2016

Improved Design of Permanent Magnet Generators for Large Scale Wind Turbines

Helena Arifa Khazdozian
Iowa State University

Improved design of permanent magnet generators for large scale wind turbines

by

Helena Arifa Khazdozian

A dissertation submitted to the graduate faculty

in partial fulfillment of the requirements for the degree of

DOCTOR OF PHILOSOPHY

Co-Major: Wind Energy Science, Engineering and Policy
Co-Major: Electrical Engineering

Program of Study Committee:
David Jiles, Major Professor
James McCalley
Nicola Elia
Ravi Hadimani
Alexander King

Iowa State University

Ames, Iowa

2016

DEDICATION

I would like to dedicate this work to my late grandfather, Rasoul Khazdozian. He was the most kind and generous man I have ever known. Education was a value he held close to his heart and my hope that is I honor him by completing this chapter in my life.

TABLE OF CONTENTS

LIST OF FIGURES

LIST OF TABLES

NOMENCLATURE

P	Power, W
T	Torque, Nm
ω	Rated speed, rad/s
K	Output coefficient
B_a	Average magnetic flux density over rotor surface or magnetic loading, T
A	Electric loading, A/m
V_r	Rotor volume, m^3
$/BH/_{max}$	Maximum theoretical energy product, kJ/m^3
$/BH/$	Energy product, kJ/m^3
B_r	Remanence, T
μ_0	Permeability of free space, H/m
μ_r	Relative permeability
D_r	Rotor diameter, m
L_{stk}	Stack length, m
k_{w1}	Fundamental harmonic winding coefficient
M_n	Magnetization, A/m
p	Number of pole pairs
g	Airgap length, m
h_m	radial thickness of magnet, m
R_s	Inner radius of stator, m
R_m	Inner radius of magnets ($R_s - g$), m

R_r	Outer radius of rotor ($R_m - h_m$), m
r	Radius at which magnet flux density is being calculated, m
α_p	Magnet pole arc to pole pitch ratio
PC	Permeance coefficient
B_m	Magnetic flux density in magnet, T
μ_{rec}	Recoil permeability
H_m	Magnetic field in magnet, A/m
H_c	Coercivity, A/m
B	Magnetic flux density, T
H	Magnetic field strength, A/m
W_h	Hysteresis loss, W
C_h	Coefficient of hysteresis loss
B_{pk}^n	Peak magnetic flux density of the material's BH curve, T
n	material dependent, ranging from 1.6 to 2.2
We	Eddy-current loss, W
C_e	Coefficient of eddy-current loss
f	Frequency, Hz
L	Inductance, H
N	No. of turns
A_c	Area of coil, m^2
l	Length of coil, m
μ	Permeability
TV	Torque density, Nm/m^3

ACKNOWLEDGMENTS

Many thanks are in order to all the family, friends, faculty and colleagues who have helped me complete this long journey.

I would like to start by thanking my committee chair and major professor Dr. David Jiles. He has been much more than an adviser – he has been a mentor and a constant source of support and wisdom. Beyond the technical discussions and questions that spurred on my research forward, I am so thankful that he has fostered my interest in energy policy and allowed me to pursue learning in this area. And more than this, when I have felt discouraged about my research, or faced obstacles in my personal life, he has been there to lift my spirits and show me the bigger picture. This has helped me to keep things in perspective and continue on with my work. I am so grateful to have had the opportunity to be a part of his research group. It has felt more like a family and community than a collection of scholars.

Thank you to my committee members, Ravi Hadimani, James McCalley, Nicola Elia and Alex King, for taking the time to review my work. The feedback they have offered has served to strengthen my work beyond what I thought possible, and their perspectives have widened my view of my research and wind energy.

I would like to thank Dr. Ravi Hadimani. More than anyone, I believe I discussed my work with him the most. Many of our discussions led to new ideas in my research and he has helped me work through many challenges in my work, all of which pushed my research further. Often times more than myself, he believed in my vision for this research and I will continue to highly value the advice he has offered me for many years to come.

I would also like to thank Dr. James McCalley for giving me the opportunity to be a part of the Wind Energy Science, Engineering and Policy (WESEP) program. It has been a truly amazing experience. He has gone above and beyond to support the WESEP students' diverse interests in WESEP 594 and done everything possible to support my degree while at Iowa State. He helped make the Wind Energy Student Organization a reality, which is the single thing I am most proud of looking back at my time at Iowa State.

Thanks to my research group, Priyam Rastogi, Neelam Prabhu-Gaunkar, Yan Ni and Xiaojing Zhong, for creating a supportive, and perhaps more importantly, a fun work environment. I am so fortunate to be part of this unique research group, surrounded by amazing and talented women who have inspired me to keep reaching higher.

To all the WESEP students, I would like to thank you for expanding not only my knowledge of wind energy, but widening my perspective of approaches to research. The experiences we have shared are something I will treasure always.

Thanks to all my family and friends who volunteered to proof read my thesis, Devin Khazdozian, Patrick Dare, Neelam Neelam Prabhu-Gaunkar, Priyam Rastogi, Jayaprakash Selvaraj, and Rose Carballeira. And a special thank you to Rose Carballeira, who has been much more than my friend, and always there to reassure me when my confidence faltered.

I would of course not have made it this far without the love and support of my family. I would to thank my parents, Lorraine Raggi and Kaveh Khazdozian, for fostering my dreams, encouraging me never to give up, and all the sacrifices they

have made for me throughout my entire life. My parents are my first role models, and I will always aspire to be like them. Thanks to my brother Devin Khazdozian who came to visit me so many times during my graduate work when I felt homesick and always knows how to make me laugh when I am struggling. I could not have asked for a more loving and supporting family. They have been the most enthusiastic cheer section anyone could ask for throughout my entire academic career and I don't think I could ask for more support than they have given me.

And finally, thank you to my life partner, Nick Scutt. He has been my shoulder to lean on through some of the toughest challenges in my life and I can truly say I would have not made it to this point without his unwavering support. He has shared with me every success and disappointment, and has always been there to remind me what's important in life. I cannot put into words how much this achievement is as much his as mine, and how thankful I am to have him in my life.

ABSTRACT

Direct-drive permanent magnet generators (DDPMGs) offer many benefits over traditional geared doubly-fed induction generators for large and offshore wind turbines. However, DDPMGs are used in less than 1% of utility scale wind turbines (>100 kW) in the U.S. wind industry due to two major barriers: significant scaling of size and mass with rated torque and power, and the use of rare earth NdFeB permanent magnets. The former is due to the need to generate high torque at low speeds by increasing the volume of the PMG, while the latter is a concern due to the high cost of the critical rare earth materials.

In this work, finite element methods were used to investigate methods to increase magnetic contribution to torque and allow for significant reduction in the PMG volume, or the use of hard ferrite permanent magnets that do not contain critical rare earth materials.

To achieve these goals, the magnetic loading, or average magnetic flux density over the rotor surface of the PMG, must be increased to compensate for torque not generated from either the PMG volume or high energy density NdFeB permanent magnets. The magnetic properties of permanent magnets needed to achieve significant size reduction in a 10 MW PMG were calculated to provide insight into suitable material developments, and mechanisms by which permanent magnets contribute to torque and power were investigated. Practical approaches to concentrating the magnetic flux over the rotor surface were also investigated. The use of Halbach arrays and a novel rotor design incorporating electrical steel flux collectors in a 3.5 kW PMG were found to allow for up to 35% or 46% reduction in

the outer diameter and axial length respectively compared to a PMG with surface mounted permanent magnets, or the use of hard ferrite, strontium iron oxide permanent magnets. Existing permanent magnet topologies were also investigated to determine which provided the highest magnetic loading and torque density to allow for size reduction. Finally, the political, environmental and social barriers to the lack of U.S. legislative action to secure a long-term, sustainable supply of rare earths were investigated.

CHAPTER 1. INTRODUCTION

1.1 Motivation

The U.S. is dependent on fossil fuels for the majority of its energy generation, with fossil fuels accounting for 67% of all electricity generation in 2015 [1]. This has many negative consequences such as the release of greenhouse gases, which contribute to climate change, and dependence on foreign oil, which threatens national energy security and energy independence. The U.S. Department of Energy (DOE) has proposed 20% wind electricity generation by 2030, with a long term goal of 35% by 2050, to reduce dependence on fossil fuels [2] [3]. In 2015, 4.7% of all electricity generation in the U.S. was generated by wind energy [1]. Continued growth of the U.S. wind industry is necessary to achieve the goal set by the DOE.

1.2 Problem Statement

The DOE has recommended larger and offshore wind turbines in order to grow the U.S. wind industry and achieve its goal of 35% wind electricity generation by 2050 [2], [3]. Currently, one of the biggest challenges faced by the wind industry is gearbox reliability. Gearbox failure accounts for the most downtime per failure in wind turbines and significantly increases operation and maintenance costs [4], [5]. Direct-drive permanent magnet generators (DDPMGs) offer a viable solution to the challenge of gearbox reliability by eliminating the gearbox, which decreases operation and maintenance costs, making DDPMGs preferred for offshore and remote wind turbines

[6], [7]. Yet, in 2014 DDPMGs account for less than 1% of all utility scale wind turbines (greater than 100 kW) in the U.S. [8].

There are two significant barriers that must be overcome to allow for increased use of DDPMGs in the U.S. wind industry. The first is the sheer size and mass of DDPMGs. DDPMGs require large rotor volumes to generate high torque at low speeds. This causes DDPMGs to scale in size and mass much more rapidly than geared doubly-fed induction generators as rated torque/power is increased [6], [7], [9]. Increased drivetrain weight is undesirable in wind turbines as it increases the load the wind turbine tower must support.

The second barrier to increased use of DDPMGs in wind turbines is their use of rare earth NdFeB permanent magnets. NdFeB permanent magnets contain rare earth elements Nd and Dy, which are considered “critical materials” by the DOE due to their supply risk and importance to renewable energy technologies [10].

1.3 Summary of Contributions

In this work, methods are explored to achieve size reduction or the use of rare earth free permanent magnets in DDPMGs. In partial fulfillment of the requirements of a doctor of philosophy degree in Wind Energy Science, Engineering and Policy, the following contributions have been made:

1. Investigated magnetic contribution of increased remanence to size reduction
2. Demonstrated the potential of Halbach cylinder rotors to achieve:
    a. significant reduction in outer diameter and axial length of PMGs (up to 35%)
    b. or the use of rare earth free, strontium iron oxide permanent magnets
3. Employed the use of electrical steel flux collectors in the rotor to concentrate magnetic flux and achieve:
    a. significant reduction in outer diameter and axial length of PMGs (up to 46%)
    b. or use of rare earth free, strontium iron oxide permanent magnets
4. Investigated the potential for size reduction by employing varied permanent magnet rotor topologies
5. Determined barriers to enacting a legislative strategy to ensure a sustainable, long-term supply of rare earths

1.4 Overview of Dissertation

In Chapter 2, an overview of the U.S. wind industry and generator technology is presented, including a review of recent developments and alternatives to these technologies. In Chapter 3, a theoretical investigation is described in which reduction in the outer diameter and axial length of a 10 MW PMG is achieved by varying the permanent magnetic properties of NdFeB permanent magnets. The magnetic characteristics of the PMG are explored to account for their contribution to achievement

of rated torque. Chapters 4 and 5 present magnetic flux focusing techniques to achieve significant size reduction or the use of rare earth free, hard ferrite permanent magnets in a 3 MW PMG. Halbach cylinders are explored in Chapter 4 and electrical steel flux collectors are explored in Chapter 5. The potential for size reduction through variation of permanent magnet topology is studied in Chapter 6. The environmental, social and political barriers to enacting a legislative policy to ensure a long-term, sustainable supply of rare earths is presented in Chapter 7. Finally, the findings of this work are summarized accompanied by recommendations for future work in Chapter 8.

CHAPTER 2. BACKGROUND & LITERATURE REVIEW

2.1 U.S. Wind Industry Overview

The first wind farms appeared in the U.S. in the 1980s, representing the birth of the U.S. wind industry. Since then, wind turbines have steadily grown in size and power rating. Wind energy has become so viable as an alternative energy source that the U.S. Department of Energy (DOE) has targeted achievement of 35% wind electricity generation by 2050 [3]. Wind energy accounted for 4.7% of total electricity generation in 2015 (Fig. 2-1), representing 35% of all renewable electricity generation including hydroelectric [1]. The DOE has recommended both larger and offshore wind farm installations to continue growth of the wind industry and achieve its stated goal [2], [3].

Through 2015, the U.S. had 74,471 MW of installed wind capacity [11], with more than 48,000 utility-scale wind turbines in 39 states and Puerto Rico [12]. Globally, the U.S. ranks second in terms of installed wind capacity (behind China) [11]. Currently the U.S. has no installed commercial offshore wind farms. Construction on the first commercial offshore wind farm in the U.S. has begun and is expected to be operational by 2016. The 30 MW Deepwater Wind project will be installed off the coast of Rhode Island, to be followed by projects off the coasts of Massachusetts and New Jersey [13].

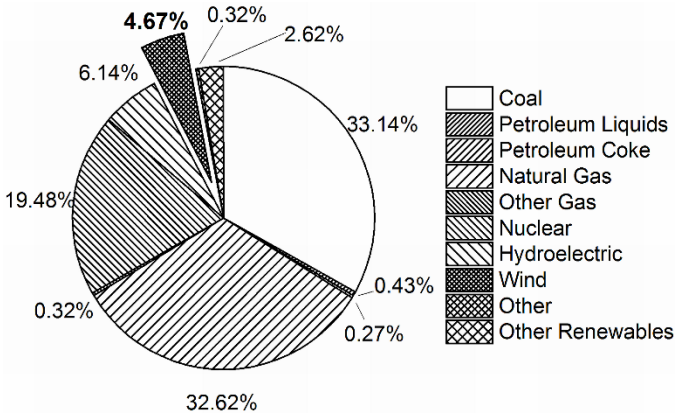

Figure 2-1. U.S. net electricity generation by source in 2015 [3].

2.2 Wind Turbine Generators

In wind turbines, the generator serves to convert mechanical to electrical energy. The mechanical energy is supplied by the rotation of the blades around the wind turbine rotor. Wind turbine generators can be broadly categorized into two types: induction or asynchronous and synchronous generators. The shaft of an induction generator needs to spin around 1800 rpm for efficient energy conversion. However, the wind turbine rotor only spins between 5 and 25 rpm and is limited by the wind speeds. To overcome this limitation, a gearbox is employed to increase the rotational speed supplied to the generator shaft for efficient conversion.

There are four broad types of wind turbines with Types 1 to 3 utilizing a geared induction generator in the drive train and Type 4 being direct-drive (Fig. 2-2). Type 1 fixed speed generators were common in the first wind turbines (Fig. 2-2a). The geared squirrel cage induction generators offered little control, operating at or around rated speed. They also consumed reactive power, necessitating a capacitor bank as a reactive power source. Type 2 generators (Fig. 2-2b) offered partial control, allowing for some variation in the speed of the generator shaft, with up to 10% slip control. Geared wound rotor induction generators were used. Some slip control was achieved with the use of variable rotor resistance, which replaced the slip rings traditionally used. Type 3 variable speed generators (Fig. 2-2c) are most commonly used in the wind industry, employing a geared doubly-fed induction generator (DFIG). Two power converters rated at 30% of full power are employed to allow up to 50% control of slip.

In a direct-drive, or Type 4, wind turbine the gearbox is eliminated and the generator

shaft spins at the same speed as the wind turbine rotor (Fig. 2-2d). Permanent magnet generators are most often employed in Type 4 wind turbines, though it should be noted wound rotor machines run synchronously or asynchronously are also employed in the industry. Variable speed control is provided by two power converters rated at full power.

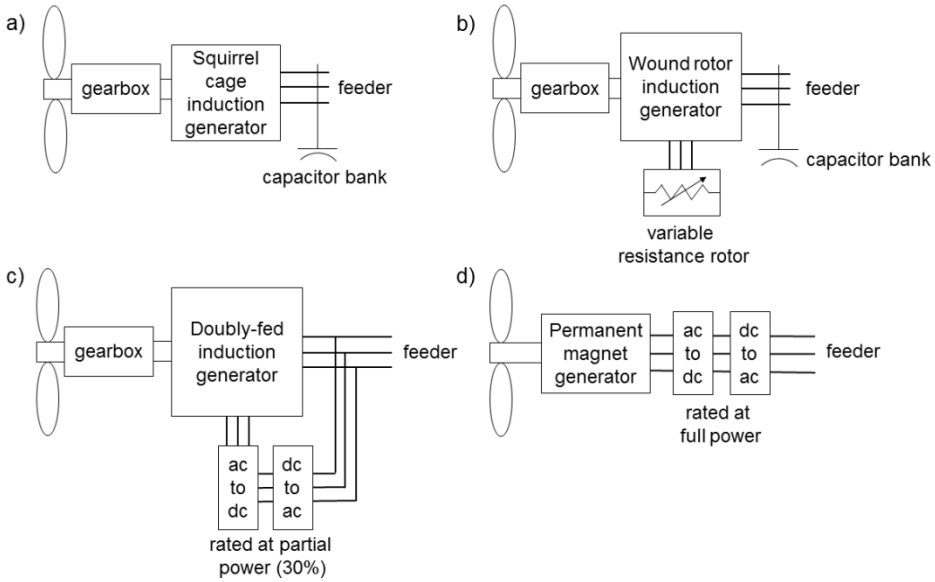

Figure 2-2. a) Type 1, b) Type 2, c) Type 3 and d) Type 4 wind turbines.

2.2.1 Geared Doubly-fed Induction Generators

Type 3 generators or DFIGs are most commonly employed in wind turbines for conversion of mechanical to electrical energy. As wind turbines have continued to increase in size and power rating, multistage gearboxes have become standard. While a three stage gearbox is most common for the use of DFIGs in wind turbines, a fourth stage may be required for larger scale wind turbines. Geared DFIGs have the advantage of being lightweight, with outer diameters of 1 to 2 meters for a 3 MW wind turbine.

Geared DFIGs are not without their disadvantages. The biggest drawback to Type 3 turbines is the gearbox. Gearboxes fail well before their 20 year design lifetime [5] and account for the most downtime per failure in wind turbines [4]. This decreases the overall reliability of the drivetrain and wind turbine. Gearboxes failures are most often tied to issues with the bearings [3], [4].

Gearbox failure accounts for increased costs of wind turbines due to the price of manufacturer warranties, which must cover such failures, as well as contingency funds the owners and operators must set aside for gearbox repair or replacement [5]. Gearboxes also account for the majority of system losses in the drivetrain, decreasing the efficiency of DFIGs overall [6]. Gearbox reliability is one of the most important issues currently faced by the wind industry, according to literature [4], [5] and wind industry [14], [15] and permanent magnet [16] experts.

2.2.2 Permanent Magnet Generators

Direct-drive permanent magnet generators (DDPMGs), or Type 4 generators, are an alternative to geared DFIGs. DDPMGs were employed in less than 1% of utility scale wind turbines (>100 kW) in the U.S. in 2014 [8]. PMGs have many advantages over traditional electrical machines including no excitation loss, higher torque density, and higher air gap flux density [7]. The most significant advantage of DDPMGs is the elimination of the gearbox. This increases wind turbine reliability, which decreases operation and maintenance costs, as well as audible noise [6], [7], [17]. DDPMGs also offer high efficiency at both full and partial load making them ideal for variable speed wind turbines. Due to these advantages, DDPMGs are used more extensively on a

global scale, especially in the European Union and China. The DOE has identified direct-drive generators and PMGs specifically as drive train technology that should be advanced in the future [3].

DDPMGs have two significant disadvantages. First, DDPMGs must generate high torque at low speeds, ranging from 5 to 25 rpm, to achieve rated power as described by equation (1). In order to increase torque, more rotor volume is required as evident in equation (2)

$$P = T\omega \quad (1)$$

$$T = KB_aAV_r \quad (2)$$

where T is torque, ω is rated speed, K is the output coefficient, B_a is the magnetic loading, A is the electrical loading, and V_r is the rotor volume. Thus, as rated torque/power is increased, DDPMGs scale in size and mass much more rapidly than geared DFIGs (Fig. 2-3). Increased drivetrain weight is undesirable in wind turbine design as it increases the load the wind turbine tower must support.

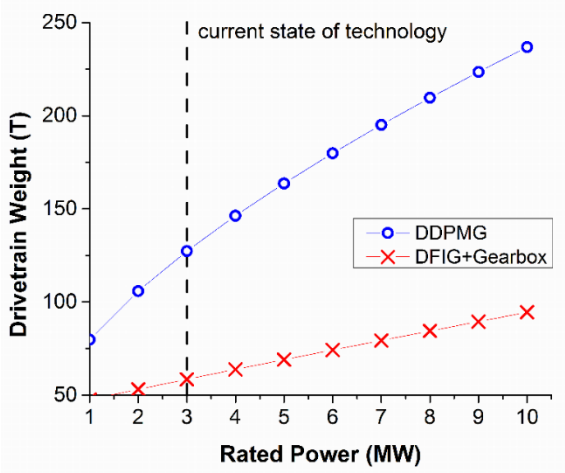

Figure 2-3. Comparison of the drivetrain weight for geared DFGIs and DDPMGs as predicted by the National Renewable Energy Laboratory Wind Turbine Design Cost and Scaling Model [9].

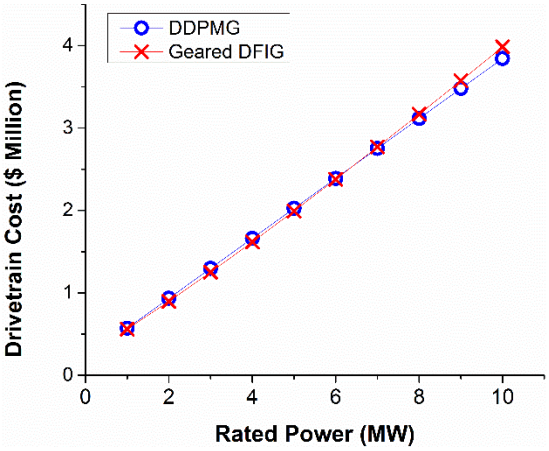

Figure 2-4. Comparison of the drivetrain cost for geared DFGIs and DDPMGs as predicted by the National Renewable Energy Laboratory Wind Turbine Design Cost and Scaling Model [9].

The second major disadvantage of PMGs are rare earth NdFeB permanent magnets. NdFeB permanent magnets increase the material cost of PMGs and have supply risks associated with them. This will be discussed further in sections 2.3.1, 2.4 and Chapter 7. It should also be noted that DDPMGs suffer from cogging torque, or torque ripple, due to low speed operation. However, several known techniques including pole skew and stator skew can be used to minimize cogging torque [18].

PMG design for wind turbines encompasses many considerations[1]. For purposes of this discussion, only brushless machines will be discussed as most modern PMGs are brushless. Choice of magnetic flux path is an important consideration with radial, axial or transverse flux (for linear machines) being general design choices. Radial flux machines are considered superior for high-speed, high-power applications while axial flux machines offer the advantages of zero-cogging torque and low cost. However, axial flux machines require a large airgap contributing to significant magnetic flux leakage, which is problematic for high torque applications such as wind turbines [18]. Thus, radial flux PMGs are most commonly used in commercial PMGs for wind turbines and will be discussed here.

Radial flux PMGs allow for choice of interior and exterior rotor configuration. Interior rotor PMGs with high pole number are best for applications that require high torque at low speeds [18], such as wind turbines, making them popular in commercial permanent magnet wind turbine installations. Additionally, interior rotor PMGs place the stator in the outer position, allowing for passive air cooling. However, exterior rotor PMGs are

[1] Stator design considerations are not mentioned here as they are not dealt with in this research. However, it should be noted that stator design, particularly the winding layout, is an important and active area of research.

becoming more common in the wind industry as power rating increases because they allow for reduced axial machine length, allowing for a more compact machine in the nacelle of the wind turbine.

Permanent magnet topology is also an important design consideration and is dependent on the application of the PMG. Interior permanent magnet (IPM) machines are preferred for applications that require rapid acceleration or deceleration of the load, such as hybrid and electric vehicles [19]. Surface mounted and bread-loaf permanent magnets are most common for wind turbine application [20].

2.2.3 Permanent Magnet Generator Design Research

Research on PMGs covers a wide range of research topics including, but not limited to, modeling and investigating losses, structural issues, reduction of cogging torque, stator winding layout, and generator control. Research on PMGs in the area of magnetics is less extensive, making this research unique.

Size and mass reduction in PMGs have been investigated with different approaches. One such approach is the use of an ironless-stator [21], [22]. Reductions in mass of over 55% in a 100 kW PMG have been reported [22]. Versteegh *et al.* designed a commercial direct-drive wind turbine, which employed a 70 meter rotor blade diameter to allow for the use of an interior rotor PMG [23]. Also, as previously discussed, the use of an exterior rotor topology can allow for reduced axial length and therefore offer a compact design.

Though many are aware of the supply risks associated with NdFeB permanent magnets (to be discussed in section 2.4), there is not an extensive body of research in

the literature on rare earth free PMG design. However, industry is certainly interested in this design issue. A patent was recently granted to UQM Technologies Inc. in which the use of U-shaped magnets allowed for the use of low coercivity, rare earth free permanent magnets, such as Alnico or FeCoW, in the permanent magnet motor [24]. The design is intended for application in hybrid and electric vehicles [25].

2.2.4 Alternative Generator Technologies

Size and weight reduction can also be achieved with alternative generator technologies. One such alternative is a hybrid wind turbine, in which a single or two stage gearbox is coupled with a PMG. Such wind turbines operate in the rage of 100 to 400 rpm. The increased speed allows for the use of compact PMGs, which reduces the drivetrain weight and material cost due to the comparatively higher torque density of PMGs compared to induction generators. The losses due to the gearbox are minimized since there are less stages. Many PMG installations in the U.S. employ a hybrid configuration. Researchers have proposed improvements such as the coupling of a coaxial magnetic gear in place of a traditional gearbox, which allows for high speed operation and compact, lightweight PMG design [26].

Another alternative is a high temperature superconducting (HTS) generator. HTS generators have been explored for direct-drive wind turbines. HTS direct-drive (HTSDD) generators have several advantages including a lightweight, compact design, high efficiency and scalability [27]. In a comparative assessment of HTSDD generators with existing wind turbine generator technologies conducted by the National Renewable Energy Laboratory, American Superconductor (AMSC) and AMSC Windtec, it was

found that HTSDDs achieve annual energy production at or exceeding that achieved by geared DFIGs and DDPMGs [27]. Furthermore, the levelized cost of energy (LCOE) was predicted to decline with increased power rating, rather than increase as is the case for geared DFIGs and DDPMGs. HTSDD generators are not yet employed in the wind industry. However, AMSC SeaTitan is currently working on a prototype 10 MW offshore wind turbine utilizing a HTSDD generator.

2.3 Permanent Magnets

Permanent magnets are magnetic materials which are able to retain magnetization in the absence of an applied magnetic field. Permanent magnets should have high remanence B_r, or magnetization remaining after the applied magnetic field is removed, and high coercivity H_c, or resistance to demagnetization. Commercially, an important figure of merit is the energy product, or energy density, of the permanent magnets [28]. The theoretical energy product of a permanent magnet is defined by the operating point on its demagnetization curve, which yields the highest product of the magnetic field H and the magnetic flux density B (Fig. 2-5a). The operating point will be defined by the intersection of load line of the permanent magnet with the demagnetization curve (Fig. 2-5a). The load line of a permanent magnet is given by its geometry. In practical applications, the operating point will yield an energy product below the theoretical limit (Fig. 2-5b).

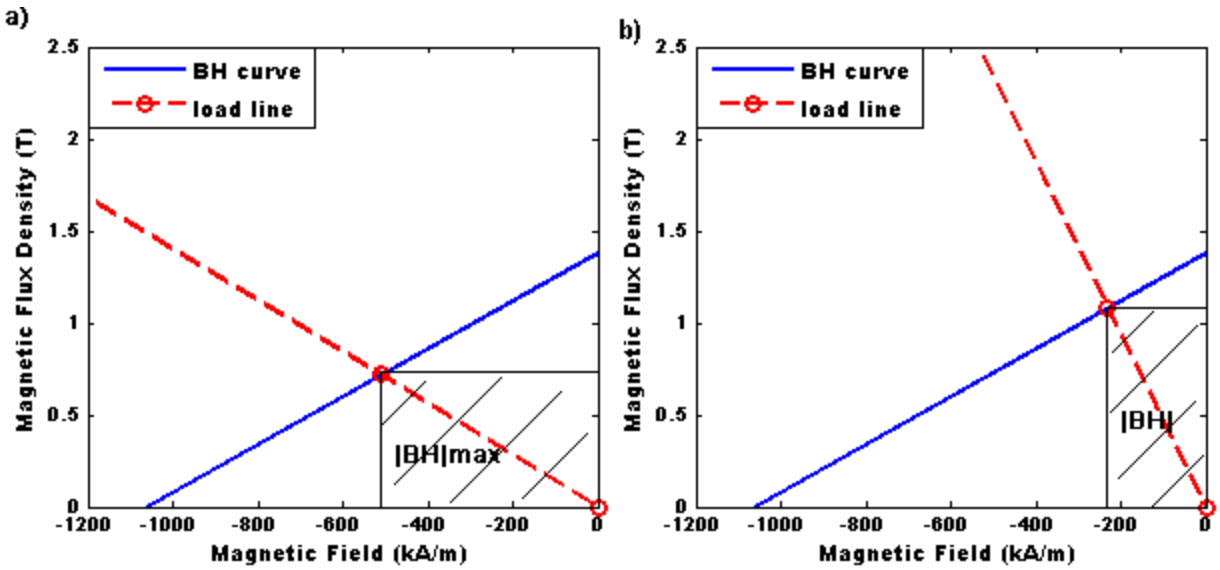

Figure 2-5. Demagnetization curve and load line for a NdFeB 48/11 grade permanent magnet in the case of a) theoretical maximum energy product given by the optimum operating point and b) practical load line yielding an energy product below the theoretical limit.

Commercial permanent magnet materials broadly include rare earth metals, NdFeB and SmCo, hard ferrites or ceramics, and alnico (Table 2-1). Hard ferrites with permanent magnet applicability include $BaFe_{12}O_{19}$ and $SrFe_{12}O_{19}$. For purposes of application in permanent magnet generators high operating temperature is desired as well as a linear demagnetization curve [28].

Table 2-1. Typical properties of commercial permanent magnets [29].

	B_r (kG)	H_c (kOe)	BH_{max} (MGOe)	T_m (°C)
NdFeB	10.8 – 14.9	11.0 – 34.0	28 – 54	220
SmCo	8.7 – 11.6	8.2 – 10.9	18 – 31.5	350
Hard Ferrites	2.0 – 4.1	1.57 – 4.0	0.8 – 4.32	300
alnico	6.6 – 13.2	0.475 – 1.475	1.35 – 10.5	538

NdFeB permanent magnets, specifically $Nd_2Fe_{14}B$, are considered far superior to other permanent magnets for PMGs as they have the highest available energy product [30]. Yet, partial substitution of Nd with Dy or Tb is necessary to achieve a linear demagnetization curve with temperature stability by increasing the anisotropy of the

NdFeB permanent magnet [31]. In practice, Dy is used more commonly than Tb to increase operating temperature as it is about half the cost of Tb. $Nd_2Fe_{14}B$ corrodes easily requiring a coating in most applications, including wind turbines. By comparison SmCo type magnets do not corrode as easily, but are more expensive and have a lower maximum energy product [28]. Hard ferrites and alnico are non-rare earths and are therefore more economical, but also have lower energy products and require significantly more volume to achieve the same magnetic flux density as NdFeB or SmCo. Hard ferrites in particular are easily produced while the demand for alnico is low, but consistent [32].

2.3.1 Rare Earths

The rare earth metals, or rare earths, consist of 17 elements including the 15 lanthanides as well as Sc and Y. The latter two elements are included due to similarity of chemical properties to the lanthanides. Rare earths are classified into the “heavy” and “light” elements (Fig. 2-6), grouped according to atomic number [33]. The heavy elements are less abundant than the light elements and therefore tend to more expensive [31]. It is important to note that Dy, which is considered to be the most critical rare earth by the DOE, is classified as a heavy rare earth.

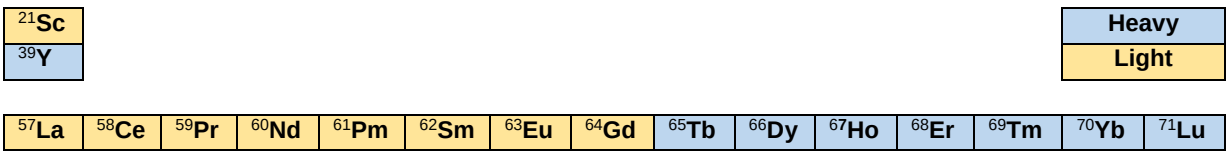

Figure 2-6. Classification of heavy and light rare earths.

The name “rare” earth is a misnomer as rare earths are actually more abundant than precious metals such as gold and silver. Rare earths are found distributed throughout the earths’ crust, combined in mineral deposits. However, large concentrations of rare earths in such mineral deposits that are economically sufficient for mining, are less common. Bastnasite deposits, a carbonate-fluoride mineral, are currently the largest source of rare earths, while monazite deposits, a phosphate mineral, are the second. With only 300 deposits identified worldwide, there is an estimated 130 million metric tonnes of rare earths, according to the U.S Geological Survey (USGS) [34]. China has the largest amount of identified reserves with an estimated 42% of world reserves, followed by Brazil and Australia (Table 2-2).

Table 2-2. Estimated mine production and reserves of rare earths in 2015 [34].

	Estimated Mine Production (Metric Tonnes)		**Estimated World Reserves (Metric Tonnes)**	
	2013	**2014**	**Share in Tonnes**	**Share by %**
China	95,000	95,000	55,000,000	42.3
United States	5,500	7,000	1,800,000	1.4
India	2,900	3,000	3,100,000	2.4
Russia	2,500	2,500	*	*
Australia	2,000	2,500	3,200,000	2.5
Thailand	800	1,100	NA	NA
Vietnam	220	200	*	*
Brazil	330	---	22,000,000	16.9
Malaysia	180	200	30,000	0.02
Other Countries	NA	NA	41,000,000	31.5
World Total (rounded)	110,000	110,000	130,000,000	100

*Included with other countries

2.4 Implications of Rare Earth Dependence

Dependence on imported rare earths has significant environmental, social, political and economic implications for the U.S. wind industry. According to the USGS, 86% of the world’s rare earth mine production took place in China in 2014 [34]. In recent years,

China has controlled up to as much as 95% of the world's rare earth market. Past Chinese policies of restricting export quotas and imposing tariffs may have contributed to historical high and volatile prices for Nd and Dy. Though the World Trade Organization (WTO) has ruled that these policies violated international trade laws and China has agreed to end these practices [35], Chinese consolidation of rare earth mines and production facilities into a few state owned facilities and efforts to stop illegal rare earth production and mining creates uncertainty about rare earth supply and price in the future.

The DOE has classified Nd and Dy as "critical materials" due to their supply risk and importance to renewable energy technologies. The DOE has recommended that the U.S. pursue domestic investment, diversification of global supply chains, and heavy research and development to develop a sustainable long-term supply of rare earths and reduce U.S. dependence on these materials. Currently, the U.S. has no stockpiles of rare earths, limited domestic production, and no congressional strategies to ensure a sustainable long term supply of rare earths [10].

2.4.1 Recycling of Rare Earths

Recycling of Nd and Dy could generate an alternative supply stream of rare earths and has been recommended by the DOE. The recycling of rare earths in general can come from three potential streams: direct recycling of pre-consumer rare earth manufacturing scrap or residue, urban mining of end of life/post-consumer products, and mining of urban and industrial waste residues [36]. However, most processes

cannot achieve economies of scale for end use in large NdFeB permanent magnets for clean energy technologies.

Up to 30% of rare earth alloy is lost during manufacturing in swarf or fine chips of filings of magnets generated from grinding of the permanent magnets [36]. Recycling swarf is already being employed in production facilities, but only recently.

Small NdFeB permanent magnets from hard disk drives and voice coil motors (usually Dy-free) can be mined from electronic waste or e-waste. Recycling shredded e-waste is chemically intensive and produces low recovery rates. Ideally, recycling would take place before shredding of e-waste to lower chemical and energy requirements, but requires demagnetization to allow for manual dismantling [36], [37]. Such recycling techniques are not currently a viable supply stream for large NdFeB permanent magnets, but may reduce the overall demand for Nd in electronic applications.

With regard to urban mining of large NdFeB permanents magnets for application in renewable energy technologies, the current supply stream is limited due to the youth of the wind and electric vehicle industries. There are currently few to no wind turbines or electric vehicles that have reached end of life/post-consumer use. However, in the long term, there will be many opportunities for recycling these large NdFeB permanent magnets, which can be used directly after removal with processing.

Future research may change the economies of scale of recycling rare earths. Recently, the Critical Materials Institute (CMI) at Ames Laboratory, Department of Energy has developed two promising recycling techniques. One technique that is under optimization has been developed to recycle SmCo directly from swarf [38]. The second technique, membrane solvent extraction, presents a viable recycling method from e-

waste. The technique is less energy and chemical intensive than established recycling methods and yields 90% recovery of Nd and Dy, free of impurities such as Fe and B. Furthermore, the rare earth oxides recovered can be used directly after recovery for some applications [39].

2.4.2 Permanent Magnetic Materials Research

Development of a rare earth free permanent magnet with comparable energy product to NdFeB would also alleviate the need to mine and import rare earths. Currently, no commercial alternative exists, but research on substitution for Nd and Dy, or a new permanent magnet material are ongoing and supported by the federal government.

Mn-based compounds are being investigated extensively. $Mn_{70}Ga_{30}$ melt spun ribbons have achieved 2.2 kOe coercivity and 10 emu/g remanence, with annealing at 973K for one hour in Ar increasing coercivity to 5.7 kOe at the cost of significantly lower remanence [40]. Mn_xGa (x=2-3) films grown by molecular beam epitaxy on Si substrates with a native layer of amorphous SiO_2 achieved coercive fields of 2.5 T, comparable to that of NdFeB (2.6 T) [41]. $Mn_{55}Al_{45}$ alloy with exchange-bias had a reported intrinsic coercivity of 19 KOe at 10K, but a coercivity of only ~4.5 kOe at the same temperature [42].

Exchange-spring magnets are a promising alternative. Investigation of FeCo/FePt(001) exchange-spring magnets by numerical methods predict a maximum coercivity of ~188 kOe and energy product of ~66 MGOe [43]. Exchange-spring FePt/Fe cluster nanocomposite permanent magnets achieved a maximum energy

product of 21 MGOe for 14 %vol of Fe after annealing at 500˚C [44], which is comparable to lower energy density SmCo and NdFeB permanent magnets. Additionally, $HfCo_7$ nanocrystals were reported to achieve a coercivity of 3.0 kOe and a magnetocrystalline anisotropy coefficient, K_1, of ~10 Mergs/cm^3 at room temperature [45].

Finally, researchers at Ames Laboratory have achieved the use of Ce in substitution of Dy in melt spun NdFeB. By employing partial doping of Ce for Nd and Co for Fe in the NdFeB alloy, high operating temperatures are achieved in the high strength NdFeB permanent magnets, though the material cannot be used in place of very high strength permanent magnets [46]. Sintered NdFeB magnets with Ce and Co have not yet been developed.

CHAPTER 3. POTENTIAL AND LIMITS OF IMPROVEMENTS OF PERMANENT MAGNETIC MATERIAL PROPERTIES IN PERMANENT MAGNET GENERARTORS

3.1 Introduction

Size reduction of DDPMGs is limited by the magnetic properties of the permanent magnets. The magnet strength per unit volume, or energy product, of commercial permanent magnets limits the maximum magnetic flux density that can be achieved in conventional PMG designs such as the surface mounted PMG. This limits the achievable magnetic contribution to torque B_a, limiting the size reduction achievable as described by the equation (2).

$$T = KB_aAV_r \tag{2}$$

The theoretical upper limit of energy product is given by

$$|BH|_{max} = B_r^2 / (4\mu_0\mu_r) \tag{3}$$

where B_r is the remanence, μ_0 is the permeability of free space and μ_r is the relative permeability. Magnetic permeability is a measure of the magnetic field formed in a material with respect to the applied magnetic field (analogous to conductivity in an electrical circuit). As discussed in Chapter 2, the highest available energy product in commercial permanent magnets is offered by NdFeB, which has a theoretical maximum energy product of 477.5 kJ/m^3 [47].

In this Chapter, theoretical limitations on improvements in the size reduction of permanent magnet generators were determined through an investigation of permanent magnetic material properties. Theoretically, if the energy product of the permanent magnet could be increased, the average flux density of the rotor surface could also be increased, thereby increasing the magnetic loading B_a, torque, and ultimately the output

power of the PMG. This would allow for reduction of the PMG volume by offsetting the torque not generated by the rotor, allowing a more compact design. A 25% reduction in outer diameter and axial length of a 10 MW PMG was proposed to demonstrate proof of concept since this would have even greater weight saving implications (rotor volume is dependent on the square of the rotor diameter). The idealized properties of a permanent magnet necessary to maintain achievement of rated torque for a 10 MW PMG with the proposed reductions in dimensions were calculated analytically. The theoretical results were then verified through finite element analysis and the magnetic contribution to achievement of rated torque was determined.

3.2 Methodology

3.2.1 Machine Design

Initially, a 3.5 kW PMG finite element was designed for initial investigation in MotorSolve^{TM} by Infolytica Corporation. A small machine design, on the order of kW, was initially selected to save computational time; it is straight forward to scale designs within the finite element software. Machine topology, inner rotor with surface mounted permanent magnets, was chosen to reflect that used by industry. This was based on discussions with a member of corporate research at ABB [20]. Such commercial PMGs have radial-flux topology with N35SH or N35UH grade NdFeB magnets in a surface mounted or bread-loaf permanent magnet topology. Inner and outer rotor topologies are both used. For direct-drive configuration in large scale wind turbines, outer rotor topology is preferential because it allows for reduction in stack length. However, for this investigation inner rotor topology was selected for ease of design.

A 3.5 kW PMG with radial-flux, surface mounted topology was designed (Table 3-1). The dimensions of the PMG were based on the design of Abdel-Khalik *et al.* [48]. Four magnetic poles were selected to minimize the number of common denominators between the pole and slot number, which is desirable to minimize cogging torque [49]. M19 26 Ga non-oriented Si steel was selected for the rotor and stator laminations [50]. Finite element software, MotorSolve^{TM} by Infolytica Corporation, aided in design. Finite element methods were used to calculate the torque, input and output power as a function of rotor position under 2D steady-state conditions. The advance angle was set to 180° to simulate generator operation at rated current (21.5 A) and rated speed (333 rpm). 24 sample points, 5 skew samples, and a harmonic amplitude threshold of $1x10^{-6}$ were used with the best periodicity possible. The effects of varying the remanence, coercivity, energy product and permanent magnet geometry were also investigated for the 3.5 kW design.

Table 3-1. General Specifications of the 3.5 kW PMG Design.

Specification	Value
Rated torque (Nm)	100
Rated speed (rpm)	333
# of phases	3
# of poles	4
# of slots	24
Outer rotor diameter (mm)	192
Inner rotor diameter (mm)	113
Outer stator diameter (mm)	348
Inner stator diameter (mm)	194
Stack length (mm)	348

3.2.1.1 Scaling of PMG Design: 3.5 kW to 10 MW

The 3.5 kW PMG design was scaled to 10 MW. NdFeB 48/11 grade magnets were selected to provide a high energy product ($|BH|_{max}$ = 367.4 kJ/m^3). The scaled 10 MW

PMG with NdFeB 48/11 permanent magnets is referred to as “Case 1.” For the rated speed of 333 rpm, a rated torque of 286,532 Nm is required to achieve 10 MW of power, according to equation (1). Rearranging equation (2), torque can be expressed as the following [51], [50]

$$T = KD_r^2 L_{stk} \tag{4}$$

$$K = \frac{k_{w1}}{\sqrt{2}} \frac{\pi^2}{4} B_a A = 1.74 k_{w1} B_a A \tag{5}$$

where k_{w1} is the fundamental harmonic winding constant. According to equation (4), each dimension must be scaled by 14.2 times to achieve this rated torque assuming the output coefficient K remains unchanged (Table 3-2).

Table 3-2. General specifications of the 10 MW PMG design where the 3.5 kW design has been scaled by 14.2 times (Case 1).

Specification	Value
Rated Torque (Nm)	286,532
Outer rotor diameter (mm)	2,726
Inner rotor diameter (mm)	1,359
Outer stator diameter (mm)	4,942
Inner stator diameter (mm)	2,754
Stack length (mm)	4,942

According to equation (2), the rated torque of the 10 MW PMG design can be maintained when the dimensions are reduced by 25% if the energy product of the permanent magnet is increased accordingly. This will increase the average flux density over the rotor surface B_a, and consequently the output coefficient K. The dimensions of the 10 MW PMG design in Table 3-2 were reduced by 25% (Table 3-3). The 10 MW PMG reduced in size by 25% with NdFeB 48/11 permanent magnets is referred to as “Case 2.”

Table 3-3. General specifications of the 10 MW PMG design where dimensions of the design in Table 3-2 have been reduced by 25% (Cases 2-3).

Specification	Value
Rated Torque (Nm)	286,532
Outer rotor diameter (mm)	2,045
Inner rotor diameter (mm)	1,020
Outer stator diameter (mm)	3,707
Inner stator diameter (mm)	2,066
Stack length (mm)	3,707

To compensate for the resulting reduction in torque due to the reduction in PMG volume, the output coefficient K must increase by 2.37 times. The output coefficient will increase linearly with an increase in the average flux density of the rotor surface as described by equation (6). Assuming the magnetic flux density will scale linearly with an increase in energy product and the electrical load remains constant, the energy product must also scale by 2.37 times. This implies the remanence of the permanent magnet must be increased by 1.54 times, as is evident from equation (3). The calculated theoretical remanence, relative permeability and upper limit on the energy product were calculated as shown below.

$$B_r = 1.54*1.39T = 2.14T \quad (6)$$

$$\mu_r = (B_r/H_c) / \mu_0 = 1.64035 \quad (7)$$

$$|BH|_{max} = 553.9kJ/m^3 \quad (8)$$

where H_c is the coercivity equal to 1,060,650 A/m and μ_0 is $4\pi x10^{-7}$ H/m. The initial remanence and coercivity are that of NdFeB 48/11. These calculations serve as a rough "back of the envelope" calculation, which give a starting point for determining the remanence needed to achieve 25% reduction in the dimensions of the PMG. The 10MW PMG reduced with dimensions reduced by 25% with idealized permanent magnets of

increased remanence and energy product is referred to as “Case 3.” A summary of each case is presented in Table 3-4.

Table 3-4. Description of each PMG case investigated.

Name	Outer Diameter (mm)	Permanent Magnet Material
Case 1	2,726	NdFeB 48/11
Case 2	2,045	NdFeB 48/11
Case 3	2,045	Idealized

A linear permanent magnet model was used to define the permanent magnets, as described in equation (9). This linear model is derived from the demagnetization curve of a permanent magnet, or hysteresis curve in the second quadrant (Fig. 3-1), where the slope is given by the remanence and coercivity and the remanence gives the intersection point for the y-axis.

$$B = \frac{B_r}{H_c} H + B_r \tag{9}$$

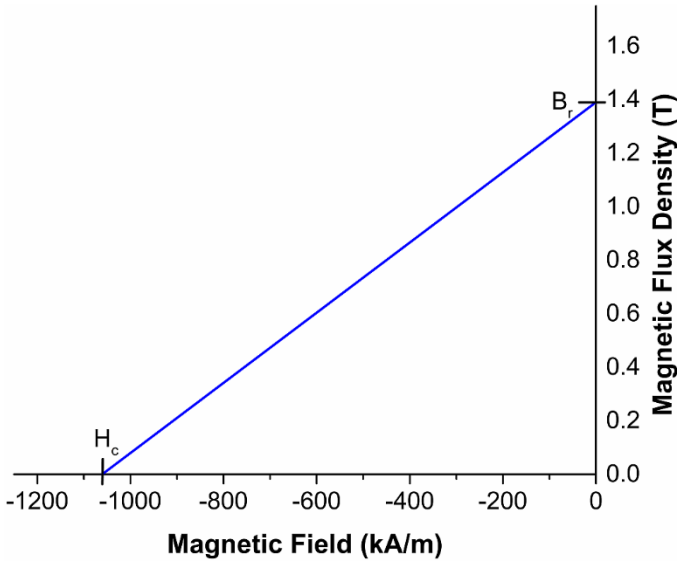

Figure 3-1. Linear model of the demagnetization curve for a NdFeB 32/31 permanent magnet.

The performance of the 10 MW PMG was simulated for 2D steady-state operation to determine the torque, input and output power, and efficiency using finite element

methods in MotorSolve™ by Infolytica Corporation, according to the same conditions described in section 3.2.1. The operating point, magnetic flux density, loss mechanisms and their effects on the torque produced were examined to determine magnetic contribution to torque. The effects of increased energy product during operation on the losses in the rotor and stator were also investigated. The aforementioned investigations are compared for Cases 1 to 3 (Table 3-5).

Table 3-5. Specifications of 10 MW PMGs of equal ratings.

	Case 1	**Case 2**	**Case 3**
Rotor Outer Diameter (mm)	2,726	2,045	2,045
Rotor Yoke (mm)	612	459	459
Stator Outer Diameter (mm)	4,942	3,707	3,707
Stator Yoke (mm)	612	459	459
Conductor Area (mm^2)	9,301	5,233	5,233
Permanent Magnet Material	NdFeB 48/11	NdFeB 48/11	Idealized
Theoretical Energy Product (kJ/m^3)	367.4	367.4	553.9
Remanence (T)	1.39	1.39	2.14

3.3.2 Model Validation

To validate the finite element model and results, the air gap flux density was determined analytically and numerically. The analytical model was developed by Zhu [52] where the air gap flux density is given by equations (10) and (11). The magnetization M_n is given in polar coordinates and assumed to be uniform for the entire magnet cross-section. The airgap flux density is calculated analytically under open-circuit conditions in 2D polar coordinates by solving the governing Laplacian/quasi-Poissonian field equations. The analytical model does not take into account the effects of stator slots and the relative recoil permeability is assumed to be constant [52]. For comparison, the numerical results were determined by finite element methods (FEM).

$$B_g(r,\theta) = \sum_{n=1,3,5\ldots}^{\infty} \frac{\mu_0 M_n}{\mu_r} \frac{np}{(np)^2-1} \left\{ \frac{(np-1)+2\left(\frac{R_r}{R_m}\right)^{np+1} - (np+1)\left(\frac{R_r}{R_m}\right)^{2np}}{\frac{\mu_r+1}{\mu_r}\left[1-\left(\frac{R_r}{R_s}\right)^{2np}\right] - \frac{\mu_r-1}{\mu_r}\left[\left(\frac{R_m}{R_s}\right)^{2np} - \left(\frac{R_r}{R_m}\right)^{2np}\right]} \right\} \cdot \left[\left(\frac{r}{R_s}\right)^{np-1} \left(\frac{R_m}{R_s}\right)^{np+1} + \left(\frac{R_m}{r}\right)^{np+1} \right] \cos(np\theta) \quad (10)$$

$$M_n = \frac{2B_r \alpha_p}{\mu_0} \frac{\sin\left(\frac{n\pi\alpha_p}{2}\right)}{\frac{n\pi\alpha_p}{2}} \quad (11)$$

where μ_r is the relative recoil permeability, p is the number of pole pairs, R_s is the inner radius of stator, R_m is the radius of magnets ($R_s - g$), g is the air gap length, R_r is the outer radius of rotor ($R_m - h_m$), h_m is the radial thickness of magnet, r is the radius at which flux density is being calculated, B_r is the remanence, and α_p is the magnet pole arc to pole pitch ratio.

The comparison between the analytical and numerical/FEM results indicates good agreement (Fig. 3-2). The fringing field which occurs in the FEM result is due to the presence of stator slots, which the analytical model ignores. There is a discrepancy in the position of the air gap flux density curves. This is due to a difference in the starting rotor location of the calculation, and will not affect the average values of torque, power and efficiency computed from the numerical model. The positions have been adjusted for alignment to compare values.

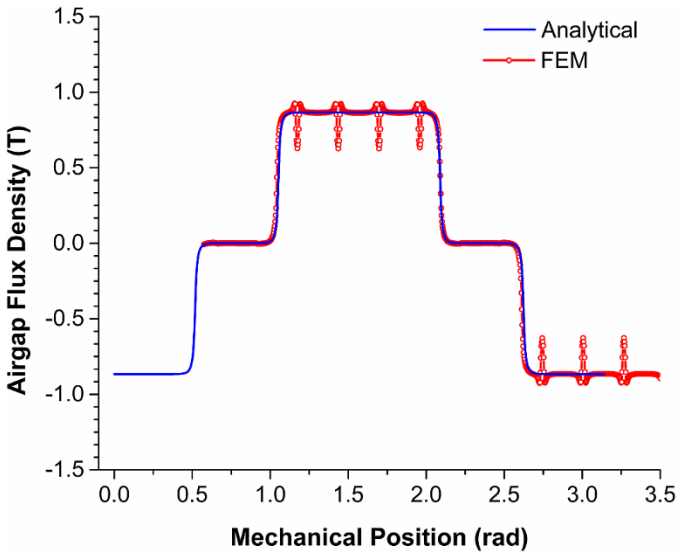

Figure 3-2. Analytical and FEM airgap flux density of a 10 MW PMG.

3.3.3 Determination of Operating Point

To find the operating point, first FEM was used to calculate the magnetic flux density and magnetic field distribution of the permanent magnets in Cases 1 to 3 for purposes of comparison; the finite element package MagNet™ by Infolytica Corporation was employed. H-adaption was used to refine the coarsest 5% of elements in the model using a tolerance of 0.5%. 2D static fields were calculated. The magnetic flux density B and magnetic field H were sampled at 1,000 points across each permanent magnet (4 poles in each generator). An average value was used for B_m and H_m in the analytical calculation of the permeance coefficient PC as described by equation (12) [53]. Equation (13) was used to determine the magnetic flux density and magnetic field of the permanent magnet. This relationship has been derived by Hendershot and Miller [53].

$$PC = B_m / (\mu_0 |H_m|) \tag{12}$$

$$B_m = B_r + \mu_0 \mu_{rec} H_m = PC \times B_r / (\mu_{rec} + PC) \tag{13}$$

where B_m and H_m are the magnetic flux density and magnetic field of the permanent magnet.

3.3.4 Magnetic Flux Distribution

The instantaneous magnetic field for Cases 1 to 3 were simulated by finite element methods using MotorSolve™ by Infolytica Corporation. The magnetic flux density distribution throughout the rotor and stator and over the rotor surface was calculated. The magnetic loading was calculated by averaging the instantaneous magnetic flux density over the rotor surface.

3.3.5 Loss Mechanisms

Ideally negligible eddy-current loss should occur in the rotor or magnets, but eddy-current loss exists due to imperfections or non-synchronous operation [15]. Hysteresis loss is anticipated in the rotor and stator yokes. 2D steady-state operation of Case 1 and Case 3 was simulated by finite element methods using MagNet™ by Infolytica Corporation. Friction and windage losses were not considered as the mechanical and thermal performance were not taken into account in the FEM. The contributions to core loss in the rotor, time averaged hysteresis and eddy current losses, were quantified as a function of generator radius and compared for both PMGs. The time averaged ohmic loss in the windings were also determined and compared. These comparisons serve to understand the implications of the changes in magnetic properties of the theoretical permanent magnet discussed in this paper.

3.4 Results & Discussion

3.4.1 Variation of Energy Product

For the 3.5 kW design, the "grade" of NdFeB magnet was varied (i.e. the properties were altered for the purpose of the calculations) in order to understand the impact of the energy product on the performance of the generator. Four grades of NdFeB magnets were selected. For each increased grade, the remanence, coercivity and energy product of the permanent magnet increased as shown in Table 3-6. The output power of the generator increased linearly with energy product, assuming all other factors were held constant. This result was expected since more magnetic flux Φ is available to excite the stator windings, inducing more voltage in the armature.

From Fig. 3-3, it is evident that increased energy product also resulted in slightly decreased efficiency. This result is less intuitive, and perhaps even surprising. It is likely that for higher energy product, stray field losses increased. Without optimization of the geometry of the permanent magnets, the flux is not well focused. Therefore, variation of permanent magnet geometry or stator teeth geometry may reduce such losses. This is an important consideration if higher energy density permanent magnets are to be considered for future use. An important conclusion here is that there is a small tradeoff between efficiency and output power for increased energy product of the permanent magnets.

Table 3-6. Magnetic Properties of Various Grades of NdFeB Magnets.

	NdFeB 28/32	NdFeB 34/22	NdFeB 40/15	NdFeB 48/11
B_r (T)	1.08	1.19	1.29	1.39
H_c (A/m)	-815,539	-894,591	-971,014	-1,060,650
μ_r	1.05554	1.06427	1.05474	1.03967
$\lvert BH \rvert_{max}$ (kJ/m^3)	220.6	267.6	312.4	367.4

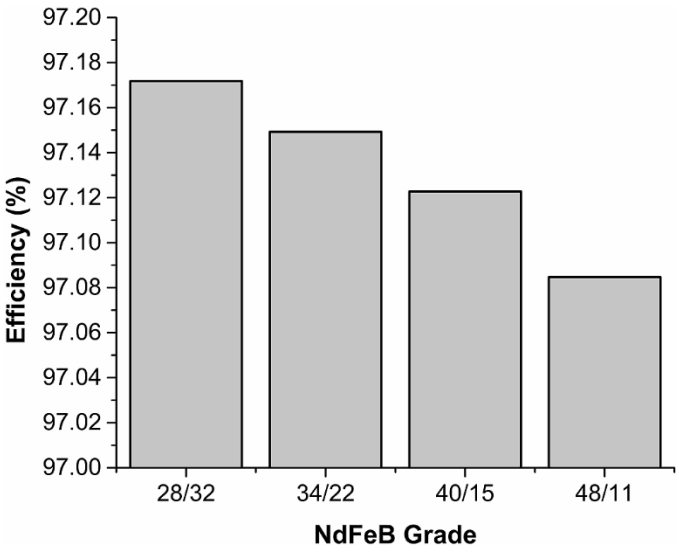

Figure 3-3. Calculated average efficiency of 3.5 kW PMG with varying permanent magnet grades.

3.4.2 Effects of Permanent Magnet Geometry

The effects of varying magnet angle and magnet thickness were also investigated. The magnet angle and magnet thickness were varied independently from their initial values of 60° and 5mm respectively; each parameter was incremented so that it resulted in an equal change in volume.

Output power was observed to increase with magnet volume in general. This result is again intuitive. For larger permanent magnet volume, more flux is available for excitation of the stator windings. It is similar to the previous result in which more output power was produced by a higher energy product. In both cases, the strength of the flux source increased.

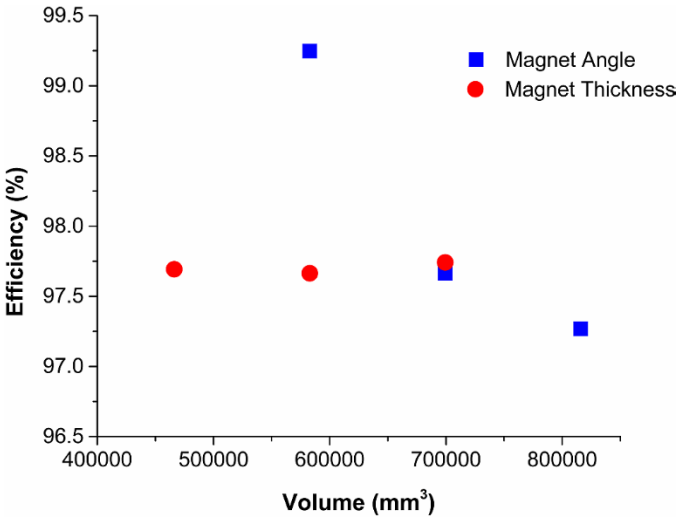

Figure 3-4. Calculated average efficiency of 3.5 kW PMG with varying permanent magnet volume by change in magnet thickness and change in magnet angle.

The efficiency was observed to decrease linearly with an increase in magnet angle (Fig. 3-4). This is consistent with the previous results in which efficiency decreased due to higher energy product. However, a linear trend was not observed between efficiency and increased magnet thickness as demonstrated in Fig. 3-4. Thus, efficiency is not related linearly to change in permanent magnet volume in general. This suggests that the geometry of the permanent magnet also contributes in some way to the efficiency.

3.4.3 Operating Point of an Idealized Permanent Magnet

The operating point of the permanent magnets in Cases 1 to 3 (10 MW PMGs) was determined for comparison of the operating conditions and the practical energy product. The operating point of a permanent magnet is determined by the intersection of the demagnetization curve (or hysteresis curve in the second quadrant) and the load line (given by the geometry of the permanent magnet). As the variation of the magnetic flux density B is linear, or approximately linear, with magnetic field H for a NdFeB

permanent magnet in the second quadrant of hysteresis, a simple linear model for the demagnetization curve was used (Fig. 3-5a) and is given by equation (9).

The slope of the load line is given by the permeance coefficient PC, determined from equation (12). The product of the magnetic flux density and magnetic field at the operating point gives the energy product, $/BH/$. The maximum theoretical energy product is frequently cited as an important figure of merit by manufacturers; it is given by the operating point at which the area given by the product of magnetic flux density and magnetic field is maximized (Fig. 3-5a). However, in practice the load line usually will not give an operating point which maximizes this area, resulting in an energy product lower than the maximum theoretical energy product (Fig. 3-5b). For these reasons, it is the practical energy product at the operating point that is of interest.

It is evident from the comparison of the practical energy product of the two PMGs that the increase in energy product needed for future permanent magnetic materials in PMGs is very ambitious. Though the maximum energy product of an idealized permanent magnet in Case 3 is ~51% higher than that of the NdFeB 48/11 grade permanent magnets in Cases 1 and 2 (Table 3-7), the practical energy product of Case 3, given by the operating point, is ~167% higher than that of Cases 1 and 2 (Table 3-8). This is a value that will be difficult to achieve. Nevertheless this calculation shows some of the theoretical limitations.

Table 3-7. Comparison of permanent magnet material properties.

	H_c (MA/m)	B_r (T)	μ_r	$\|BH\|_{max}$ (kJ/m^3)
Idealized	-1.06	2.14	1.64	553.9
NdFeB 48/11	-1.06	1.39	1.04	367.4

Table 3-8. Comparison of the operating point and energy product of the permanent magnets in two 10 MW PMGs.

	Operating Point		*Energy Product*
	H (MA/m)	**B (T)**	**|BH| (kJ/m^3)**
Case 1	-0.172	1.037	177.79
Case 2	-0.175	1.029	180.19
Case 3	-0.322	1.478	474.77

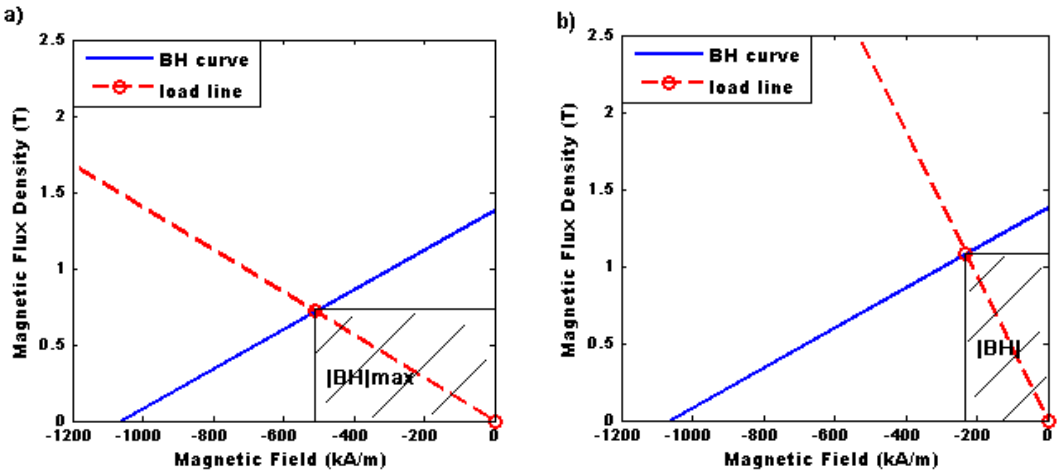

Figure 3-5. a) Energy product given by the optimal operating point for NdFeB 48/11, b) practical operating point and corresponding energy product given by the intersection of the demagnetization curve and load line for NdFeB 48/11 (Case 1).

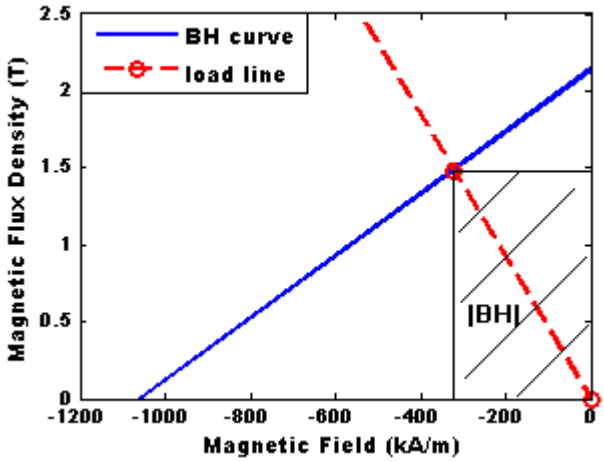

Figure 3-6. Operating point of idealized permanent magnet (Case 3) given by the intersection of the demagnetization curve and the load line.

This substantial difference in the practical energy product (in the idealized permanent magnets in Case 3 compared to that of the NdFeB 48/11 grade permanent magnets in

Cases 1 and 2) would be a result of an increase in the magnetic field strength and magnetic flux density of ~87% and ~43% respectively in the idealized permanent magnet if practically realized. This significant increase in energy product could be caused by a comparatively small increase in the remanence of the idealized permanent magnet of 35%. This demonstrates the potential of future development of permanent magnets in PMGs for large scale wind turbines; a large practical energy product could be achieved as a consequence of a comparatively small increase in the remanence. Finally, for the case of both PMGs, the operating point does not put the permanent magnets in danger of demagnetization.

3.4.4 Torque Generation/Analysis

As previously discussed, the operating point of a permanent magnet determines its practical energy product. This is an important consideration for PMG design. Higher energy product can increase the input torque provided by the permanent magnet by increasing the magnetic loading (average magnetic flux density over the rotor surface) B_a. This is evident from Fig. 3-5 and 3-6. There is an average increase in magnetic flux density throughout the rotor yoke in Case 3 of ~36% (Fig. 3-5a) compared to Cases 1 and 2 (Fig. 3-5b).

Since the magnetic flux source is stronger for Case 3, more magnetic flux Φ propagates through the rotor yoke and ultimately reaches the rotor surface. The magnetic loading B_a for Case 3 is ~41% higher than Cases 1 and 2 (Fig. 3-6). Recalling equations (1) and (2), it is clear that the increased magnetic flux density over the rotor surface accounts for the achievement of rated torque in Case 3. This analysis validates

our approach to size reduction of PMGs, which shows that the rated performance is achievable providing improved materials can be produced with the necessary magnetic properties.

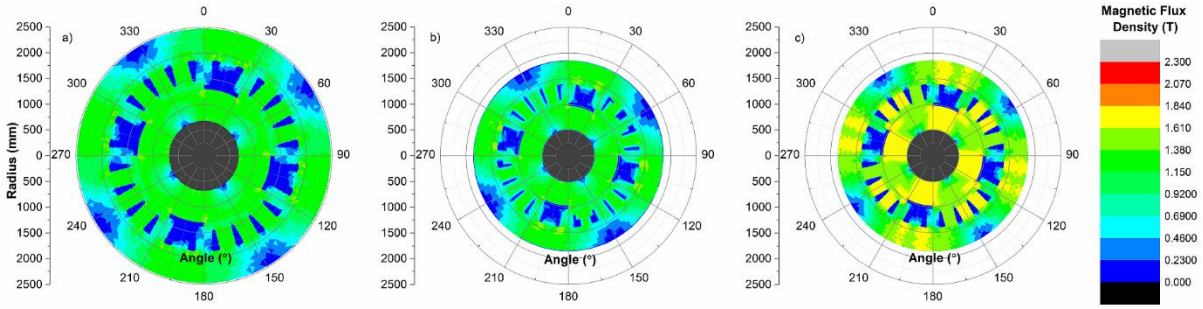

Figure 3-5. Comparison of magnetic flux density *B* in a) Case 1, b) Case 2, and c) Case 3.

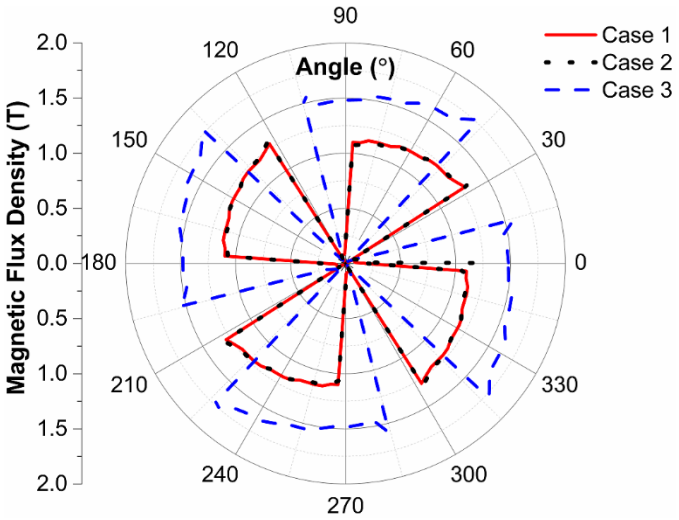

Figure 3-6. Comparison of the magnetic flux density over the rotor surface for two 10 MW PMGs.

3.4.5 Loss Mechanisms

PMGs are advantageous in wind turbine application due to their high efficiency at both full and partial load. Due to the increase in energy product of the idealized permanent magnet in Case 3, and therefore increased magnetic flux density B throughout the rotor as previously demonstrated in section 3.4.2, increased core loss

was expected in the rotor and stator compared to Case 1. Case 2 was not considered because it did not achieve rated performance. Though the efficiency of Case 3 remains high (97%), the losses of Case 3 should be considered carefully to understand if any tradeoffs exist between increased permanent magnet energy product and efficiency.

It is evident from Fig. 3-7 that, because of the permanent magnets, the eddy-current losses in the rotor and stator can be considered negligible when compared to the hysteresis loss. In general, the core losses in the stator decrease as one moves radially outward through the stator. This result is intuitive; the further away from the magnetic flux source, the lower the magnetic field and the lower the associated losses should be. The same trend is true in the rotor.

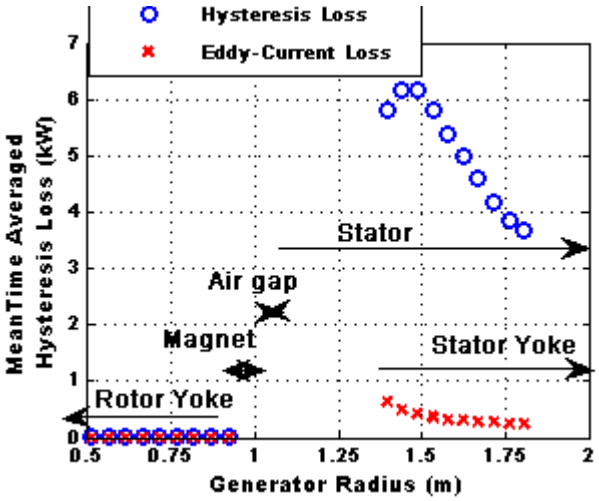

Figure 3-7. Mean time averaged hysteresis and eddy-current loss in Case 3.

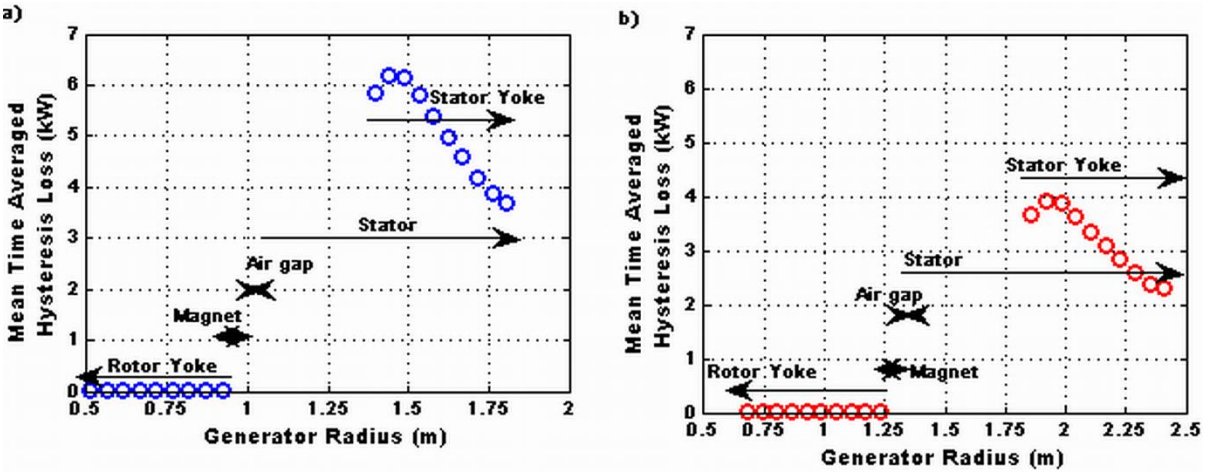

Figure 3-8. Comparison of a) mean time averaged hysteresis loss in Case 3 and b) mean time averaged hysteresis loss in Case 1.

An increase in core loss was found to occur in Case 3 compared to Case 1 (Fig. 3-8). Hysteresis and eddy-current losses in the rotor increased by a factor of 6.6 and 9.9 respectively in Case 3 compared to that of Case 1. In the stator the increased loss was less substantial; the hysteresis and eddy-current losses increased by a factor of 1.7 and 1.9 respectively. Classically, both hysteresis and eddy-current losses should increase with amplitude of the magnetic flux density in a material given by the Steinmetz equation [14]. The Steinmetz equation is a set of empirical formulas used to predict core or Fe loss.

$$W_h = C_h B_{pk}^n \tag{14}$$

$$W_e = C_e B_{pk}^2 f^2 \tag{15}$$

where C_h is the hysteresis loss coefficient, B_{pk} is the peak magnetic flux density, n is a material dependent parameter varying between 1.2 to 2.2, C_e is the eddy-current loss coefficient and f is the frequency [14].

In Case 3, the presence of a stronger magnetic flux source increases the magnetic flux density throughout the electrical steel of the rotor and stator yoke as demonstrated in the section 3.4.2. Therefore, the peak magnetic flux density in the electric steel of the rotor and stator yoke will also increase, contributing to an increase in core losses as described by the direct dependence on peak magnetic flux density in equations (14) and (15). The eddy-current losses were found to increase more than hysteresis loss as a result of this increase in the peak magnetic flux density in the electrical steel. It is logical to conclude that the material dependent exponent n must lie in the lower bounds of the range given, which would give the eddy-current loss a stronger dependence on the peak magnetic flux density, accounting for the simulated results.

Additionally, the ohmic loss in Case 3 increased by 77.6% compared to Case 1 (Table 3-8). The increase in ohmic loss is easily accounted for. The PMGs discussed have equivalent current flowing through the Cu windings in the stator. However, the conductor area of the windings in Case 3 is 56% smaller than that of Case 1. Thus, the same current is flowing through a smaller area, which will inevitably lead to increased resistance and therefore increased heating of the windings and, consequently, more ohmic loss.

Table 3-8. Comparison of ohmic loss in Case 1 and Case 3.

	Time Averaged Ohmic Losses (Ω)	
	Case 1	**Case 3**
Phase A Coils	6.64	11.8
Phase B Coils	20.7	36.7
Phase C Coils	6.64	11.8

Future design of PMGs employing permanent magnets with higher energy products should give careful consideration to the design of the rotor and stator in PMGs. Specific

attention should be given to the thermal losses in the stator. Though higher energy products can increase input torque and output power in PMGs, increased core and ohmic losses need to be taken into account and minimized if possible to prevent the necessity of additional cooling of the PMG. Furthermore, this substantiates the previous finding that the increasing the energy product of the permanent magnet results in a small decrease in efficiency. However, it is also important to note that the efficiency of Case 3, while lower than Case 1, did not decrease significantly.

3.4.6 Sizing Requirement Investigation

The average input and output power, torque and efficiency of the three PMG cases were compared to determine whether or not the performance was maintained for the 10 MW PMG of reduced size and idealized permanent magnets. Case 1 and 3 should theoretically be able to provide the same rated torque with sufficient rotor volume and magnetic loading respectively. From Fig. 3-9 and 3-10, the reduction in average output power and torque in Case 2 (compared to Case 1) demonstrates the principle of the sizing requirements for PMGs described by equation (2). For Case 2, the PMG volume was insufficient to achieved rated torque or power. It is apparent from Fig. 3-9 and 3-10a that rated power and rated torque were achieved for both Cases 1 and 3. In Case 3, the increased energy product of the idealized permeant magnet was able to compensate for the lack of torque provided by the rotor volume.

The results suggest that ideally the permanent magnetic material would allow for a reduction in the outer diameter and axial length of 25%, translating to a reduction in

rotor volume of 58%. It is also important to note that high efficiency of the PMG was maintained for reduced dimensions and increased energy product as shown in Fig. 3-10b.

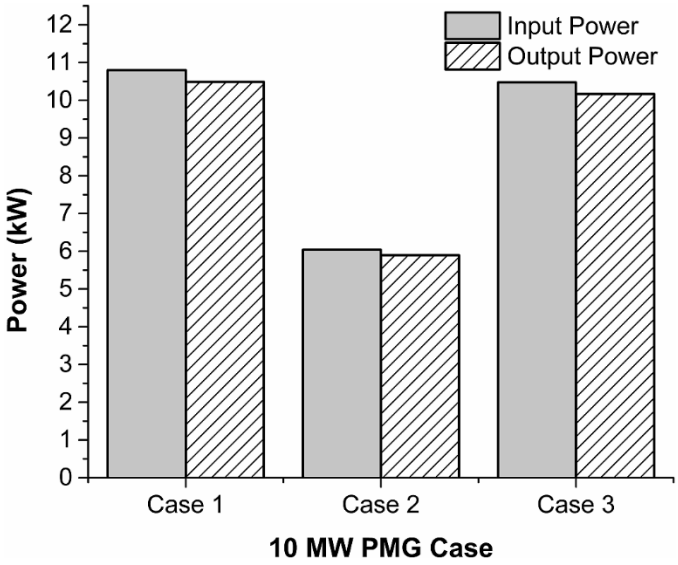

Figure 3-9. Comparison of the average input and output power of 10 MW PMGs.

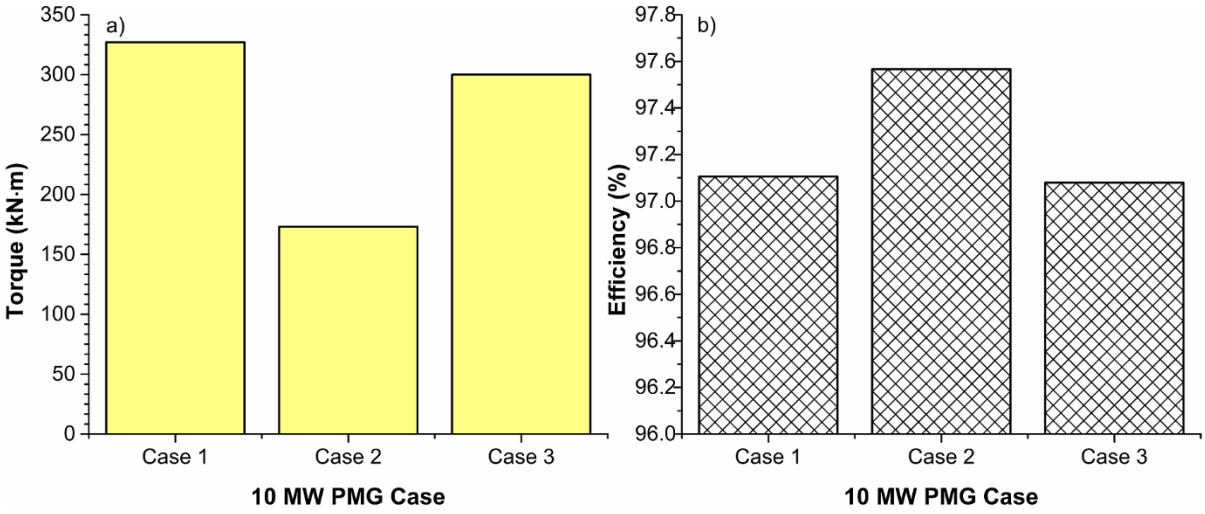

Figure 3-10. Average a) torque and b) efficiency for 10 MW PMGs.

3.5 Conclusions

A 10 MW PMG was designed by the simple process of scaling a 3.5 kW PMG. The effects of varying design parameters such as permanent magnet volume, geometry and energy product were studied. Efficiency of PMGs seem to be dependent on the volume as well as the geometry of the permanent magnets. It was noticeable that a small, but unexpected, tradeoff exists between output power and efficiency when increasing the energy product of the permanent magnet for a given PMG design.

Through investigation of the permanent magnets in a 10 MW PMG with design innovation, we validated our approach to size reduction of PMGs. In the case of the 10 MW PMG design, the change in the operating point of the idealized permanent magnets provided an increase in the energy product of 167% compared to NdFeB 48/11. This increased the magnetic flux density over the rotor surface by 41% and achieve rated torque. The core and ohmic losses were found to increase slightly as a result of the magnetic properties of the idealized permanent magnet; however, average efficiency for this 10 MW PMG was not sacrificed despite these losses. Improvements in the properties of permanent magnet materials such as the idealized permanent magnet discussed in this chapter could have significant implications for size reduction of PMGs for large scale wind turbines.

The implications of increasing the energy product of permanent magnets in PMGs for large scale wind turbines has been discussed. The idealized permanent magnet investigated in this paper had increased remanence, and consequently energy product, compared to NdFeB 48/11. However, application of such findings is contingent on the discovery of new permanent magnet materials. Thus, other techniques should be

investigated to increase the magnetic loading. Magnetic flux focusing techniques are investigated in Chapters 4 and 5 as a means to increase magnetic loading and achieve significant size reduction without the need for the development of new permanent magnetic materials.

CHAPTER 4. HALBACH CYLINDER ROTOR APPLICATIONS

4.1 Introduction

In the previous Chapter, it was determined that significant increase in the energy product of permanent magnets is required to allow for 25% reduction in the outer diameter and stack length of a 3.5 kW permanent magnet generator (PMG). The applicability of these results is dependent on the development of new, higher energy density permanent magnets. Alternatively, the magnetic flux can be concentrated over the rotor surface in order to increase the magnetic flux density and effectively create a higher energy density permanent magnet without the need for new permanent magnet materials. In this Chapter, Halbach arrays are investigated for purposes of increasing magnetic loading, or the average magnetic flux density over the rotor surface, to achieve two goals:

1. reduction of rotor volume
2. use of permanent magnets that do not contain rare earths

Currently, the achievable magnetic loading is limited by the energy product of the permanent magnet, meaning either a stronger permanent magnet is needed, or more magnet volume is needed to increase magnetic loading. The former is contingent on the development of new permanent magnet materials and the latter is undesirable as the components in the wind turbine nacelle should be as compact and lightweight as possible. In order to increase magnetic loading, magnetic flux can be concentrated over the rotor surface.

Halbach arrays can be employed to concentrate magnetic flux. A Halbach array is an arrangement of permanent magnets that focus magnetic flux to one side of the magnet

array, such as the magnetization scheme depicted in Fig. 4-1a. A Halbach array can be arranged in a cylinder, or Halbach cylinder (HC), for application in machine design by focusing magnetic flux inside or outside of the HC (Fig. 4-1b), thereby eliminating the need for a rotor back-iron and offering the benefit of sinusoidal airgap flux density and back-EMF [55], [56]. Halbach arrays and HCs are currently limited in commercial application, but do find use in niche applications. For a review of Halbach applications the reader is referred to reviews by Z. Q. Zhu and D. Howe [55], [56].

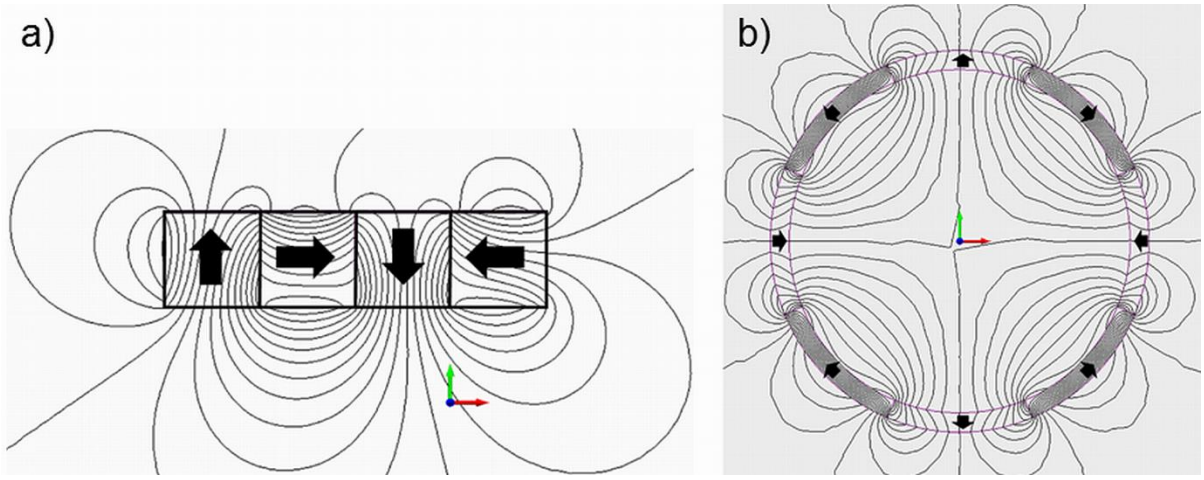

Figure 4-1. Magnetic flux profile of a) 4 segment Halbach array and b) 8 segment Halbach cylinder calculated with MagNet™ by Infolytica Corporation. Arrows indicate magnetization direction.

HCs have not yet been employed in PMGs in the wind industry, which is facing significant challenges in terms of gearbox reliability. The use of HCs may allow for wider deployment of direct-drive PMGs (DDPMGs) in the U.S. wind industry by concentrating magnetic flux over the rotor surface and allowing for reduction in rotor volume or the use of rare earth free permanent magnets. Thus, HCs are explored for direct-drive wind turbine application. The use of HCs is explored here to concentrate magnetic flux over the rotor surface and determine the maximum size reduction of the PMG possible for

the proposed HCs, and to see if the use of hard ferrite permanent magnets is possible.

In this Chapter, the magnetic flux focusing capabilities of HCs with varying number of magnetic poles as an isolated unit and as the rotor in a 3.5 kW PMG design are investigated for purposes of rotor volume reduction or use of rare earth free permanent magnets. The number of stator slots was also varied for each PMG design and the performance was investigated for each design variation. Finally, selected designs were scaled to 3 MW to investigate the performance in a commercial scale machine.

4.2 Methodology

A HC employing the magnetization scheme depicted in Fig. 4-1a was designed. The number of magnetic poles (one magnet segment per pole) was varied while maintaining a constant rotor volume, resulting in HCs with 4, 8, 16, 20, 28, 32, 40 and 44 poles. The magnet flux focusing ability of the HCs was investigated with finite element methods under static conditions, employing MagNet™ by Infolytica Corporation.

The HC was then employed as the rotor in a 3.5 kW Halbach PMG (HPMG), based on an existing generator design [48], to determine the magnetic flux density distribution in the HPMGs (Fig. 4-2). An outer rotor PMG with a motor aspect ratio (ratio of stack length to outer diameter) of 1/3 was selected to allow for reduced stack length, contributing to reduction in the rotor volume of the PMG (Table 4-1). NdFeB 32/31 permanent magnets (energy product of 256 kJ/m^3 at 20°C) were selected. The stator slot number was varied for each HPMG

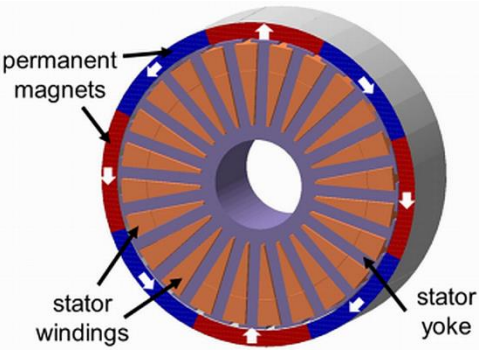

Figure 4-2. HPMG topology.

design; the slot-to-pole ratio plays an important role in the efficiency of the magnetic flux path between the rotor and stator.

Table 4-1. 3.5 kW HPMG design specifications.

Specification	Value
Rated Power (kW)	3.5
Rated Torque (Nm)	100
Rated Speed (rpm)	333
Outer Diameter (mm)	300
Stack Length (mm)	100

The torque, input and output power, magnetic loading, airgap flux density, and cogging torque (or torque ripple) of the HPMGs were calculated as function of mechanical position in MotorSolve^{TM} by Infolytica Corporation using 2D finite element analysis under steady-state conditions at rated speed, and compared to evaluate the potential for size reduction or use of rare earth free permanent magnets. The advance angle was set to 180° to simulate generator operation at rated current (21.5 A) and rated speed (333 rpm). 24 sample points, 5 skew samples, and a harmonic amplitude threshold of $1x10^{-6}$ were used with the best periodicity possible. Cogging torque was investigated because it should be minimized for wind turbine application; fluctuations in the torque, or torque ripple, result in voltage ripple. In wind turbine application, voltage ripple is undesirable due to its negative impact on the quality of voltage transferred to the grid. In the analysis, the torque, input power and output power were averaged over the position. Efficiency was calculated simply by dividing the output power by the input power.

Designs that achieved high magnetic loading and consequently high torque and output power above the rated values were identified. First, the potential reduction of the

outer diameter and axial length were calculated. The HPMGs were then reduced in size and their performance was investigated by employing the same finite element conditions described above. Second, but separately, ceramic 11 (C11), a strontium iron oxide, hard ferrite permanent magnet (containing no rare earths), was substituted as the permanent magnet material in the HPMGs with all other design factors remaining constant including the rotor volume. C11 permanent magnets were selected as the rare earth free permanent magnet because it has one of the highest energy products among ceramic permanent magnets (Table 4-2), 32.9 kJ/m^3 at 20°C, with a remanence of 0.42 T and a coercivity of 313 kA/m at 20˚C [57].

Table 4-2. Permanent magnet properties.

	B_r (kG)	H_c (kOe)	BH_{max} (MGOe)
C11	4.3	3.94	4.1
NdFeB 32/31	11.7	11	32

Finite element methods were also employed to determine the time-averaged hysteresis and eddy-current losses in each conducting component (stator windings and yoke) with 2D steady-state motion analysis in MagNet by Infolytica Corporation™. Instantaneous windage losses were determined in MotorSolve™. Stray losses and thermal effects are ignored in these calculations.

Finally, for each study, selected designs were scaled to 3 MW to investigate the performance in a commercial scale machine, again employing the same finite element conditions described above. It should be noted that the construction and assembly of the designs have not been considered to allow for an investigation of the theoretical limitations on achievable size reduction.

4.3 Results

4.3.1 HC Flux Density

The magnetic flux density produced by 8 HCs with 4, 8, 16, 20, 28, 32, 40 and 44 segments and NdFeB permanent magnets was investigated. The average magnetic flux density over the inner radius of the HC (135mm) was calculated (Fig. 4-3), which corresponds to the rotor surface in the HPMG. With the exception of the 4 segment HC, the number of poles had little impact on the average magnetic flux density achieved at the inner radius of the HC. The 4 segment HC did not efficiently focus the magnetic flux over its inner radius, with more than half of the magnetic flux distributed outside the HC (Fig. 4-1). This accounts for its comparatively low achievement of magnetic flux density over its inner radius. While the 8 segment HC achieved the highest magnetic flux density over its inner radius, varying the number of magnet segments between 8 and 44 had little effect on how efficiently the magnetic flux was focused over the inner radius of the HC.

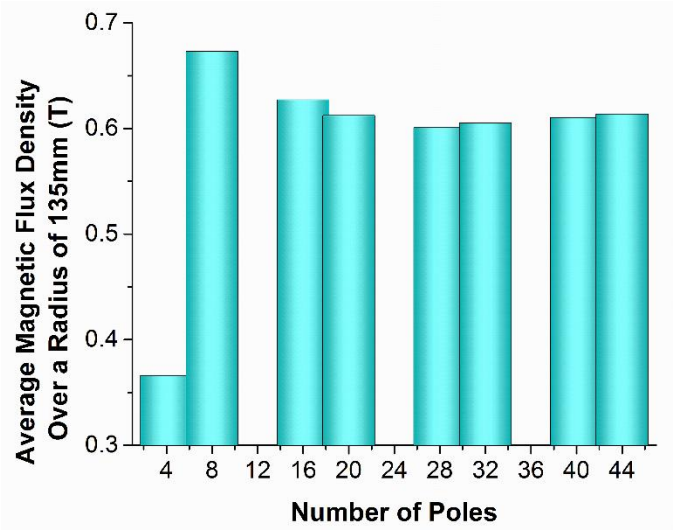

Figure 4-3. Comparison of average magnetic flux density over inner radius of HCs with varying number of poles and NdFeB permanent magnets.

4.3.2 HPMG Flux Density

The magnetic loading, or average magnetic flux density over the rotor surface, B_a of each HPMG was determined, excluding the 4 and 8 pole HPMGs since these designs did not achieve rated torque or power (see section 4.3.3 HPMG Performance). It is evident from Fig. 4-4a that varying the number of slots, for constant pole number, had little effect on the average magnetic flux density achieved over the rotor surface. In contrast, we observed a direct relationship between an increase in pole number, for constant slot number, and the magnetic loading. This differs from the case of the isolated HC (Fig. 4-3), where pole number had little impact on concentrating magnetic flux over the rotor surface. This difference is due to the path provided for the magnetic flux by the stator yoke in the HPMG.

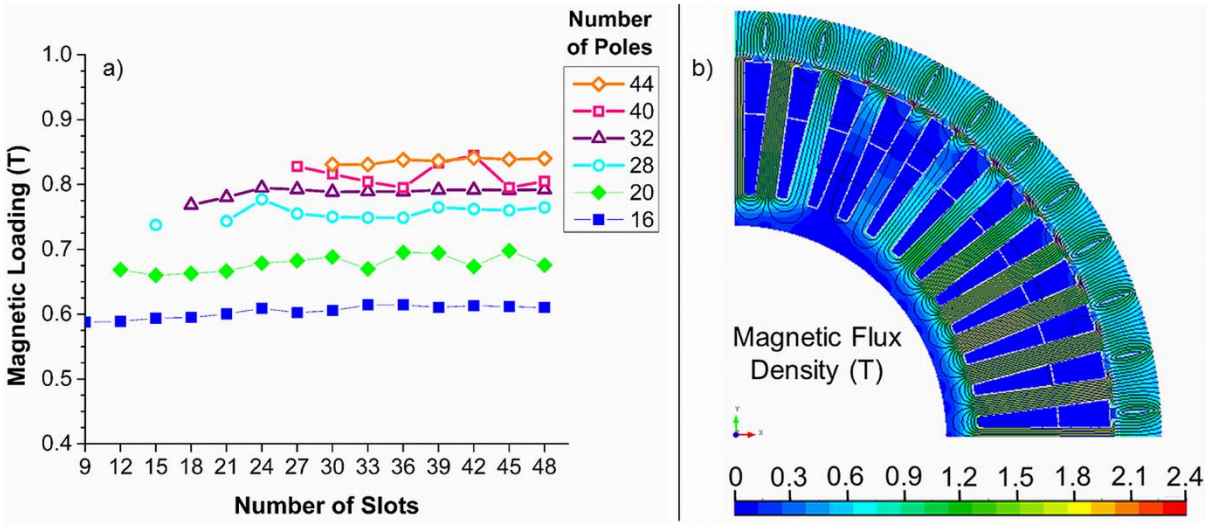

Figure 4-4. a) Average magnetic flux density over rotor surface achieved in 3.5 kW HPMGs with NdFeB permanent magnets and varying slot-to-pole ratio and b) magnetic flux density distribution in a 3.5 kW HPMG with NdFeB permanent magnets, 44 poles and 48 slots. MotorSolve$_{TM}$ by Infolytica Corporation was used for calculating the magnetic flux density distribution.

4.3.3 HPMG Performance

The performance of 3.5 kW outer rotor HPMGs with NdFeB permanent magnets and varying pole and slot number, rated at 100 Nm, was investigated. The metrics for performance were defined as cogging torque as well as average torque, output power and efficiency. It was found that for the 4 and 8 pole HCs rated torque and power were not achieved for any slot-to-pole ratio (Fig. 4-5). It was observed that for constant pole number, an increased number of slots, or higher slot-to-pole ratio, resulted in an increase in the average torque and output power achieved by the HPMG. Additionally, it was found that in general for a higher number of poles in the HC, higher torque and output power were achieved in the HPMG. The HPMG designs which achieved more than the rated power (3.5 kW) corresponded to those that achieved more than rated torque. Furthermore these designs all achieved average efficiency greater than 90% at rated speed.

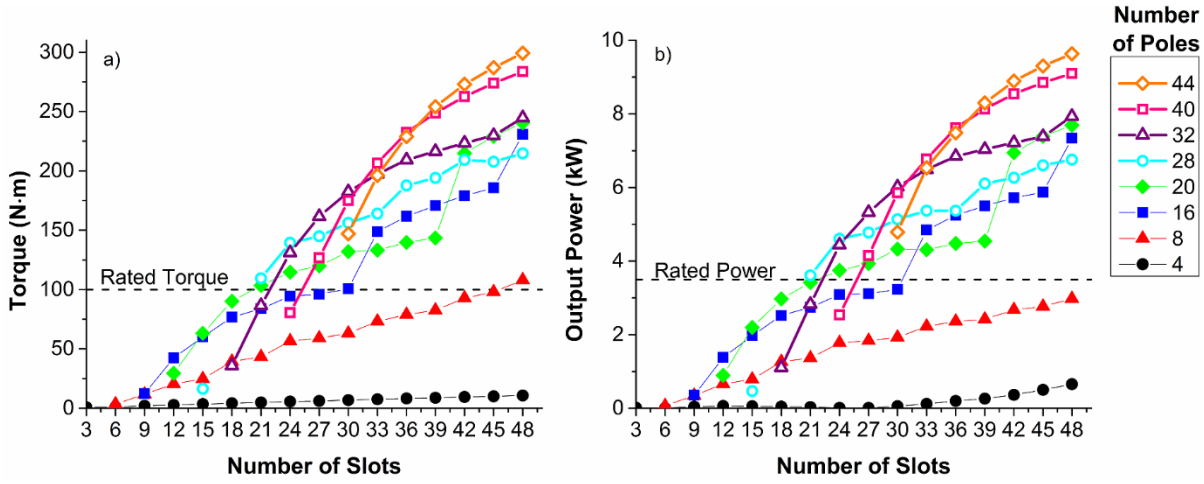

Figure 4-5. Average a) torque and b) output power achieved in 3.5 kW HPMGs with NdFeB permanent magnets and varying slot-to-pole ratio.

The airgap flux density was calculated for each design condition. Significant variation in the airgap flux density can be seen for changing pole and slot number (Fig. 4-6). For constant pole number, an increase in the number of slots resulted in more fringing present in the airgap flux density curve. Slotting is known to cause this fringing effect [52]. For lower slot number, the airgap flux density resembles that of a Halbach cylinder with 2 magnet segments per pole, as expected [55]. However for higher slot number, the airgap flux density resembles that of a radially magnetized HC [55]. Furthermore, for constant slot number, the fringing due to slotting was most prominent for low pole number than for high pole number in general (Fig. 4-7).

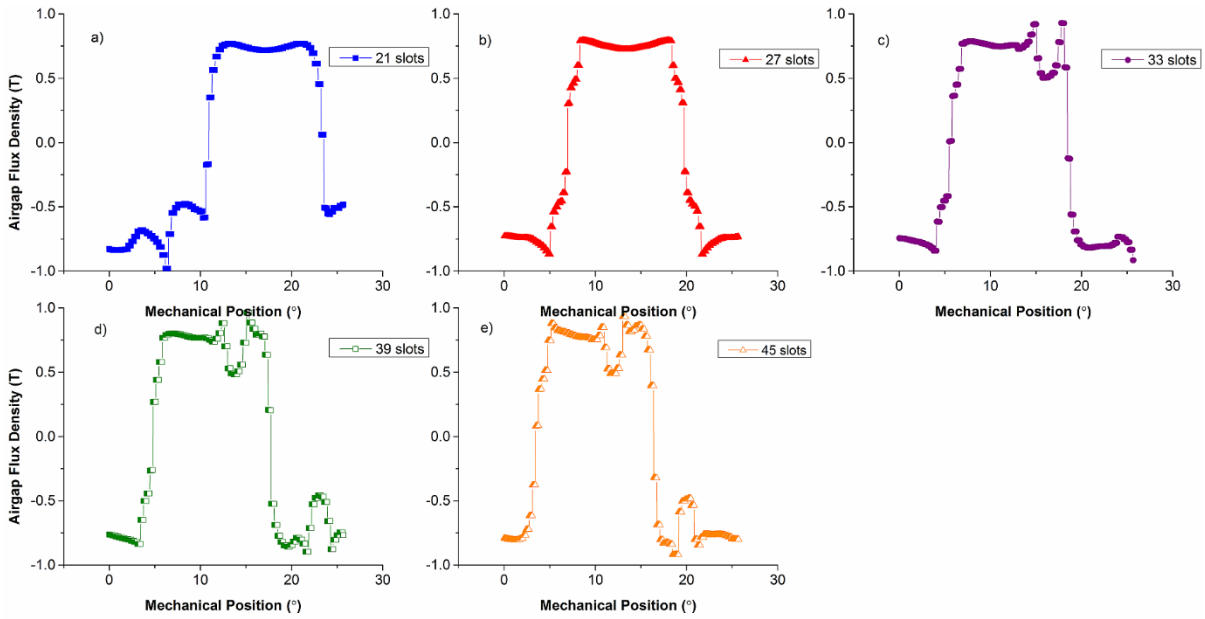

Figure 4-6. Calculated airgap flux density of 3.5 kW HPMGs with NdFeB permanent magnets, 28 slots and a) 21 slots, b) 27 slots, c) 33 slots, d) 39 slots, and e) 45 slots.

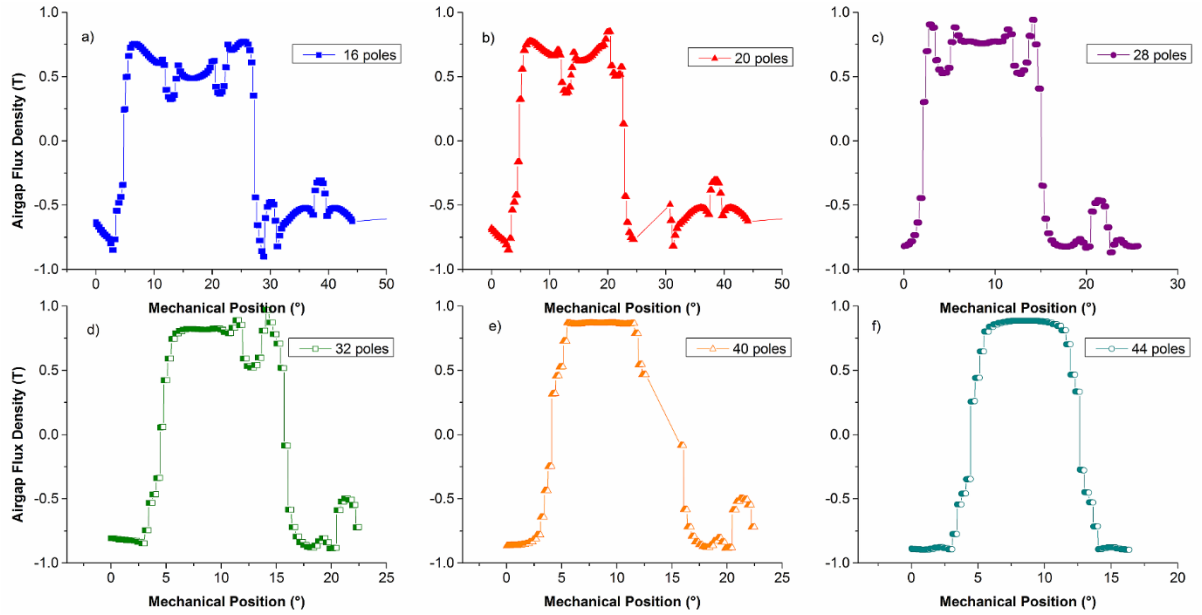

Figure 4-7. Calculated airgap flux density of 3.5 kW HPMGs with NdFeB permanent magnets, 42 slots and a) 16 poles, b) 20 poles, c) 28 poles, d) 32 poles, e) 40 poles, and f) 44 poles.

There was no linear trend observed between cogging torque and variation of slot or pole number. Slot-to-pole ratio appeared to have some influence on the cogging torque. For the design variations associated with each pole number, a slot-to-pole ratio of 0.75 resulted in maximum cogging torque with amplitudes varying from 75.6 to 89.0 Nm (Table 4-3). A slot-to-pole ratio of 1.5 also resulted in very large cogging torque. Cogging torque was not minimized for any one slot-to-pole ratio, but cogging torque with amplitude of less than 0.5 Nm was achieved for many cases, giving a wide range of design choices (Table 4-3).

Table 4-3. Amplitude of cogging torque in 3.5 kW HPMGs with NdFeB permanent magnets and varying slot-to-pole ratio.

No. of Slots	Cogging Torque (Nm)					
9	2.839					
12	75.632	42.168				
15	1.097	86.868	0.433			
18	7.154	2.757	0.751	2.705		
21	0.784	0.155	88.985	0.057	0.185	
24	61.102	19.965	1.974	88.708	54.969	
27	0.390	0.179	0.091	0.138	0.164	
30	2.379	66.883	0.322	0.147	84.182	0.147
33	0.087	0.272	0.188	0.163	0.319	80.199
36	17.584	7.381	5.632	2.910	0.277	1.387
39	0.080	0.138	0.061	0.246	0.198	0.042
42	1.088	0.411	71.908	0.087	0.183	0.251
45	0.165	15.366	0.034	0.065	1.743	0.448
48	58.501	2.588	2.462	77.134	4.870	0.449
No. of Poles	**16**	**20**	**28**	**32**	**40**	**44**

4.3.4 Size Reduction

For the HPMG designs that achieved torque and power exceeding the rated values and high magnetic loading, reduction in the rotor volume is possible. It was found that the range of designs investigated allows for reduction in the outer diameter and axial length of the 3.5 kW HPMGs of up to 35%.

The performance of the 3.5 kW HPMGs with NdFeB permanent magnets of reduced dimensions were compared to that of a 3.5 kW PMG with surface mounted NdFeB permanent magnets based on a design by Abdel-Khalik *et al*. [48]. Rated torque and power are achieved in the HPMGs of reduced size and compare favorably of the surface mounted PMG (Table 4-4). However, a trade-off does exist between achievable size reduction and efficiency.

Table 4-4. Comparison of performance of selected 3.5 kW HPMGs with NdFeB permanent magnets reduced in size with a surface mounted PMG (no size reduction).

	HPMG				Surface Mounted PMG
# Poles	20	28	32	44	20
# Slots	24	24	48	24	24
Outer Diameter mm)	255	225	215	195	300
Torque (Nm)	118.62	126.74	127.25	118.69	112.13
Output Power (kW)	3.89	4.14	3.52	3.16	3.68
Efficiency (%)	93.96	93.50	79.14	76.20	94.09
% Size Reduction	15	25	28	35	NA

These results demonstrate as proof of concept the ability to significantly reduce the size of a PMG through practically realizable techniques. The use of HCs as the rotor in a 3.5 kW outer rotor PMG allows for up to 35% reduction in the outer diameter of the rotor and the stack length. This translates up to reduction in the combined volume of the electrical steel (Si-Fe) in the rotor and stator yoke of up to 90% and reduction in the volume of Cu in the windings of up to 91% (Table 4-5).

Table 4-5. Comparison of estimated material volume in 3.5 kW HPMGs with NdFeB permanent magnets of reduced size with a surface mounted PMG design (no size reduction).

		Material Volume (cm^3)		
PMG	**% Size Reduction**	**NdFeB**	**Cu**	**Si-Fe**
20 poles (HPMG)	15	811	0.726	519
28 poles (HPMG)	25	556	0.499	169
32 poles (HPMG)	28	485	0.161	201
44 poles (HPMG)	35	361	0.108	152
Surface Mounted PMG	NA	141	1.179	1530

However, the required volume of NdFeB permanent magnets in the HCs is significantly increased compared to a conventional design. Therefore, a trade-off exists. HCs allow for reduced size and volume of the PMG, which reduces the amount of Si-Fe and Cu material used, as well as reduces the load imposed on the wind turbine tower by

the nacelle. However, this comes at the cost of increased NdFeB material use, which increases materials costs and dependence on imported rare earths. Also, any simplifications in manufacturing due to the reduction in size of the machine must also be considered against the increased complexity of manufacturing the HC.

4.3.5 Ceramic PMs

For the 3.5 kW HPMGs with NdFeB permanent magnets that achieved at least twice the value of rated torque (100 Nm) and power (Table 4-6), C11 permanent magnets were substituted as the permanent magnet material leaving all other design parameters constant. Almost all the HPMG designs with C11 permanent magnets achieved rated torque on average at rated speed (Fig. 4-8a) with the exception of three designs (32 poles and 45 slots, 40 poles and 39 slots, and 44 poles and 39 slots). However, only 3 HPMG with C11 permanent magnets designs achieved rated power on average at rated speed (Fig. 4-8b).

Table 4-6. 3.5 kW HPMGs with NdFeB 32/31 grade PMs which achieved twice (or more) the value of rated torque and power.

# Poles	# Slots	Torque (Nm)	Output Power (kW)	Input Power (kW)	Efficiency (%)	Magnetic Loading (T)
32	45	229.91	7.38	8.03	92.00	0.791
32	48	244.78	7.94	8.55	92.87	0.792
40	39	248.77	8.13	8.68	93.67	0.833
40	42	262.63	8.55	9.17	93.22	0.845
40	45	273.83	8.85	9.56	92.61	0.795
40	48	283.58	9.10	9.90	91.91	0.805
44	39	254.17	8.30	8.87	93.55	0.836
44	42	273.00	8.89	9.53	93.32	0.841
44	45	286.93	9.30	10.02	92.87	0.839
44	48	299.14	9.64	10.44	92.28	0.840

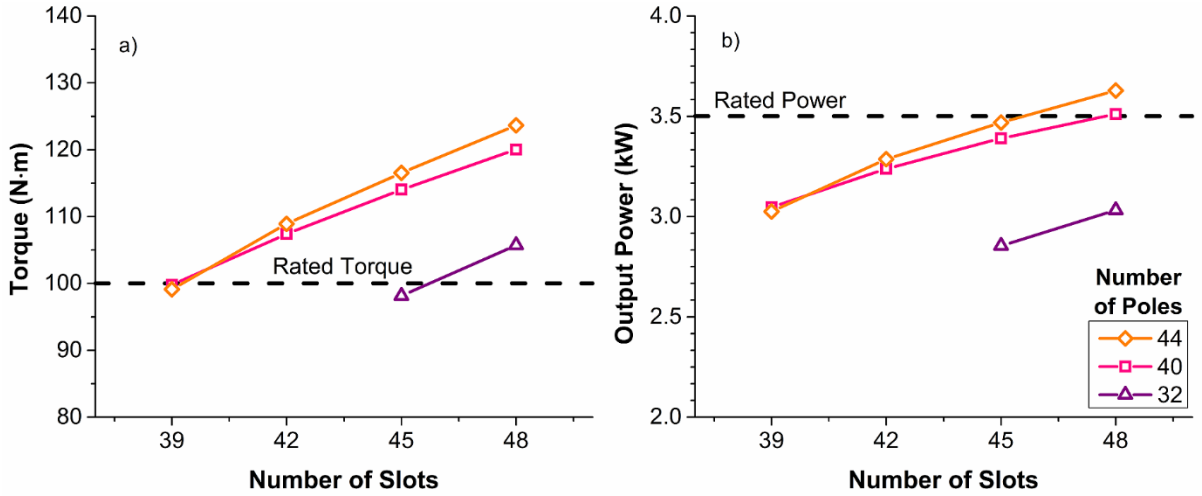

Figure 4-8. Average a) torque and b) output power achieved in 3.5 kW HPMGs with C11 permanent magnets and varying pole and slot number.

In the 3.5 kW HPMGs with C11 permanent magnets, it was observed that high pole and slot number contributed to achievement of higher torque and power (Fig. 4-8), agreeing with the previous results (section 4.3.3). However, for constant pole number, the slot-to-pole ratio did not significantly affect the magnetic loading achieved, with standard deviations of less than 1% (Fig. 4-9). This is also consistent with previous results (section 4.3.3).

The profile of airgap flux density of the HPMGs with C11 permanent magnets is consistent with the HPMGs with NdFeB permanent magnets (Fig. 4-10). From Fig. 4-11 it is apparent that for the C11 HPMGs, fringing was also more significant for higher slot number, though less amplified due to the high pole number.

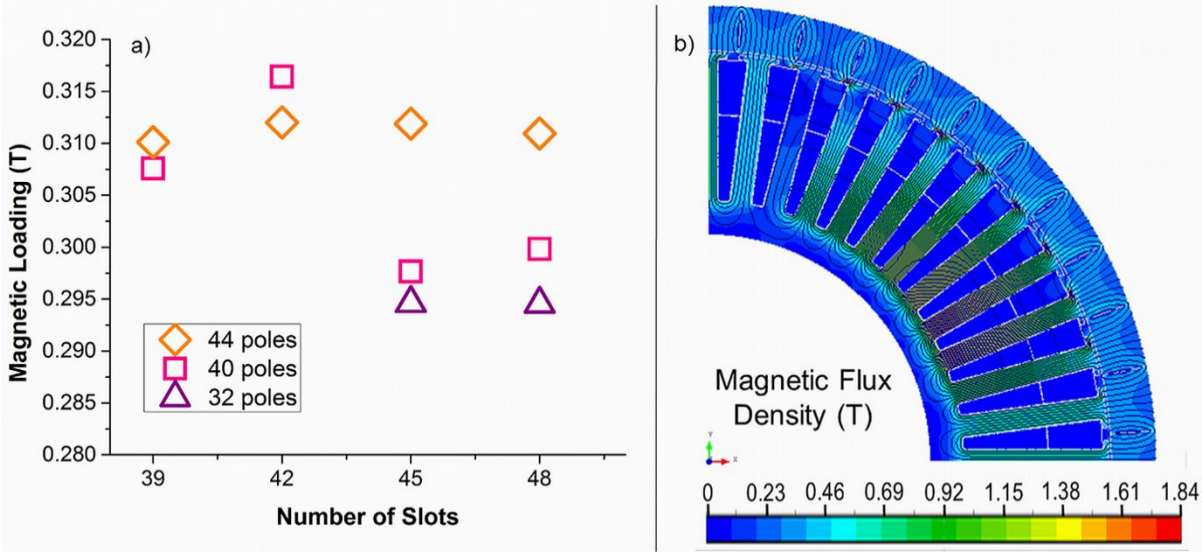

Figure 4-9. Magnetic loading of 3.5 kW HPMGs with C11 permanent magnets and varying slot and pole number (a) and magnetic flux density distribution in a 3.5 kW HPMG with C11 permanent magnets and 44 poles and 48 slots (b).

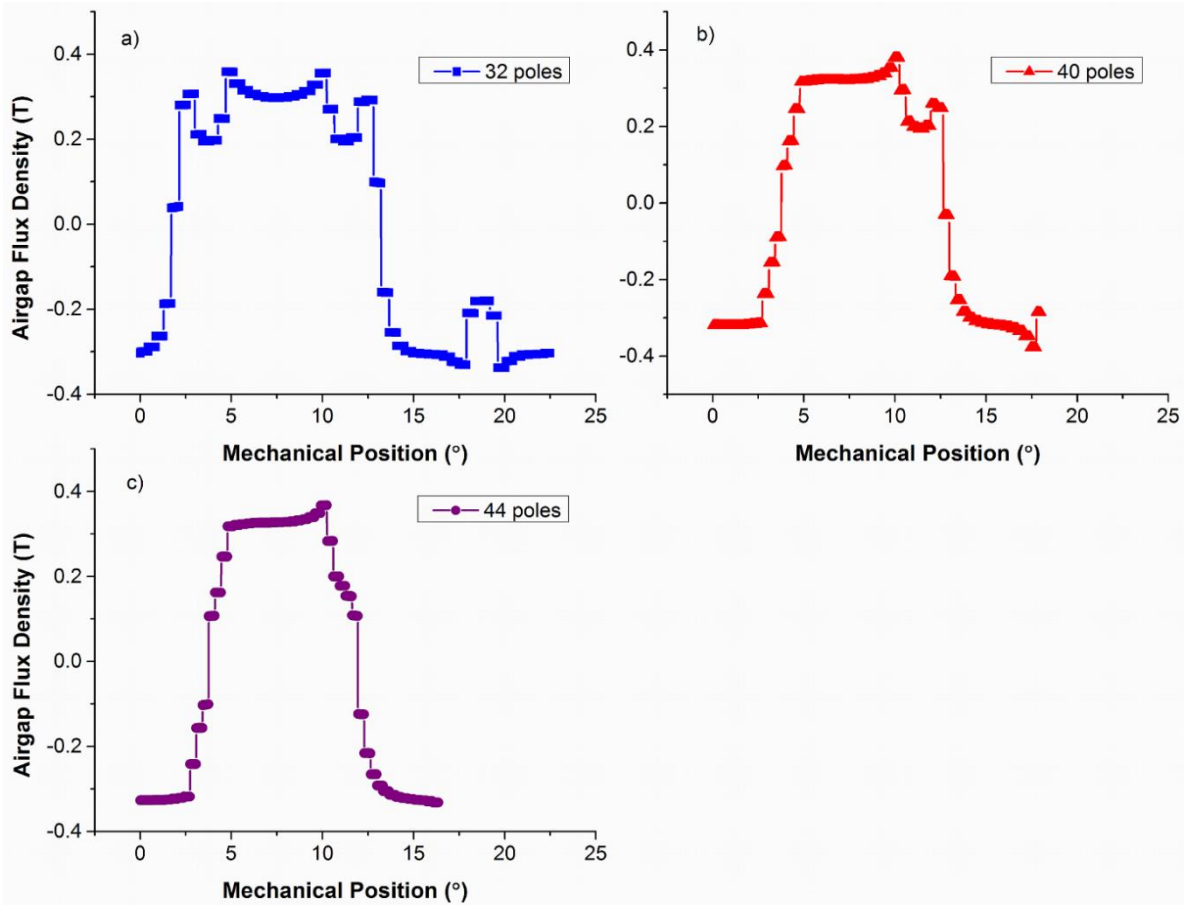

Figure 4-10. Airgap flux density of 3.5 kW HPMGs with C11 permanent magnets, 48 slots and a) 32 poles, 40 poles, and c) 44 poles.

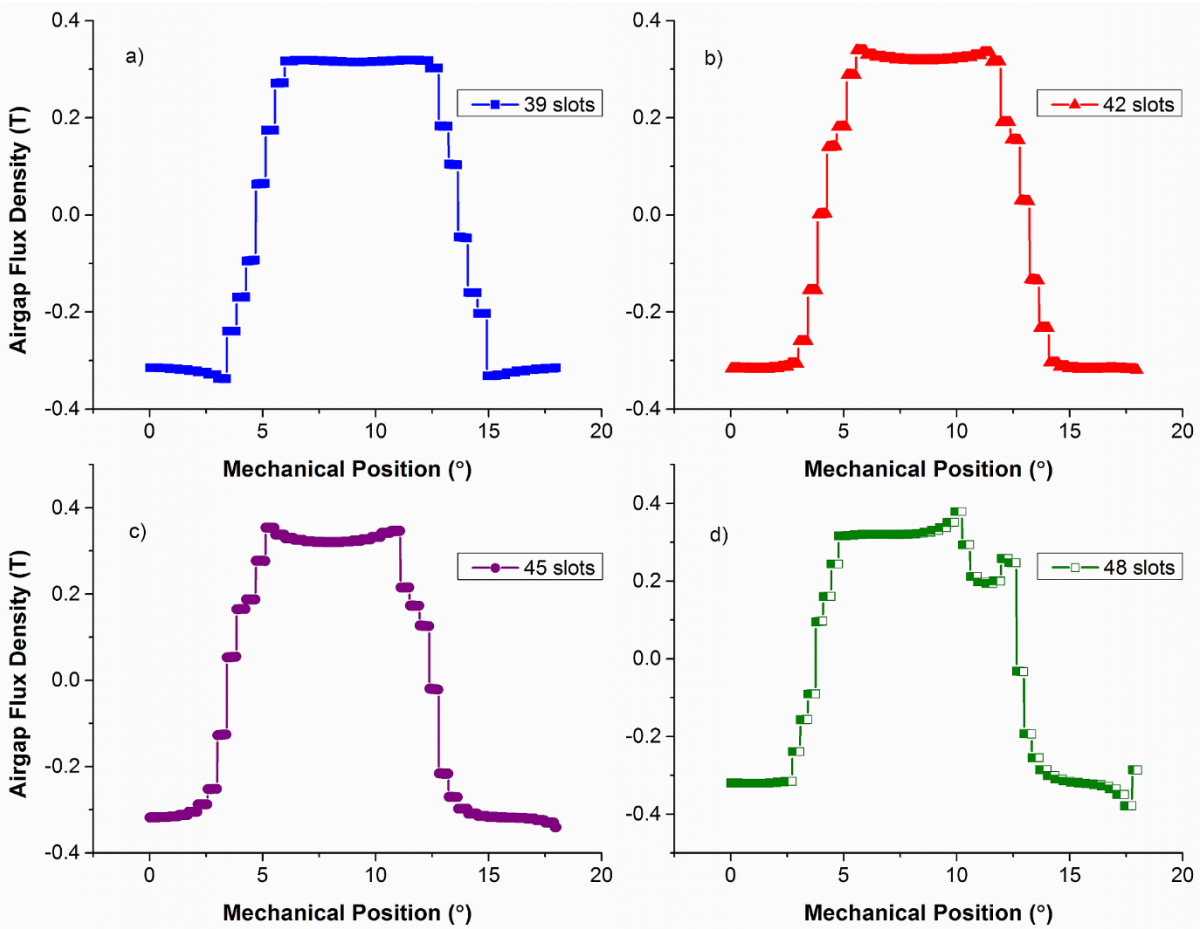

Figure 4-11. Airgap flux density of 3.5 kW HPMGs with C11 permanent magnets, 40 poles and a) 39 slots, b) 42 slots, c) 45 slots, and d) 48 slots.

The cogging torque of the HPMGs with C11 permanent magnets was found to be less than half a percent of rated torque with the exception of one machine (32 poles and 48 slots) as shown in Table 4-7. The periodicity and shape of the cogging torque was a function of the generator design, specifically the slot-to-pole ratio. However, the amplitude was directly related to the permanent magnet material. While the shape of the cogging torque was identical for the HPMGs regardless of permanent magnet material, the cogging torque of the NdFeB HPMGs was significantly higher than for the C11 HPMGs (Fig. 4-12). This is intuitive since the overall torque is reduced for the HPMGs

with C11 permanents compared to NdFeB permanent magnets due to the reduction of energy product and consequently magnetic loading.

Table 4-7. Cogging torque of 3.5 kW HPMGs with varying pole and slot number and permanent magnet material.

	Cogging Torque (Nm)	
Pole and slot configuration	**C11**	**NdFeB 32/31**
32 poles, 45 slots	0.0082	0.0651
32 poles, 48 slots	8.7857	77.1343
40 poles, 39 slots	0.0040	0.1980
40 poles, 42 slots	0.0240	0.1826
40 poles, 45 slots	0.0610	1.7432
40 poles, 48 slots	0.0294	4.8703
44 poles, 39 slots	0.0040	0.0416
44 poles, 42 slots	0.0240	0.2514
44 poles, 45 slots	0.0610	0.4478
44 poles, 48 slots	0.0294	0.4486

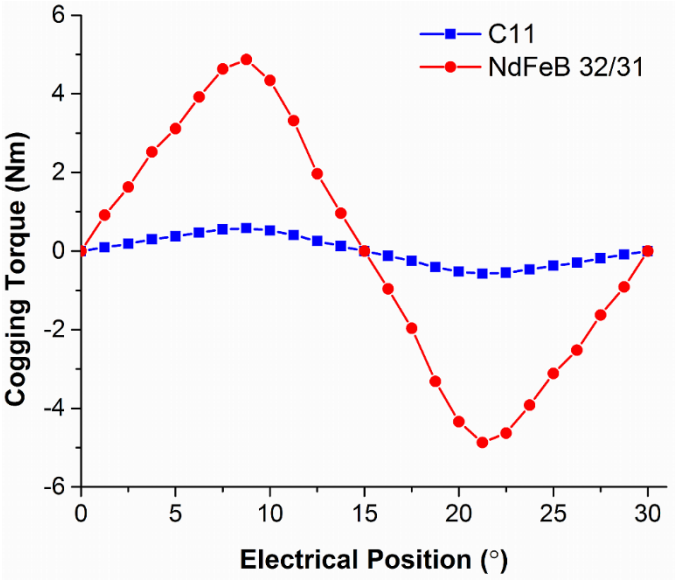

Figure 4-12. Comparison of cogging torque for a 3.5 kW HPMG with 40 poles, 38 slots, and varying permanent magnet material.

It was found that the efficiency of the 3.5 kW HPMGs at rated speed (333 rpm) was reduced to between 82 and 87% with the use of C11 permanent magnets, compared to

efficiencies between 91 and 93% for NdFeB permanent magnets (Table 4-8). The losses in the HPMGs for each permanent magnet material were explored. Machine losses include Joule or copper losses W_{Cu}, iron losses W_{Fe}, friction and windage losses W_{mech}, and stray losses W_{stray}

$$W_T = W_{Cu} + W_{Fe} + W_{mech} + W_{stray} \quad (16)$$

$$W_{Cu} = mI_{ph}^2 R_{ph} \quad (17)$$

$$W_{Fe} = W_h + W_e \quad (18)$$

where W_T is the total loss, m is the number of phases (3), I_{ph} is the RMS phase current, R_{ph} is the phase resistance, W_h is the hysteresis loss and W_e is the eddy-current loss [54].

Table 4-8. Average efficiency of 3.5 kW HPMGs at rated speed with varying pole and slot number and permanent magnet material.

	Average Efficiency (%)	
Pole and slot configuration	**C11**	**NdFeB 32/31**
32 poles, 45 slots	83.31	92.00
32 poles, 48 slots	82.15	92.87
40 poles, 39 slots	87.49	93.67
40 poles, 42 slots	86.38	93.22
40 poles, 45 slots	85.16	92.61
40 poles, 48 slots	83.81	91.91
44 poles, 39 slots	87.43	93.55
44 poles, 42 slots	86.45	93.32
44 poles, 45 slots	85.27	92.87
44 poles, 48 slots	84.07	92.28

The total losses were determined for each design variation from the difference between the input and output power. The time-averaged ohmic, hysteresis and eddy-

current losses were calculated as described in the methodology section. Copper losses are sometimes referred to as ohmic losses due to dependence on the resistance of the copper coils as shown in equation (17). Iron losses are composed of hysteresis and eddy-current losses as shown in the relationship in equation (18). Windage losses were calculated in MotorSolve and found to be on the order of 10^{-7} kW/mm^3 and thus were considered negligible. As described in the methodology section, friction and stray losses are ignored by the finite element calculations because no thermal analysis was performed and stray losses are generally negligible.

The percent of total losses due to iron losses decreased overall for the use of the C11 permanent magnets with a decrease in both hysteresis and eddy-current contributions (Fig. 4-13).

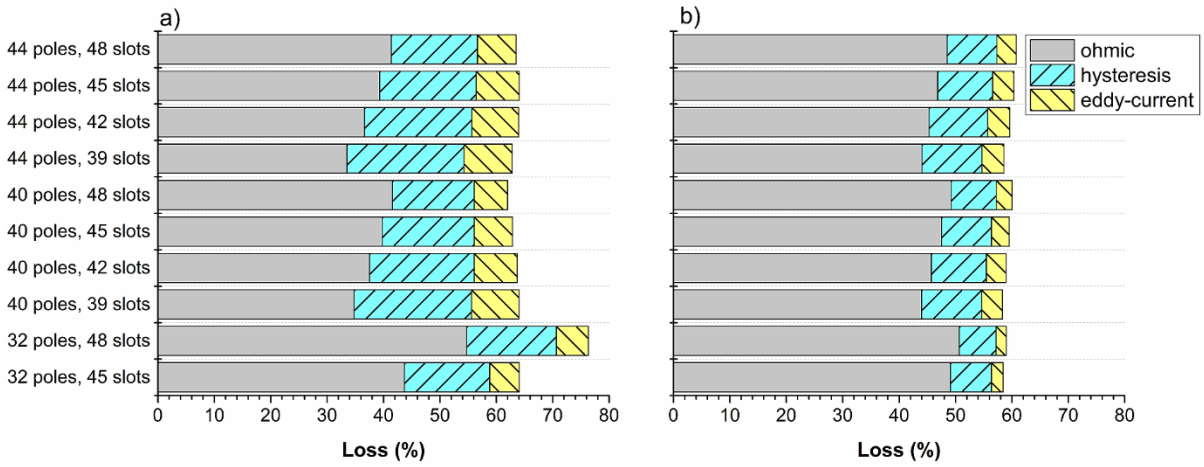

Figure 4-13. Calculated losses in terms of percent loss for 3.5 kW HPMGs with a) NdFeB permanent magnets and b) C11 permanent magnets.

This is explained by the dependence of hysteresis and eddy-current loss on the peak magnetic flux density, recalling the relationships in equation (14) and (15) respectively [54]. The peak magnetic flux density is higher for the use of NdFeB 32/31 permanent

magnets because of higher energy product and remanence than C11 permanent magnets.

$$W_h = C_h B_{pk}^n \tag{14}$$

$$W_e = C_e B_{pk}^2 f^2 \tag{15}$$

In terms of the percent of total losses, ohmic losses were increased slightly for the use of the C11 permanent magnets. However, it should be noted that the value of ohmic losses was equal for each HPMG design variation regardless of permanent magnet material due to the fact that the stator design was unchanged. Thus ohmic losses only accounted for a greater percentage of the total losses for the C11 HPMGs because the iron losses were reduced.

From Fig. 4-13, it is clear that the ohmic and iron losses do not account for 100% of the losses in the 3.5 kW HPMGs of either permanent magnetic material. In permanent magnet machines, Joule losses will not be purely resistive. Self and mutual inductance in the coils will add a reactive component to the windings impedance, likely accounting for the remaining losses.

The only variable design factor in each 3.5 kW HPMG design was the permanent magnetic material. Thus, the change in permanent magnetic material properties must be responsible for the reduction in efficiency in the HPMGs with C11 permanent magnets. To determine which property or properties were responsible for the reduction in efficiency, the energy product, remanence, coercivity and relative permeability of the NdFeB 32/31 permanent magnets were independently set to that of C11 and the torque,

input and output power were calculated with finite element methods using the same methods described in the methodology section.

The reduced coercivity of the C11 permanent magnets was ultimately found to account for the decreased efficiency of the 3.5 kW HPMGs with C11 permanent magnets. The difference in coercivity of the C11 permanent magnets accounts for the higher relative permeability of the C11 permanent magnets with respect to the NdFeB 32/31 permanent magnets. To substantiate this, the coercivity of the NdFeB 32/31 permanent magnets was varied in a 3.5 kW HPMG with 44 poles and 48 slots, while *all* other parameters were left constant. From Fig. 4-14 below it is clear that there is a direct relationship between a decrease in coercivity of the permanent magnet and the efficiency, explaining the reduced efficiency of the HPMGs with C11 permanent magnets.

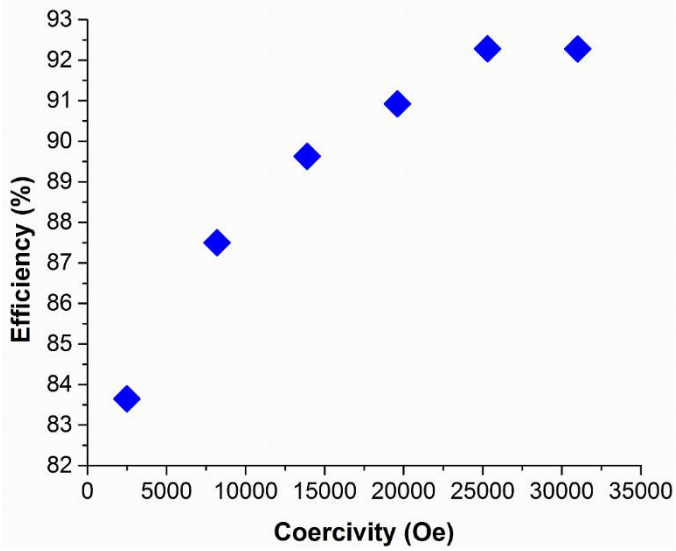

Figure 4-14. Variation of efficiency with coercivity of NdFeB 32/31 permanent magnets in a 3.5 kW HPMG with 44 poles and 48 slots.

4.3.6 3 MW HPMGs: Rotor Volume Reduction

The three 3.5 kW HPMG designs which achieved the greatest size reduction were scaled to 3 MW, a power rating on par with commercial generators in the U.S wind industry. HPMGs with 44 poles and 42, 45 and 48 slots were selected. Rated torque (85959.89 Nm) and power (3 MW) were achieved for all three designs on average (Fig. 4-15). Efficiency was increased for the scaled designs, ranging from 92 to 93% on average for rated speed, an improvement over the 3.5 kW HPMGs. It is well known that larger machines are more efficient than smaller machines. Additionally, for the 3 MW HPMGs investigated, higher slot number allowed for the greatest size reduction (Table 4-9), with outer diameters not exceeding 2.25 m.

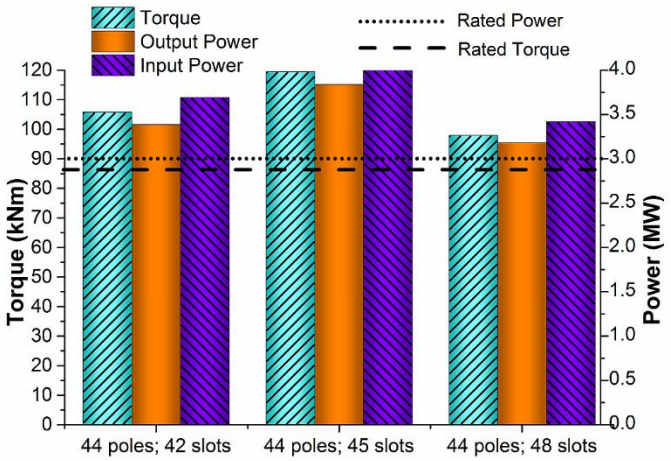

Figure 4-15. Average torque and power achieved in 44 pole, 3 MW HPMGs with varying slot number.

Table 4-9. Dimensions of 44 pole, 3 MW HPMGs.

# Slots	42	45	48
Outer Diameter (mm)	2250	2200	2000
Stack Length (mm)	750	733	667

The peak airgap flux density and shape of the airgap flux density curve was comparable for all three 3 MW HPMGs (Fig. 4-16). Fringing due to slotting was only

present in the airgap flux density of the 48 slot 3 MW HPMG. Cogging torque was most significant for the 3 MW HPMG with 48 slots (Fig. 4-17), which agrees with the results for the 3.5 kW HPMGs. The amplitude of the cogging torque was less than 1% of the rated value of torque in all cases. Magnet skew and stator skew will be investigated in the future to further reduce cogging torque in the 3 MW HPMGs.

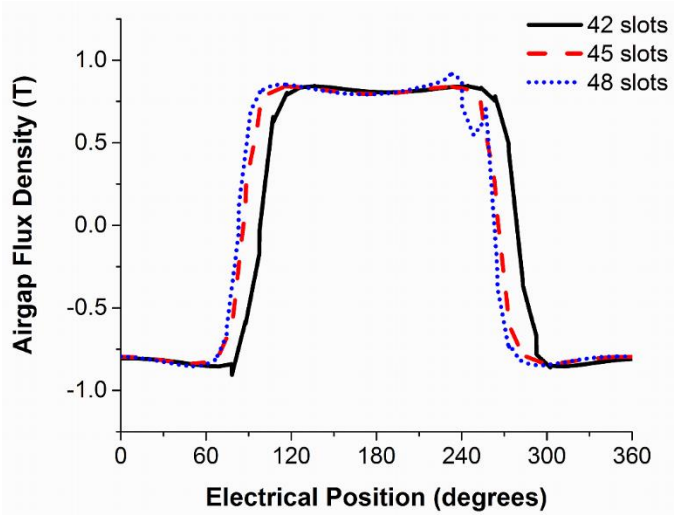

Figure 4-16. Airgap flux density of 44 pole, 3 MW HPMGs with varying slot number.

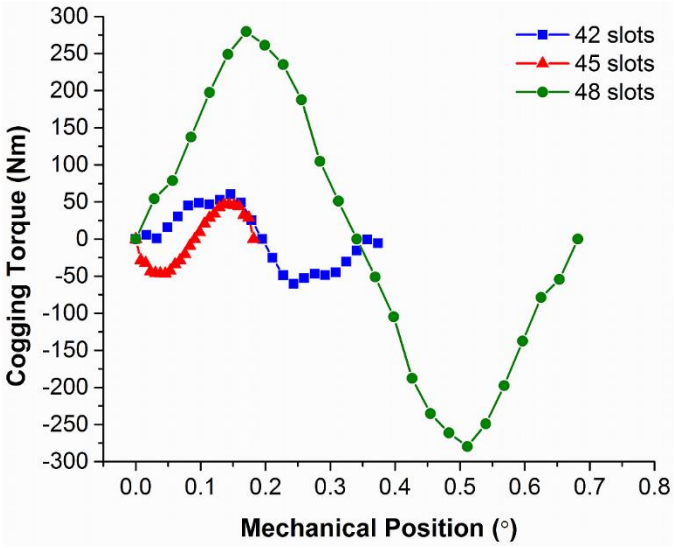

Figure 4-17. Cogging torque in 44 pole, 3 MW HPMGs with varying slot number.

4.3.7 3 MW HPMGs: Rare Earth Free Permanent Magnets

The 3.5 kW HPMG designs with C11 permanent magnets that achieved rated torque (100 Nm) and power (3.5 kW) were scaled to 3 MW. For the 3 MW HPMGs with C11 permanent magnets, rated torque (85989.89 Nm) and power (3 MW) were achieved for all 3 designs (Fig. 4-18). 94% efficiency was achieved for all 3 HPMGs on average at rated speed. Larger machines tend to be more efficient than smaller ones, and it was found that ohmic losses were significantly reduced for the scaled 3 MW HPMG.

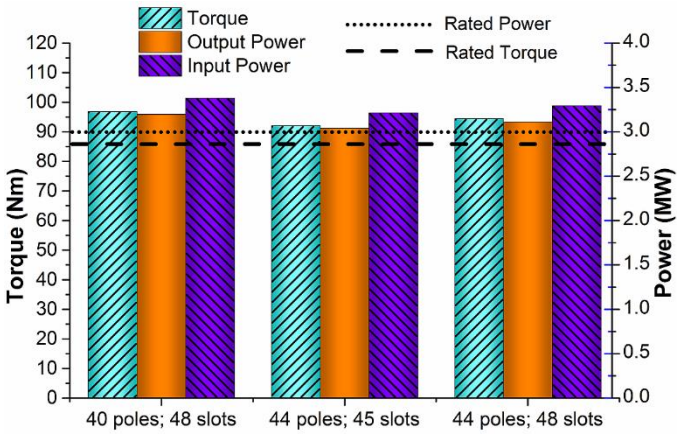

Figure 4-18. Average torque and power achieved in 3 MW HPMGs with C11 permanent magnets and varying number of poles and slots.

When comparing the 3 MW HPMGs with C11 permanent magnets, it was observed that higher pole number allowed for significant overall size reduction of the HPMG with the 44 pole machines being over 1 meter smaller in outer diameter than the 40 poles HPMG (3 meters vs. 4.1 meters) as shown in Table 4-10.

Table 4-10. Dimensions of 3 MW HPMGs with C11 permanent magnets.

# Poles		40	44	44
# Slots		48	45	48
Outer Diameter (mm)		4,100	3,000	3,000
Stack Length (mm)		1,367	1,000	1,000

The peak and profile of the airgap flux density seemed to be independent of the pole-slot combinations investigated (Fig. 4-19). Fringing due to slotting is again more apparent for higher slot number and more prevalent for lower pole number in the 3 MW HPMGs, which is consistent with the results for the 3.5 kW HPMGs. Finally, the cogging torque of the 3 MW HPMG with C11 permanent magnets, 40 poles and 48 slots was significant (Fig. 4-20), but still less than 3% of the rated torque, while the cogging torque of the 44 pole, 3 MW HPMGs was less than 0.5% of rated torque. This gives some design flexibility when designing the 3 MW HPMG – with the 44 pole, 45 slot machine being the best option in terms of cogging torque.

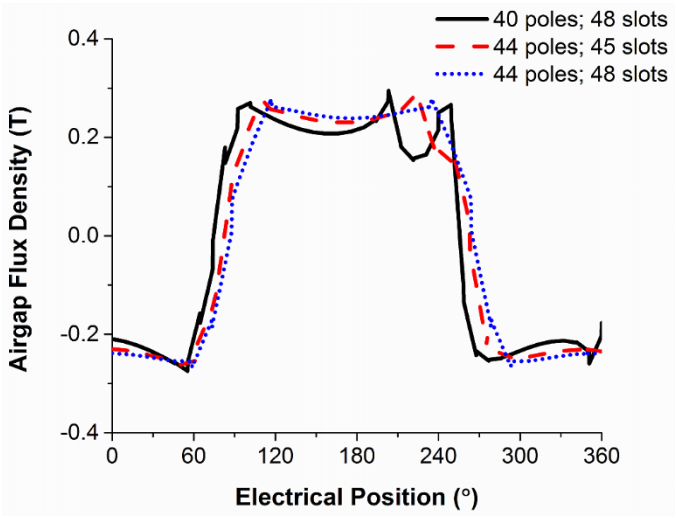

Figure 4-19. Airgap flux density for 3 MW HPMGs with C11 permanent magnets and varying number of poles and slots.

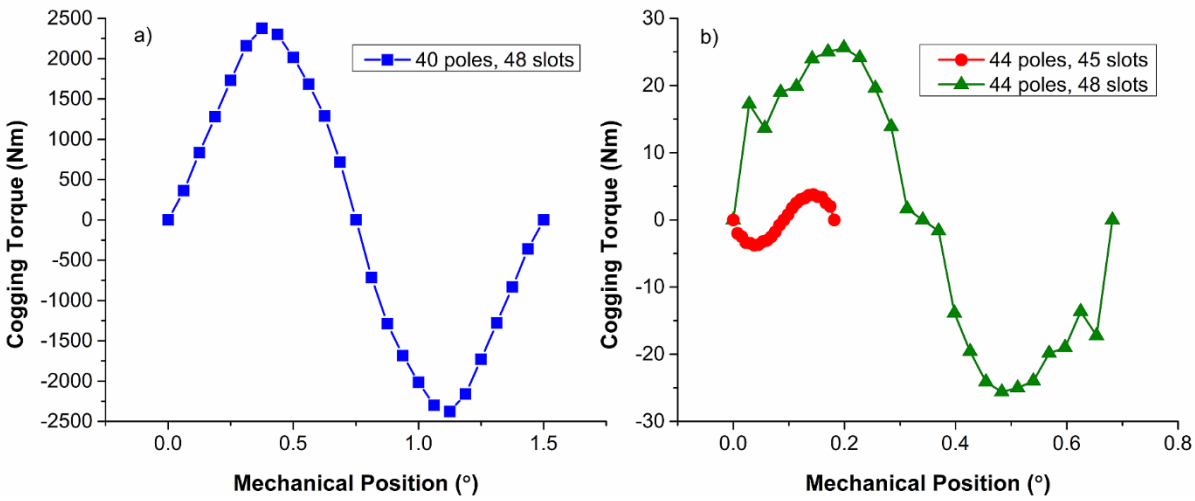

Figure 4-20. Cogging torque of 3 MW HPMGs with C11 permanent magnets and a) 40 poles and 48 slots and b) 44 poles and 45 or 48 slots.

4.4 Conclusions

The performance characteristics of 3.5 kW HPMGs with varying designs were studied. It was found that for high pole and slot number, magnetic loading could be significantly increased, resulting in torque and output power up to twice the rated values. Through appropriate selection of slot-to-pole ratio, cogging torque was reduced to less 0.5 Nm.

Two major achievements were demonstrated. For high pole and slot number, up to 35% reduction in the outer diameter and axial length of the HPMGs can be achieved. For the 3.5 kW HPMGs of reduced size, rated performance was achieved. However, a trade-off was found to exist between efficiency and size reduction at this power rating. Furthermore, while reduction in the volume of the Si-Fe and Cu of up to 90% and 91% respectively can be achieved, this comes at the cost of the need for increased NdFeB material volume.

Secondly, for high pole and slot number, rare earth free C11 permanent magnets can be used as the permanent magnet material in the 3.5 kW HPMGs without increasing the rotor volume. Though rated performance was achieved, at the 3.5 kW scale, reactive contributions losses increase significantly due to the permanent magnet material, thereby reducing efficiency.

When HPMGs designs with highest size reduction potential were scaled to 3 MW, we found that rated performance was achieved at reduced rotor volume of just over 2 meter in outer diameter, comparing favorably to outer PMG diameters of between 4m and 7 m for commercial DDPMGs. The 3 MW HPMGs achieved rated performance and high efficiency at rated speed (333 rpm).

Furthermore, rated torque and power was achieved for scaling of the 3.5 kW HPMGs with C11 permanent magnets to 3 MW on average at rated speed. High efficiency was achieved for the 3 MW HPMGs, demonstrating the potential for eliminating rare earth permanent magnets in commercial scale wind turbine generators. In future work, the use of HCs will be explored for PMGs rated at speeds in the range of direct-drive wind turbines.

CHAPTER 5. ELECTRICAL STEEL FLUX COLLECTORS

5.1 Introduction

In the previous Chapter, Halbach cylinder rotors were investigated for purposes of reducing the volume of permanent magnet generators (PMG) or using rare earth free, hard ferrite permanent magnets by focusing the magnetic flux to reach the desired magnetic flux density. In this Chapter, an alternative approach for focusing the magnetic flux is investigated – the use of electrical steel flux collectors. The use of electrical steel flux collectors is employed in magnetic levitation applications such as maglev trains to obtain high magnetic field gradients [58]. In these systems, electrical steel flux collectors are placed between permanent magnets of opposing magnetization (Fig. 5-1). The high permeability of the electrical steel provides a path for the magnetic flux, guiding the magnetic flux into a concentrated area (Fig. 5-2). In this Chapter, the use of electrical steel flux collectors are investigated to concentrate magnetic flux over the rotor surface and allow for achievement of two goals:

1. reduction or rotor volume
2. use of rare earth free permanent magnets

It is found that the concentration of magnetic flux over the rotor surface is sufficient to allow for substantial reduction in the outer diameter and axial length of the PMG, or for the use of rare earth free, hard ferrite permanent magnets while simultaneously allowing for some small reduction in the PMG volume for high pole and slot number.

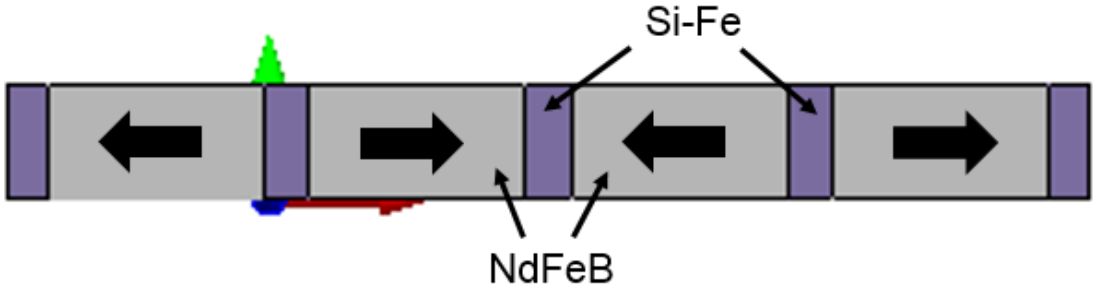

Figure 5-1. NdFeB permanent magnet array with Si-Fe flux collectors. Arrow indicate magnetization direction.

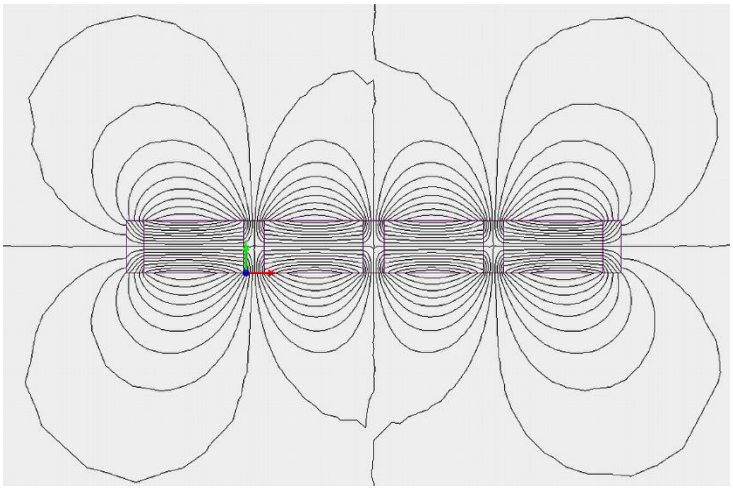

Figure 5-2. Magnetic flux profile of NdFeB permanent magnet array with Si-Fe flux collectors.

5.2 Methodology

A 3.5 kW outer rotor, surface mounted permanent magnet generator (PMG) was designed based on an existing generator design [48]. A novel rotor was designed with electrical steel flux collectors placed between permanent magnets of opposing magnetization (Fig. 5-3) with a rotor back-iron. Two magnets were defined per pole. The initial design parameters for the base model are

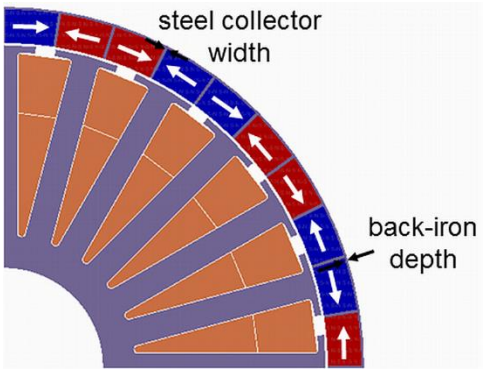

Figure 5-3. Quarter cross-section of PMG finite element model with electrical steel flux collectors.

described in Table 5-1. NdFeB 32/31 grade permanent magnets were selected (Table 5-2) and M19 26 Ga non-oriented Si-Fe. Several design parameters were varied to investigate the torque and output power achievable in the PMG with electrical steel flux collectors. These parameters included the rotor back-iron depth, electrical steel flux collector width, number of poles, and number of slots. The rotor volume, outer diameter, and stack length were kept constant.

Table 5-1. Specifications of the base model for a 3.5 kW PMG with electrical steel flux collectors.

Specification	Value
Rated Power (kW)	3.5
Rated Torque (Nm)	100
Rated Speed (rpm)	333
Outer Diameter (mm)	300
Stack Length (mm)	100
Airgap Length (mm)	1
Rotor Back-Iron Depth (mm)	1
Steel Collector Width (°)	1
Number of Poles	20
Number of Slots	24

For each design variation, finite element methods were used to calculate the torque, output power, input power, cogging torque, and airgap flux density as a function of the rotor position under 2D steady-state conditions. MotorSolve™ by Infolytica Corporation was used for the finite element calculations. The advance angle was set to 180° to simulate generator operation at rated current (21.5 A) and rated speed (333 rpm). 24 sample points, 5 skew samples, and a harmonic amplitude threshold of $1x10^{-6}$ were used with the best periodicity possible. In the analysis, each value was averaged over the position. The magnetic loading was calculated by averaging the instantaneous magnetic flux density over the rotor surface at a rotor position of 0 degrees. The torque density TV was calculated for each design variation, defined by equation (15) [50].

$$TV = \frac{T}{V_r} = \frac{T}{\pi D_r^2 L_{stk}/4} \quad (18)$$

where T is the torque, V_r is the rotor volume, D_r is the rotor diameter and L_{stk} is the stack length.

For design variations which achieved significantly more than rated torque (100 N·m) and power (3.5 kW), the outer diameter and axial length were reduced as much as possible without performing below the PMG ratings. All other dimensions were scaled accordingly. Additionally, for the design variations which achieved greater than rated torque and power, a rare earth free, hard ferrite permanent magnet C11 (Table 5-2) was substituted as the permanent magnet material to see if rated torque and power could still be achieved. C11 is a high grade, strontium iron oxide ceramic or hard ferrite permanent magnet.

Table 5-2. Properties of permanent magnet materials at 20°C.

	Coercivity (kA/m)	Remanence (T)	Energy Product (kJ/m^3)
NdFeB 32/31	874	1.17	256
C11	313	0.42	32.9

The results were compared to the performance of 3.5 kW Halbach PMGs with the same slot and pole combinations to determine which approach achieved the highest torque density and most reduction in the outer diameter and axial length. Finally, a comparison of the PMGs with electrical steel flux collectors and Halbach cylinders to PMGs with surface mounted magnets and bread-loaf magnets was performed (Fig. 5-4). Surface mounted permanent magnets and bread-loaf permanent magnets are very similar. Both have alternating north-south magnetization. However, while surface mounted permanent magnets are arced (Fig. 5-4a), bread-loaf permanent magnets are not (Fig. 5-4b). Surface mounted and bread-loaf magnet topologies were selected as

they are common topologies used by the wind industry. The same PMG volume and pole and slot combinations were selected for comparison.

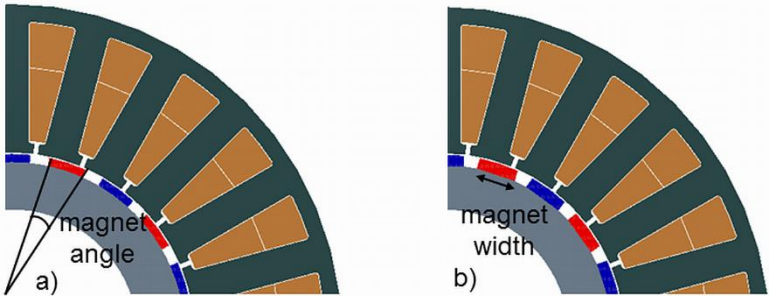

Figure 5-4. Quarter cross-section of PMG with a) surface mounted and b) bread-loaf permanent magnets.

5.3 Results & Discussion

5.3.1 Rotor Back-Iron Depth

The initial back-iron depth was varied slightly to determine if increasing or decreasing the back-iron depth was more beneficial in terms of increasing the magnetic loading, torque and power. It was found that decreasing the back-iron depth increased the magnetic loading, torque and power (Fig. 5-5a). This is because the magnetic flux leakage was reduced for a smaller back-iron depth, allowing a greater percentage of the magnetic flux to travel into the airgap of the PMG. Thus, a rotor back-iron depth of 0.5mm was selected for the initial base design (Table 5-1).

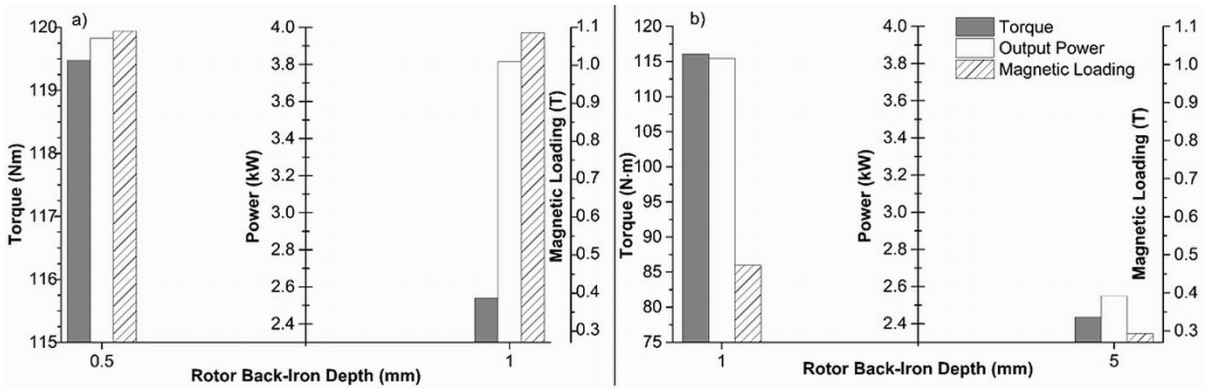

Figure 5-5. Average torque, output power and magnetic loading for a 3.5 kW PMG with electrical steel flux collectors for a) decreased rotor back-iron depth and b) increased rotor back-iron depth.

5.3.2 Electrical Steel Collector Width

After selecting a rotor back-iron depth of 0.5 mm (see section 5.3.1) for the 20 pole, 24 slot PMG with electrical steel flux collectors, the electrical steel collector width was varied by increasing the angle it spanned from 5° to 15° in increments of 1 degree. The rotor volume and stator design remained constant. It was found that the peak airgap flux density decreased linearly with increase in electrical steel collector width (Fig. 5-6). This result is intuitive since as the electrical steel

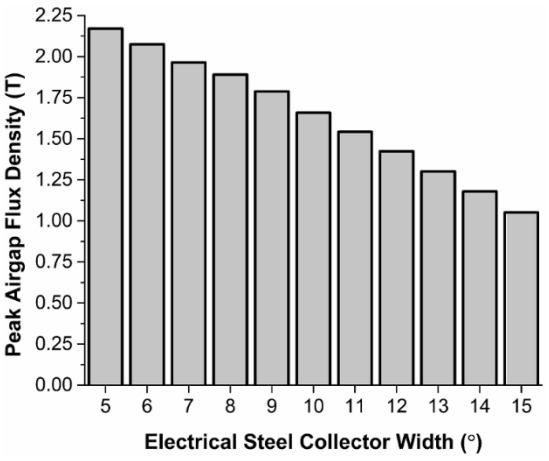

Figure 5-6. Peak airgap flux density for a 3.5 kW PMG with varied electrical steel collector width.

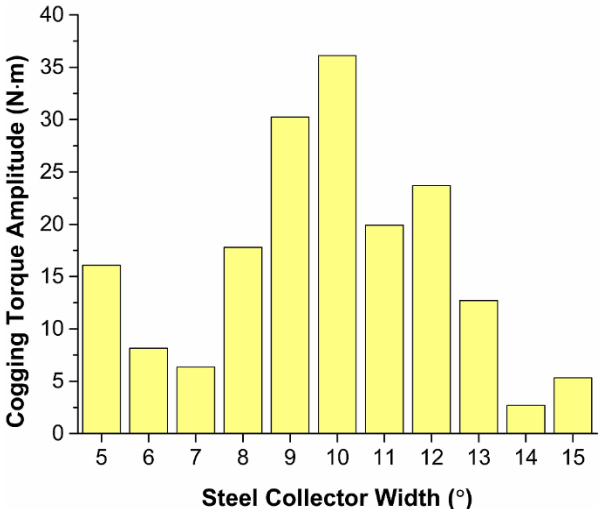

Figure 5-7. Cogging torque for varying electrical steel collector width for a 3.5 kW PMG.

collector width is increased, the permanent magnet volume is decreased, thereby reducing the magnetic flux crossing the airgap. A direct relationship was not established between the cogging torque and the electrical steel collector width (Fig. 5-7). Rather certain widths were found to minimize cogging torque including 7, 14 and 15 degree spans.

The average torque, power, efficiency and magnetic loading did not exhibit a direct relationship with the width of the electrical steel collectors. Instead there seemed to be an "optimal" width for which the magnetic flux path through the electrical steel collectors was most efficient (Fig. 5-8).

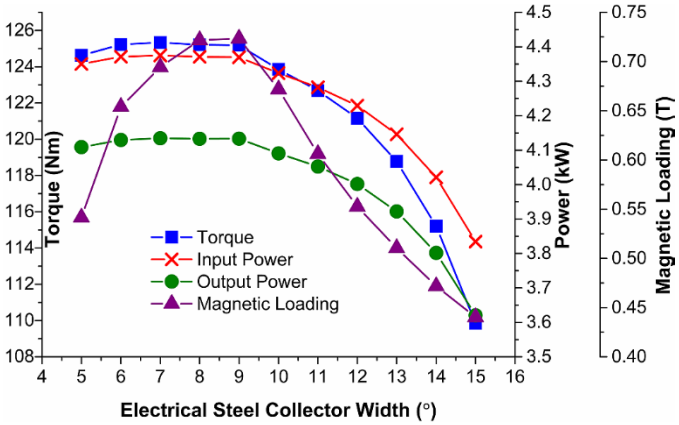

Figure 5-8. Average torque, output power and magnetic loading for a 3-5 kW PMG with varied electrical steel collector width.

The optimal width was determined to span 7 degrees because it achieved high average torque, power and magnetic loading without sacrificing efficiency or significantly increasing cogging torque.

5.3.3 Variation of Pole and Slot Number

The pole number was varied at 28, 32, 40 and 44 poles for the 3.5 kW PMG with electrical steel flux collectors. For each of these design variations the slot number was varied from 24 to 48 slots. These pole and slot combinations were chosen to maintain consistency with the Halbach cylinder study in Chapter 4 for purposes of direct

comparison. The ratio of electrical steel collector width to magnet width was optimized for variation of pole number (Table 5-3). It was found that the ratio of electrical steel collector width to permanent magnet width that formed the most efficient path for the magnetic flux was not constant for all designs.

Table 5-3. Dimensions of 3.5 kW PMGs with electrical steel flux collectors.

# Poles	Steel Collector Width (°)	Permanent Magnet Width (°)	Ratio of Collector to Magnet Width
20	7	11	0.64
28	3	3.43	0.87
32	3	2.63	1.14
40	2	2.5	0.8
44	2	2.09	0.96

For constant pole number, the average torque was generally found to increase linearly with increase in slot number (Fig. 5-9a). Though higher pole number was found to be beneficial for increasing the torque (by increasing the magnetic loading), a direct relationship between the two was not exhibited for constant slot number. For constant pole number, the average output power was also found to increase linearly with slot number, and again a direct relationship between pole number and torque was not exhibited, though high pole number was found to be desirable in the design (Fig. 5-9b).

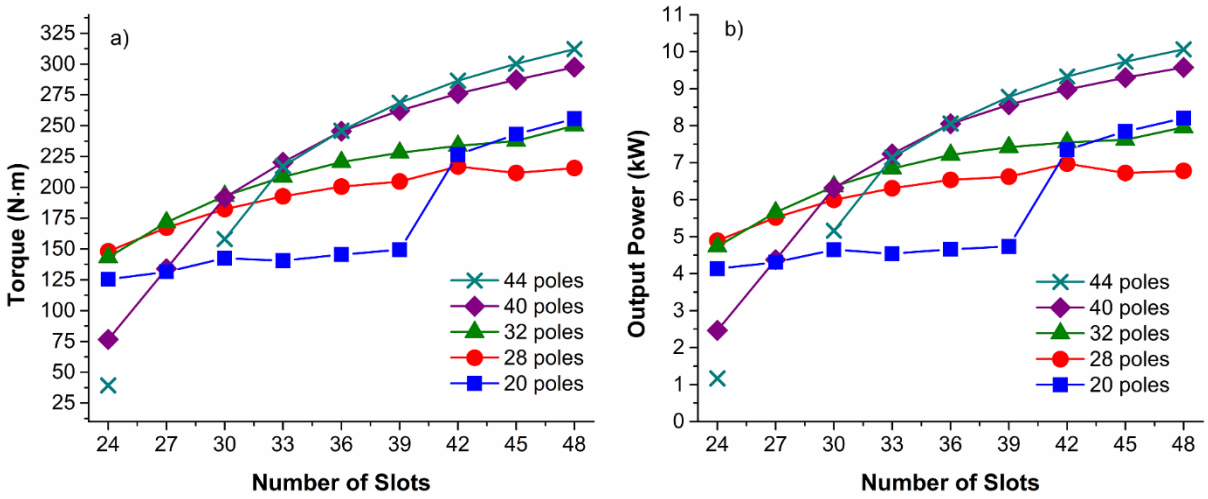

Figure 5-9. Average a) torque and b) output power of 3.5 kW PMGs with electrical steel flux collectors and varying number of slots and poles.

In contrast, average efficiency was found to decrease linearly for increase in slot number (with constant pole number) to a small degree (Fig. 5-10). However, the reduction in performance was not significant, with the average efficiency remaining above 90% in general.

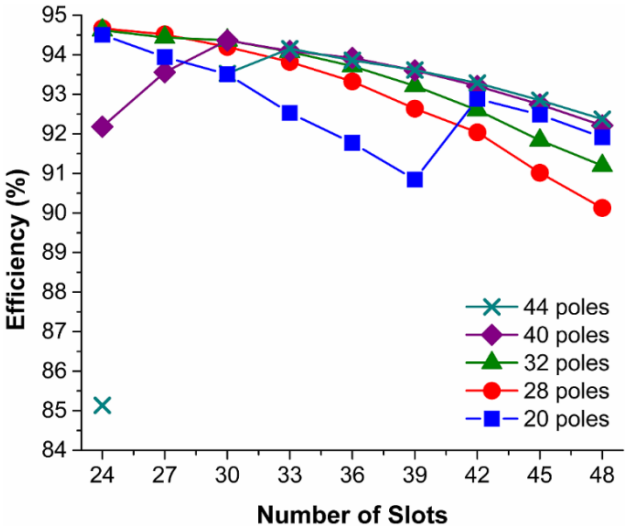

Figure 5-10. Average efficiency of 3.5 kW PMGs with electrical steel flux collectors and varying number of slots and poles.

For the slot and pole configurations investigated, it was found that for a high pole and slot number, more than twice the value of rated torque was achieved. In general, higher slot number had a greater influence on increasing the achieved torque and output power.

5.3.4 Size Reduction

The outer diameter and stack length of 3.5 kW PMGs with electrical steel flux collectors were reduced appropriately to allow for achievement of rated torque and power for those design variations which significantly increased torque density and magnetic loading. It was found that the outer diameter and axial length could be reduced by up to 46% and still allow for achievement of rated performance (Table 5-4). However, the average efficiency was significantly reduced for the PMGs of reduced size.

Table 5-4. Dimensions and average performance of 3.5 kW PMGs with electrical steel flux collectors and of reduced size.

Pole-Slot Configuration	32 poles, 48 slots	40 poles, 48 slots	44 poles, 48 slots
Outer Diameter (mm)	183	165	162
Stack Length (mm)	61.2	55.2	54.2
Airgap Length (mm)	0.61	0.55	0.54
Torque (Nm)	143.941	148.690	150.049
Output Power (kW)	3.614	3.529	3.508
Efficiency (%)	71.92	67.99	66.98

5.3.5 Ceramic PMG

For the 3.5 kW PMGs with electrical steel flux collectors that achieved more than rated torque and power, C11 permanent magnets (Table 5-2) were substituted as the permanent magnet material. For 13 of the design variations (varying slot and pole number), the use of C11 was possible (Fig. 5-11). A tradeoff was observed between increasing the average torque and power with efficiency, which decreased for increasing slot number. For high pole and slot number, the torque and power achieved was greater than rated values, indicating some reduction in the outer diameter and axial length would be possible if desired. However, this might also further reduce the efficiency of the PMG (sec. 5.3.4).

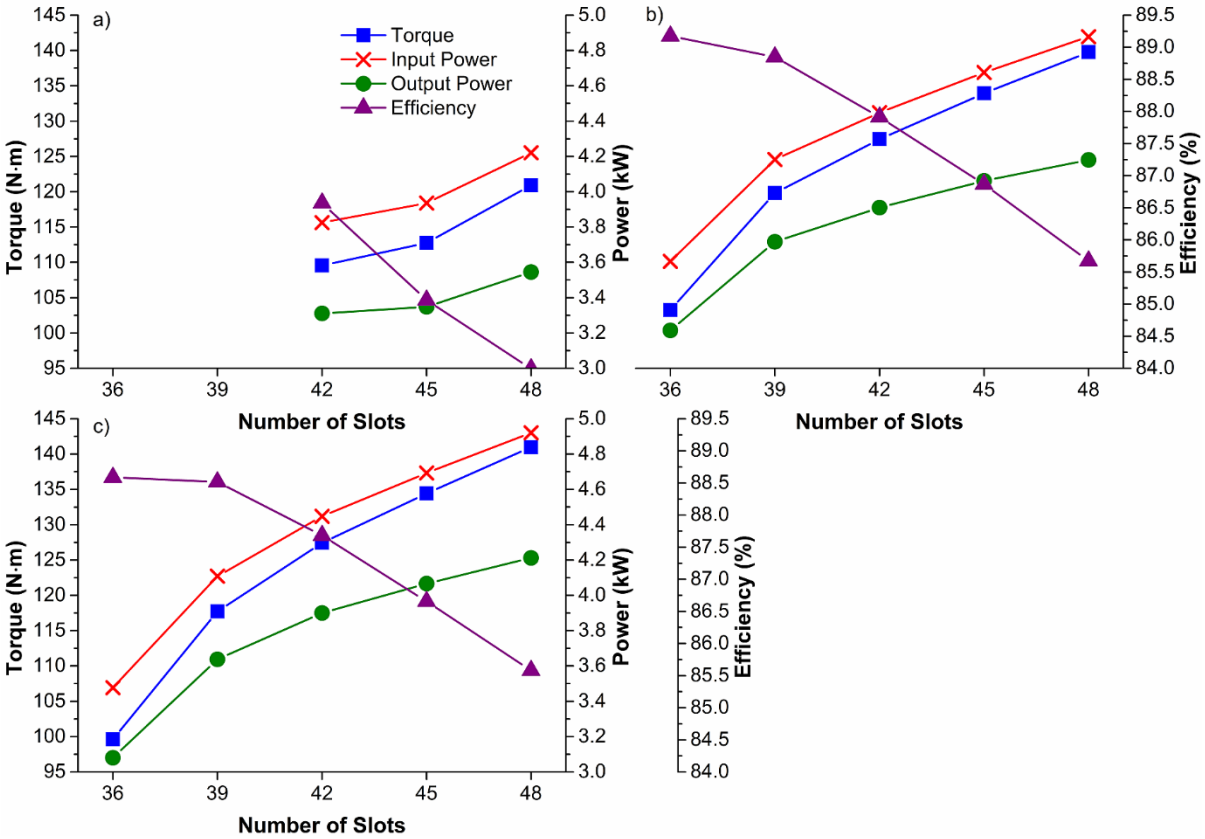

Figure 5-11. Average performance of 3.5 kW PMGs with electrical steel flux collectors, C11 permanent magnets, varying number of slots and a) 32 poles, b) 40 poles, and c) 44 poles.

5.3.6 Halbach vs. Steel Collector

The 3.5 kW PMGs with electrical steel flux collectors were able to achieve either significant reduction in the outer diameter and axial length or the use of rare earth free, strontium iron oxide permanent magnets with the potential for a small reduction in the PMG volume as well. These PMGs were compared to those with Halbach cylinder rotors, or Halbach PMGs (HPMGs) of equal ratings and pole-slot configurations.

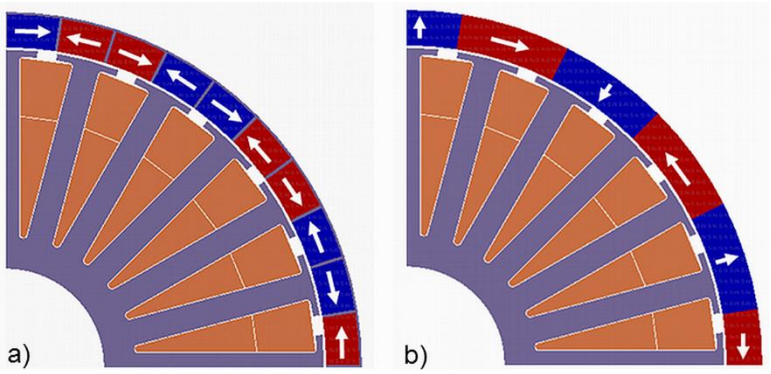

Figure 5-12. Quarter cross-section of 3.5 kW PMGs with a) electrical steel flux collectors and b) Halbach cylinder. Arrows indicate magnetization direction.

First, the 3.5 kW PMGs were compared for equal PMG volume, rotor volume, and varying number of slot and poles to see which technique achieved greater concentration of magnetic flux. It was found that for all slot and pole combinations investigated, the 3.5 kW PMG with electrical steel flux collectors achieved slightly higher torque density than the HPMGs (Fig. 5-13).

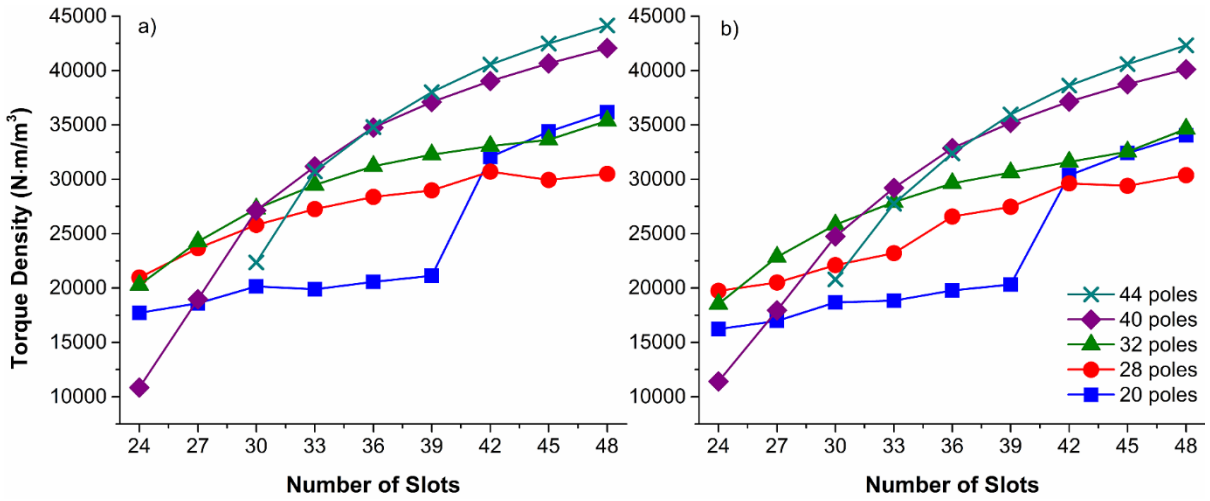

Figure 5-13. Average torque density in 3.5 kW PMG with a) electrical steel flux collectors and b) Halbach cylinder.

The PMGs with electrical steel flux collectors achieved higher peak airgap flux density for all pole and slot combinations compared to the HPMGs (Fig. 5-14). However, if the

airgap flux density profiles are compared, it is evident that the HPMG achieve a more homogeneous distribution than that PMG with electrical steel flux collectors (Fig. 5-15).

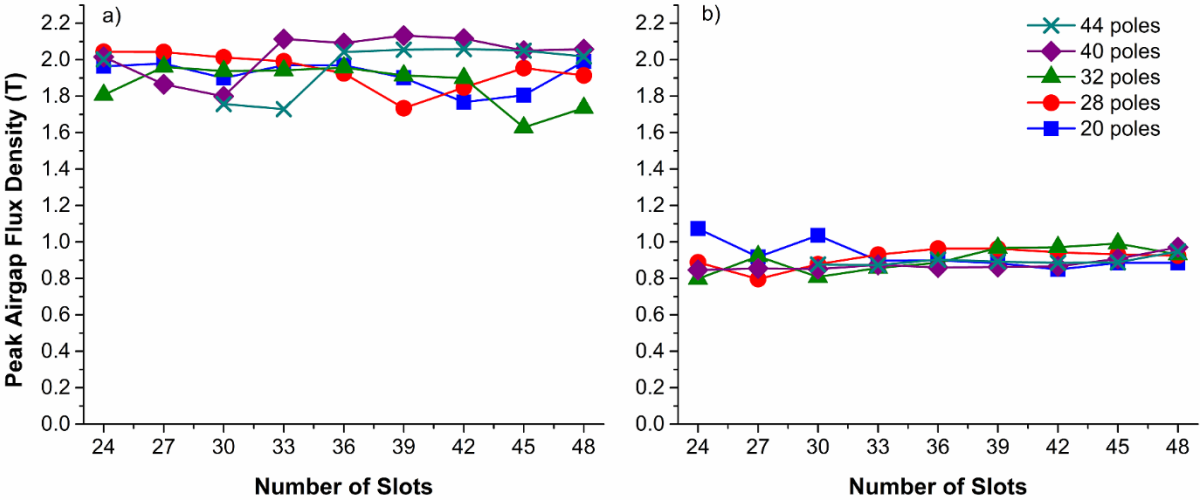

Figure 5-14. Peak airgap flux density in 3.5 kW PMG with a) electrical steel flux collectors and b) Halbach cylinder.

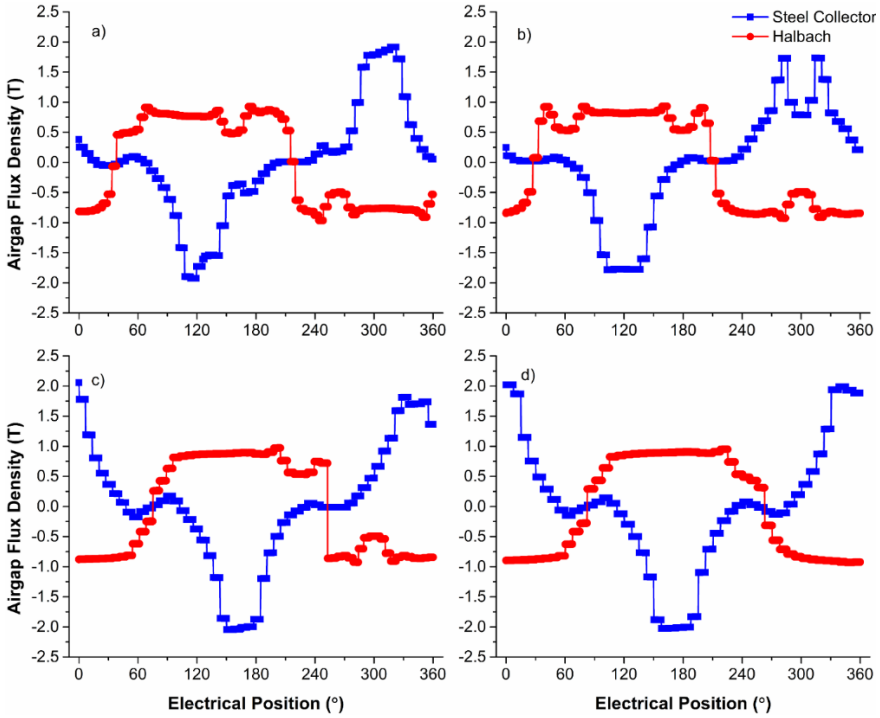

Figure 5-15. Airgap flux density of 3.5 kW PMG with electrical steel flux collectors and Halbach cylinders with 48 slots and a) 28 poles, b) 32 poles, c) 40 poles, and d) 44 poles.

The average efficiency of the HPMG and PMG with electrical steel flux collectors were quite comparable (Fig. 5-16). Generally, the HPMG had slightly higher average efficiency, but by less than 1% in most cases.

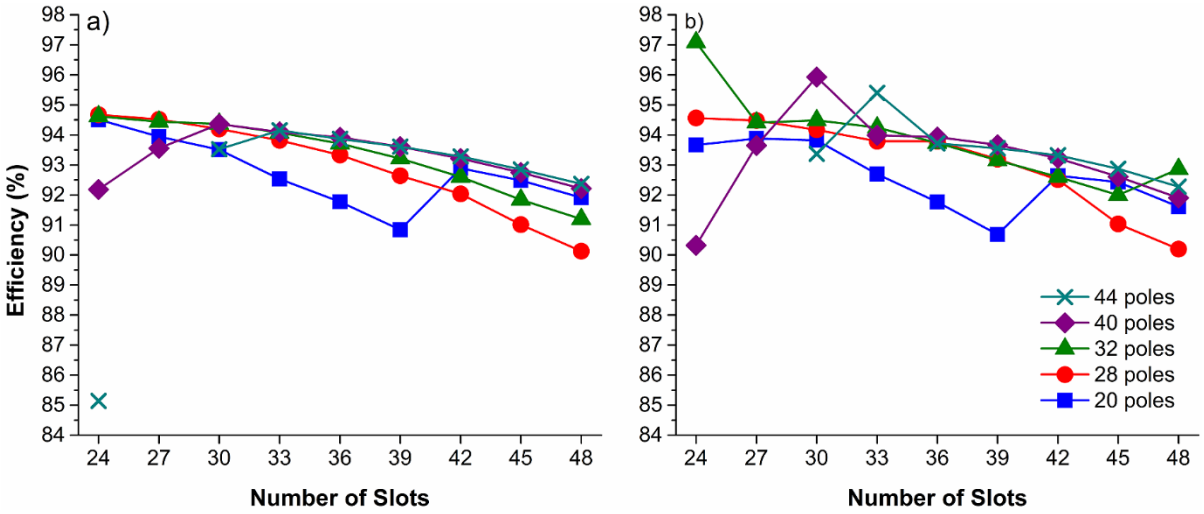

Figure 5-16. Average efficiency 3.5 kW PMG with electrical steel flux collectors and Halbach cylinders with a) electrical steel flux collectors and b) Halbach cylinder.

Both techniques allowed for reduction in the outer diameter and the axial length of the 3.5 kW PMG. The PMG with electrical steel flux collectors achieved greater reduction in the dimensions than the HPMGs (Table 5-5). Additionally, the PMGs with electrical steel flux collectors require less permanent magnet volume either for the same size or reduced size than the HPMGs, helping to reduce on the material cost.

Table 5-5. Dimensions of 3.5 kW PMGs with electrical steel flux collectors and Halbach cylinders of reduced size.

Pole-Slot Configuration	Rotor Type	Outer Diameter (mm)	Stack Length (mm)
32 poles 48 slots	Steel Collector	183	61.2
	Halbach	215	71.7
44 poles 48 slots	Steel Collector	162	54.2
	Halbach	225	75

Both magnetic flux focusing techniques allowed for the use of C11 hard ferrite permanent magnets. The higher torque density and airgap flux density of the 3.5 kW

PMGs with electrical steel flux collectors allowed for a wider range of designs to successfully utilize the C11 permanent magnets than was possible with the HPMGs (Fig. 5-17). For these designs, the PMGs with electrical steel flux concentrators achieved slightly higher average torque, output power and efficiency (Fig. 5-18). Based on these results, the electrical steel flux collectors are the preferred choice for the use of the C11 permanent magnets as it allows for more design flexibility.

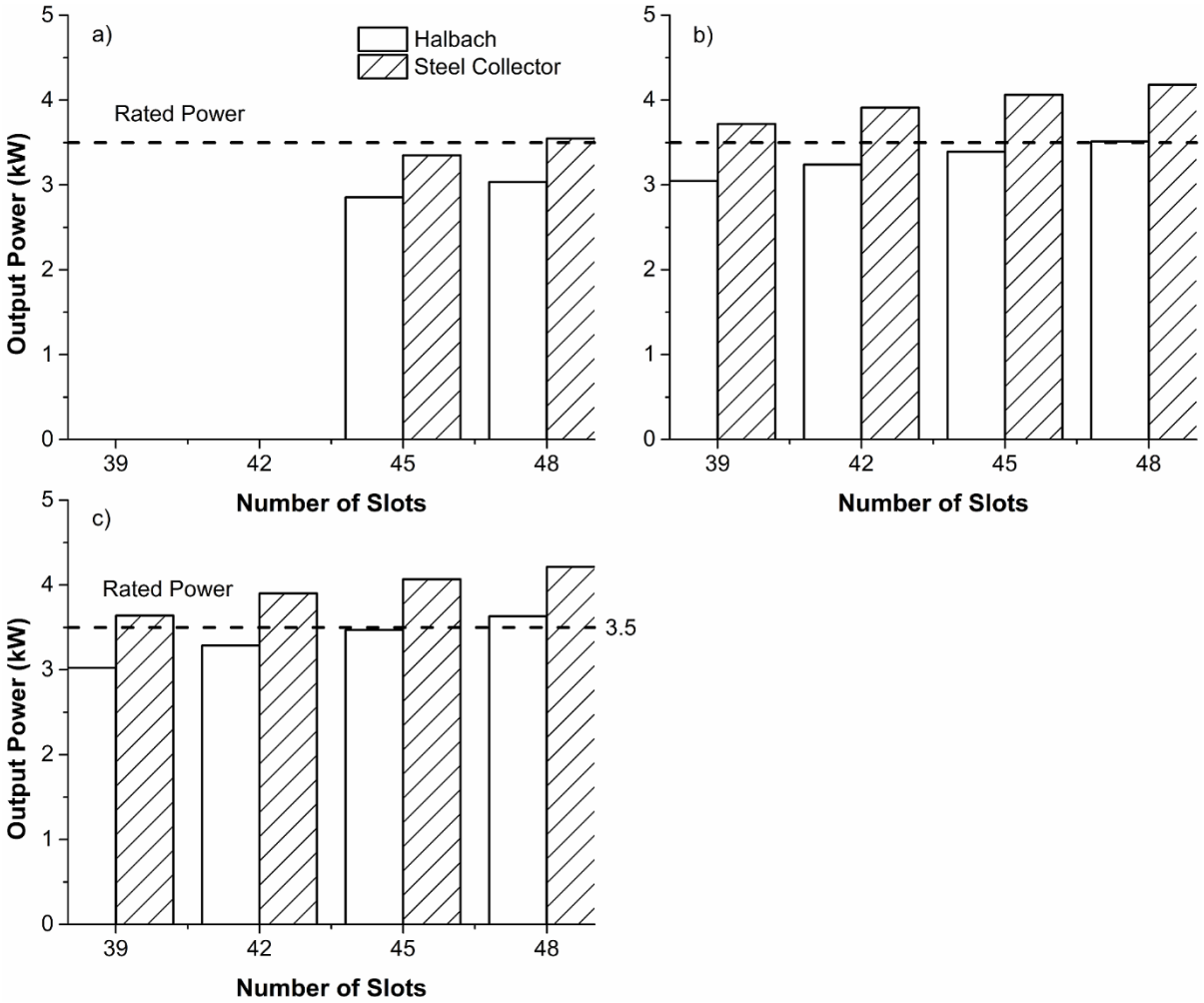

Figure 5-17. Average output power of 3.5 kW PMG with electrical steel flux collectors and Halbach cylinders and a) 32 poles, b) 40 poles, and c) 44 poles.

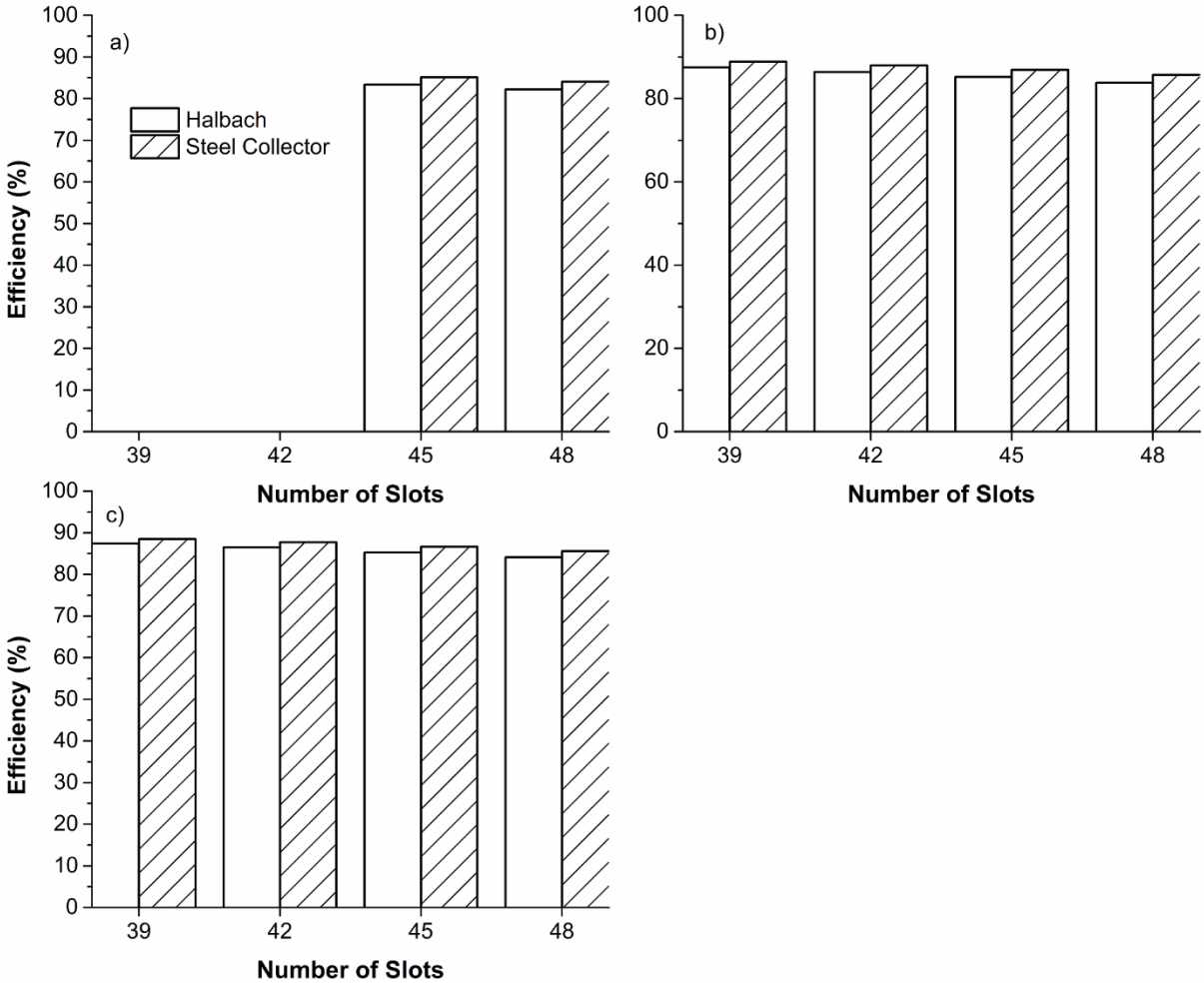

Figure 5-18. Average efficiency of 3.5 kW PMG with electrical steel flux collectors and Halbach cylinders and a) 32 poles, b) 40 poles, and c) 44 poles.

5.3.4 Comparison to Other Topologies

The performance of the 3.5 kW PMGs with electrical steel flux collectors and Halbach cylinders were compared to that of PMGs with surface mounted and bread-loaf permanent magnets. For this comparison, only the permanent magnet topology was varied. Each 3.5 kW PMG had 20 poles and 24 slots. The outer diameter, axial length and overall PMG volume remained constant. However, the dimensions of each design selected allowed for achievement of the rated torque and power without greatly

exceeding these values. Thus, the outer diameter, axial length and overall PMG volume varied for this comparison.

From Table 5-6, it is evident that when sized according to the rating, no rotor topology offers any benefit in terms of average efficiency. The use of magnetic flux focusing techniques allows for the PMG with electrical steel flux collectors and Halbach cylinder to reduce the overall PMG volume. However, the permanent magnet volume increases for the use of the rotor topologies that concentrate magnetic flux. The PMG with electrical steel flux collectors requires less permanent magnet volume than the HPMG.

Table 5-6. Average performance and dimensions of 3.5 kW PMGs with varying rotor topology.

Rotor Topology	Torque (N·m)	Output Power (kW)	Efficiency (%)	Magnetic Loading (T)	Outer Diameter (mm)
Surface Mounted	107.805	3.537	93.98	0.8223	300
Bread-loaf	106.921	3.502	93.84	0.6216	300
Steel Collector	107.147	3.502	93.62	0.6986	259
Halbach	107.005	3.509	93.95	0.6869	283

In terms of cogging torque, the PMG with electrical steel flux collectors performed better than the other topologies in terms of the amplitude (Fig. 5-19). However, the use of two magnets per pole did increase the ripple that occurs, which would in turn increase the voltage ripple seen by the grid. The PMG with electrical steel flux collectors achieved the highest peak airgap flux density of the topologies investigated, while the other rotor topologies provided a more homogeneous distribution of the airgap flux (Fig. 5-20).

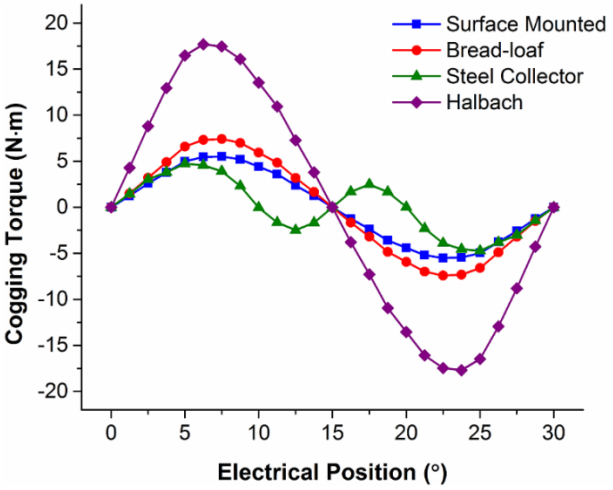

Figure 5-19. Cogging torque for 3.5 kW PMGs with varying rotor topology.

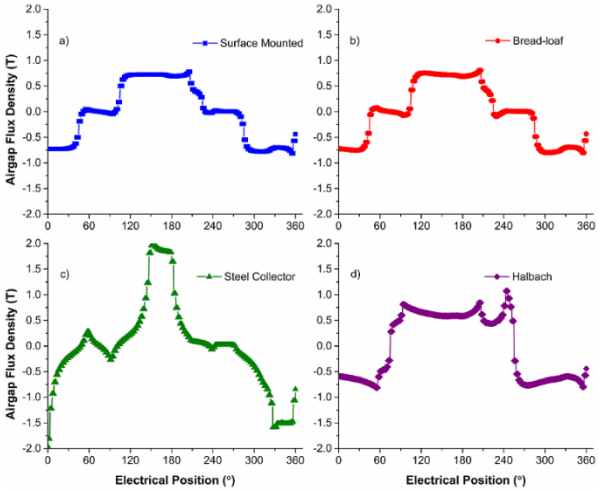

Figure 5-20. Airgap flux density for 3.5 kW PMGs with a) surface mounted magnets, b) bread-loaf magnets, c) electrical steel collectors and d) Halbach cylinder rotor.

5.4 Conclusions

The use of electrical steel flux collectors in a 3.5 kW PMG was studied for the purpose of focusing the magnetic flux to allow for size reduction or the use of rare earth free, hard ferrite permanent magnets. With the addition of a thin back-iron and optimization of the collector width, the efficiency of the path of the magnetic flux was increased. The use of electrical steel flux collectors was ultimately found to provide a greater potential for size reduction and use of C11, strontium iron oxide permanent magnets than for the use of a Halbach cylinder. Up to 46% reduction in the outer diameter and axial length was demonstrated to be achievable with the use of electrical steel flux collectors. The PMGs with electrical steel flux collectors and C11 permanent magnets suffered from less efficiency loss than for reduction of the size with NdFeB 32/31 grade permanent magnets, and also demonstrate the potential for a small degree of size reduction. Furthermore, more design flexibility is achievable for the C11

permanent magnets than for the HPMGs. When comparing to conventional topologies used in the wind industry, the electrical steel flux collectors were found to reduce the amplitude of cogging torque, though increasing the periodicity of the torque ripple. However, more permanent magnet volume is required to achieve size reduction. Thus, it is recommended that electrical steel flux collectors be used to further explore the design of rare earth free permanent magnets.

CHAPTER 6. PERMANENT MAGNET TOPOLOGY INVESTIGATION

6.1 Introduction

The wind industry typically uses permanent magnet generators (PMGs) with a surface mounted or bread-loaf permanent magnet topologies (Fig. 6-1) [20]. However, there is a wide range of permanent magnet topologies that can be employed in PMG design. These range from inset to spoke permanent magnet topology (Fig. 6-1). The aim of this Chapter is to investigate the various permanent magnet topologies for PMGs to determine whether any other topology provides significant benefits, in terms of increasing magnetic loading and torque density as compared to surface mounted or bread-loaf topologies in order to allow for significant PMG volume reduction. The permanent magnet topology of a 10 kW PMG was varied to determine the relative advantages and disadvantages of each topology. It was found that while the spoke permanent magnet topology (Fig. 6-1e) produced the highest magnetic flux density, the value of magnetic flux was highly variable contributing to significant cogging torque, or torque ripple. The bread-loaf permanent magnet topology (Fig. 6-1c) was ultimately determined to be the best choice relative to the other topologies in terms of providing reduction in the PMG volume without sacrificing performance.

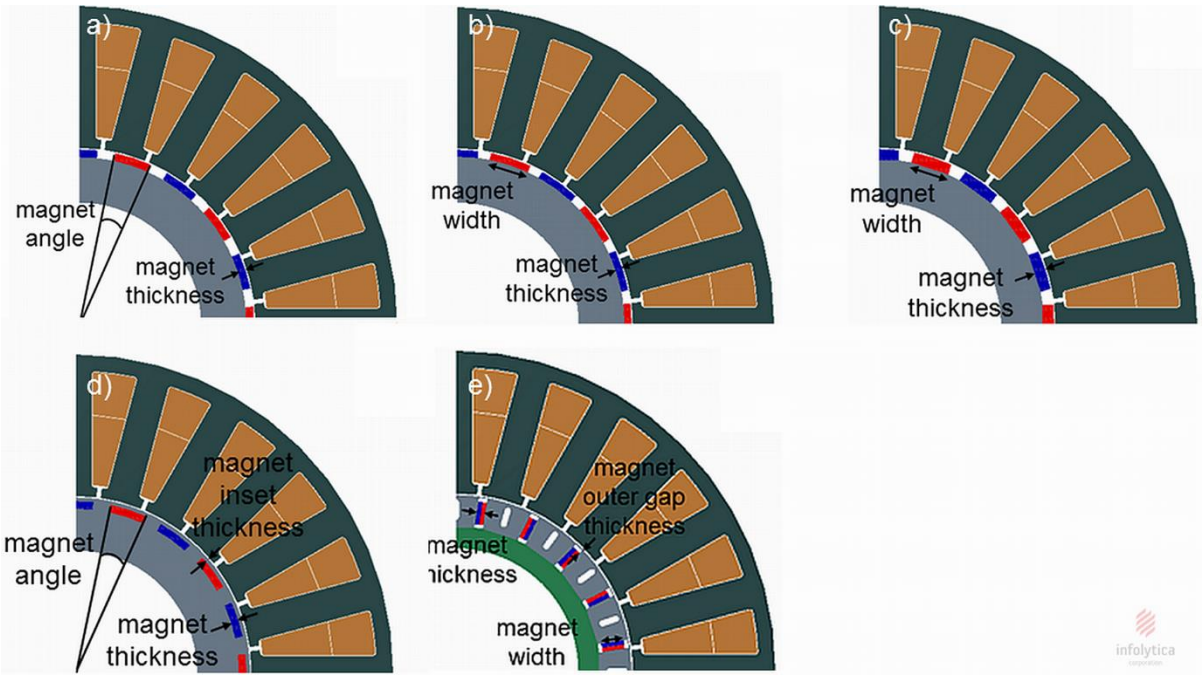

Figure 6-1. Quarter cross-section of PMGs with a) surface mounted with radial magnets, b) surface mounted with parallel magnets c) bread-loaf, d) inset and e) spoke permanent magnet topologies.

6.2 Methodology

A 10 kW surface mounted PMG with radial magnets and an interior rotor (Fig. 6-2) was designed, rated at 100 rpm (Table 6-1). The PMG was sized to allow for achievement of rated torque and power to serve as the "base model," but not optimized initially for reduction in the outer diameter or stack length. The topology of the permanent magnets in the base model was varied, while maintaining the constant PMG volume, outer diameter and stack length, pole and slot number, and permanent magnet material (NdFeB 32/31). PMG designs which

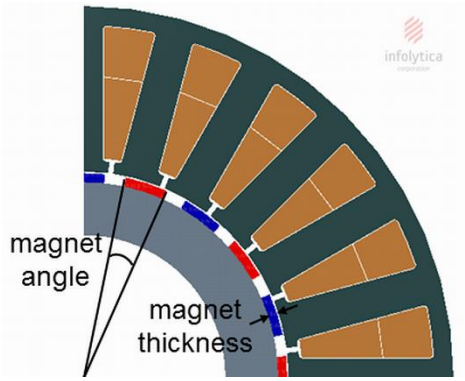

Figure 6-2. Quarter cross-section of surface mounted PMG with radial magnets.

achieved more than rated torque and power were investigated for potential to significantly increase magnetic loading, thereby allowing for reduction of PMG volume. These topologies included bread-loaf, inset, spoke and parallel surface mounted permanent magnets (Fig. 6-1). For each of these permanent topologies, different design parameters were varied to study how this variation affected the machine performance including magnet thickness, magnet width or angle (depending on the shape of the magnet), slot number, pole number, slot-to-pole ratio, inset magnet gap for the case of inset magnet topology, and magnet outer gap thickness for the case of the spoke magnet topology. The surface mounted PMG with radial magnets was also optimized to see whether other permanent magnet topologies could provide greater size reduction than the “base model”. For purposes of comparison, several design parameters were fixed based on the results from the wide range of possibilities investigated. These parameters included a slot-to-pole ratio of 2.25 with 54 slots and 24 poles, which were found to significantly increase torque and output power produced (section 6.3).

Table 6-1. Specifications of a 10 kW surface mounted PMG with radial magnets and interior rotor.

Specification	Value
Rated Power (kW)	10
Rated Torque (Nm)	954.927
Rated Speed (rpm)	100
Outer Diameter (mm)	833.33
Stack Length (mm)	1250
Airgap Length (mm)	1.62
Rotor Outer Diameter (mm)	417.2
Rotor Inner Diameter (mm)	319
Stator Outer Diameter (mm)	833.33
Stator Inner Diameter (mm)	462
Magnet Thickness (mm)	10.2
Magnet Angle (°)	12
Number of Poles	20
Number of Slots	24

Finite element methods were used to calculate the torque, cogging torque, input and output power, and airgap flux density as a function of rotor position under 2D steady-state conditions using MotorSolve^{TM} by Infolytica Corporation. An advance angle of 180° was used to simulate the performance of the machine as a generator at rated speed (100 rpm) and rated current (106A). 24 sampling points per period for the best periodicity, 5 skew samples, and a harmonic amplitude threshold of $1x10^{-6}$ were used. Magnetic loading was determined by calculating the instantaneous magnetic flux density throughout each PMG and averaging the magnetic flux density at the rotor surface radius. In the analysis, the torque, input power and output power were averaged over the position. Efficiency was taken as the average output power over the average input power. An undergraduate research assistant, Melissa Flood, assisted generating some of the numerical results with finite element methods.

The parameters which were identified to increase magnetic loading, torque and output power were combined in a final “optimized” design. Then the PMG was resized to produce the rated parameters to see how much volume reduction was possible.

6.3 Results & Discussion

The torque, input and output power, and efficiency were averaged over the rotor position for each 10 kW PMG. Several permanent magnet topologies were identified as having potential to increase magnetic loading to allow for achievement exceeding the rating parameters including bread-loaf with non-embedded magnets, inset magnets, spoke with embedded magnets, and surface mounted with parallel and radial magnets as highlighted in Table 6-2 below.

Table 6-2. Average performance of 10 kW PMGs with varying permanent magnet topology.

	Average			
PMG Topology	**Torque (N·m)**	**Input Power (kW)**	**Output Power (kW)**	**Efficiency (%)**
Bread loaf with two non-embedded magnets per pole	930.914	9.749	9.050	92.72
Bread loaf with non-embedded magnets	1,015.220	10.631	9.873	92.87
Bread loaf with 12 non-embedded magnets	289.528	3.032	2.912	96.04
Inset magnets	982.287	10.286	9.599	93.31
IPM with angled barrier	869.773	9.108	8.494	93.26
IPM with curved magnets	873.486	9.147	8.554	93.52
IPM with variable orientation magnets	727.284	7.616	7.193	94.44
IPM with lateral magnets	523.298	5.480	5.201	94.90
Spoke with non-embedded magnets	784.685	8.217	7.733	94.10
Spoke with embedded magnets	991.189	10.380	9.624	92.72
Surface mounted with parallel magnets	1,169.363	12.246	11.259	91.95
Surface mounted with radial magnets (base model)	1,085.780	11.370	10.542	92.72

6.3.1 Surface mounted with radial magnets (base model)

The surface mounted PMG with radial magnets (Fig. 6-2) served as the base model (Table 6-1) for the study. It was optimized for volume reduction to see whether any other permanent magnet topologies could achieve more volume reduction than the base model. The magnet angle, magnet thickness, slot number, pole number, and slot-to-pole ratio were varied for this topology.

6.3.1.1 Magnet Angle

The magnet angle was varied from 6 to 18 degrees in increments of 2 degrees. The magnet angle is a measure of the magnet width for arced magnets (Fig. 6-2). It should be noted that at an angle of 18° the gap between magnets was eliminated. The average torque and average output power were found to increase linearly with increase in magnet angle, while average efficiency was found to decrease linearly (Fig. 6-3). However, the average efficiency remained above 90% for all magnet angles investigated so a significant trade-off was not found between torque and efficiency or output power and efficiency. The increase in torque and output power with magnet angle is intuitive. As magnet angle increases, so too does the permanent magnet volume, thereby increasing the magnetic flux density at the surface of the rotor, which by definition will increase the magnetic loading and torque.

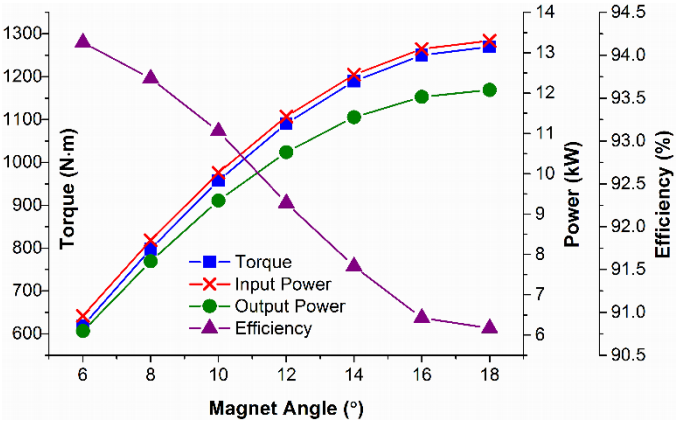

Figure 6-3. Average performance of surface mounted PMG with radial magnets and varying magnet angle.

6.3.1.2 Magnet Thickness

The magnet thickness was varied from 5 to 55 mm in increments of 5 mm. The variation in magnet thickness was found to have little effect on the

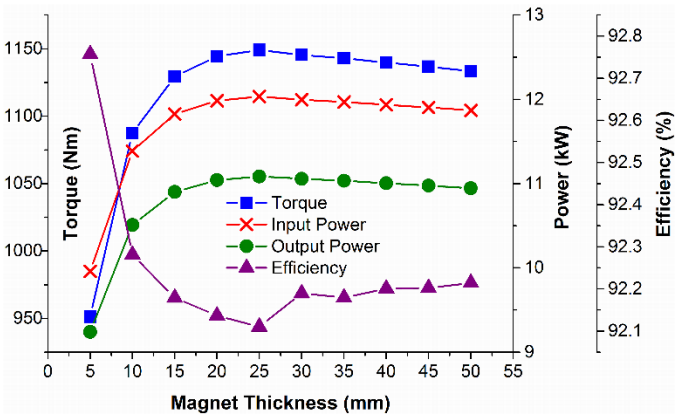

Figure 6-4. Average performance of surface mounted PMG with radial magnets and varying magnet thickness.

average torque, output power and efficiency produced (Fig. 6-4). A thickness of 25 mm maximized the average torque and output power. Although the increase in magnet thickness also increases the permanent magnet volume, the distance between the surface of the rotor back-iron and stator is increased, thereby increasing the airgap distance between the rotor back-iron and the stator. Thus, the magnetic flux leakage will likely increase for the increase in magnet thickness, offsetting additional magnetic flux density from the increased permanent magnet volume and accounting for the relatively constant value of average torque, power and efficiency with change in magnet thickness.

6.3.1.3 Slot and Pole Number

The pole number was varied from 8 to 32 poles in increments of 6. For each pole number, the slot number was also varied from 15 to 39 in increments of 6 to give a wide range of design options. It was found that for higher pole and slot number, higher average torque and average output power was achieved (Fig. 6-5a and 6-5b), but average efficiency was reduced (Fig. 6-5c). For a constant pole number, there was a clear increase in average torque and average power with increase in slot number. However, for constant slot number, increasing pole number did not have a clear benefit, indicating the slot-to-pole ratio plays an important role. The best compromise between rated performance and efficiency was achieved for the surface mounted PMG with radial magnets with 14 poles and 39 slots.

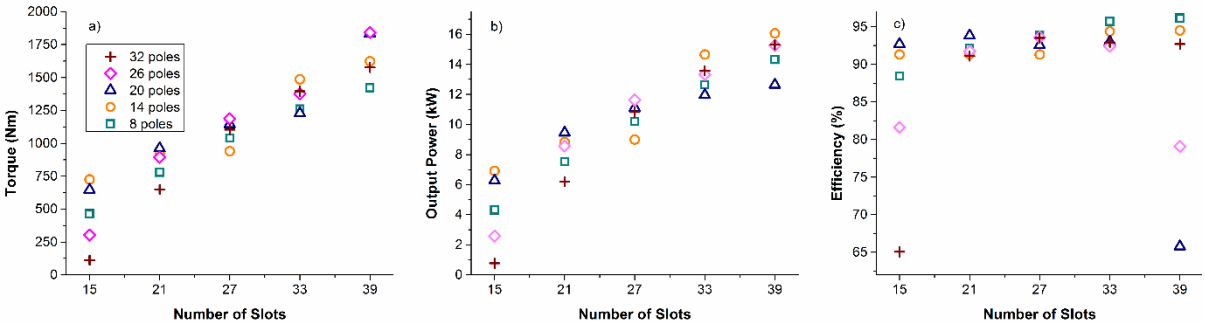

Figure 6-5. a) Average torque, b) average output power, and c) average efficiency of surface mounted PMG with radial magnets and varying slot and pole number.

6.3.1.4 Slot-to-Pole Ratio

The number of slots and poles were varied, keeping a constant slot-to-pole ratio of 2.25, which was found to be a desirable slot-to-pole ratio for achieving high magnetic loading, torque, power and efficiency (see section 6.3.2.4). For higher pole and slot number, the average torque and average output power were increased well beyond the rated values (Fig. 6-6). This is also an intuitive result since higher pole number will increase magnetic loading. Average efficiency remained fairly constant for all slot and pole combinations, above 93% for all slot and pole combinations.

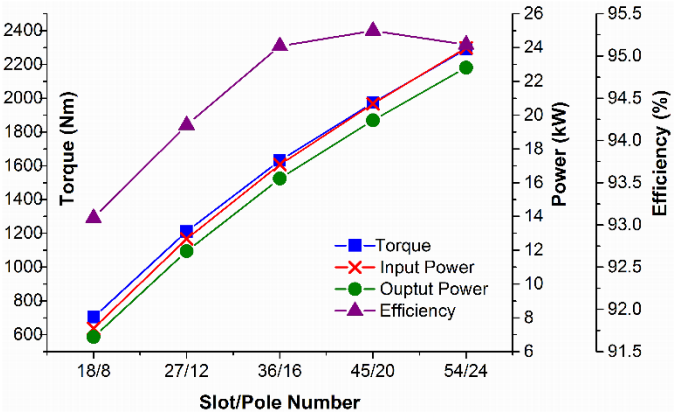

Figure 6-6. Average performance of surface mounted PMG with radial magnets and varying slot and pole number and slot-to-pole ratio.

6.3.1.5 Volume Reduction

Fixing parameters including the slot and pole number at 54 and 24 respectively (to give a slot-to-pole ratio of 2.25), additional design parameters which were identified to maximize average torque and average output power without sacrificing efficiency were employed in the surface mounted PMG design. These included the largest magnet angle allowable and a magnet thickness of 25 mm (Table 6-5). Upon combining these parameters in the design, the surface mounted PMG with radial magnets was able to produce average torque and average output power at more than twice the rated values (Table 6-4), and allow for reduction in the outer diameter and stack length of over 50% (Table 6-5).

Table 6-4. Average output of 10 kW surface mounted PMGs with radial magnets.

PMG Description	Torque (Nm)	Output Power (kW)	Input Power (kW)	Efficiency (%)
Base	1,085.914	10.528	11.372	92.58
Optimized	2,799.627	27.676	29.318	94.40
Reduced Volume	1,013.805	10.018	10.617	94.36

Table 6-5. Specifications of 10 kW surface mounted PMGs with radial magnets.

Specification	Optimized PMG	Reduced Volume PMG
Rated Power (kW)	10	10
Rated Torque (Nm)	954.927	954.927
Rated Speed (rpm)	100	100
Outer Diameter (mm)	833.33	321
Stack Length (mm)	1250	482
Airgap Length (mm)	1.62	0.626
Rotor Outer Diameter (mm)	458	177
Rotor Inner Diameter (mm)	339	131
Stator Outer Diameter (mm)	833.33	321
Stator Inner Diameter (mm)	462	178
Magnet Thickness (mm)	25	9.63
Magnet Angle (°)	15	15
Number of Poles	24	24
Number of Slots	54	54

6.3.2 Bread-loaf with embedded magnets

The 10 kW bread-loaf PMG with embedded magnets (Table 6-6) achieved greater than rated torque and power with no optimization (Table 6-2). The magnet thickness, magnet width, pole number, and slot-to-pole ratio were varied for this topology (Fig. 6-7).

Table 6-6. Specifications of a 10 kW bread-loaf PMG with non-embedded permanent magnets

Specifications	Value
Rated Power (kW)	10
Rated Torque (Nm)	954.927
Rated Speed (rpm)	100
Outer Diameter (mm)	833.33
Stack Length (mm)	1250
Airgap Length (mm)	1.62
Rotor Outer Diameter (mm)	458
Rotor Inner Diameter (mm)	319
Stator Outer Diameter (mm)	833.33
Stator Inner Diameter (mm)	462
Magnet Thickness (mm)	5.96
Magnet Width (mm)	50.1
Number of Poles	20
Number of Slots	24

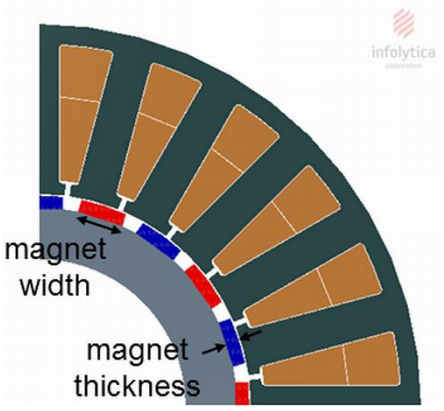

Figure 6-7. Quarter cross-section of bread-loaf PMG with embedded magnets.

6.3.2.1 Magnet Width

The magnet width was varied from 10 to 70 mm in increments of 6 mm. The average torque and average output power were found to increase linearly with increase in magnet width (Fig. 6-8). It should be noted that at 70 mm, the gap between magnets was

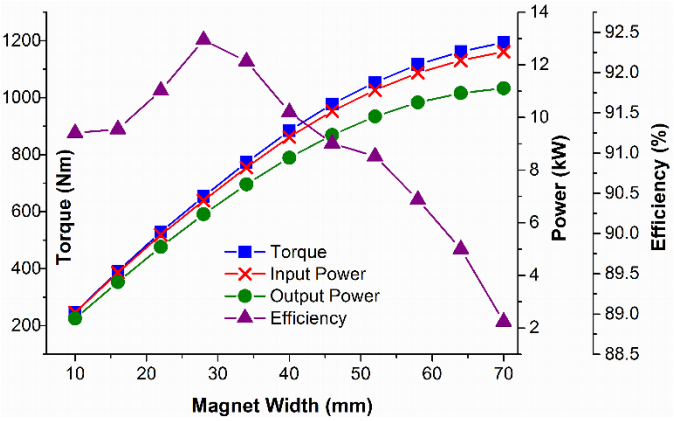

Figure 6-8. Average performance of bread-loaf PMG with non-embedded magnets and varying magnet width.

eliminated. The direct relationship between torque/output power and magnet width was attributed to the linear increase in magnetic loading with magnet width, due to the increased permanent magnet volume and consequently magnetic flux density over the rotor surface. A trade-off was again observed between increased torque and output power with efficiency. The average efficiency did not decrease linearly with magnet width, with the lowest average efficiency equal to 89% for a magnet width of 70 mm. At this magnet width, the gap between magnets was eliminated, ultimately altering the magnetic flux path between the rotor and stator, likely accounting for the decrease in efficiency.

6.3.2.2 Magnet Thickness

The magnet thickness was varied from 2 to 20 mm in increments of 2 mm. The average torque and average output power were found to increase in general with increased magnet thickness, although not linearly, with the highest torque and output power being achieved for 20 mm magnet thickness (Fig. 6-9). This result is expected because as the thickness of the magnet is increased, the overall permanent magnet volume is increased, providing more magnetic flux density to the PMG overall and contributing to higher torque. Magnetic loading was found to increase with magnet thickness. The magnetic loading at 4 mm magnet thickness and below was not sufficient to achieve

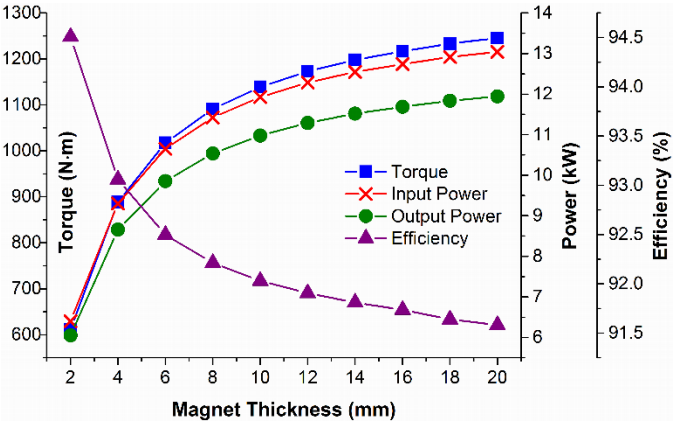

Figure 6-9. Average performance of bread-loaf PMG with non-embedded magnets and varying magnet thickness.

rated torque, while rated power was not achieved for magnet thicknesses below 6 mm. Furthermore a small trade-off was found to exist between output power and efficiency. The decrease is efficiency was not significant; the efficiency remained above 91% for all thicknesses investigated.

6.3.2.3 Pole Number

The pole number was varied from 4 to 28 in increments of 4 for a constant slot number of 27. Higher average torque and average output power was achieved for higher pole number in general (Fig. 6-10). The highest average torque and average output power was achieved for 12 poles, at a slot-to-pole ratio of 2.25. The average efficiency was reduced most significantly for 16 poles, but remained above 90% for all pole numbers investigated.

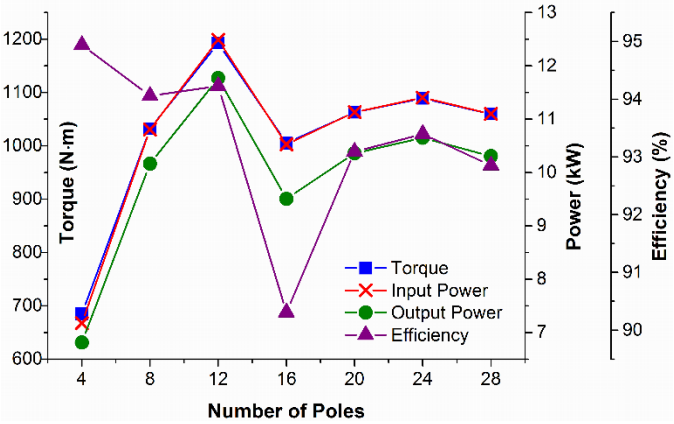

Figure 6-10. Average performance of bread-loaf PMG with non-embedded magnets and varying pole number and slot-to-pole ratio.

6.3.2.4 Slot-to-Pole Ratio

It was found that for a slot-to-pole ratio of 2.25, the torque and power achieved could be increased significantly (section 6.3.2.3). Other slot/pole combinations which gave a

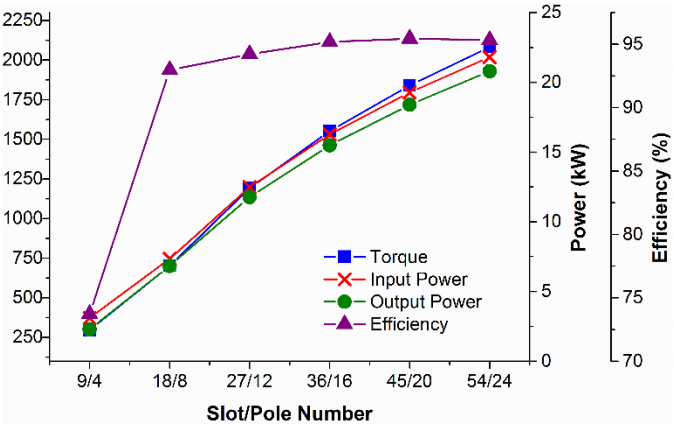

Figure 6-11. Average performance of bread-loaf PMG with non-embedded magnets and varying slot and pole number.

slot-to-pole ratio of 2.25 were investigated for the 10 kW bread-loaf PMG with non-embedded magnets. It was found that higher number of poles and slots achieved the highest average torque and average output power (Fig. 6-11). Average efficiency was not greatly affected by the change in slot/pole combination, remaining fairly constant at about 95% with the exception of the slot/pole combination 9/4. The magnetic loading was not sufficient for achievement of rated performance due to the low pole number.

6.3.2.4 Volume Reduction

Fixing parameters including the slot and pole number at 54 and 24 respectively (to give a slot-to-pole ratio of 2.25), additional design parameters which were identified to maximize average torque and average output power without sacrificing efficiency were employed in the surface mounted PMG design. Maximizing the magnet width (without eliminating the gap between magnets) was found to increase torque and output power more significantly than for maximizing magnet thickness. Thus, the magnet width was first maximized and then the magnet thickness increased appropriately (Table 6-8). Upon combining these parameters in the design, the bread-loaf PMG with non-embedded magnets was able to produce average torque and average output power at more than twice the rated values (Table 6-7), and allow for reduction in the outer diameter and stack length of over 50% (Table 6-8).

Table 6-7. Average output of 10 kW bread-loaf PMGs with non-embedded magnets.

PMG Description	Torque (Nm)	Output Power (kW)	Input Power (kW)	Efficiency (%)
Base	1,015.220	10.631	9.873	92.87
Optimized	2,013.539	20.197	21.086	95.78
Reduced Volume	1,016.324	10.037	10.643	94.30

Table 6-8. Specifications of 10 kW bread-loaf PMGs with non-embedded magnets.

Specification	Optimized PMG	Reduced Volume PMG
Rated Power (kW)	10	10
Rated Torque (Nm)	954.927	954.927
Rated Speed (rpm)	100	100
Outer Diameter (mm)	833.33	316
Stack Length (mm)	1250	474
Airgap Length (mm)	1.62	0.616
Rotor Outer Diameter (mm)	458	174
Rotor Inner Diameter (mm)	339	128
Stator Outer Diameter (mm)	833.33	316
Stator Inner Diameter (mm)	462	175
Magnet Thickness (mm)	5	7.58
Magnet Width (mm)	59	20.9
Number of Poles	24	24
Number of Slots	54	54

6.3.3 Inset magnets

The 10 kW PMG with inset magnets or “inset PMG” (Table 6-9) achieved greater than rated torque and power with no optimization (Table 6-2). The magnet thickness, magnet angle, magnet inset depth/thickness, pole number, slot number, and slot-to-pole ratio were varied for this topology (Fig. 6-12).

Table 6-9. Specifications of a 10 kW inset PMG.

Specification	Value
Rated Power (kW)	10
Rated Torque (Nm)	954.927
Rated Speed (rpm)	100
Outer Diameter (mm)	833.33
Stack Length (mm)	1250
Airgap Length (mm)	1.62
Rotor Outer Diameter (mm)	458
Rotor Inner Diameter (mm)	319
Stator Outer Diameter (mm)	833.33
Stator Inner Diameter (mm)	462
Magnet Thickness (mm)	14
Magnet Angle (°)	12
Magnet Inset Depth (mm)	0.943
Number of Poles	20
Number of Slots	24

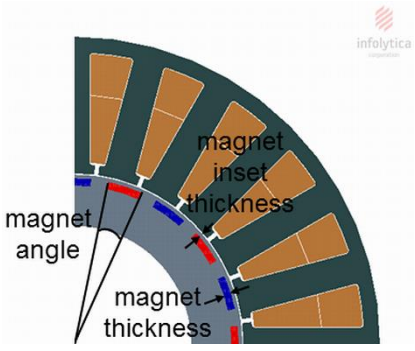

Figure 6-12. Quarter cross-section of inset PMG.

6.3.3.1 Magnet Angle

The magnet angle was varied from 6 to 16 degrees in increments of 2 degrees. The average torque and average output power were found to increase linearly with magnet angle, while the efficiency decreased linearly with magnet angle (Fig. 6-13).

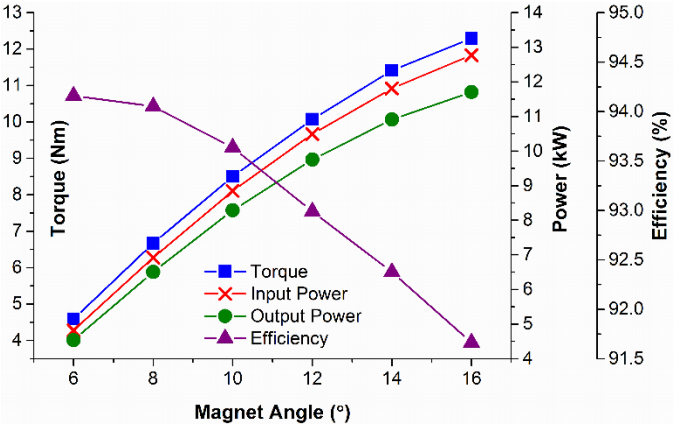

Figure 6-13. Average performance of inset PMGs with radial magnets and varying magnet angle.

However, average efficiency still remained above 91% on average at rated speed, so the trade-off was not significant. The magnetic loading was also found to increase with magnet angle, though not linearly. At 16°, the magnet angle achieved the highest torque and output power. At this angle, a gap still existed between the magnets; it was found that for elimination of this gap (18°), the finite element solution could not be found.

6.3.3.2 Magnet Thickness

The magnet thickness was varied from 10 to 50 mm in increments of 10 mm. Above 20 mm, the increase in the magnet thickness had little effect on the average torque, average output power and average efficiency achieved in the PMG with inset magnets (Fig. 6-14). The increase in permanent magnet volume in the inset permanent magnet

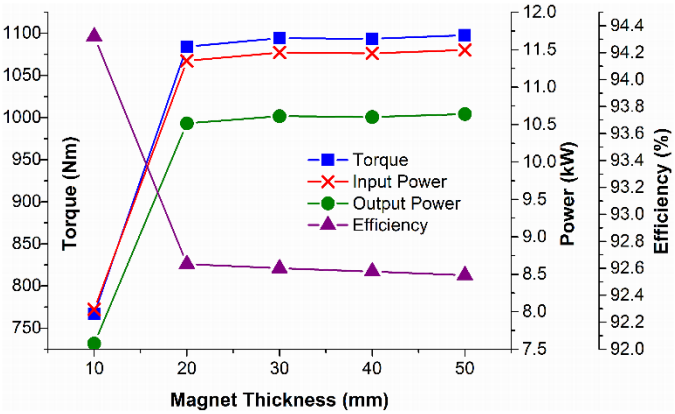

Figure 6-14. Average performance of inset PMGs with radial magnets and varying magnet thickness.

thickness resulted in permanent magnet volume increase inside the rotor back-iron rather than on the rotor surface like for the surface mounted or bread-loaf topologies. Thus, the magnetic loading was not directly increased. The additional magnetic flux density provided by the increase in permanent magnet volume in the inset PMG was likely lost as magnetic flux leakage in the rotor back-iron since the permeability of the back-iron is much higher than that of the airgap.

6.3.3.3 Magnet Inset Depth

The magnet inset depth was varied from 0 to 1.5 mm in increments of 0.5 mm. 10mm was also investigated. It was found that the torque and output power were maximized for 0 mm magnet inset depth where the magnets were closest to the rotor surface (Fig. 6-15). For any significant increase in magnet inset depth (>10 mm), the average torque and average output power produced were well below the rated values. This result is intuitive. If the distance between the magnet flux source (permanent magnets) and the stator are increased, the magnetic field strength in the airgap will be weakened.

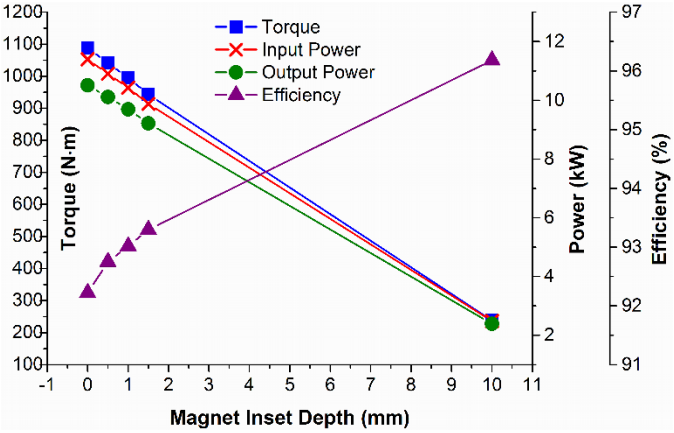

Figure 6-15. Average performance of inset PMGs with radial magnets and varying magnet inset depth.

6.3.3.4 Slot and Pole Number

The numbers of slots and poles were varied. The slot number was varied at 21, 27, 33 and 39 slots. For each of these slot numbers the pole number was varied from 8 to

32 in increments of 6. It was found that for constant slot number, there was no trend between increased pole number and average torque or average output power (Fig. 6-16a and Fig. 6.16b). For constant pole number, an increase in the slot number clearly increased the average torque and average output power. Average efficiency was above 91% regardless of the slot and pole number, and no trend was apparent (Fig. 6-16c). In terms of maximizing efficiency, torque and output power, the best slot and pole combination was 39 slots and 14 poles.

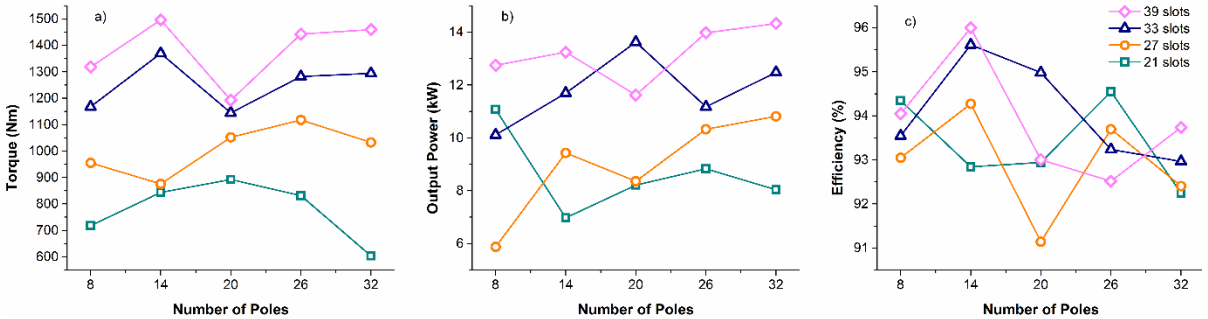

Figure 6-16. Average performance of inset PMGs with radial magnets and varying slot and pole number.

6.3.3.5 Slot-to-Pole Ratio

Slot/pole combinations which gave a slot-to-pole ratio of 2.25 were investigated for the 10 kW inset PMGs. It was found that in general, for high slot and pole number, average torque and average output power were increased, agreeing with previous results (Fig. 6-17). Average efficiency was also found to increase for higher slot and pole number, remaining above 92% for all cases studied.

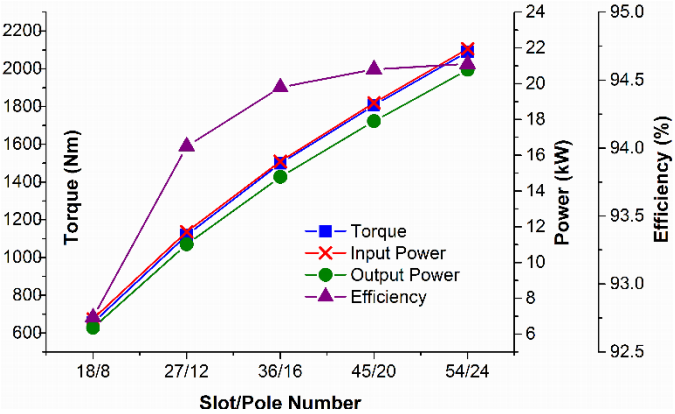

Figure 6-17. Average performance of inset PMGs with radial magnets and varying slot and pole number.

6.3.3.6 Volume Reduction

Fixing parameters including the slot and pole number at 54 and 24 respectively (to give a slot-to-pole ratio of 2.25), additional design parameters which were identified to maximize average torque and average output power without sacrificing efficiency were employed in the inset PMG. Maximizing the magnet angle (without eliminating the gap between magnets) was found to increase torque and output power more significantly than for maximizing magnet thickness. Thus, the magnet width was first maximized and then the magnet thickness increased appropriately (Table 6-11). Additionally, an inset magnet depth of 0 mm was used. Upon combining these parameters in the design, the inset PMG was able to produce average torque and average output power at more than twice the rated values (Table 6-10), and allow for reduction in the outer diameter and stack length of over 50% (Table 6-11).

Table 6-10. Average output of 10 kW inset PMGs.

PMG Description	Torque (Nm)	Output Power (kW)	Input Power (kW)	Efficiency (%)
Base	982.287	10.286	9.599	93.31
Optimized	2,765.790	27.358	28.963	94.46
Reduced Volume	1,023.768	10.126	10.721	94.45

Table 6-11. Specifications of 10 kW inset PMGs.

Specification	Optimized PMG	Reduced Volume PMG
Rated Power (kW)	10	10
Rated Torque (Nm)	954.927	954.927
Rated Speed (rpm)	100	100
Outer Diameter (mm)	833.33	330
Stack Length (mm)	1250	495
Airgap Length (mm)	1.62	0.644
Rotor Outer Diameter (mm)	458	181
Rotor Inner Diameter (mm)	273	134
Stator Outer Diameter (mm)	833.33	330
Stator Inner Diameter (mm)	462	183
Magnet Thickness (mm)	20	7.92
Magnet Angle (°)	24	14
Magnet Inset Depth (mm)	0	0
Number of Poles	24	24
Number of Slots	54	54

6.3.4 Spoke with embedded magnets

The 10 kW PMG with embedded spoke magnets or “spoke PMG” (Table 6-12) achieved greater than rated torque and power with no optimization (Table 6-2). The magnet thickness, magnet width, magnet outer gap thickness, pole number, and slot-to-pole were varied for this topology (Fig. 6-18).

Table 6-12. Specifications of a 10 kW spoke PMGs.

Specification	Value
Rated Power (kW)	10
Rated Torque (Nm)	954.927
Rated Speed (rpm)	100
Outer Diameter (mm)	833.33
Stack Length (mm)	1250
Airgap Length (mm)	1.62
Rotor Outer Diameter (mm)	458
Rotor Inner Diameter (mm)	319
Stator Outer Diameter (mm)	833.33
Stator Inner Diameter (mm)	462
Magnet Thickness (mm)	11
Magnet Width (mm)	32.4
Magnet Outer Gap Width (mm)	3.09
Number of Poles	20
Number of Slots	24

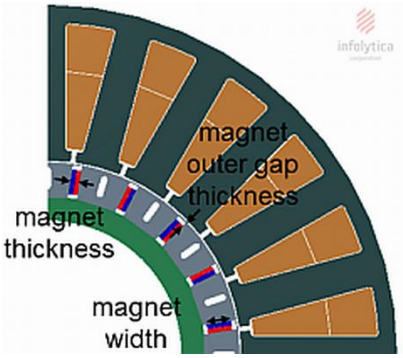

Figure 6-18. Quarter cross-section of a spoke PMG with embedded magnets.

6.3.4.1 Magnet Width

The magnet width was varied from 10 to 70 mm in increments of 10 mm. The average torque and average output power were found to increase linearly with increase in magnet width, while the average efficiency was found to decrease linearly (Fig. 6-19), though the trade-off was not significant as the average efficiency was not reduced significantly. Again, the increased permanent magnet volume contributed to the increase in torque and output power by providing additional magnetic flux density at the rotor surface, thereby increasing the magnetic loading.

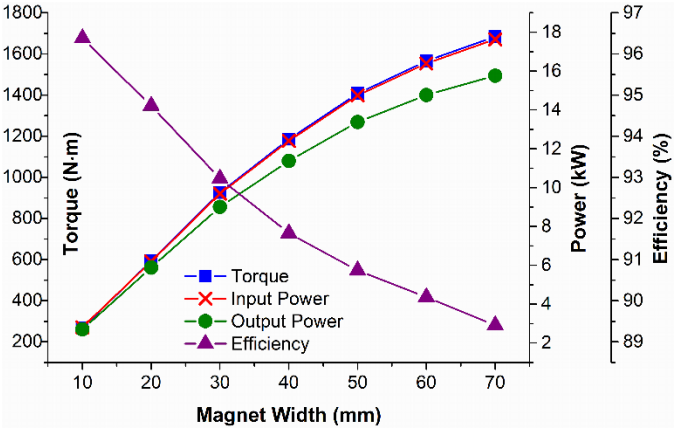

Figure 6-19. Average performance of spoke PMGs with embedded permanent magnets and varying magnet width.

6.3.4.2 Magnet Thickness

The magnet thickness was varied from 10 to 50 mm in increments of 10 mm. The average torque and average output power were found to increase in general from 10 to 40 mm (Fig. 6-20); at a magnet thickness of 50mm, the average torque and average output power decreased with respect to a magnet thickness of 30 and 40 mm, demonstrating

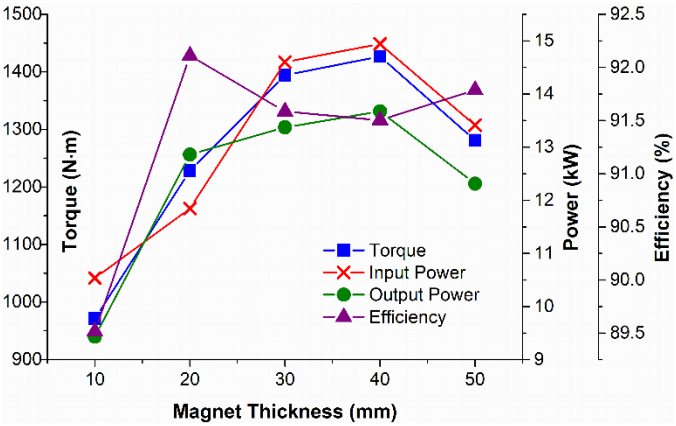

Figure 6-20. Average performance of spoke PMGs with embedded permanent magnets and varying magnet thickness.

that the increase in permanent magnet volume was not beneficial and again the geometry of the permanent magnet played a role in the performance of the PMG. Average efficiency did not vary greatly with magnet thickness.

6.3.4.3 Magnet Outer Gap Width

The magnet outer gap width was varied from 1 to 5 mm in increments of 0.5 mm. The average torque and average output power were found to increase linearly with increased magnet outer gap width from 1 to 4.5 mm (Fig. 6-21), while the average efficiency was found to decrease linearly for this range. For magnet outer gap width above 5 mm, the permanent magnet volume was decreased too substantially to allow for achievement of rated torque or power.

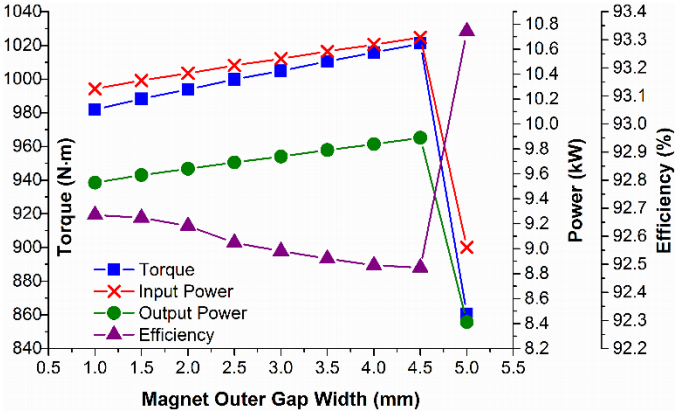

Figure 6-21. Average performance of spoke PMGs with embedded permanent magnets and varying magnet outer gap width.

6.3.4.4 Pole Number

For a constant slot number of 27 the pole number was varied at 8, 12, 14, 20 and 26 poles. No trend was observed between the pole number and the average torque, output power or efficiency (Fig. 6-22), demonstrating

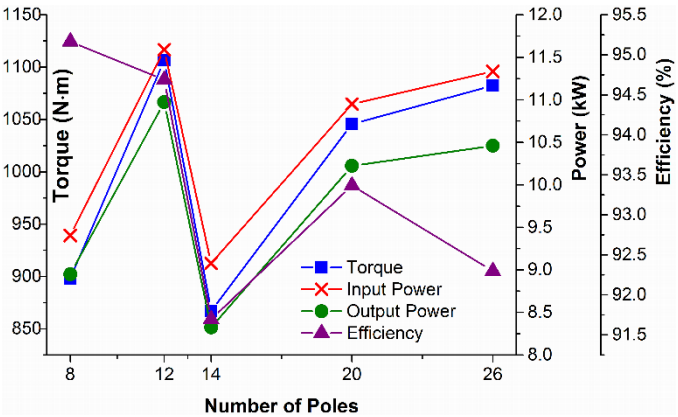

Figure 6-22. Average performance of spoke PMGs with embedded permanent magnets and varying pole number and slot-to-pole ratio.

once again that the slot-to-pole ratio played an important role in the performance of the PMG by contributing to the magnetic flux path between the rotor and stator.

6.3.4.5 Slot-to-Pole Ratio

Slot/pole configurations which gave a slot-to-pole ratio of 2.25 were investigated. For higher slot and pole number, higher average torque and average output power were achieved (Fig. 6-23). The average efficiency was also found to increase slightly with slot and pole number.

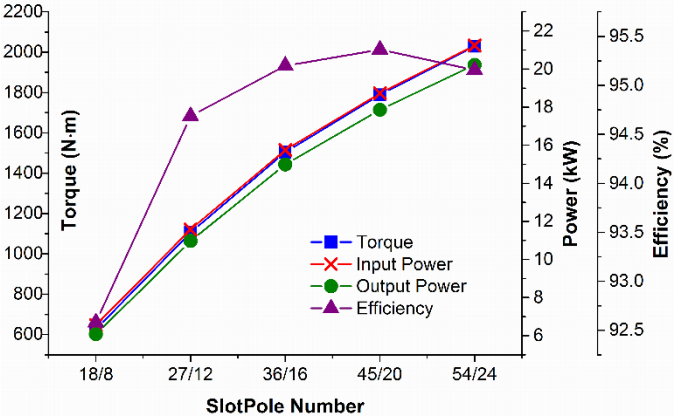

Figure 6-23. Average performance of spoke PMGs with embedded permanent magnets and varying slot and pole number.

6.3.4.6 Volume Reduction

Fixing parameters including the slot and pole number at 54 and 24 respectively (to give a slot-to-pole ratio of 2.25), additional design parameters which were identified to maximize average torque and average output power without sacrificing efficiency were employed in the inset PMG. Maximizing the magnet width was found to increase torque and output power more significantly than for maximizing magnet thickness. Thus, the magnet width was first maximized and then the magnet thickness increased appropriately (Table 6-14). Additionally, a magnet outer gap thickness of 4.5 mm was used. Upon combining these parameters in the design, the spoke PMG was able to produce average torque and average output power at more than twice the rated values

(Table 6-13), and allow for reduction in the outer diameter and stack length of over 50% (Table 6-14).

Table 6-13. Average output of 10 kW spoke PMGs.

PMG Description	Torque (Nm)	Output Power (kW)	Input Power (kW)	Efficiency (%)
Base	991.189	10.380	9.624	92.72
Optimized	3,300.144	32.342	34.559	93.59
Reduced Volume	1,024.158	10.069	10.725	93.88

Table 6-14. Specifications of 10 kW spoke PMGs.

Specification	Optimized PMG	Reduced Volume PMG
Rated Power (kW)	10	10
Rated Torque (Nm)	954.927	954.927
Rated Speed (rpm)	100	100
Outer Diameter (mm)	833.33	300
Stack Length (mm)	1250	450
Airgap Length (mm)	1.62	0.585
Rotor Outer Diameter (mm)	458	165
Rotor Inner Diameter (mm)	320	111
Stator Outer Diameter (mm)	833.33	300
Stator Inner Diameter (mm)	462	166
Magnet Thickness (mm)	30	12.2
Magnet Width (mm)	64	23
Magnet Outer Gap Width (mm)	4.5	1.62
Number of Poles	24	24
Number of Slots	54	54

6.3.5 Surface mounted with parallel magnets

The 10 kW surface mounted PMG with parallel magnets (Table 6-15) achieved greater than rated torque and power with no optimization (Table 6-2). The magnet thickness, magnet angle, pole number, slot number, and slot-to-pole ratio were varied for this topology (Fig. 6-24).

Table 6-15. Specifications of a 10 kW surface mounted PMG with parallel magnets.

Specification	Value
Rated Power (kW)	10
Rated Torque (Nm)	954.927
Rated Speed (rpm)	100
Outer Diameter (mm)	833.33
Stack Length (mm)	1250
Airgap Length (mm)	1.62
Rotor Outer Diameter (mm)	458
Rotor Inner Diameter (mm)	319
Stator Outer Diameter (mm)	833.33
Stator Inner Diameter (mm)	462
Magnet Thickness (mm)	9.23
Magnet Width (mm)	53.7
Number of Poles	20
Number of Slots	24

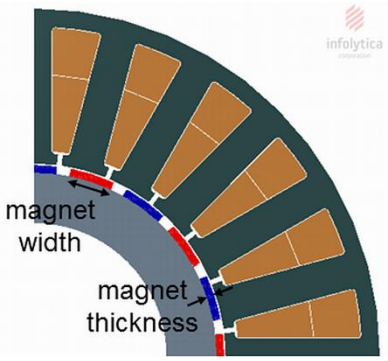

Figure 6-24. Quarter cross-section of surface mounted PMG with parallel magnets.

6.3.5.1 Magnet Width

The magnet width was varied from 10 mm to 70 mm in increments of 6 mm. From 10 mm to 64 mm, the torque and output power were found to increase linearly with increase in magnet width, while the efficiency was found to decrease linearly (Fig. 6-25).

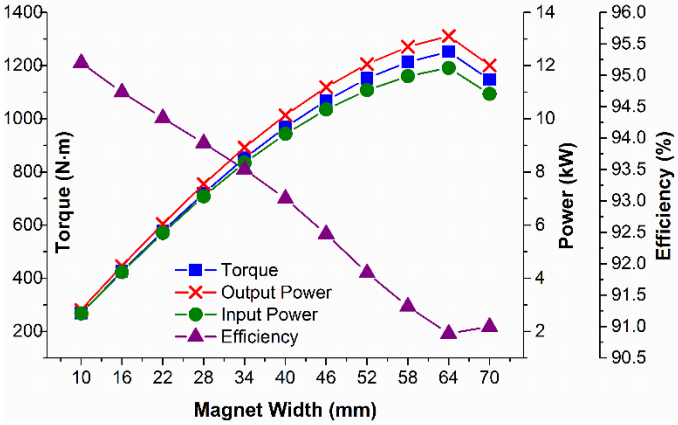

Figure 6-25. Average performance of surface mounted PMGs with parallel magnets varying magnet width.

At 70 mm, the torque and output power decreased slightly and the efficiency increased slightly; at this width, the gap between permanent magnets was almost eliminated, likely accounting for the slight degradation in performance with respect to a magnet width of 60 mm.

6.3.5.2 Magnet Thickness

The magnet thickness was varied from 5 mm to 50 mm in increments of 5 mm. The variation in magnet thickness was found to have little effect on the performance of the surface mounted PMG with parallel magnets (Fig. 6-26). Magnetic loading was found to increase linearly with increase in magnet thickness, due to the increase in permanent magnet volume, and thus the increase in magnetic flux density. A magnet thickness of 30 mm was found to give the highest torque and output power.

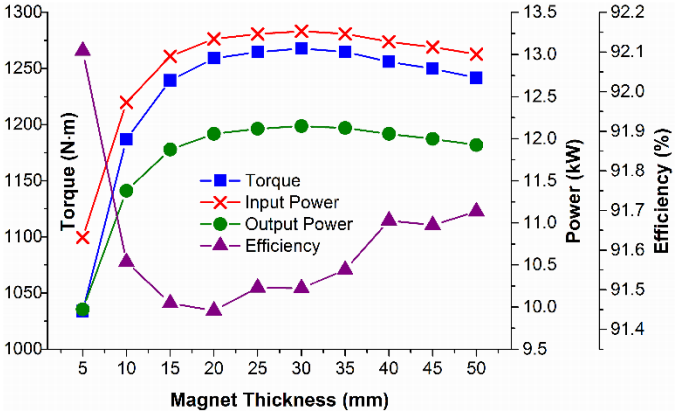

Figure 6-26. Average performance of surface mounted PMGs with parallel magnets varying magnet thickness.

6.3.5.3 Slot and Pole Number

The pole number was varied from 8 to 38 poles in increments of 6 poles for a constant slot number of 24. The pole number was also varied from 4 to 28 poles in increments of 4 poles for a constant slot number of 27. For a constant slot

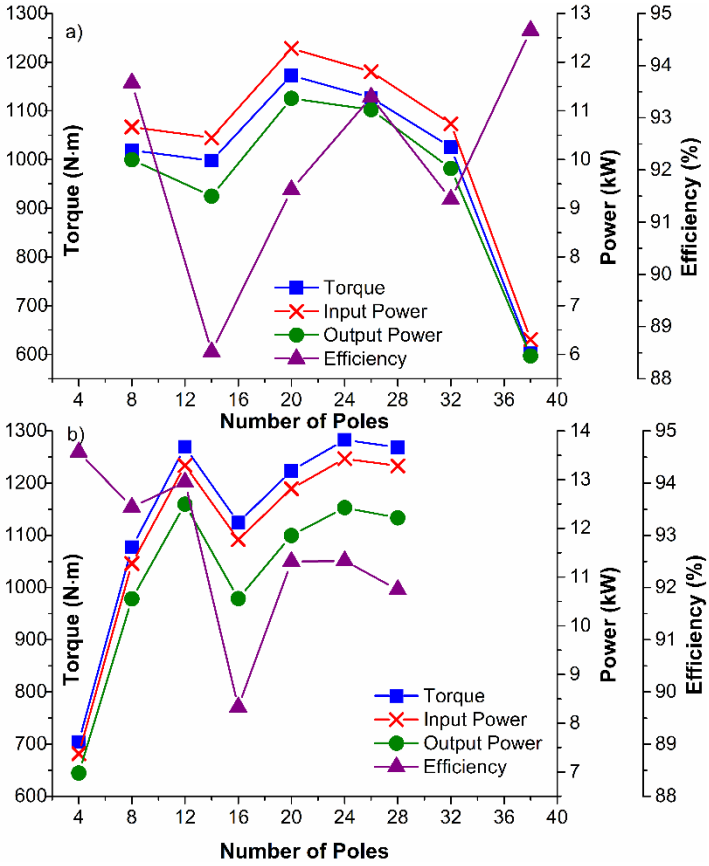

Figure 6-27. Average performance of surface mounted PMGs with parallel magnets pole number and slot-to-pole ratio for a) 24 slots and b) 27 slots.

number of 24, increasing pole number did not increase average torque and output power in general (Fig. 6.27a), while for a constant slot number of 27, increase in pole number did increase average torque and power in general. Comparing the two slot number studies, the higher slot number seemed to contribute overall to greater achievement of torque and power for the same pole number. This once again demonstrates the importance of slot-to-pole ratio over simply choosing more slots and poles in the PMG design.

6.3.5.4 Slot-to-Pole Ratio

For a constant slot-to-pole ratio of 2.25, varying slot and pole numbers were investigated. Consistent with all previous results, the average torque and output power were found to increase for high slot and pole number (Fig. 6-28). Average efficiency was slightly improved for high pole and slot number as well.

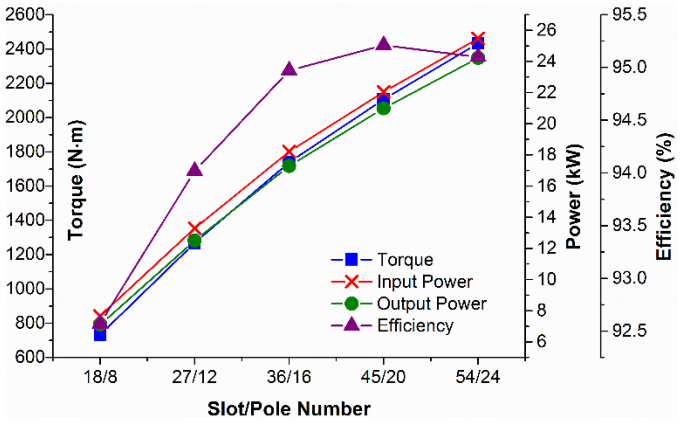

Figure 6-28. Average performance of surface mounted PMGs with parallel magnets varying slot and pole number.

6.3.5.5 Volume Reduction

Fixing parameters including the slot and pole number at 54 and 24 respectively (to give a slot-to-pole ratio of 2.25), additional design parameters which were identified to maximize average torque and average output power without sacrificing efficiency were employed in the surface mounted PMG with parallel magnets. Maximizing the magnet

width (without eliminating the gap between magnets) was found to increase torque and output power more significantly than for maximizing magnet thickness. Thus, the magnet width was first maximized and then the magnet thickness increased appropriately (Table 6-17). Upon combining these parameters in the design, the surface mounted PMG with parallel magnets was able to produce average torque and average output power at more than twice the rated values (Table 6-16), which allows for reduction in the outer diameter and stack length of over 50% (Table 6-17).

Table 6-16. Average output of 10 kW surface mounted PMGs with parallel magnets.

PMG Description	Torque (Nm)	Output Power (kW)	Input Power (kW)	Efficiency (%)
Base	1,169.363	11.259	12.246	91.95
Optimized	2,804.320	27.733	29.367	94.44
Reduced Volume	1,041.661	10.317	10.908	94.58

Table 6-17. Specifications of 10 kW surface mounted PMGs with parallel magnets.

Specification	Optimized PMG	Reduced Size PMG
Rated Power (kW)	10	10
Rated Torque (Nm)	954.927	954.927
Rated Speed (rpm)	100	100
Outer Diameter (mm)	833	330
Stack Length (mm)	1,250	495
Airgap Length (mm)	1.62	0.644
Rotor Outer Diameter (mm)	458	181
Rotor Inner Diameter (mm)	339	134
Stator Outer Diameter (mm)	833	330
Stator Inner Diameter (mm)	462	183
Magnet Thickness (mm)	14	5.54
Magnet Width (mm)	24	21.4
Number of Poles	24	24
Number of Slots	54	54

6.3.6 Comparison of Results

Several permanent magnet topologies allowed for reduction in the overall volume of the 10 kW PMG base model (Table 6-18). By increasing the number of poles and slots in the PMG and choosing an appropriate slot-to-pole ratio, significant reduction in the

PMG volume and permanent magnet volume with respect to the base model was possible. Insights were gained into the benefits of varying the permanent magnet topology. The spoke permanent magnet topology achieved the greatest reduction in the outer diameter and stack length with the highest torque density of all the permanent magnet topologies, but required the most permanent magnet volume to generate rated torque (955 Nm) and output power (10 kW) as shown in Table 6-18. In the surface mounted permanent magnet topology, radial magnets produced a slightly higher torque density than the parallel magnets, but requested significantly more permanent magnet volume to achieve this and provided only one millimeter additional reduction in the outer diameter and stack length. The bread-loaf magnet topology generated a higher torque density than either surface mounted permanent magnet topology, allowing for greater PMG volume reduction, although requiring more permanent magnet volume than the surface mounted PMG with parallel magnets.

Table 6-18. 10 kW PMGs dimensions with varying permanent magnet topology.

PMG Description	Outer Diameter (mm)	Stack Length (mm)	Airgap Length (mm)	PM Volume (cm^3)	Torque Density (m^3)
Base Model	833	1,250	1.62	11,135.068	5,776.183
Surface mounted with radial magnets	321	482	0.626	2,228.197	85,481.311
Bread-loaf with non-embedded magnets	316	474	0.616	1,802.209	90,170.711
Surface mounted with parallel magnets	322	483	0.628	1,310.696	85,322.593
Inset magnets	330	495	0.644	1,897.587	80,380.233
Spoke magnets	300	450	0.585	3,030.480	106,437.992

No topology offered a particular benefit over the others in terms of average efficiency, with all topologies achieving 94% average efficiency at rated speed. While the spoke PMG did allow for the greatest reduction in PMG volume, it also had the highest

cogging torque of all the permanent magnet topologies investigated (Fig. 6-29). The permanent magnet topology itself contributed to the cogging torque. The magnetic flux density distribution over the rotor surface was compared for the spoke and inset PMGs in Fig. 6-30. While the spoke PMG did achieve significantly higher peak magnetic flux density at its rotor surface than the inset PMG, the extreme variation of the magnetic flux density contributed to significant cogging torque. In contrast, the uniformity of the magnet flux density distribution of the inset PMG contributed to cogging torque with an amplitude of less than 1% of the rated torque.

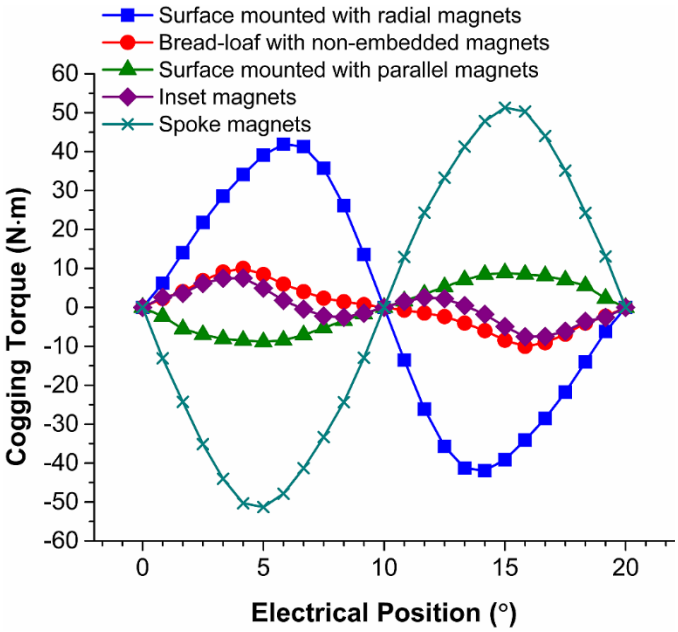

Figure 6-29. Cogging torque of 10 kW PMGs with varying permanent magnet topology.

The effect extreme variation of the magnetic flux density over the rotor surface of the spoke PMG was also apparent the in magnetic loading. Though the peak magnetic flux density of the spoke PMG was significantly higher than for the inset PMG, the minimum magnetic flux density of the spoke PMG was also significantly

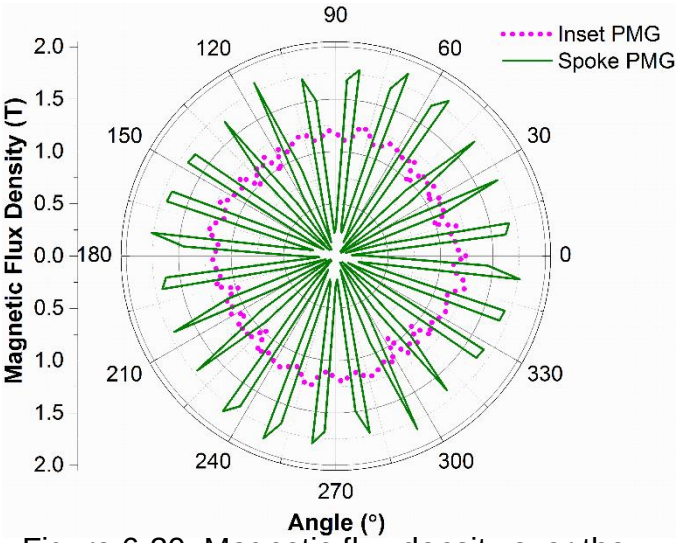

Figure 6-30. Magnetic flux density over the rotor surface of 10 kW PMGs with varying permanent magnet topology.

lower than for the inset PMG. This accounted for the lower magnetic loading of the spoke PMG than the inset PMG (Table 6-19).

Table 6-19. Magnetic loading of 10 kW PMGs with varying permanent magnet topology.

PMG Description	Magnetic Loading (T)
Surface mounted with radial magnets	1.093
Bread-loaf with non-embedded magnets	1.136
Surface mounted with parallel magnets	1.097
Inset magnets	1.139
Spoke magnets	0.915

6.4 Conclusions

By varying the permanent magnet topology of a 10 kW PMG with interior rotor, insights were gained into the relative advantages and disadvantages of each topology. It was demonstrated that the spoke topology produced the highest magnetic flux density and torque density, allowing for the greatest reduction in PMG volume. However, the topology of the spoke permanent magnets in the rotor back-iron contributed to large variation in the magnetic flux density over the rotor surface, ultimately contributing to significant cogging torque relative to the other topologies. The bread-loaf topology was found to be the most desirable of the topologies considered, achieving the second largest reduction in the outer diameter and stack length with significantly less permanent magnet volume and low cogging torque. Additionally, it was demonstrated through varying design parameters that the slot-to-pole ratio plays a significant role in the achievement of additional torque and output power in PMGs by shaping the path of magnetic flux between the rotor and stator. High pole and slot number were found to be desirable at an appropriate slot-to-pole ratio. Finally, it was found that increasing

magnet width (or angle) was more effective than increasing magnet thickness in increasing torque and power because the magnetic flux density over the rotor surface was directly increased, making the geometry of the permanent magnet as important as the increase in permanent magnet volume.

CHAPTER 7. ENVIRONMENTAL, SOCIAL AND POLITICAL BARRIERS TO LEGISLATIVE STRATEGY FOR LONG-TERM SUSTAINABLE SUPPLY OF RARE EARTHS

7.1 Abstract

Rare earth elements are critical to renewable energy technologies such as permanent magnet generators employed in direct-drive wind turbines. Such technology is vital to the development of offshore wind turbines in the U.S. The U.S. currently has no existing stockpiles of rare earths, limited domestic production, and no legislative strategies to ensure a sustainable long term supply of rare earths. An investigation has been conducted to determine why the U.S. congress has not taken legislative action regarding its rare earth supply. It was determined that high environmental and social costs of rare earth production, lack of public awareness, and political party divides have contributed to the lack of legislative action. Finally, through deeper investigation, it was determined that Congress has been able to support the R&D approaches recommended by the DOE in the *Critical Materials Strategy* to develop recycling techniques, substitutes and improved stewardship of critical materials through appropriations bills.

7.2 Introduction

Direct-drive permanent magnet generators (DDPMGs) rely on imported rare earth NdFeB permanent magnets that are associated with serious social and environmental costs. A background on rare earth elements is given in section 2.3.1. This dependence on rare earths raises important questions regarding the U.S. strategy for securing a long

term sustainable supply of these elements, which are not only vital to renewable energy technologies such as wind turbines and hybrid/electric vehicles, but to everyday modern technologies such as cell phones and computers.

The U.S. was the leading producer of rare earths in the 1980s, producing enough rare earths to be self-sufficient. Currently, the U.S. has no active rare earth mines (Molycorp Inc. ceased operations at the Mountain Pass mine in 2015 [59]) and relies heavily on imports. In 2015, an estimated 85% of all rare earths were mined in China [60]. Chinese facilities currently produce about 86% of NdFeB permanent magnets and the rare earth oxides used to produce them. Following the “rare earths crisis” in 2011 (discussed in section 7.3.1), prices have stabilized. A possible contributing factor to the rare earths crisis was export quotas and tariffs placed on rare earths by Chinese policy makers. Though the World Trade Organization (WTO) has ruled that these policies violated international trade laws, and the Chinese government has agreed to end these practices [35], the majority of rare earths are still mined and produced in China. This makes U.S. industry heavily dependent on a single supply source for imported rare earths, with 71% of imported rare earths coming from Chinese producers from 2011 to 2014 [60]. This may have contributed to the U.S. wind industry’s aversion to DDPMGs.

According to the U.S. Department of Energy (DOE), wind turbines greater than 2.5 MW are more likely to use DDPMGs [10]; thus, the dependence of the U.S. wind industry on rare earth permanent magnets is likely to increase in the future. According to the *Critical Materials Strategy* by the DOE, the NdFeB permanent magnets used in renewable energy technologies are dependent on “critical materials” (Nd and Dy), which are associated with short-term and long-term supply risks. In this report, the DOE states

that the U.S. should pursue a three pillar strategy heavily based on R&D: diversifying supply, developing substitutions, and improved stewardship of materials use [10].

Though R&D is being actively pursued by the DOE and supported by Congress, the U.S. has no existing stockpiles of rare earths, limited domestic mining and production, and no enacted legislation to ensure a sustainable long term supply of rare earths. In this Chapter, we consider why the U.S. Congress has not been more proactive in pursuing legislative solutions to what the Department of Defense (DoD) has identified as an issue of national security [61], and investigate what actions have been taken to follow the recommendations of the DOE. To assess this, a literature review was conducted, content analysis of popular media coverage on the topic of rare earths was performed, rare earth legislation and corresponding congressional voting trends were analyzed, and appropriations bills were investigated. It was found that while no legislation has been enacted through Congress to support the three pillars set forth by the DOE, appropriations bills have been passed as part of the annual budget to support R&D efforts aligned with the DOE's *Critical Materials Strategy*. Furthermore, it was found that the lack of enacted legislation is due in part to high social and environmental costs associated with rare earth product, lack of public awareness and political party divides. Based on these findings, a set of recommendations was developed, aimed to create a more sustainable supply of rare earths in the short-term and reduce dependence of the wind industry on rare earth magnets in the long-term. These recommendations include continued research and development into recycling and

substitutes, practicing environmental justice[2] in domestic or foreign mine development as well as financial transactions with Chinese industry, federal subsidies for domestic rare earth mines, and finally a public awareness campaign reframed as domestic economic development.

7.3 Background

7.3.1 The Rare Earth Crisis

Worldwide, rare earths are primarily mined and produced in China [60]. After the discovery of rare earths in China, production was increased by 40% between 1978 and 1989. The increased production in China increased the supply of rare earth oxides worldwide, which reduced prices. Many producers in the U.S. could not compete with the low market prices and limited production or closed altogether. This eventually contributed to the closure of all U.S. rare earth mining and production facilities [62].

In 2011, during what is referred to as the “rare earth crisis,” rare earth prices increased up to six times their previous prices [63]. For example, from 2010 to 2011, the price of Nd-oxide increased from $108 to $245 per kg, while the price of Dy-oxide increased by 200% during this same period, costing $1200 per kg in 2011 [8]. Chinese policies of export quotas and tariffs may have contributed to this price increase.

During this time of concern about rare earth prices by governments in the U.S., E.U., Canada and Japan, a political dispute between China and Japan heightened this concern. Japanese and Chinese governments both claim ownership of fishing waters

[2] Environmental justice is a social framework in which the enforcement of environmental regulations or policies should impact all people equally without regard for income, race or ethnicity [113].

near the Senkaku Islands. In these disputed waters, Japanese coast guards apprehended a Chinese fisherman who crossed into Japanese waters in 2011. In response, the Chinese government unofficially cut-off all rare earths exports to Japanese buyers for four months [63].

Though the WTO has ruled that export quotas and tariffs imposed by Chinese policy makers violated international law and the Chinese government has agreed to remove them [35], the U.S. government remains concerned about the long-term supply of rare earths.

7.3.2 Current U.S. Policy & Strategy

U.S. government concern about domestic supply of rare earths heightened after the rare earths crisis in 2011. The DOE recommended the U.S. government develop a strategy based on three pillars: diversifying supplies, developing substitutes and improved stewardship of material use [10]. To diversify supplies Molycorp Inc. reopened one rare earth mine in Mountain Pass, California. One hope was that reopening this mine would reduce U.S. dependence on imports in 2012. From 2012 to 2013, annual mine production in the U.S. increased from 800 to 4,000 tons. This contributed to a decrease in the value of imported rare earths of an estimated $259 million [64]. In 2013, exploration into the development of mines in 10 additional states was being conducted in the U.S. However, by May 2015, Molycorp Inc. filed for bankruptcy and ceased mining operations in October 2015 [59]. One contributing factor to this was the decline in prices of rare earths after the rare earth crisis. Furthermore, predicted shortages of rare earths did not come true as demand for rare earths decreased worldwide [65].

There have been considerable congressional efforts to address the concern of long-term supply of rare earths in response to the DOE's *Critical Materials Strategy*. In terms of legislations, 21 bills were introduced between 2010 and July 2015 regarding this issue, though no bills were enacted as legislation. However, to support the heavily focused R&D approach recommended by the DOE, Congress has funded R&D activities to develop substitutes[3] and improve stewardship of materials (e.g. recycling and improvement of production processes) through passing of appropriations bills. One example of this is the Rare Earth Alternatives in Critical Technologies (REACT) program, funded by the Advanced Research Projects Agency-Energy (ARPA-E), in which funding was awarded to research projects to investigate development of substitutes for critical materials [66]. One such project was awarded to Ames Laboratory to investigate the use of Ce as a substitute for Dy in NdFeB permanent magnets for electric vehicle motors. Ames Laboratory has demonstrated substitution of Ce for Dy in high temperature NdFeB permanent magnets at the laboratory scale [46].

It is also worth noting that the U.S. DoD issued a *Strategic and Critical Materials 2013 Report on Stockpile Requirements* in which the DoD recommend the following rare earths be stockpiled: Dy, Y, Er, Tb, Tm and Sc [61]. The U.S. government currently has no existing stockpile of rare earths [64]. However, in Sec. 1412 of the National Defense Authorization Act for fiscal year 2014, or Public Law No. 113-66, Congress allocated about $41 million for purchase of six materials including Dy [67], [68]. It is worth noting that in the updated report by the DoD (*Strategic and Critical Materials 2015 Report on*

[3] The USGS states that there are currently no suitable substitutes available for most rare earths, and those that do exist result in lower performance than rare earths [114].

Stockpile Requirements), Dy and Nd are not included in the list of materials recommended for stockpiling [67], indicating the concern about these particular rare earths has been mitigated, likely due to the decline and stabilization in prices. Furthermore, in a report issued by the U.S. Government Accountability Office (GAO), *Rare Earth Materials: Developing a Comprehensive Approach Could Held DOD Better Manage National Security Risks in the Supply Chain*, the GAO found inconsistencies with how difference offices in the DoD defined "critical materials," and in the approaches the different offices took to develop recommendations to address the issue [69].

7.4 Methodology

7.4.1 Literature Review

A literature review was conducted to gain an understanding of the environmental and social consequences of rare earth mining and production. A survey was conducted on the established recycling practices of rare earths and potential for future recycling. The life cycle of rare earths was also investigated. Finally, current events regarding rare earths were followed and incorporated into the literature review where relevant.

7.4.2 Content Analysis: Media Coverage of Rare Earths

The objective of this study was to determine whether or not widely read/circulated newspapers have covered the topic of rare earths, and whether any trends in the extent of coverage exist. This study serves to gain an understanding of the public awareness regarding the issue of rare earth supply and to gauge the media's interest in the topic. The most widely circulated newspapers (in print or digital) were determined [70]–[75].

Search terms included “most popular newspapers in USA” and “most circulated newspapers in USA.” The top three newspapers that were consistently cited as the most circulated were selected. They include *USA Today*, *The Wall Street Journal*, and *The New York Times*. Initial findings indicated coverage by *The Wall Street Journal* and *The New York Times*, but almost no coverage of rare earths by *USA Today*, which is the most widely read newspaper in the U.S. Thus, the study was extended to the top six most widely circulated newspapers including *The Los Angeles Times*, *The Daily News of New York*, and *The New York Post* to determine whether other newspapers were covering the issues surrounding rare earths.

Each newspaper was searched over a time period of 1/1/2009 to 6/26/2015 to determine the extent of media coverage of rare earths. For each year it was determined how many articles, blogs, and multimedia coverage there were on the topic of “rare earths.” Widespread concern about the issue of renewable energy technology dependence on rare earths and their supply risks did not arise until 2011 when rare earth prices rose drastically. Additionally, Congress has introduced 21 bills regarding rare earths and critical materials since 2010. These factors serve as justification for the time period selected.

Newspaper search terms[4] included “rare earth(s)” and “critical materials.” The results for each of these search terms were evaluated to determine whether or not they related to the subject of rare earths. Articles with titles related to rare earths/critical materials applications were further investigated to determine whether or not they were on topic.

[4] Initial search terms also included “permanent magnets,” “neodymium,” “dysprosium,” and “NdFeB” but were not found to generate results different than for “rare earth(s).”

Title keywords include (but are not limited to): rare earths, China, North Korea, hybrid/electric vehicles, Silicon Valley, mine/mining, Japan, Greenland, Australia. Furthermore, it was found that results for the search term “critical materials” did not yield different results from that of “rare earth(s)” and therefore can be considered a subset of “rare earth(s).” Thus, analysis was performed only on results yielded from the “rare earth(s)” search term.

7.4.3 Investigation of Congressional Legislation

Twenty one bills have been introduced in Congress regarding rare earths between January 2010 and July 2015. However, only four have come to a vote; of these four, only three passed in the House of Representatives. The three bills that made it to the Senate never made it out of committee consideration. This investigation serves to understand the voting patterns in the House of Representatives. The objectives were to determine whether representatives’ votes were motivated by party affiliation or state self-interest (states having identified rare earth deposits may stand to benefit from rare earth legislation) and to determine reasons for support and opposition of these bills.

For each bill, it was determined who introduced the bill (state and party affiliation) and the voting records as well as the congressional records were examined. The party and state affiliation of each voting representative was determined. It was also determined which states had identified rare earth deposits at the time of the vote by examining the USGS Mineral Commodity Summaries report for the corresponding year.

7.4.4 Investigation of Congressional Appropriation Bills

Congress can fund agencies through an appropriation of funds in budget resolutions. The Congress presiding during the period of interest (2010-2015) was relatively less successful in enacting legislation than previous Congresses (Fig. 7-1) [76]. However, Congress was able to appropriate funds to the DOE to support R&D regarding rare earths. Appropriations bills were investigation to determine the funding amount allocated to the various offices in the DOE, programs were investigated to determine initiatives to support R&D for rare earths, and linkages between the two investigated.

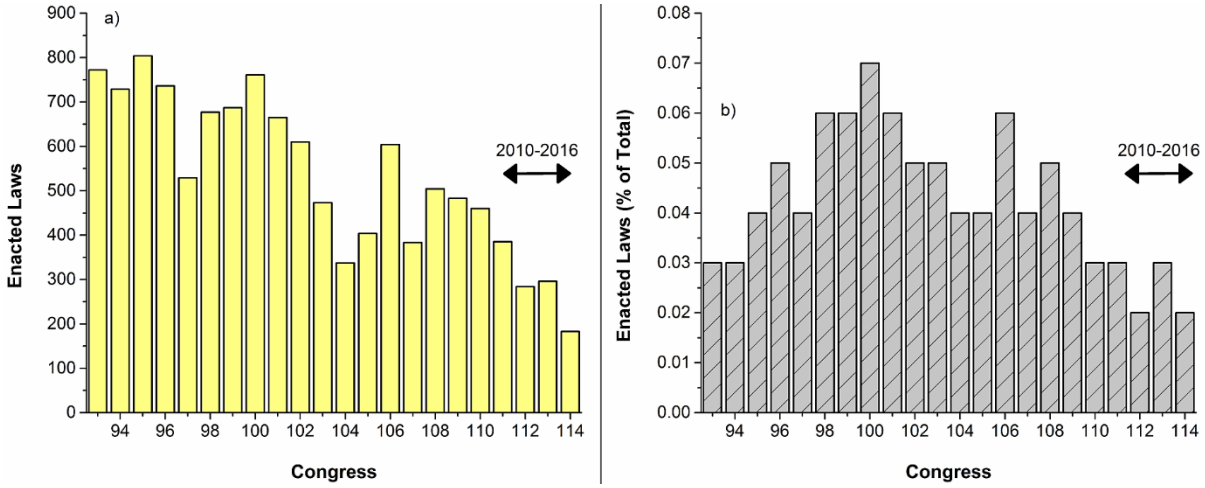

Figure 7-1. a) Number of laws enacted by each Congress and b) enacted laws by each Congress as a percentage of the total bills introduced [76].

7.5 Results & Discussion

7.5.1 Environmental & Social Consequences of Rare Earth Production

While the U.S. wind industry has moved away from DDPMGs in part due to the high prices of NdFeB permanent magnets, they should also be aware of the consequences of producing this technology. Articles have been published with titles such as “Big Wind’s Dirty Little Secret: Toxic Lakes and Radioactive Waste” [77]. While such articles

exaggerate the extent of the U.S. wind industry's dependence on rare earths (less than 1% of utility scale wind turbines in the U.S. use DDPMGs [8]), the concern is justified. The U.S. wind industry should be an active participant in practices of "environmental justice[5]", helping to ensure protection of human and environmental health both domestically and abroad.

Mining and especially refinement of rare earths present a serious hazard to human and environmental health. The lack of environmental regulations on the part of Chinese policy makers in China, where the majority of rare earths are mined and produced, has also contributed to high social consequences. In China, communities surrounded rare earth mining and refinement facilities are subject to serious health risks. The risks described in this section present a major barrier to U.S. domestic production of rare earths. They are risks that the U.S. government and wind industry should carefully consider when developing rare earth strategies.

According to the U.S. Environmental Protection Agency (EPA), hard rock mining risks are well documented. This includes environmental contamination risks as well as the release of Al, As, Ba, Be, Cu, Mn, Zn and Pb, which are known and documented to be a risk to human and environmental health [78]. In China, rare earths are primarily mined in Bayan-Obo, producing 120,000 tons of rare earth ore in 2006. This ore contains 0.04% Th, an element with radioactive decay products, exposing workers to radioactive dust [37]. If the radionuclides are inhaled, the radioactive decay takes place in the lungs

[5] Concerns about "environmental justice" can be applied within a nation, or globally. "Environmental injustice" occurs when environmental regulations or industry practices place populations of lower income, specific race or specific ethnicity as disproportionately higher levels of risk e.g. proximity to hazardous waste sites.

where the release of gamma rays has the potential to dislodge electrons from water, protein, and DNA [78].

Refinement of rare earth mineral deposits to produce rare earth oxides presents an even greater risk to human and environmental health. According to the EPA, for every ton of rare earths produced, 1 ton of radioactive waste is produced [78]; the USGS estimates that Chinese rare earth facilities produced 105,000 metric tonnes of rare earths in 2011. This makes waste management a crucial issue to prevent damage to human and environmental health. The risks of rare earths as contaminants and their movement through the environment are not yet well understood. However, the chemical processes used to produce rare earth oxides are well understood. The chemical processes used to isolate rare earth elements from mineral deposits include sulfide mineral dissolution, which can leak metals into the environment and create acid water, as well as carbonate dissolution, which can lead to the release of alkaline minerals that also threaten the pH balance of the water. These contaminants can be distributed by air, soil and water. In addition to radioactive waste, for every ton of rare earths produced, 8.5 kg F dust, 13 kg flue dust, 9600-12000 m^3 gas containing flue dust concentrate, HFl, sulfur dioxide and sulfuric acid, and 75 m^3 acidic waste water are produced [8], [78], [62].

Because the risk to human and environmental health is so high, lack of regulations on rare earth mining and refinement facilities have serious environmental and social consequences. For example, in the City of Baotou, China (located in Inner Mongolia) where the primary producer of rare earth oxides in China is located, 10 million tons of wastewater are generated annually. The farmland surrounding the refinement facility

served as the source of livelihood for the surrounding residents. However, since the opening of the refinement facility, the quality of the farmland and water supply have been severely degraded due to the release of wastewater. The neighboring lake is so polluted that neither fish nor algae can survive in the lake and crops will no longer grow on the farmland [79]. The water has been deemed to be unfit for human or animal consumption, or irrigation by the Chinese government [80].

This has had a devastating effect not only on the environment, but on the farmers who depended on it. Their livestock have died from the pollution and they have been stripped of their only means to make a living. The population has dropped from 2,000 to 300 in the past 10 years. However, farmers who do leave face discrimination due to the fact that they are labeled as a farmer on their identity card, and are treated like second class citizens [79]. Furthermore, the residents of Baotou have unusually high incidence of cancer and it has been reported that over 50% of the residents have black lung [62]. No scientific or medical studies have been conducted to determine whether the rare earth refiners have contributed to these medical conditions.

The developed world's dependence on these critical materials has led to global "environmental injustice". While this is often true within a single nation, it has become a global reality in the case of rare earths in which the Chinese population is exposed to disproportionately higher health risks from the release of hazardous chemicals into the environment than populations living in the U.S. or E.U., whose governments both have ambitious renewable energy goals. The environmental consequences of the renewable energy technologies such as wind turbines and electric/hybrid vehicles have been

externalized to the developing world, where Chinese citizens living near rare earth refineries or working in mines are exposed to the very serious risks.

The high environmental and social costs of mining and refinement of rare earths present a major barrier to domestic mining and production in the U.S. Rare earth mines in the U.S. closed, in part due to low prices of rare earths. The U.S. government and industry may be unwilling to deal with the environmental costs associated with rare earths. Thus, concentration of production of rare earths in China is due in part to lack of environmental regulations on the part of Chinese policymakers. This idea is supported by the fact that little production of rare earths has taken place in the U.S. between 2012 and 2015. Even with the short lived mining activities at the Mountain Pass mine, most rare earth mineral ore was still sent to Chinese facilities for refinement into rare earth oxide. This once again transfers the environmental and social risks from the developed world to the developing world as the refinement process has much more serious environmental risks than mining.

7.5.2 Content Analysis: Media Coverage of Rare Earths

The top six most widely read/circulated newspapers were examined to determine the extent of media coverage on the topic of rare earths from 1/1/2009 until 6/26/2015. This study served to gain understanding of the extent of public awareness on the topic of rare earths, and to determine whether any trends existed in the coverage over the period examined.

7.5.2.1 Overall Trends in Rare Earth Media Coverage

The overall media coverage for all six newspapers investigated is presented in Fig. 7-2, which demonstrates very little coverage of rare earth in 2009, a spike in coverage from 2010 to 2012, and a comparative decline in coverage from 2013 to 6/26/2015 with respect to 2010 to 2012. From 2010 to 2011, the prices of rare earths peaked, causing concern within the U.S. government and federal agencies. This may account for the similar spike in media coverage from 2010 to 2012, when the concern of Chinese control of the rare earth market first came to fruition. Since 2012, the price of rare earths has stabilized, and though rare earths prices are still high relative to prices before 2010, concern may have attenuated.

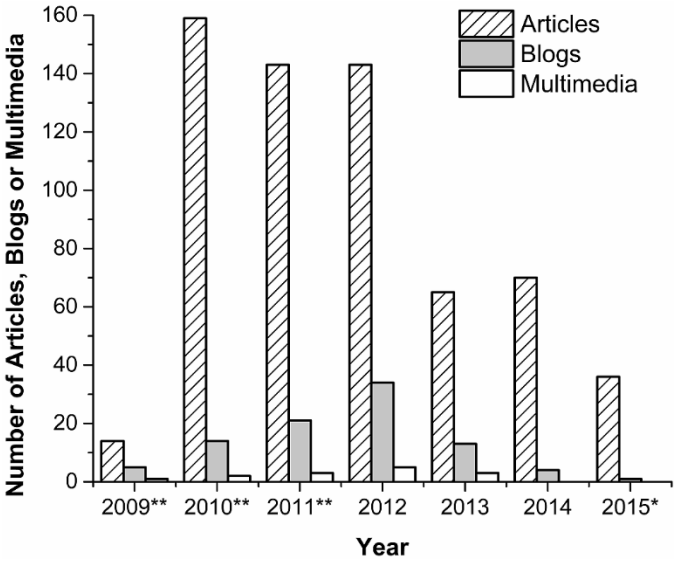

*Coverage through 6/26/15
**Blogs and multimedia data not available for The Wall Street Journal before 3/26/11 (see section 7.5.2.2)
Figure 7-2. Cumulative media coverage on the topic of “rare earth(s)” in the six most widely circulated newspapers in the U.S.

The Wall Street Journal and *The New York Times* had significantly more coverage on rare earths than the other newspapers, with *The Wall Street Journal* having the most extensive coverage. From Fig. 7-3, it is apparent that newspapers other than *The Wall*

Street Journal and *The New York Times* had very little to no coverage on rare earths, with at most 3 mentions in all media coverage per year. Furthermore, the only article covered by *The Daily News of New York* was about a girl who swallowed a rare earth permanent magnet, which while on the topic of rare earths, is not on the topic of issues surrounding global supply on rare earths or U.S. dependence on imported rare earths. This may indicate the knowledge of the issues surrounding rare earths is limited to a small, business oriented portion of the U.S. population.

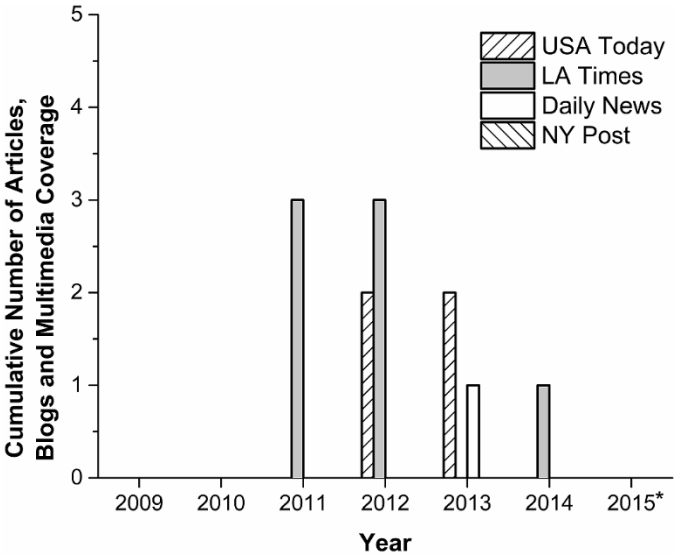

*Coverage through 6/26/15

Figure 7-3. Media coverage on the topic of “rare earth(s)” for *USA Today, LA Times*, *Daily News of NY*, and the *NY Post*.

It is also apparent that the primary form of media coverage is through articles, rather than blogs or multimedia such as videos (Fig. 7-2). It is difficult to determine whether the number of blogs has also decreased since 2013 compared to that of 2010 to 2012 since blog and multimedia data were not available for *The Wall Street Journal* before 3/26/11 (see section 7.5.2.2). However, *The Wall Street Journal* and *The New York Times* also have significantly more blogs on rare earths compared to the other newspapers for the

period of available data. These blogs are authored by various journalists or reporters who either work for the newspaper or are free-lance journalists. This is evidence that knowledge of the issues surrounding rare earths are limited to a specialized audience, in this case the media, rather than the general public.

7.5.2.2 The Wall Street Journal

Online access to archived media from *The Wall Street Journal* through the newspapers' website is only available for the last four years at the time of search (before 3/26/11 for this study). Archived articles for *The Wall Street Journal* and *The Wall Street Journal Online* are available for the time period of interest through ProQuest, an online depository of various resources including newspapers articles, but not including blog or multimedia archives for *The Wall Street Journal*. Thus, ProQuest was used to determine how many articles on the topic of "rare earth(s)" were published for each year and *The Wall Street Journal* online search engine was used to determine how many blogs and multimedia stories exist for each year. Thus, data on blogs and multimedia were not available before 3/26/11.

In 2009, there were only two articles on rare earths in *The Wall Street Journal*; then from 2011 to 2012 the coverage increased significantly (Fig. 7-4). Furthermore, the number of articles on rare earths actually increased each year from 2010 to 2012. Media coverage declined relative to this increased coverage from 2013 to 6/26/15. This is similar to the overall trend discussed in the previous section. Again, this is likely due to the price spike of rare earths in 2010 and 2011 and decline in prices recently. It should also be noted that while the media coverage has declined recently compared to

that of 2010 to 2012, it remains at much higher levels than in 2009. This may indicate a sustained interest in the topic, either by the media or by its readership.

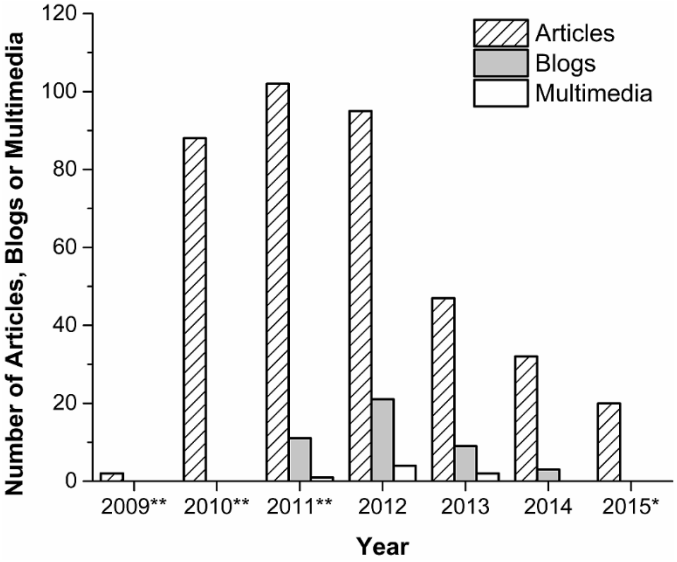

*Coverage through 6/26/15
**Blogs and multimedia data not available for *The Wall Street Journal* before 3/26/11.
Figure 7-4. Media coverage on the topic of “rare earths” by *The Wall Street Journal*.

7.5.2.3 The New York Times

Media coverage of rare earths by *The New York Times* in 2009 was also quite low compared to the significant increase in coverage from 2010 to 2012 (Fig. 7-5). Unlike *The Wall Street Journal*, coverage by *The New York Times* decreased each year from 2010 to 2012. Similar to the overall trend, media coverage declined from 2013 to 6/26/15 (relative to 2010 to 2012), likely due to stabilization of rare earth prices. Furthermore, although the media coverage has declined recently, the number of articles on rare earths did increase from 2013 to 2014 with coverage comparable to that of 2012 and still much greater than the coverage in 2009 before the price spike in rare earths. Again, this may indicate sustained interest in the topic either by the media or its readership.

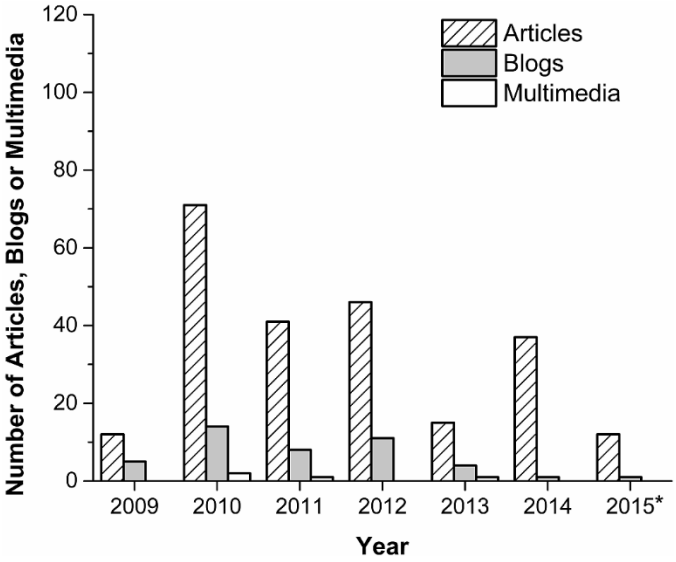

Coverage through 6/26/15

Figure 7-5. Media coverage on the topic of “rare earths” by *The New York Times*.

7.5.3 Congressional Legislation

Despite the strategy developed by the DOE, the U.S. Congress has not enacted any legislation regarding rare earths. However, there have been significant efforts. Following the price peak of rare earths in 2010 through 2011, 21 bills were introduced between January 2010 and July 2015 to address U.S dependence on imported rare earths or critical materials. Fig. 7-6 depicts a timeline of when these bills were introduced chronologically. Those with the prefix “H.R.” were introduced in the House of Representatives and those with the prefix “S.” were introduced in the Senate. Additionally, blue indicates a bill introduced by a Democrat and red indicates a bill introduced by a Republican.

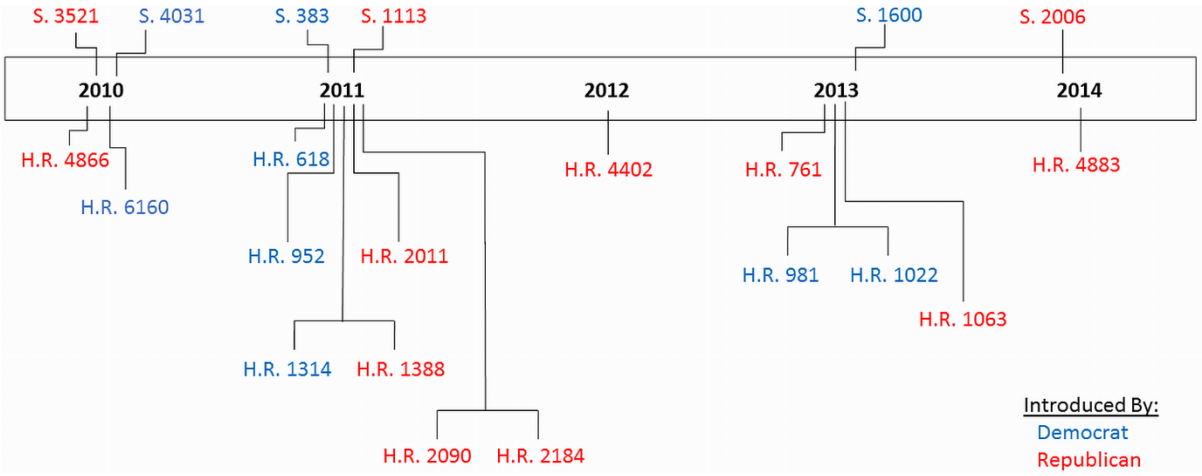

Figure 7-6. Timeline of recently introduced rare earth legislation.

The House of Representatives has been more active in introducing legislation than the Senate, but both political parties have been actively sponsoring these bills (Fig. 7-7). However, despite these efforts, not a single bill regarding critical material legislation has passed both congressional houses. Since the rare earth crisis in 2010, no legislation has been passed to establish a congressional strategy to ensure a secure and sustainable supply of rare earths for renewable energy or military application. Furthermore, all legislation discussed (except where noted) was never brought to a vote by either congressional house.

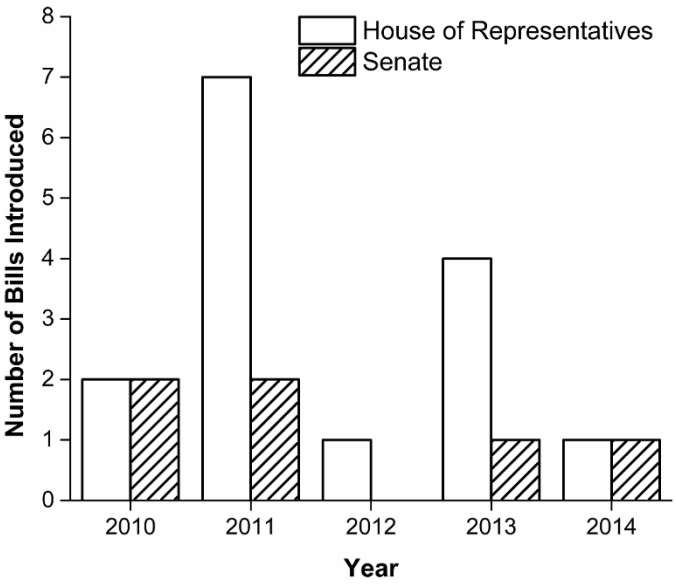

Figure 7-7. Number of bills introduced by each congressional house from 2010-2014.

Initial legislation, the *Rare Earths and Critical Materials Revitalization (RESTART) Act* [81], sought to reestablish domestic supply of rare earths by promoting domestic mining, refining and production of rare earths as well as by developing and understanding of restrictions of these practices and international trade law. Legislation of this nature has been continually introduced in consecutive years including the *National Strategic and Critical Materials Policy Act of 2011*, *Critical Minerals Policy Act of 2011*, *National Strategic and Critical Minerals Production Act of 2012* (passed by the House), *National Strategic and Critical Minerals Production Act of 2013* (passed by the House), and the *National Rare-Earth Cooperative Act of 2014* [82]–[86]. The two bills which passed a vote in the House of Representatives did not make it out of committee consideration in the Senate.

Legislation introduced by the Senate in 2010 (*RESTART Act*) also included an effort to establish a “Rare Earth Policy Task Force” to promote rare earth development, reestablish domestic supply and provide loan guarantees for domestic production of

rare earths [87]. This act was reintroduced again by the Senate later in 2010, modifying the loan guarantees to apply only to new and improved commercial applications of rare earths through amendment of the *Energy Policy Act of 2005*. It also sought to repeal the *National Critical Materials Act of 1984*. The House of Representatives introduced similar bills in 2011, the Rare *Earth Policy Task Force and Materials Act* and the *RESTART Act*, which included an effort to get an inventory of Nd and Dy specifically [88], [89].

Additional legislation introduced by the House of Representatives in 2010 included the *Rare Earths and Critical Materials Revitalization Act of 2010*, which sought to develop a program under the DOE to ensure long term security and stability of a rare earths supply [90]. This act also included amendment of the *Energy Policy Act of 2005* to establish loan guarantees for new or improved commercial applications of rare earths, and sought to repeal the *National Critical Materials act of 1984*. These bills were all introduced in the House of Representatives and include the *Rare Earths and Critical Materials Revitalization Act of 2011*, *Energy Critical Elements Renewal Act of 2011*, *National Strategic and Critical Minerals Policy Act of 2013*, and the *Security Energy Critical Elements and American Jobs Act of 2014* [85], [91], [92]. The latter bill was voted on, but did not get the two-thirds majority needed to pass.

Finally, a number of bills have been introduced for the purpose of resource assessment of critical materials in the United States and abroad. These bills include the *Resource Assessment Act of 2011*, *Energy Critical Elements Advancement Act of 2011*, *RARE Act of 2013*, and the *National Rare Earth Cooperative Act of 2014* [93]–[96].

7.5.4 Analysis of Voting Trends

This investigation serves to understand the voting patterns in the House of Representatives by studying the 4 bills [of 21 introduced in both congressional houses] which made it to a vote. Of these 4 bills, 3 passed, but never made it out of committees in the Senate. From this analysis, it was determined that political affiliations, rather than identified rare earth deposits in a representative's state, motivated votes for or against the bills discussed.

7.5.4.1 Rare Earths and Critical Materials Revitalization Act of 2010 (H.R. 6160)

The purpose of the *Rare Earth and Critical Materials Revitalization Act of 2010*, or H.R. 6160, was to establish a program under the DOE to ensure long-term security and sustainability of rare earths. It was introduced by a Democrat, Kathleen Dahlkemper of Pennsylvania, and was co-sponsored by representatives Coffman (R-CO), Carnahan (D-MO) and Lewis (D-GA), demonstrating the bipartisanship of the bill. None of these representatives came from a state with identified rare earth deposits at that time [97]. The bill passed when it came to a vote. While the Democrats almost unanimously supported the bill, Republicans were split over the issue, with more against than in favor of the bill (Fig. 7-8). This demonstrates party loyalty in general as a Democrat introduced the bill. States with identified rare earth deposits in 2011 include California, Wyoming, Idaho and Nebraska [97]. In general, representatives from these states voted for if they were a Democrat and against if they were Republican. This evidence supports the idea that party affiliation was more likely to motivate voting than state affiliation.

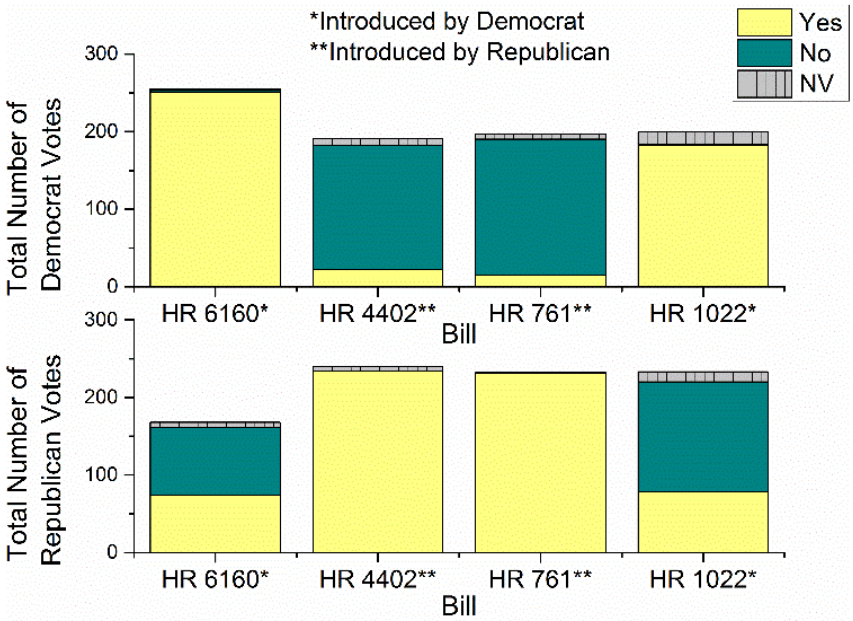

Figure 7-8. Voting record in House of Representatives on bills regarding rare earth policy.

According to the congressional record [98], Dahlkemper (D-PA) framed the bill as an issue of national security due to the supply risk of rare earths posed by lack of domestic rare earth mining and production and military dependence on the materials. Republicans who spoke out against the bill did not support loan guarantees because they felt that it allowed the government to pick “winners” and “losers” rather than let the market decide which companies would succeed. Representative Bilbray (R-CA) expressed concern that too many government regulations would prohibit the development of domestic natural resources such as rare earths.

7.5.4.2 National Strategic and Critical Minerals Production Act of 2012 (H.R. 4402)

The *National Strategic and Critical Minerals Production Act of 2012*, or H.R. 4402, sought to establish a lead agency that would both conduct and permit the exploration of

new mines including environmental review. The bill was introduced by a Republican, Mark E. Amodei (R-NV); Nevada did not have identified rare earth deposits at that time [99]. The bill passed when it came to a vote. While Republicans supported the bill unanimously, Democrats overwhelmingly voted against the bill (Fig. 7-7). This again demonstrates party loyalty in general as a Republican introduced the bill. Again, representatives from states with identified rare earth deposits, including California, Wyoming, Idaho, Nebraska and Montana [99], seemed to be motivated by party affiliation rather than state affiliation when voting.

According to the congressional record, Van Hollen (D-MD) spoke out in opposition of the bill, stating that it reduced and even eliminated environmental review for mines on public land, urging a no-vote. There was heated debate between the two parties regarding this bill [100]. Democrats were against the bill for two major reasons. First, they felt the bill defined “critical materials” too broadly, allowing sand, gravel and clay to be classified as such, in addition to rare earths. Second, the Democrats claimed the bill allowed for new mines to circumvent environmental review and that overall the bill was “a giveaway” for mining corporations. Republicans maintained that the bill was about creating jobs and a more efficient process for mining approval, which Democrats claimed was faster than it had even been under the Obama administration. Furthermore, President Obama had stated he was opposed to the bill. Amodei, who introduced the bill, argued that the bill did not allow for mining corporations to bypass environmental review and that material such as gravel, which help build infrastructure like roads, were just as critical to the U.S. as rare earths.

7.5.4.3 National Strategic and Critical Minerals Production Act of 2013 (H.R. 761)

Similarly to H.R. 4402, the *National Strategic and Critical Minerals Production Act of 2013*, or H.R. 761, sought to establish a lead agency that would both conduct and permit the exploration of new mines including environmental review. Amodei (R-NV) also introduced this bill. At this time, Nevada did have identified rare earth deposits [101]. The bill passed when it came to a vote. Republicans again supported the bill unanimously while Democrats overwhelmingly opposed it (Fig. 7-8). This once again demonstrates party loyalty in general as a Republican introduced the bill. Again, representatives from states with identified rare earth deposits, including California, Wyoming, Idaho, Nebraska, Montana, Arizona, Missouri, Texas, Nevada and Arkansas [101], seemed to be motivated by party affiliation rather than state affiliation when voting.

Again, Van Hollen (D-MD) urged a no vote on this bill as he believed it sought to eliminate environmental review on public land [102]. The debate over this bill was similar to its previous version [103]. Democrats still felt that the bill had little to do with rare earth supply security, arguing that the definition of “critical materials” was too broad, environmental review would be circumvented and that mines were approved 17% more quickly under the Obama administration than before. Republicans again argued that the bill sought to create jobs and eliminate red tape associated with domestic mining of rare earths. Amodei (R-NV), who introduced the bill, again argued that the future of supplies such as Cu, Pt, and gravel were uncertain, and thus also critical, and maintained that the bill language did not suggest eliminating environmental

review. It is also interesting to note that Smith (R-MO) expressed concern about the supply risk of Pb in the future, which was not considered under the bill.

7.5.4.4 Securing Energy Critical Elements and American Jobs Act of 2014 (H.R. 1022)

The purpose of the *Securing Energy Critical Elements and American Jobs Act of 2014*, or H.R. 1022, was to establish a program under the DOE which sought to ensure long term security and sustainability of rare earths. The bill was introduced by Eric Swalwell (D-CA); California had known rare earth deposits at the time [101]. The bill failed to pass when it came to a vote. While the Democrats voted almost unanimously in favor of the bill, twice as many Republicans voted against it than voted for it (Fig. 7-7). This demonstrates party loyalty in general as a Democrat introduced the bill; this is substantiated by the fact that many of the Democratic members of this Congress who voted for this bill voted against H.R. 761, while many of the Republicans who voted for H.R. 761 voted against this bill. Again, representatives from states with identified rare earth deposits, including California, Wyoming, Idaho, Nebraska, Montana, Arizona, Missouri, Texas, Nevada and Arkansas [101], seemed to be motivated by party affiliation rather than state affiliation when voting.

According to the Congressional Record [104], Democrats amended the bill to exclude loan guarantees at the request of Republican committee members to gain bipartisan support. However, the Heritage Foundation decided to include this vote on their scorecard, which “measures votes, co-sponsorships, and other legislative activity to show how conservative Members of Congress are” [105]. The Heritage Foundation supports global free market solutions and was against this bill, stating that it subsidized

American technologies, in violation of free market principles [106]–[108]. Thus, House Republicans were under pressure to vote against the bill [108], accounting for why the bill did not pass the vote despite bipartisan support initially.

7.5.5 Congressional Appropriation Bills

Though Congress was not able to effectively pass any legislation regarding rare earths due to political party divides, they were able to indirectly support R&D efforts through the end of the year appropriations bills. In these appropriation bills, funding is appropriated to the DOE, often specifically to energy and science programs such as Energy or Science under the Office of Energy Efficiency & Renewable Energy (EERE). In this way, Congress was able to fund R&D aligned with the goals of the *Critical Materials Strategy*.

On 10/28/2009, the 111th Congress passed Public Law No. 111-85, or H.R. 3183, the Energy and Water Development and Related Agencies Appropriations Act of 2010 as a Regulator Appropriation [109]. This awarded the DOE a total of $4,903,710,000 under Title III: Department of Energy. Of this sum, $15,000,000 was restricted for allocation to the Advanced Research Projects Agency-Energy (ARPA-E). Additionally, $76,890,000 was specifically allocated to “Congressionally Directed Science Projects” as described in the accompanying conference report [110]. ARPA-E later awarded $156,000,000 to R&D efforts under the REACT program, or Rare Earth Alternatives in Critical Technologies. The REACT program was created in direct response to the rare earths crisis, and supported research efforts to create technologies, such as permanent magnets, which were free of critical materials. For example, Ames Laboratory was

awarded $3,065,922 to develop “Novel High Energy Permanent Magnets Without Critical Materials” in which Ce based magnets were investigated for electric vehicle motors [66]. Ames Laboratory has since demonstrated substitution of Ce for Dy in high temperature NdFeB permanent magnets at the laboratory scale [46].

On 03/26/2013 Congress passed the H.R. 9333, the Consolidation and Further Continuing Appropriations Act of 2013, or Public Law No. 113-6 [111]. In this appropriations bill, under Title II: Energy and Water Development, the DOE was awarded $1,814,091,000 for EERE by the 113th Congress. In 2013, the Critical Materials Institute (CMI) was created as an Energy Innovation Hub by the DOE (through a funding announcement by the EERE), which awarded $120 million to Ames Laboratory over five years to specifically address the R&D needs surrounding critical materials like rare earths [112]. The CMI is a collaboration across many organizations across the U.S. demonstrating the commitment to addressing the need for recycling, developing substitutes and improved stewardship of critical materials from DOE national laboratories, universities, and industry[6].

7.6 Conclusions & Discussion

Following the rare earths crisis in 2011, the U.S. DOE raised concern regarding the dependence of renewable technologies on critical materials such as Nd and Dy. The

[6] These organizations include Ames National Laboratory, Idaho National Laboratory, Lawrence Livermore National Laboratory, Oak Ridge National Laboratory, Brown University, Colorado School of Mines, Florida Industrial and Phosphate Research Institute, Iowa State University, Purdue University, Rutgers, University of California at David, Advanced Recovery, Cytec Inc., General Electric, Graver Technologies, Molycorp, OLI Systems, Simbol Materials.

DOE recommended a strategy to reduce U.S. dependence on rare earths based on three pillars: diversifying supplies, development of substitutes, and improved stewardship of materials use through more efficient use, processing and recycling.

The U.S. government and industry has managed to diversify supplies to some extent, reducing dependence on imports from Chinese producers from 91% to 71% [97],[60]. However, the U.S. Congress has not been successful in enacting a legislative strategy to secure a long-term, sustainable supply of rare earths. Furthermore, the U.S. has no existing stockpiles of rare earths and Congress has not taken actions to significantly develop domestic mining potential.

According to the USGS, no substitutes currently exist that yield the same performance as rare earths. However, it has been demonstrated that Ce is a feasible substitute for Dy in high temperature NdFeB laboratory scale permanent magnets. While Ce is currently in surplus, it is rare earth element and thus has high environmental and social risks associated with it.

R&D being performed is motivated and funded by federal agencies that are funded by Congress indirectly through appropriations bills which give funding to the DOE to support these efforts. Significant R&D efforts have been conducted in reducing manufacturing waste and developing recycling techniques. Recycling techniques are not a viable supply stream for large NdFeB permanent magnets at this time due to the youth of the wind and electric car industry.

In contrast, the Japanese government has an existing stockpile of rare earths and has invested heavily in diversifying supply of imported rare earths, reducing its dependence on Chinese imports from 91% to 60% in part by helping develop mines in Vietnam.

Japan has also showed a significant interest in developing mines in North Korea; the North Korean government claims to have 216 million tons of rare earth resources. Chinese, Russian and South Korean governments have also demonstrated an interest; the Chinese government estimates that existing rare earth reserves in North Korea are approximately 48 million tons.

Based on this investigation, it has been determined that three major factors are contributing to the lack of U.S. legislation regarding rare earths:

1. High environmental and social costs of rare earth mining and production present a major barrier to further domestic development.
2. Lack of public awareness about the supply risks of rare earths or the wind industry's dependence on rare earths.
3. Political party divides prevent Congress from passing legislation.

High environmental and social costs of rare earth mining and production present a major barrier to further domestic development. While the mine at Mountain Pass was reopened, the majority of refinement takes place in China facilities rather than in U.S. facilities. This supports the idea that the U.S. government and industry is unwilling to risk environmental degradation or pay the high costs necessary to avoid it.

It was determined that in general, media coverage of rare earths was highest from 2010 to 2012, and has declined more recently over the course of 2013 to 6/26/2015. This correlates to the prices of rare earths, which spiked in 2010 and 2011 and have stabilized more recently. Thus, it is likely that there was more concern about rare earths in the period of higher coverage than during the period of decline in coverage more recently. However, the media coverage since 2013 is still much greater than in 2009,

before the price spike in rare earths, indicating that either the media or its readership remain interested or concerned about the topic.

USA Today is the most widely read newspaper in the U.S. Yet, *USA Today* and other popular non-business oriented newspapers have very little to no media coverage of rare earths. Only the more business oriented newspapers, *The Wall Street Journal* and *The New York Times*, have devoted media coverage to the topic of rare earths. Even with a large readership, it is unlikely that media coverage of rare earths has reached a large portion of the audience considering that at most 83 articles were published in one year by any one newspaper. This indicates that little overall media attention has been given to the topic of rare earths and the issue of rare earths is likely limited to a very small audience. Furthermore, media coverage of rare earths has attenuated recently. This is an issue because media attention translates to public awareness. If the media doesn't inform the public about rare earths, they will not even be aware of the issue, let alone be concerned about the potential consequences.

Lack of public awareness directly influences lack of congressional action. While members of Congress are aware of media coverage about rare earths, there was no mention of public opinion in the congressional record. Based on the analysis of voting in the House of Representatives, it is clear that political party divides present a significant barrier in passing any rare earth legislation (or any legislation in general). From the debates described in the congressional record, deep party divides exist in the House of Representatives, and disagreements about other legislation fuels disagreements about rare earth legislation. Political party divides remain a major barrier in passing rare earth legislation. Furthermore, it is evident from the congressional record that members of

Congress are aware of media coverage on the issue of rare earth supply risk, as well as the importance of rare earths to military and clean energy technologies. Lack of pressure from representatives' constituents leaves Congress with little incentive to compromise. However, it is important to note that Congress is heavily supporting R&D efforts recommended by the DOE through appropriations bills.

7.7 Recommendations

The DOE has put forth a strategy to obtain a sustainable, long-term supply of rare earths and ultimately reduce U.S. dependence on them. These recommendations include:

- Diversifying supply
- Developing substitutes
- Improved stewardship of materials through more efficient materials use, manufacturing and recycling

It is recommended in this Chapter that the U.S. strategy supported by Congress should extend beyond the currently funded R&D to address the needs of the U.S. wind industry, as well as other rare earth dependent industries, and ensure achievement of the DOE's goal of 20% wind electricity generation by 2030.

Long term, development of rare earth free permanent magnets (as recommended by the DOE) will offer the best solution for the wind industry. Rare earth free permanent magnets will allow for elimination of U.S. industry dependence on imported rare earths and significantly reduce the demand for rare earths overall, which would mitigate environmental and social costs associated with rare earth mining and refinement.

Development of new permanent magnetic materials is actively being pursued by academia, industry and national laboratories. Within academia and national laboratories, federal agencies like the DOE largely fund such initiatives, provided by appropriations passed by Congress. Congressional action in the form of a bill regarding R&D is not believed to be necessary, but continued financial support allotted to such federal agencies is.

In the short term, there are no new commercial permanent magnetic materials. In order to allow for use of DDPMGs in wind turbines, R&D should be pursued to develop a substitute for Dy. Such work is actively being pursued in and Ce has been demonstrated to be a suitable substitute at the laboratory scale by Ames Laboratory [46]. In addition to recycling of swarf[7] already being implemented, development of cost-efficient recycling methods of small NdFeB permanent magnets found in hard disk drives and voice coil motors is recommended to help offset the need for mining and production of Nd. Manual dismantling is believed to be preferable as it is less energy and chemical intensive.

In order for any U.S. policy or strategy to succeed, it should have public support. It is important that the public contributes to the discussion about rare earths and know how they may be impacted by solutions currently being proposed. Therefore, a public awareness campaign is highly recommended to inform the public to start a public discourse on the issue. The correct framing for the issue of rare earths needs to be identified. Within congressional debates, the issue has been framed both as one of

[7] Fine chips of filings of magnets generated from grinding of the permanent magnets.

national security, due to military dependence on rare earths, as well as energy security or independence, due to the dependence of renewable energy technologies on rare earths. These frameworks have failed in motivating congressional action in both congressional houses. It is recommended that the issue be framed in terms of domestic job creation from domestic mining and production, which would generate both “blue-collar” and “white-collar” jobs. An emphasis on the end products being made in America is recommended, as it may instill a sense of national pride. Additionally, the media is likely to follow the lead of the government if efforts are made to communicate the issues of rare earths to the public. Finally, a public discourse on the issue could generate new ideas and solutions not previously considered by federal agencies or Congress.

Domestic production and global diversification of the U.S. rare earth imports are recommended. All nations’ governments and policy makers are likely to act in the best interest of the nation they are serving, and thus depending so heavily on a single imported supply source of rare earths may be a risky strategy. In order for domestic rare earths mines to be successful, it is recommended that government subsidies be given. This will enable mines to overcome the barrier of environmental regulations without sacrificing environmental health, or the health of surrounding communities, and help domestic mines compete under low price market conditions. Congress should continue to pursue legislation that makes the rare earth mining approval process more efficient without sacrificing environmental review. It is the authors’ viewpoint that the bill be limited to rare earths, since other materials, while important to other aspects of the economy, are not critical to energy and national security. Political party divides are

difficult to overcome, but public pressure may result from a public awareness campaign, which could in turn result in successful legislation.

Finally, the issue of “environmental justice” should carefully be considered in development of domestic or foreign mines, as well as in economic transactions with Chinese industry. While the U.S. government and rare earth industry need to carefully consider the costs of human and environmental health for domestic mining and production of rare earths, responsibility should also take for contribution to the “environmental injustice” surrounding rare earths. Chinese industry is able to produce rare earths at a lower cost than other countries due to lack of environmental regulations and protection of workers. Industries in the U.S., as well as the E.U. and Japan are also heavily dependent on these technologies, and the industries and governments in these nations should agree to continue investment in Chinese rare earths oxides and products in order to allow for Chinese industry to cover the costs of increasing environmental regulations and protection of workers through trade agreements.

Industries in the U.S. should bear some responsibility for global environmental health by demonstrating willingness to pay prices which support a fair wage and mitigate risks to human and environmental health. The environmental disaster in Baotou should be prevented with support of the U.S. industry and government. Though this would mean higher costs for mine development, the long term costs of pollution and human deaths are far greater. Furthermore, instead of trying to compete for “control” of the rare earths market, it is recommended the U.S. policy makers recognize that the U.S. economy is interdependent with that of the Chinese economy. Due to this interdependence, there should be solutions which will promote benefits on both sides, such as a steady supply

of rare earths from China to the U.S. This could include trade agreements that would allow Chinese policy makers and industry to improve human and environmental health associated with rare earth mining and production. Again, this may require the willingness of the U.S. industry and government to pay prices for rare earths that support such conditions. Though the short term costs may be higher, the long term costs of not protecting environmental and human health will be greater. In reducing dependence on fossil fuels which contribute to climate change with wind turbines, the same mistakes of short sightedness should be avoided with rare earths.

CHAPTER 8. CONCLUSIONS AND FUTURE WORK

8.1 Conclusions

Direct-drive permanent magnet generators (DDPMGs) are a practical solution to the problem of gearbox reliability in large and offshore wind turbines, but are currently used in less than 1% of utility scale wind turbines (>100 kW) in the U.S. wind industry. Two major barriers exist to increased use of DDPMGs in the U.S. wind industry: (i) significant scaling of size and mass with increased rated torque and power, and (ii) the use of expensive rare earth NdFeB permanent magnets. Thus, the motivation for improvements in PMG design for large scale wind turbines are not only technical, but political and economic as well.

To address these barriers, methods have been investigated in this project to increase the magnetic loading, or average magnetic flux density over the rotor surface, thereby increasing magnetic contribution to torque and allowing for either size reduction or the use of lower energy density permanent magnets that do not contain rare earths. In Chapter 3, permanent magnet material properties necessary for a 25% reduction in the outer diameter and axial length of a 10 MW PMG were quantified. It was found that the remanence of a NdFeB 48/11 grade permanent magnet would need to be increased from 1.39 T to 2.14 T, giving a theoretical maximum energy product of 553.9 kJ/m^3, an increase of 167% from existing NdFeB 48/11. This is a very ambitious goal and while it would have significant implications in terms of reducing PMG volume if implemented, it is dependent on the discovery and development of new permanent magnet materials.

Alternatively, practically realizable techniques to concentrate the magnetic flux over the rotor surface to increase magnetic loading were investigated. Halbach arrays and electrical steel flux collectors were both utilized in the outer rotor of a 3.5 kW PMG to concentrate the magnetic flux. It was found that both designs allowed for significant reduction in the outer diameter and axial length of the 3.5 kW PMG – up to 35% for the Halbach PMG (HPMG) and up to 46% for the novel electrical steel flux collector PMG design. Ultimately the PMG with electrical steel flux collectors achieved higher magnetic loading than the HPMG, giving more design flexibility and at the same time being more practical from a manufacturing perspective.

Existing permanent magnet topologies were explored to compare performance and determine if any provided significant benefits over the others. It was found that the spoke permanent magnet topology achieved the highest torque density for an interior rotor, 10 kW PMG. However, the “spoke” permanent magnet topology also contributed to large variation of the magnetic flux distribution over the rotor surface, causing significant cogging torque, which is undesirable for wind turbine applications. Ultimately, the bread-loaf permanent magnet topology was found to be the most desirable as it allowed significant size reduction without sacrificing performance.

Finally, the barriers to passing rare earth legislation were investigated. It was found that high environmental and social costs, lack of public awareness, and political party divisions were the major factors contributing to the lack of U.S. legislation on securing a long-term, sustainable supply of rare earths, but that Congress has been able to support R&D efforts in the DOE to address these needs through appropriation of funding.

8.2 Future Work

In this work, the initial foundation was laid for designs that allow for significant reduction in PMG volume, or the use of hard ferrite permanent magnets by providing proof of concept with finite element models and calculations. In the future, this work should be expanded to address several additional goals. The investigation of starting torque in the speed range of a direct-drive machine as well as calculation of the thermal and mechanical properties of the PMG designs are recommended. Another technique that could be explored to increase magnetic loading, and allow for significant size reduction or the use of hard ferrite permanent magnets, is the use of high permeability magnetic flux guides in the rotor and/or stator yoke by employing high permeability materials such as permalloy. Finally, the materials work at Ames Laboratory includes the development of Dy free NdFeB as well as improved alnico permanent magnets for use in PMGs. Collaboration should be pursued to include these materials in the finite element PMG models for wind turbine application.

REFERENCES

[1] "Electric Power Monthly," U.S. Energy Information Administration, July 2015, [Online]. Availale: http://www.eia.gov/electricity/monthly/pdf/epm.pdf.

[2] U.S. Department of Energy, "20% Wind Energy by 2030," U.S. Department of Energy, Oak Ridge, TN. Tech. Rep. DOE/GO-102008-2567, July 2008.

[3] "Wind Vision: A New Era for Wind Power in the United States," U.S. Department of Energy, Oak Ridge, TN. Tech. Rep. DOE/GO-102015-4557, Apr. 2015.

[4] S. Sheng, "Report on Wind Turbine Subsystem Reliability - A Survey of Various Databases," National Renewable Energy Laboratory, Golden, CO, Rep. NREL/PR-5000-59111, June 2013.

[5] W. Musial, W. Butterfield, and B. McNiff, "Improving Wind Turbine Gearbox Reliability," in *2007 European Wind Energy Conference*, 2007.

[6] R. Scott Semken, M. Polikarpova, P. Röyttä, J. Alexandrova, J. Pyrhönen, J. Nerg, A. Mikkola, and J. Backman, "Direct-drive permanent magnet generators for high-power wind turbines: benefits and limiting factors," *IET Renew. Power Gener.*, vol. 6, no. 1, pp. 1–8, 2012.

[7] G. Shrestha, "Structural Flexibility of Large Direct Drive Generators for Wind Turbines," Technical University of Delft, 2013.

[8] "private communication." American Wind Energy Association, Sept. 2014.

[9] L. Fingersh, M. Hand, and a Laxson, "Wind Turbine Design Cost and Scaling Model Wind Turbine Design Cost and Scaling Model," National Renewable Energy Laboratory, Golden, CO, Rep. NREL/TP-500-40566, p. 38, Dec. 2006.

[10] "Critical Materials Strategy," U.S. Department of Energy, Oak Ridge, TN, Tech. Rep. DOE/PI-0009, Jan. 2012.

[11] "Global Wind Statistics 2015," Global Wind Energy Council, Brussels, Belgium, 2016. [Online]. Available: http://www.gwec.net/wp-content/uploads/vip/GWEC-PRstats-2015_LR_corrected.pdf

[12] "Wind Energy Facts at a Glance," *American Wind Energy Association*, 2015. [Online]. Available: http://www.awea.org/Resources/Content.aspx?ItemNumber=5059.

[13] D. Henry, "Work begins on nation's first offshore wind farm | TheHill," *The Hill*, 2015. [Online]. Available: http://thehill.com/policy/energy-environment/240184-work-begins-on-nations-first-offshore-wind-farm. [Accessed: 02-Jul-2015].

[14] A. El-Refaie, G.E. Global Research Center, “private communcation,” Mar. 2015.

[15] M. Snodgrass, MidAmerican Energy Company, “private communication,” Apr. 2015.

[16] A. King, Critial Materials Institute, Ames Laboratory, U.S. Department of Energy, “private communication,” Mar. 2015.

[17] R. Thresher, M. Robinson, and P. Veers, “Wind Energy Technology: Current Status and R&D Future,” in *Physics of Sustainable Energy Conference*, 2008.

[18] J. R. Hendershot and T. J. E. Miller, *Design of Brushless Permanent-Magnet Machines*. Venice, FL: Motor Design Books LLC, 2010.

[19] J. R. Hendershot and T. J. E. Miller, “Machine Types and Applications,” in *Design of Brushless Permanent-Magnet Machines*, Venice, FL: Motor Design Books LLC, 2010, p. 28.

[20] D. Tremelling, ABB, “private communication,” Feb. 2013.

[21] E. Spooner, P. Gordon, J. R. Bumby, and C. D. French, “Lightweight ironless-stator PM generators for direct-drive wind turbines,” in *IEEE Proceedings of Electric Power Applications*, 2005, pp. 17–26.

[22] M. a. Mueller and A. S. McDonald, “A lightweight low-speed permanent magnet electrical generator for direct-drive wind turbines,” *Wind Energy*, vol. 12, no. 8, pp. 768–780, 2009.

[23] C. Versteegh and G. Hassan, “Design of the Zephyros Z72 wind turbine with emphasis on the direct drive PM generator,” *Proc. Nord. Work. power Ind. Electron.*, vol. 31, no. 0, pp. 14–16, 2004.

[24] J. Lutz and J. Ley, “Brushless PM machine construction enabling low coercivity magnets,” US8928198 B2, 2015.

[25] “Motor ‘delivers rare-earth performance without rare-earths,’” *Drives & Controls*, 21-Jan-2015. [Online]. Available: http://www.drivesncontrols.com/news/fullstory.php/aid/4696/Motor__delivers_rare-earth_performance_without_rare-earths_.html

[26] L. Jian, K. T. Chau, and J. Z. Jiang, “A magnetic-geared outer-rotor permanent-magnet brushless machine for wind power generation,” *IEEE Trans. Ind. Appl.*, vol. 45, no. 3, pp. 954–962, 2009.

[27] B. Maples, M. Hand, and W. Musial, “Comparative Assessment of Direct Drive High Temperature Superconducting Generators in Multi-Megawatt Class Wind Turbines,” Natioanl Renewable Energy Laboratory ,Golden, CO, Tech. Rep. NREL/TP-5000-49086, 2010.

[28] K. H. J. Buschow, *Permanent Magnet Materials and Their Applications*. Trans Tech Publications LTD, 1998.

[29] “Products,” Arnold Magnetic Technologies, 2015. [Online]. Available: http://www.arnoldmagnetics.com/Products.aspx

[30] M. J. Melfi, S. D. Rogers, S. Evon, and B. Martin, “Permanent Magnet Motors for Energy Savings in Industrial Applications,” *2006 Rec. Conf. Pap. - IEEE Ind. Appl. Soc. 53rd Annu. Pet. Chem. Ind. Conf.*, vol. 1, no. c, pp. 1–8, Sep. 2006.

[31] P. C. Dent, “Rare earth elements and permanent magnets (invited),” *J. Appl. Phys.*, vol. 111, no. 7, p. 07A721, 2012.

[32] J. M. D. Coey, “Permanent magnets: Plugging the gap,” *Scr. Mater.*, vol. 67, no. 6, pp. 524–529, Sep. 2012.

[33] “REE Handbook,” Investor Intel, ProEdge Media, 2013. [Online]. Available: http://www.reehandbook.com/.

[34] “Mineral commodity summaries 2015: U.S. Geological Survey,” U.S. Geological Survey, pp. 196, 2015. [Online]. Available: http://dx.doi.org/10.3133/70140094

[35] A. Panda, “WTO Finds Chinese Rare Earth Export Restrictions in Violation of International Trade Law,” *The Diplomat*, Mar-2014.

[36] K. Binnemans, P. T. Jones, B. Blanpain, T. Van Gerven, Y. Yang, A. Walton, and M. Buchert, “Recycling of rare earths: a critical review,” *J. Clean. Prod.*, vol. 51, pp. 1–22, Jul. 2013.

[37] B. Sprecher, Y. Xiao, A. Walton, J. Speight, R. Harris, R. Kleijn, G. Visser, and G. J. Kramer, “Life cycle inventory of the production of rare earths and the subsequent production of NdFeB rare earth permanent magnets.,” *Environ. Sci. Technol.*, vol. 48, no. 7, pp. 3951–8, Apr. 2014.

[38] “New Process Recycles Magnets from Factory Floor,” *Product Design & Development*, 01-Jul-2015.

[39] D. Lockwood, “Recycling Rare Earths From E-Waste More Sustainably,” *Chemical & Engineering News*, 08-Jul-2015.

[40] T. Saito and R. Nishimura, “Hard magnetic properties of Mn-Ga melt-spun ribbons,” *J. Appl. Phys.*, vol. 112, p. 252506, 2012.

[41] T. J. Nummy, S. P. Bennett, T. Cardinal, and D. Heiman, “Large coercivity in nanostructured rare-earth-free MnxGa films,” *Appl. Phys. Lett.*, vol. 99, p. 252506, 2011.

[42] F. Jiménez-Villacorta, J. L. Marion, T. Sepehrifar, M. Daniil, M. A. Willard, and L. H. Lewis, “Exchange anisotropy in the nanostructured MnAl system,” *Appl. Phys. Lett.*, vol. 100, p. 112408, 2012.

[43] D. Kim and J. Hong, “Rare earth free exchange spring magnet FeCo/FePt(011): Giant

magnetic anisotropy and energy product," *Surf. Sci.*, vol. 606, pp. 1960–1964, 2012.

[44] X. Rui, J. E. Shield, Z. Sun, L. Yue, Y. Xu, D. J. Sellmyer, Z. Liu, and D. J. Miller, "High-energy product exchange-spring FePt/Fe cluster nanocomposite permanent magnets," *J. Magn. Magn. Mater.*, vol. 305, pp. 76–82, 2006.

[45] B. Das, "HfCo7-Based Rare-Earth-Free Permanent-Magnet Alloys," *IEEE Trans. Magn.*, vol. 49, pp. 3330–3333, 2013.

[46] V. K. Pathak, A. K., Khan, M., Gschneidner Jr, K. A., McCallum, R. W., Zhou, L., Sun, K., Dennis, K. W., Zou, C., Pinkerton, F. D., Kramer, M. J., Pecharsky, "Cerium: An Unlikely Replacement of Dysprosium in High Performance Nd-Fe-B Permanent Magnets," *Adv. Mater.*, vol. 27, no. 16, pp. 2663–2667, 2015.

[47] O. Gutfleisch, M. a Willard, E. Brück, C. H. Chen, S. G. Sankar, and J. P. Liu, "Magnetic materials and devices for the 21st century: stronger, lighter, and more energy efficient.," *Adv. Mater.*, vol. 23, no. 7, pp. 821–42, Feb. 2011.

[48] A. S. Abdel-Khalik, S. Ahmed, A. M. Massoud, and A. a. Elserougi, "An Improved Performance Direct-Drive Permanent Magnet Wind Generator Using a Novel Single-Layer Winding Layout," *IEEE Trans. Magn.*, vol. 49, no. 9, pp. 5124–5134, Sep. 2013.

[49] T. Morcos, "Permanent Magnet & Motor Design Workshop." Orlando, 2014.

[50] J. R. Hendershot and T. J. E. Miller, "Basic Design Choices," in *Design of Brushless Permanent-Magnet Motors*, Oxford: Magna Physics Publishing and Claredon Press, 1994, pp. 3–27.

[51] J. R. Hendershot and T. J. E. Miller, "Sizing and Computer-Aided Design," in *Design of Brushless Permanent-Magnet Motors*, New York: McGraw-Hill, Inc., 1994, pp. 12–2 – 12–6.

[52] Z. Q. Zhu, D. Howe, E. Bolte, and B. Ackermann, "Instantaneous Magnetic Field Distribution i n Brushless Permanent Magnet dc Motors , Part I : Open-circuit Field," *IEEE T*, vol. 29, no. 1, pp. 124–135, 1993.

[53] J. R. Hendershot and T. J. E. Miller, "Flux, EMF and Torque," in *Design of Brushless Permanent-Magnet Machines5*, Venice, FL: Motor Design Books LLC, 10AD, pp. 158–163.

[54] J. R. Hendershot and T. J. E. Miller, "Losses and Cooling," in *Design of Brushless Permanent-Magnet Machines*, Venice, FL: Motor Design Books LLC, 2010, pp. 555–556.

[55] Z. Q. Zhu and D. Howe, "Halbach permanent magnet machines and applications: a review," *IEE Proc. - Electr. Power Appl.*, vol. 148, no. 4, p. 299, 2001.

[56] Z. Q. Zhu, "Recent Development of Halbach Permanent Magnet Machines and Applications," *Power Convers. Conf. - Nagoya, 2007. PCC '07*, p. K–9 – K–16, 2007.

[57] "Arnox Permanent Magnets," Rochester, 2003.

[58] L. Schultz, O. deHaas, P. Verges, C. Beyer, S. Rohlig, H. Olsen, L. Kuhn, D. Berger, U. Noteboom, and U. Funk, “Superconductively Levitated Transport System—The SupraTrans Project,” *IEEE Trans. Appiled Supercond.*, vol. 15, no. 2, pp. 2301–2305, Jun. 2005.

[59] C. Jamasmie, “Molycorp shuts down Mountain Pass rare earth plant,” *Mining.com*, 2015. [Online]. Available: http://www.mining.com/molycorp-shuts-down-mountain-pass-rare-earth-plant/.

[60] “Mineral commodity summaries 2016: U.S. Geological Survey,” U.S. Geological Survey, pp. 202, 2016. [Online]. Available: http://dx.doi.org/10.3133/70140094.

[61] “Strategic and Critical Materials 2013 Report on Stockpile Requirements,” U.S. Department of Defense, RefID: 2-9B1D9E6, Jan. 2013. [Online]. Available: http://mineralsmakelife.org/assets/images/content/resources/Strategic_and_Critical_Materials_2013_Report_on_Stockpile_Requirements.pdf

[62] C. Hurst, “China’s Rare Earth Elements Industry: What Can the West Learn ?,” Institute for the Analysis of Global Security, Mar. 2010.

[63] C. B. Blakely, J. Cooter, A. Khaitan, I. Sincer, and R. Williams, “Rare Earth Metals & China,” Gerald R. Ford School of Public Policy, Ann Arbor, 2012.

[64] “Mineral commodity summaries 2014: U.S. Geological Survey,” U.S. Geological Survey, pp. 196, 2016. [Online]. Available: http://minerals.usgs.gov/minerals/pubs/mcs/2014/mcs2014.pdf

[65] K. Majcher, “What Happened to the Rare-Earths Crisis?,” *MIT Technology Review*, Feb-2015.

[66] “REACT,” *ARPA-E*, 2011. [Online]. Available: http://arpa-e.energy.gov/?q=arpa-e-programs/react.

[67] “Strategic and Critical Materials 2015 Report on Stockpile Requirements,” U.S. Department of Defense, Rep. RefID: 9-05A8E24, 2014.

[68] *H.R.3304 - National Defense Authorization Act for Fiscal Year 2014*. 2013.

[69] “Rare Earth Materials: Developing a Comprehensive Approach Could Held DOD Better Manage National Security Risks in the Supply Chain,” U.S. Government Accountability Account, Rep. GAO-16-161 Rare Earth Materials, 2016.

[70] A. Press, “Top 10 Newspapers By Circulation: Wall Street Journal Leads Weekday Circulation,” *Huffington Post*, 01-Jul-2013.

[71] “Top 10 US Daily Newspapers,” *Cision*, 18-Jun-2014.

[72] “Top 50 United States Newspapers Accessed on OnlineNewspapers Last Month,”

OnlineNewspapers.com, 04-Mar-2015.

[73] "Top 25 U.S. Newspapers for March 2013," *Alliance for Audited Media*, 2015.

[74] "USA Top 10 Newspapers," *Paperboy*, Mar-2013.

[75] "Leading daily newspaper in the United States from April to September 2014, by circulation," *Statista*, 2015.

[76] "Statistics and Historical Comparison," *govtrack.us*. [Online]. Available: https://www.govtrack.us/congress/bills/statistics#.

[77] T. Fisher and A. Fitzsimmons, "Big Wind's Dirty Little Secret: Toxic Lakes and Radioactive Waste," Institute for Energy Research, 2013. [Online]. Available: http://instituteforenergyresearch.org/analysis/big-winds-dirty-little-secret-rare-earth-minerals/. [Accessed: 20-Apr-2015].

[78] J. Paul and G. Campbell, "Investigating Rare Earth Element Mine Development in EPA Region 8 and Potential Environmental Impacts," 2011.

[79] "Rare-earth mining in China comes at a heavy cost for local villages," The Guardian, 07-Aug-2012.

[80] L. Hilsum, "Are Rare Earth Minerals Too Costly for Environment?," PBS, United States, 2009.

[81] M. Coffman, H.R.4866 - RESTART Act. House of Representatives, 2010.

[82] D. Lamborn, H.R.2011 - National Strategic and Critical Minerals Policy Act of 2011. House of Representatives, 2011.

[83] L. Murkowski, S.1113 -Critical Minerals Policy Act of 2011. Senate, 2011.

[84] M. Amodei, H.R.4402 - National Strategic and Critical Minerals Production Act of 2012. House of Representatives, 2012.

[85] M. Amodei, H.R.761 - National Strategic and Critical Minerals Production Act of 2013. House of Representatives, 2013.

[86] S. Stockman, "H.R.4883 - 113th Congress (2013-2014): National Rare-Earth Cooperative Act of 2014," 17-Jun-2014. [Online]. Available: https://www.congress.gov/bill/113th-congress/house-bill/4883?q=%7B%22search%22%3A%5B%22H.R.+4883%22%5D%7D. [Accessed: 20-Apr-2015].

[87] E. Bayh, S.4031 - RESTART Act. Senate, 2010.

[88] M. Coffman, H.R.2184 - Rare Earth Policy Task Force and Materials Act. House of Representatives, 2011.

[89] M. Coffman, H.R.1388 - RESTART Act. House of Representatives, 2011.

[90] K. Dahlkemper, H.R.6160 - Rare Earths and Critical Materials Revitalization Act of 2010. House of Representatives, 2010.

[91] L. Boswell, H.R.618 - Rare Earths and Critical Materials Revitalization Act of 2011. House of Representatives, 2011.

[92] E. Swalwell, H.R.1022 - Securing Energy Critical Elements and American Jobs Act of 2013. House of Representatives, 2014.

[93] H. Johnson, H.R.1314 - Resource Assessment of Rare Earths Act of 2011. House of Representatives, 2011.

[94] B. Miller, H.R.952 - Energy Critical Elements Renewal Act of 2011. House of Representatives, 2011.

[95] H. Johnson, H.R.981 - RARE Act of 2013. House of Representatives, 2014.

[96] R. Blunt, S.2006 - National Rare Earth Cooperative Act of 2014. Senate, 2014.

[97] “Mineral commodity summaries 2010: U.S. Geological Survey,” U.S. Geological Survey, pp. 198, 2010. [Online]. Available: http://minerals.usgs.gov/minerals/pubs/mcs/2010/mcs2010.pdf

[98] “Rare Earths and Critical Materials Revitalization Act of 2010,” Congr. Rec., vol. 156, no. 132, p. H7060, 2010.

[99] “Mineral Commodity Summaries 2012: U.S. Geological Survey,” U.S. Geological Survey, pp. 198, 2012. [Online]. Available: http://minerals.usgs.gov/minerals/pubs/mcs/2012/mcs2012.pdf

[100] “Providing for Consideration of H.R. 4402, National Strategic and Critical Minerals Production Act of 2012,” Congr. Rec., vol. 158, no. 103, p. H4791, 2012.

[101] “Mineral Commodity Summaries 2013: U.S. Geological Survey,” U.S. Geological Survey, pp. 198, 2013. [Online]. Available: http://minerals.usgs.gov/minerals/pubs/mcs/2013/mcs2013.pdf

[102] “Representative Van Hollen (MD), National Strategic and Critical Minerals Production Act of 2013,” Congr. Rec., vol. 159, no. 124, p. E1341, 2013.

[103] “Providing for Consideration of H.R. 761, National Strategic and Critical Minerals Production Act of 2013,” Congr. Rec., vol. 159, no. 123, p. H5600, 2013.

[104] “Securing Energy Critical Element and American Jobs Act of 2014,” Congr. Rec., vol. 160, no. 115, p. H6592, 2014.

[105] “Scorecard,” Heritage Action for America, 2016. [Online]. Available: http://www.heritageactionscorecard.com/.

[106] “‘NO’ ON SWALWELL’S RARE EARTH MINERAL BILL (H.R. 1022),” Heritage Action for America, 2014. [Online]. Available: http://heritageaction.com/key-votes/swalwells-rare-earth-mineral-bill-h-r-1022/.

[107] N. Loris, “Rare Earths Bill Should Open Markets, Not Create Government Programs,” The Daily Signal, 22-Jul-2014.

[108] D. Johnson, “House Republicans Blocked Critical ‘Make It In America’ Bill,” Campaign for America’s Future, 24-Jul-2014.

[109] “Energy and Water Development and Related Agencies Appropriations Act of 2010,” Congr. Rec., 2009.

[110] H. Rept. 111-278 - ENERGY AND WATER DEVELOPMENT AND RELATED AGENCIES APPROPRIATIONS ACT, 2010. 2009.

[111] H.R.933 - Consolidated and Further Continuing Appropriations Act of 2013. 2013.

[112] “Ames Laboratory to Lead New Research Effort to Address Shortages in Rare Earth and Other Critical Materials,” Energy.gov, 09-Jan-2013.

[113] P. Mohai, D. N. Pellow, and J. T. Roberts, “Environmental Justice,” Annu. Rev. Environ. Resour., vol. 34, pp. 405–430, 2009.

[114] “Mineral commodity summaries 2015: U.S. Geological Survey,” U.S. Geological Survey, pp. 196, 2015. [Online]. doi: 10.3133/70140094.

APPENDIX A. PUBLISHED CONFERENCE PROCEEDINGS

- **H. A. Khazdozian**, R. L. Hadimani, D. C. Jiles, “Use of Non-Rare-Earth Permanent Magnets in Halbach Cylinder Rotor Permanent Magnet Generator,” *IEEE Magnetics Conference (INTERMAG) 2016*, San Diego, CA, BJ-12, Jan. 2016, in press.

- **H. A. Khazdozian**, R. L. Hadimani, D. C. Jiles, “Size reduction of Permanent Magnet Generators for Wind Turbines Using Halbach Cylinders,” *IEEE Magnetics Conference (INTERMAG) 2015*, Beijing, China, pp. 1, Jan. 2016. doi: 10.1109/INTMAG.2015.7156819

- **H. A Khazdozian**, R. L. Hadimani, D. C. Jiles, “Size reduction of Permanent Magnet Generators for Wind Turbines With Higher Energy Density Permanent Magnets,” *North American Power Symposium (NAPS) 2014*, Pullman, WA, pp. 1-6, Sept. 2014. doi: 10.1109/NAPS.2014.6965439

CONTROL ID: 2356594

TITLE: Use of Non-Rare-Earth Permanent Magnets in Halbach Cylinder Rotor Permanent Magnet Generator

AUTHORS (LAST NAME, FIRST NAME): Khazdozian, Helena A.[1, 2]; Hadimani, Ravi L.[2]; Jiles, David C.[1, 2]

INSTITUTIONS (ALL):

1. Wind Energy Science, Engineering and Policy Program, Iowa State University, Ames, IA, United States.
2. Dept. of Electrical and Computer Engineering, Iowa State University, Ames, IA, United States.

ABSTRACT BODY:

Abstract Body: Direct-drive permanent magnet generators (DDPMGs) in wind turbines offer increased reliability and efficiency over the more commonly used doubly-fed induction generator [1-2]. Yet, DDPMGs are only employed in an estimated 5 to 10% of wind turbines in the U.S. wind industry due to reliance on NdFeB permanent magnets (PMs), which contain rare earth elements Nd and Dy, considered as “critical materials” by the U.S. Department of Energy [3-4]. Elimination of NdFeB PMs in DDPMGs is desirable to allow for their increased use in the U.S. wind industry. The magnetic loading in a PMG can be increased by concentrating magnetic flux over the rotor surface to allow for the use of rare earth free permanent magnetic material. We investigated the use of ceramic PMs in place of NdFeB PMs in a 3.5kW Halbach PMG (HPMG). Halbach cylinders with varying number of poles were employed as the rotor in a 3.5kW HPMG with NdFeB 32/31 grade PMs (energy product of 256kJ/m^3 at 20°C) to concentrate magnetic flux over the rotor surface. The slot-to-pole ratio was also varied as it plays an important role in the efficiency of the magnetic flux path. We found that for high pole and slot number, the magnetic flux density and torque density achieved in the 3.5kW HPMG were sufficient to allow for the use of C11, a ceramic strontium iron oxide grade PM. C11 offers one of the highest energy products among ceramic PMs, 32.9kJ/m^3 at 20°C [5]. While rated torque and power were maintained for the use of the C11 PMs, their increased permeability (as compared with NdFeB) was found to increase inductance and thus the reactive contribution to the Joule losses in the stator windings (Fig. 1). This decreased the average efficiency at rated speed. For scaling of the ceramic HPMGs to 3MW, rated performance and high efficiency (reduced Joule losses) were achieved on average at rated speed (Fig. 2), demonstrating the potential for elimination of rare earth PMs in commercial scale wind turbine generators.

Acknowledgment: NSF Grant No. 1069283

References: 1. R. S. Semken, M. Polikarpova, P. Röyttä, J. Alexandrova, J. Pyrhönen, J. Nerg, A. Mikkola, J. Backman. “Direct-drive permanent magnet generators for high-power wind turbines: benefits and limiting factors,” *IET Renewable Power Generation*, vol. 6, pp.1-8, 2012.

2. G. Shrestha, H. Polinder, D. Bang, J. A. Ferreira. “Structural Flexibility: A Solution for Weight Reduction of Large Direct-Drive Wind-Turbine Generators,” *IEEE Tran. Energy Convers.*, vol. 25, pp. 732-740, Sept. 2010.

3. “Critical Materials Strategy,” U.S. Department of Energy, Oak Ridge, TN, Dec. 2011.

4. S. Constantinides. “The Demand for Rare Earth Materials in Permanent Magnets,” Arnold Magnetic Technologies, COM 2012, Niagara Fall, Canada, 1-2 Oct. 2012.

5. “ARNOX® Permanent Magnets: Hard Ferrite Material,” Arnold Magnetic Technologies, Apr. 2003, [Online], http://www.arnoldmagnetics.com/WorkArea/DownloadAsset.aspx?id=5146.

KEYWORDS: Halbach, ceramic, permanent magnet generator, wind energy.

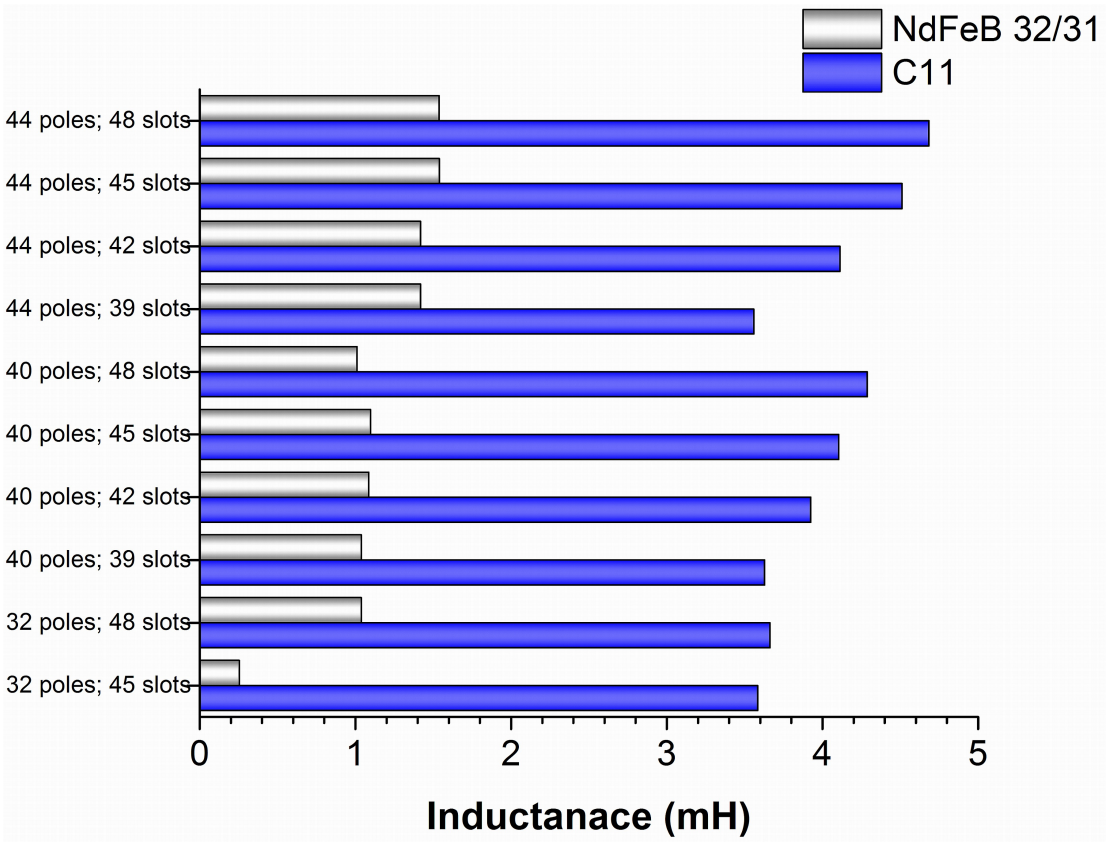

Fig. 1. Comparison of coil A inductance of 3.5kW HPMGs with NdFeB 32/31 and C11 permanent magnets.

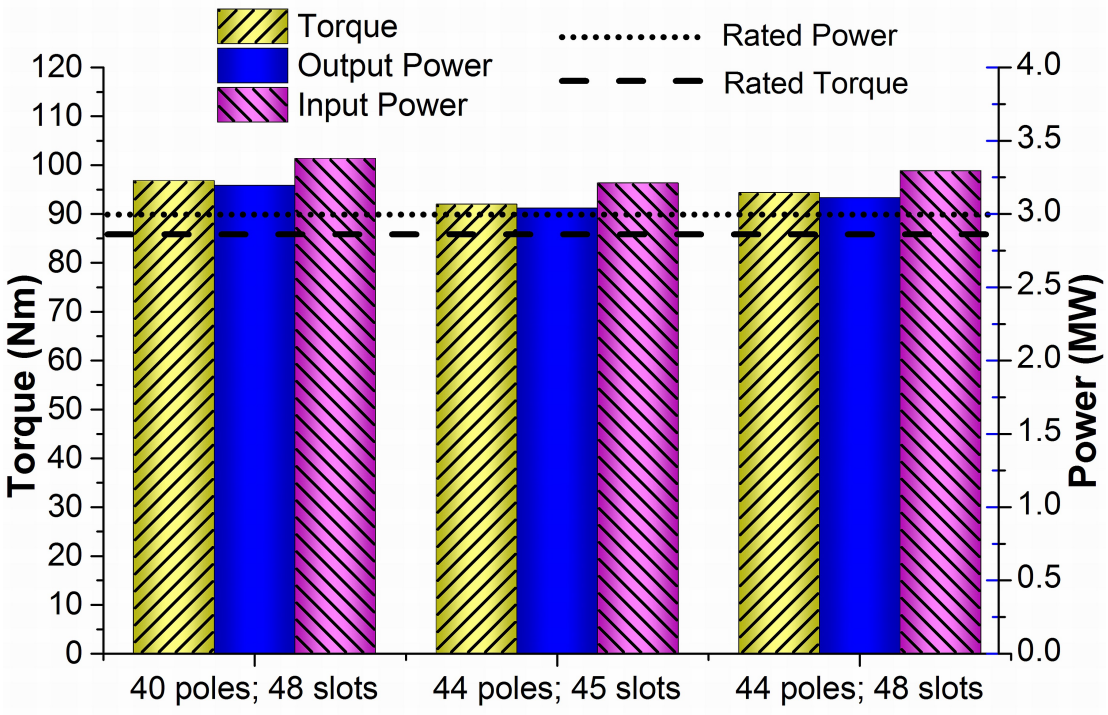

Fig. 2. Average torque and power achieved in ceramic 3MW HPMGs with varying pole and slot number.

CONTACT (NAME ONLY): Helena Khazdozian
CONTACT (E-MAIL ONLY): helenak@iastate.edu
PRESENTATION TYPE: Oral
CURRENT CATEGORY: X. Sensors (not Magnetic Recording), High Frequency and Power Devices
CURRENT SUB-CATEGORY: i. Motors: Motor Modeling and Simulations

Size Reduction of Permanent Magnet Generators for Wind Turbines Using Halbach Cylinders.

H. A. KHAZDOZIAN[1,2], R. L. HADIMANI[2], D. JILES[2]
1. Wind Energy Science, Engineering and Policy, Iowa State University, Ames, IA; 2. Electrical and Computer Engineering, Iowa State University, Ames, IA

I. INTRODUCTION

The U.S. is currently dependent on fossil fuels for electricity generation, resulting in negative consequences such as carbon emissions. To reduce this dependence the U.S. Department of Energy (DOE) has proposed 20% electricity generation from wind by 2030 as wind energy presents a viable and renewable alternative to fossil fuels. The DOE has targeted larger and offshore wind turbines to achieve this goal [1].

For offshore and remote wind turbines, direct drive permanent magnet generators (DDPMGs) are preferred over doubly-fed induction generators (DFIGs) as they eliminate the gearbox, which decreases reliability. However, the size and mass of DDPMGs scale much more rapidly than DFIGS with rated power according to the following sizing equations

$T=KD_r^2L_{stk}$ (1)

$K=1.74k_{w1}BA$ (2)

where T is torque, D_r is rotor diameter, L_{stk} is stack length, k_{w1} is the fundamental harmonic winding constant, B is average magnetic flux density over the rotor surface and A is electrical loading. To reduce the size of large scale PMGs, the magnetic flux density over the rotor surface can be increased to provide torque that is not provided by the rotor volume [2]. Halbach arrays are proposed to focus the magnetic flux density over the rotor surface, allowing for size reduction or potentially even the use of rare earth free permanent magnets (PMs).

II. METHODOLOGY

Halbach cylinders of finite volume and varying number of segments were designed and their magnetic flux focusing ability investigated with finite element methods employing MagNet™ by Infolytica Corporation. Four magnet segments or magnetic poles were used to define one array with a clockwise rotation of 90° in the magnetization direction for each segment in sequence. Only allowed pole combinations for a 27 slot machine that were also multiples a four were studied. The Halbach cylinder replaced the rotor of an outer rotor 3.5kW PMG rated at 100Nm, based on an existing design [3], eliminating the rotor back iron. An outer rotor PMG was selected to allow for reduced stack length. NdFeB 32/31 grade PMs were selected. The performance of the Halbach PMGs were simulated in MotorSolve™ by Infolytica Corporation and compared to evaluate the size reduction potential. Finally, the possibility of the use of rare earth free PMs in the Halbach machine was investigated.

III. RESULTS AND DISCUSSION

The performance of 8 Halbach PMGs with Halbach cylinders composed of 4, 8, 16, 20, 28, 32, 40 and 44 segments was investigated. It was found that for the 4 and 44 segment Halbach cylinders, rated torque and power were not achieved. Though the 40 and 44 segment Halbach cylinders had similar values of magnetic flux density over the rotor surface as 28 and 32, the resulting torque of the 40 and 44 segment Halbach PMGs were dramatically lower than that of the 28 and 32 segment Halbach PMGs (Fig. 1). This is unexpected as torque depends directly on the magnetic flux density over the rotor surface. Magnetic flux leakage may be one of the contributing factors which will be investigated in future work.

The 16 segment Halbach PMG achieved the highest magnetic flux density over the inner rotor surface, with more magnet segments generally achieving higher magnetic flux density over the rotor surface (Fig. 1). This differs from the Halbach cylinder alone where 8 segments achieved the highest magnetic flux density at its inner radius. The path provided for the magnetic flux by the stator back iron in the PMG may account for this difference.

The Halbach PMGs which achieved more than rated torque and high magnetic flux density over the rotor surface hold the greatest potential for size reduction of the 3.5kW PMG. For the 32 segment Halbach PMG, it was found that the outer diameter of rotor could be reduced by up to 25% while achieving rated torque and power and without significant loss of efficiency. This translates to 29% reduction in the rotor volume and 25% reduction in the NdFeB PM volume with respect to the conventional 3.5kW PMG design.

For the high torque PMGs, ceramic 11 grade PMs, which have the highest energy product among ceramic PMs, were substituted for the NdFeB. None were able to achieve rated torque or power (Fig. 2). The 28 segment Halbach cylinder PMG came closest, reaching torque and power of 82Nm and 2.7kW respectively.

IV. CONCLUSION

It has been demonstrated that by employing a Halbach cylinder as the rotor in an outer rotor 3.5kW PMG, size reduction is possible. By varying the number of magnet segments in the Halbach cylinder, the outer diameter of the rotor can be reduced by up to 25%, translating to a 29% reduction in rotor volume. The potential for reduction of material use is significant for large wind turbine application. However, the Halbach cylinders investigated do not produce sufficient magnetic flux density over the rotor surface to allow for the use of rare earth free PMs. Halbach cylinders with a smaller angle of rotation of magnetization direction between magnet segments will be investigated in future work.

V. ACKOWLEDEMENT

This work was supported by the National Science Foundation under Grant No. 1069283 and a Barbara and James Palmer Endowment at the Department of Electrical and Computer Engineering of Iowa State University.

1) "20% Wind Energy by 2030," U.S. Department of Energy, Oak Ridge TN, Tech. Rep. DOE/GO 102008-2567, July 2008.
2) H. A. Khazdozian, R. L. Hadimani, D. C. Jiles. "Size Reduction of Permanenet Magnet Generators for Wind Turbines with Higher Energy Density Permanent Magnet," North American Power Symposium (NAPS), 2014, pp. 1-6, 7-9 Sept. 2014, doi: 10.1109/NAPS.2014.6965439.
3) A. S. Abdel-Khalik, S. Ahmed, A. M. Massoud, A. A. Elserougi. "An improved performance direct-drive permanent magnet wind generator using a novel single-layer winding layout," IEEE Trans. Magn., vol. 49, pp. 5124-5134, Sept. 2013.

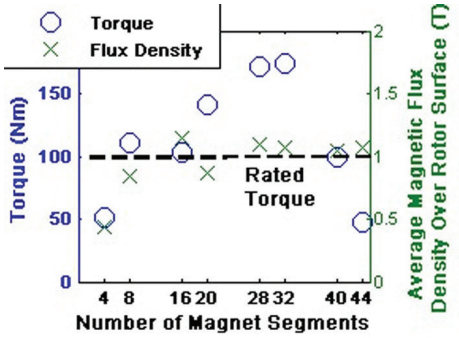

Fig. 1. Averaged torque and magnetic flux density over the inner rotor surface in Halbach PMGs with varying number of magnet segments.

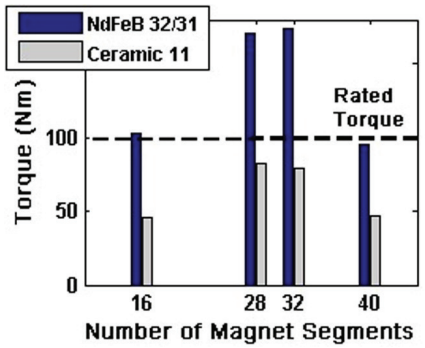

Fig. 2. Comparison of achieved torque in Halbach PMGs with varying PM material.

Size Reduction of Permanent Magnet Generators for Wind Turbines with Higher Energy Density Permanent Magnets

H. A. Khazdozian[1,2], R. L. Hadimani[2], D. C. Jiles[2]
[1]Wind Energy Science, Engineering and Policy Program
[2]Department of Electrical & Computer Engineering
Iowa State University
Ames, IA 50011

***Abstract*— Permanent magnet generators' (PMGs) dimensions scale with rated power due the sizing law for PMGs, which necessitates increased rotor volume to provide additional torque, preventing use of PMGs in large scale wind turbines. The use of higher energy density permanent magnets may offset the need to scale dimensions to achieve higher input torque. The properties of a permanent magnet necessary to achieve 25% reduction in dimensions in a 10MW wind turbine were calculated. A 29% increase in torque as a result of a 34% increase in the energy product of the permanent magnet is demonstrated.**

***Keywords*— permanent magnets, permanent magnet generators, wind energy**

I. Introduction

Wind capacity in the United States has more than doubled since the inception of the wind industry as demonstrated in Fig. 1. Currently, the U.S has 60GW installed wind capacity; this translates to 3.6% of total electricity generation [1]. The U.S. Department of Energy has proposed that 20% of electricity generation in the U.S. should be obtained from wind by 2030 [2]. Clearly, wind turbines with higher power ratings are necessary to achieve this goal. These larger wind turbines, as well as offshore development, will allow access to faster, more sustainable winds necessary to provide more power.

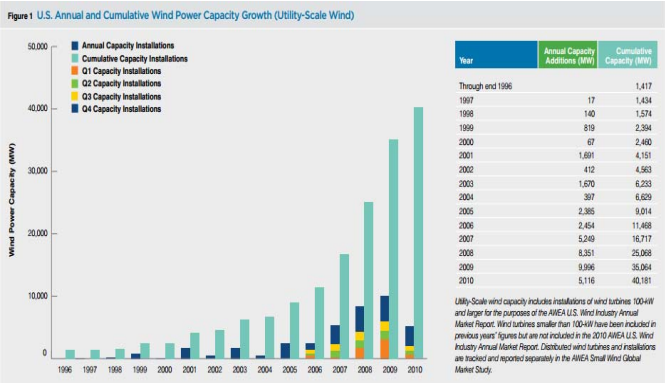

Fig. 1. U.S. annual and cumulative wind power capacity growth [1].

The majority of wind turbines currently employ doubly-fed induction generators (DFIG) to convert mechanical to electrical energy in the nacelle. DFIGs require a gearbox to increase the rotational speed of the shaft for efficient energy conversion. However, gearboxes are one of the most frequent causes of wind turbine failures and account for the greatest downtime [3], which results in a loss of profits for the wind farm. Gearbox failure significantly increases the operating and maintenance costs, requiring the use of expensive crane rentals [4]. Gearbox repair or replacement is even more challenging for offshore wind. It is desirable to eliminate the need for gearboxes in large scale wind turbines, especially for those that are offshore. Direct drive permanent magnet generators (PMGs) offer an alternate solution to DFIGs.

II. Permanent Magnet Generators

A. Fundamental Principles

In PMGs, the permanent magnets provide the magnetic flux necessary to induce a voltage in the stator windings by Faraday's law of induction. Permanent magnet properties such as coercivity, remanence and energy product are important parameters for PMG design. Coercivity is the ability of a permanent magnet to withstand demagnetization. Remanence is the magnetic flux density of the magnet after magnetization, representing the upper limit on flux density provided by the magnet. Finally, the energy product is defined as the maximum amount of energy stored in the magnet. The theoretical upper limit of energy product is given by

$$|BH|_{max} = B_r^2 / (4\mu_0\mu_r) \quad (1)$$

where B_r is the remanence, μ_0 is the permeability of free space and μ_r is the relative permeability. Magnetic permeability is a measure of the ease with which magnetic flux flows through a material. The energy product is the most widely quoted figure of merit for permanent magnets [5]. A combination of high remanence and high coercivity is desirable in permanent magnets.

978-1-4799-5904-4/14/$31.00 ©2014 IEEE

Permanent magnets fall into four families: Alnico, ceramics or hard ferrites, SmCo and NdFeB magnets. NdFeB is the industry standard in PMGs for wind turbines because it has the highest energy product (up to 477.5kJ/m^3) [5]. The energy product is the energy density of the magnet, so less volume of NdFeB is required to provide a specified flux density than other permanent magnet materials. The weight of the nacelle is an important design consideration in wind turbines, so decreasing the weight of permanent magnets is desirable. However, it should be noted that NdFeB does have limitations on its operating temperature [5-6] because of its Curie temperature of 312° C, which effectively means that its highest practical operating temperature is about 170°C. Other permanent materials such as SmCo offer a higher operating temperature and coercivity; NdFeB is preferred for PMG wind turbine application due to its higher maximum energy product, high cost of Co and the relatively low price of Nd with respect to Sm [5-6].

B. *Sizing Law*

PMGs offer several advantages over DFIGs. In a direct drive configuration, PMGs eliminate the need for a gearbox; the generator shaft rotates at the same speed as the blade rotor. Also, PMGs are more efficient than DFIGs. However, in the literature there are conflicting claims regarding which generator is more cost effective [7]. For instance, PMGs require a full size power converter, while the power converter for a DFIG is rated at only one third of the stator power rating. Yet, DFIGs result in higher operation and maintenance costs due to gearbox failure.

The primary argument for DFIGs over PMGs is that at larger outputs DFIGs are smaller and less massive. To achieve 6000kNm of input torque, the drivetrain weight with a PMG is approximately twice that of with a DFIG [8]. PMG dimensions scale much more dramatically as input torque is increased. This is due to the sizing law for PMGs, which is given by

$$T = kD_r^2L \tag{2}$$

where T is torque, k is a sizing constant, D_r is the rotor diameter and L is the stack length [9-10]. Higher input torque is required to achieve larger power output as described by the familiar relation below

$$P = T\omega \tag{3}$$

where P is the power and ω is the rated speed of the generator. From equations (2) and (3) it is evident that the size of the PMG must increase to provide larger output power. This increases the weight of PMGs, prohibiting their application in large scale wind turbines. The turbine tower must support the entire weight of the nacelle and rotor hub, so large, massive PMGs are undesirable in wind turbine design.

However, the torque (and output power) may be increased by another means. The sizing constant k is given by

$$k = 1.74k_{w1}BA \tag{4}$$

where k_{w1} is the fundamental harmonic winding factor, B is the average flux density of the rotor surface and A is the electrical loading [9,11]. Currently, increasing the average flux density of the rotor surface is limited by the energy density of the permanent magnet. However, if the energy product of the permanent magnet could be increased, the average flux density of the rotor surface could also be increased, thereby increasing the sizing constant, torque, and ultimately the output power of the PMG. This would help offset the need for increasing the dimensions of the PMG. A 25% reduction in dimensions of a 10MW PMG is proposed to demonstrate proof of concept since this would have even greater weight saving implications (rotor volume would be reduced by 58%). The theoretical properties of a permanent magnet necessary to provide the same level of input torque for a 10MW PMG with the proposed reductions in dimensions are calculated analytically. The theoretical results are then verified through finite element analysis.

III. METHODOLOGY

Initially, a small scale 3.5kW PMG was designed, and then scaled to 10MW. General machine topology was chosen to reflect that of industry based on discussions with a member of corporate research at ABB. Such commercial PMGs are radial-flux with N35SH or N35UH grade NdFeB magnets in a surface mounted or inset permanent magnet topology. Inner and outer rotor topologies are both used. For direct drive configuration in large scale wind, outer rotor topology is preferential because it allows for reduction in stack length. However, for this investigation inner rotor topology was selected for ease of design.

A radial-flux, surface mounted 3.5kW PMG was designed. The dimensions of the PMG were based on the design of Abdel-Khalik *et al.* [12]. Only 4 magnetic poles were selected to minimize the number of common denominators between the pole and slot number, which is desirable to minimize cogging torque. M19 26 Ga non-oriented Si steel was selected for the rotor and stator laminations [13]. Finite element software, MotorSolve by Infolytica Corporation, aided in design and was used to characterize the instantaneous performance of the generator at varying rotor position. The effects of varying the energy product and permanent magnet geometry were investigated for the 3.5kW design. The hypothesis of this paper was tested for the 10MW design; the input and output power, torque and efficiency were averaged over all rotor positions.

TABLE I. GENERAL SPECIFICATIONS OF THE 3.5KW PMG DESIGN

Rated torque (Nm)	100
Rated speed (rpm)	333
# of phases	3
# of poles	4
# of slots	24
Outer rotor diameter (mm)	192
Inner rotor diameter (mm)	113
Outer stator diameter (mm)	348
Inner stator diameter (mm)	194
Stack length (mm)	348

A. Model Validation

A finite element model of the 3.5kW PMG was developed using MotorSolve. To validate the results, the air gap flux density was determined analytically and numerically. The analytical model was developed by Zhu [14] where the air gap flux density is given by

$$B_g(r,\theta) = \sum_{n=1,3,5\ldots}^{\infty} \frac{\mu_0 M_n}{\mu_r} \frac{np}{(np)^2-1} \left\{ \frac{(np-1)+2\left(\frac{R_r}{R_m}\right)^{np+1} - (np+1)\left(\frac{R_r}{R_m}\right)^{2np}}{\frac{\mu_r+1}{\mu_r}\left[1-\left(\frac{R_r}{R_s}\right)^{2np}\right] - \frac{\mu_r-1}{\mu_r}\left[\left(\frac{R_m}{R_s}\right)^{2np} - \left(\frac{R_r}{R_m}\right)^{2np}\right]} \right\} \cdot \left[\left(\frac{r}{R_s}\right)^{np-1}\left(\frac{R_m}{R_s}\right)^{np+1} + \left(\frac{R_m}{r}\right)^{np+1}\right]\cos(np\theta) \quad (5)$$

$$M_n = \frac{2B_r\alpha_p}{\mu_0} \frac{\sin\left(\frac{n\pi\alpha_p}{2}\right)}{\frac{n\pi\alpha_p}{2}} \quad (6)$$

where μ_0 = permeability of free space
M_n = magnetization
μ_r = relative permeability
p = number of pole pairs
R_s = inner radius of stator
R_m = radius of magnets = $R_s - g$
g = air gap length
R_r = outer radius of rotor = $R_m - h_m$
h_m = radial thickness of magnet
r = radius at which flux density is being calculated
B_r = remanence
α_p = magnet pole arc to pole pitch ratio.

The comparison between the analytical and numerical results indicates good agreement (Fig. 2). The fringing field which occurs in the numerical result is an effect due to the presence of stator slots, which the analytical model ignores. There is a discrepancy in the position of the air gap flux density curves. This indicates a difference in the location of the permanent magnets and will not affect the average values of torque, power and efficiency computed from the numerical model.

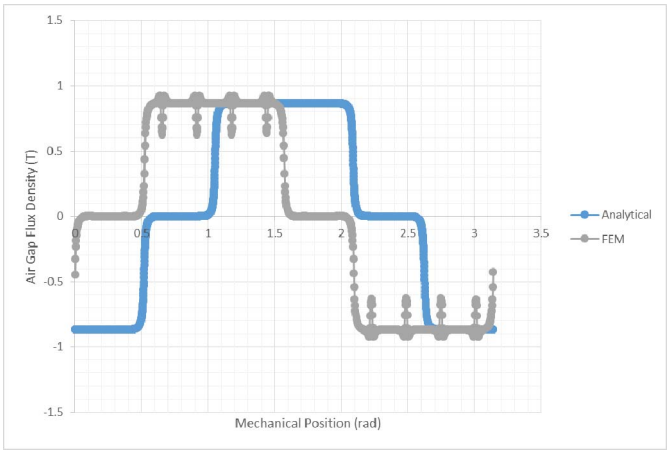

Fig. 2. Comparison of air gap flux density calculated with an analytical model and finite element model (FEM).

B. Scaling of PMG Design: 3.5kW to 10MW

The 3.5kW design was scaled to achieve a rated power of 10MW. NdFeB 48/11 grade magnets were selected to provide a high energy product. For the rated speed of 333rpm, a rated torque of 286,532Nm is required to achieve 10MW of power, as evident from equation (3). According to equation (2), each dimension must be scaled by 14.2 times to achieve this rated torque assuming the sizing constant k remains unchanged.

TABLE II. GENERAL SPECIFICATIONS OF THE 10MW PMG DESIGN WHERE DIMENSIONS OF THE 3.5KW DESIGN HAVE BEEN SCALED BY 14.2 TIMES (CASE 1)

Rated Torque (Nm)	286532
Outer rotor diameter (mm)	2726
Inner rotor diameter (mm)	1359
Outer stator diameter (mm)	4942
Inner stator diameter (mm)	2754
Stack length (mm)	4942

It has been hypothesized that the rated torque of the 10MW PMG design can be maintained when the dimensions are reduced by 25% if the energy product of the permanent magnet is increased. This will increase the average flux density of the rotor surface, and consequently the sizing constant k. The dimensions of the 10MW PMG design in Table II were reduced by 25% (Table III). To account for the resulting reduction in torque, the sizing constant k must increase by 2.37 times. The sizing constant will increase linearly with an increase in the average flux density of the rotor surface as described by equation (4). Assuming this flux density will scale linearly with an increase in energy product and the electrical load remains constant, the energy product must also scale by 2.37 times. This implies the remanence of the permanent magnet must be increased by 1.54 times, as evident from equation (1). The calculated theoretical remanence, relative permeability and upper limit on the energy product were calculated as shown below.

$$B_r = 1.54*1.39T = 2.14T$$

$$\mu_r = (B_r/H_c) / \mu_0 = 1.64035$$

$$|BH|_{max} = 553.9 kJ/m^3$$

where H_c is the coercivity equal to 1,060,650A/m and μ_0 is $4\pi x10^{-7}$ H/m. The initial remanence and coercivity are that of NdFeB 48/11.

TABLE III. GENERAL SPECIFICATIONS OF THE 10MW PMG DESIGN WHERE DIMENSIONS OF THE DESIGN IN TABLE II HAVE BEEN REDUCED BY 25% (CASES 2-3)

Rated Torque (Nm)	286532
Outer rotor diameter (mm)	2045
Inner rotor diameter (mm)	1020
Outer stator diameter (mm)	3707
Inner stator diameter (mm)	2066
Stack length (mm)	3707

IV. RESULTS & DISCUSSION

A. Variation of Energy Product

For the 3.5kW design, the "grade" of NdFeB magnet was varied (i.e. the properties were altered) in order to understand the impact of the energy product on the performance of the generator. Four grades of NdFeB magnets were selected. For increased grade, the remanence, coercivity and energy product of the permanent magnet increased as demonstrated in Table IV. **The output power of the generator increased linearly with energy product**, assuming all other factors were held constant. This result is expected since more magnetic flux is available to excite the stator windings, inducing more voltage in the armature.

From Fig. 3, it is evident that **increased energy product also resulted in decreased efficiency**. This result is less intuitive, and perhaps even surprising. It is likely that for high energy product, stray field losses increased. Without optimization of the geometry of the permanent magnets, the flux density is not well focused. Variation of permanent magnet geometry or stator teeth geometry may reduce such losses. This is an important consideration if higher energy density permanent magnets are to be considered for future use. There is a tradeoff between efficiency and output power for increased energy product of the permanent magnets.

TABLE IV. Magnetic Properties of Various Grades of NdFeB Magnets.

	NdFeB 28/32	NdFeB 34/22	NdFeB 40/15	NdFeB 48/11
B_r (T)	1.08	1.19	1.29	1.39
H_c (A/m)	-815539	-894591	-971014	-1060650
μ_r	1.05554	1.06427	1.05474	1.03967
$\|BH\|_{max}$ (kJ/m^3)	220.6	267.6	312.4	367.4

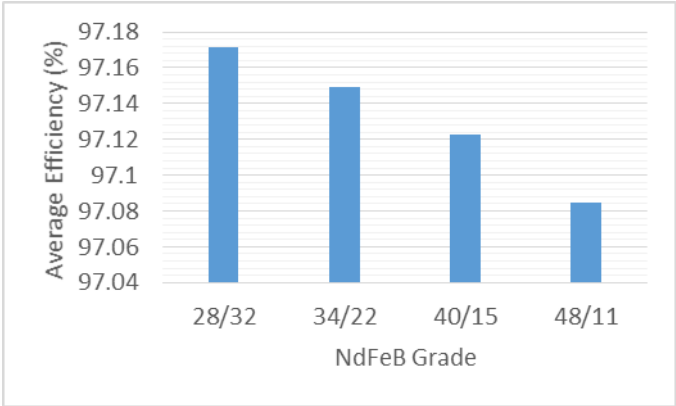

Fig. 3. Average efficiency of 3.5kW PMG with varying permanent magnet grades.

B. Effects of Permanent Magnet Geometry

The effects of varying magnet angle and magnet thickness were investigated. The magnet angle and magnet thickness were varied independently from their initial values of 60° and 5mm respectively; the change in each parameter resulted in equal change in volume.

Output power was observed to increase with magnet volume in general. This result is again intuitive. For larger permanent magnet volume, more flux is available for excitation of the stator windings. It is similar to the previous result in which more output power was produced due to higher energy product. In both cases, the strength of flux source increased.

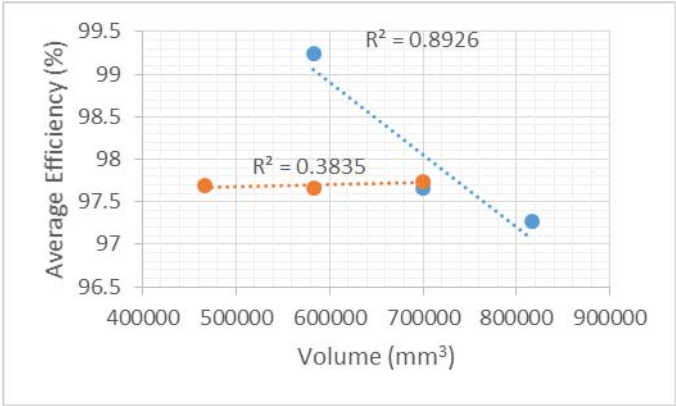

Fig. 4. Average efficiency of 3.5kW PMG with varying permanent magnet volume by change in magnet thickness (orange) and change in magnet angle (blue).

The efficiency was observed to decrease linearly with an increase in magnet angle (Fig. 4). This is consistent with the previous results in which efficiency decreased due to higher energy product. However, a linear trend was not observed between efficiency and increased magnet thickness as demonstrated by the poor linear fit in Fig. 4. Thus, efficiency is not related linearly to change in permanent magnet volume in general. This suggests that the geometry of the permanent magnet also contributes to the efficiency.

C. Sizing Law Investigation

The average input and output power, torque and efficiency of the three PMG cases were compared to determine the validity of the proposed hypothesis. Case 1 refers to the 10MW design presented in Table II in which only the dimensions of the 3.5kW PMG were scaled to achieve rated torque. Case 2 refers to a 25% reduction in dimensions (Table III) with no change in the permanent magnet properties. Case 3 refers to the 10MW design presented in Table III in which the remanence and energy product were increased to the values previously determined to achieve rated torque. Thus, case 1 and 3 should theoretically be able to provide the same rated torque. From Figs. 5 and 6, the reduction in average output power and torque in case 2 (compared to case 1) demonstrates the principle of the sizing law. It is apparent from Figs. 5 and 6 that rated power and rated torque were achieved for both cases 1 and 3. In case 3, the increased permanent magnet energy product was able to compensate for the lack of torque provided by the size of the PMG. Thus, the hypothesis has been validated.

The results suggest that ideally the permanent magnetic material would allow for a reduction in dimensions of 25%, translating to a reduction in rotor volume of 58%. It is also important to note that high efficiency of the PMG was maintained for reduced dimensions and increased energy product as shown in Fig. 7.

V. Conclusions

A 10MW PMG was designed by the simple process of scaling a 3.5kW PMG. The effects of varying design parameters such as permanent magnet volume, geometry and energy product were studied. Efficiency of PMGs seem to be dependent on the volume as well as the geometry of the permanent magnets. It was noticeable that an unexpected tradeoff exists between output power and efficiency when increasing the energy product of the permanent magnet for a given PMG design. It was demonstrated that the dimensions of the 10MW PMG can be reduced by 25% through increasing the energy product of the permanent magnet. This translates to a rotor volume reduction of 58%. The improvement of permanent magnetic materials in the form of increased energy product has significant implications for the future use of PMGs in large scale wind turbines.

VI. Future Work

By way of example, it has been proven that increased remanence and energy product of permanent magnets allow for reductions in the size of PMGs. However, there are many issues left to be addressed. In order for PMGs to compete with DFIGs in large scale wind turbine application, PMG size and mass must be reduced. Further size reduction is possible and should be aligned with industry objectives. The remanence represents the upper limit of achievable flux density supplied by the permanent magnet in the absence of an applied field. This value cannot exceed the saturation of the Si steel laminations in the rotor and stator. For M19 non-oriented Si steel laminations, saturation occurs at approximately 2.4T. Therefore, the remanence could be increased slightly, allowing for further reduction in the size of the PMG. The dimensions could also be reduced further through the use of outer rotor topology as previously discussed.

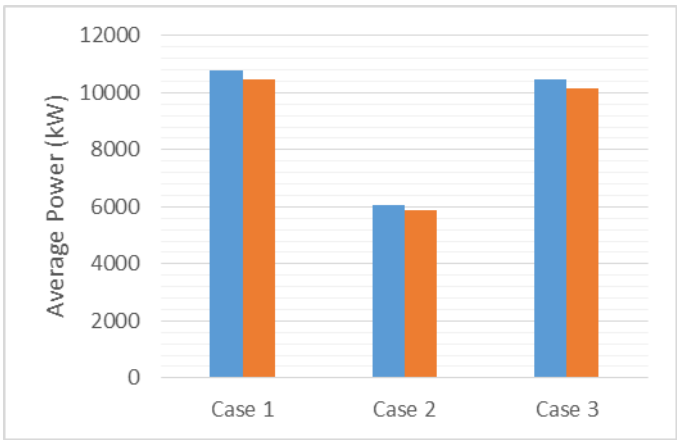

Fig. 5. Comparison of the average input power (blue) and output power (orange) of each PMG.

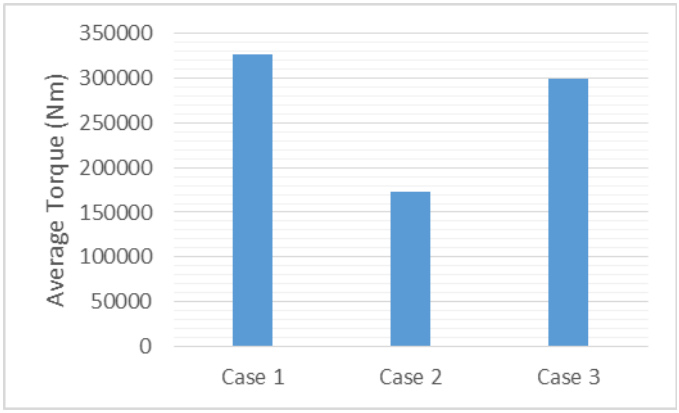

Fig. 6. Comparison of the average torque of each PMG.

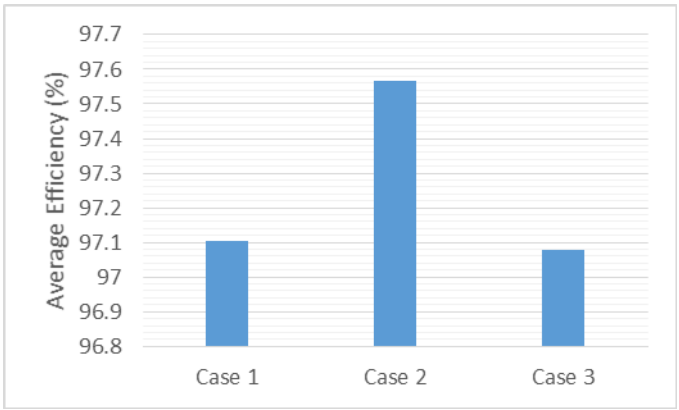

Fig. 7. Comparison of the average efficiency of each PMG.

ACKNOWLEDGMENT

The authors would like to acknowledge that this work was supported by the National Science Foundation under Grant No. 1069283 as well as a Barbara and James Palmer Endowment at the Department of Electrical and Computer Engineering of Iowa State University. The authors would like to thank Dr. J. D. McCalley of Iowa State University and Dr. D. D. Tremelling of ABB for useful discussions regarding this work.

REFERENCES

[1] "AWEA U.S. Wind Industry Annual Market Report Year Ending 2010," American Wind Energy Association, 2011.

[2] "20% Wind Energy by 2013," U. S. Department of Energy, Oak Rdige, TN, Tech. Rep. DOE/GO 102008-2567, July 2008.

[3] S. S. Sheng. "Report on Wind Turbine Subsystem Reliability – A Survey of Various Databases," National Renewable Energy Laboratory, Golden, CO, Tech. Rep. NREL/PR-5000-59111, June 2013.

[4] K. S. Morey. (2014, Feb. 27). "GE opens wind turbine repair, innovation lab in Albany," *Albany Business Review* [Online]. Available: http://www.bizjournals.com/albany/news/2014/02/26/ge-opens-wind-turbine-repair-facility.html?page=all.

[5] O. Gutfleisch *et al.* "Magnetic materials and devices for the 21st century: stronger, lighter, and more energy efficient," *Adv. Mater,*. vol. 23, pp. 821-842, Feb. 2011.

[6] L Lewis, F. Jiménez-Villacorta. "Perspectives on permanent magnetic materials for energy conversion and power generator,"*Metall. Mater. Trans. A,* vol. 44A, pp. S2-S20, Jan. 2013.

[7] J. Purahen. (2014, Apr. 21). "The Big Wind Energy Drive Train Technology Debate," *Renewable Energy World* [Online]. Available: http://www.renewableenergyworld.com/rea/news/article/2014/04/the-big-wind-energy-drive-train-technology-debate?cmpid=WNL-Wednesday-April23-2014.

[8] R. Qu. "Development and Challenges of Permanent Magnet Wind Generators," presented at Workshop on Next-Generation Wind Power, RPI, May 2010.

[9] J. R. Hendershot, TJE Miller. "Sizing & Computer-Aided Design," in *Design of Brushless Permanent-Magnet Motors*. Oxford, UK, Magna Physics Publishing and Clarendon Press, 1994, ch. 12, sec. 12.2, pp. 12-2 – 12-5.

[10] D. C. Hanselman. "Basic Concepts," in *Brushless Permanent-Magnet Motor Design.* New York, McGraw-Hill, Inc., 1994, ch. 1, pp. 11-12.

[11] J. R. Hendershot, T. J. E. Miller, "Basic Design Choices," in *Design of Brushless Permanent-Magnet Machines.* Venice, U.S., Motor Design Books LLC, 2010, ch. 3, sec. 3.3.1, pp. 87-91.

[12] A. S. Abdel-Khalik, S. Ahmed, A. M. Massoud, A. A. Elserougi. "An improved performance direct-drive permanent magnet wind generator using a novel single-layer winding layout," *IEEE Trans. Magn.,* vol. 49, pp. 5124-5134, Sept. 2013.

[13] J. R. Hendershot, TJE Miller. "Basic Design Choices," in *Design of Brushless Permanent-Magnet Motors*. Oxford, UK, Magna Physics Publishing and Clarendon Press, 1994, ch. 3, sec. 3.7, pp. 3-27.

[14] Z. Q. Zhu. "Instantaneous magnetic field distribution in permanent magnet dc motors, part I: open-circuit field," *IEEE Trans. Magn*., vol. 29, pp. 124-135, Jan. 1992.

APPENDIX B. CONFERENCE PRESENTATIONS

- **H. A. Khazdozian**, R. L. Hadimani, D. C. Jiles. “Alternatives to Rare Earth Permanent Magnets for Energy Harvesting Applications,” to be presented at the *American Physical Society March Meeting 2016*, Baltimore, MD, Mar. 2016. (poster).

- **H. A. Khazdozian**, R. L. Hadimani, D. C. Jiles, “Use of Non-Rare-Earth Permanent Magnets in Halbach Cylinder Rotor Permanent Magnet Generator,” *IEEE Magnetics Conference (INTERMAG) 2016*, San Diego, CA, Jan. 2016.

- **H. A. Khazdozian**, R. L. Hadimani, D. C. Jiles, “Improved Design of Permanent Magnet Generators for Large Scale Wind Turbines,” Poster Presentation at the Electrical and Computer Engineering Graduate Poster Session, Iowa State University, Ames, IA, Oct. 2015.

- **H. A. Khazdozian**, R. L. Hadimani, D. C. Jiles, “Improved Design of Permanent Magnet Generators for Large Scale Wind Turbines,” Poster Presentation at the Wind Energy Industry Symposium, Iowa State University, Ames, IA, Sept. 2015.

- **H. A Khazdozian**, R. L. Hadimani, D. C. Jiles, “Size reduction of Permanent Magnet Generators for Wind Turbines Using Halbach Cylinders,” *IEEE Magnetics Conference (INTERMAG) 2015*, Beijing, China, pp. 1-2, May 2015. (poster)

- **H.A. Khazdozian**, R. L. Hadimani, D. C Jiles, “Size Reduction Techniques for Large Scale Permanent Magnet Generators in Wind Turbines,” *American Physical Society March Meeting 2015*, San Antonio, TX, Mar. 2015.

- **H. A. Khazdozian**, R. L. Hadimani, D. C. Jiles, “Size Reduction of Permanent Magnet Generators for Wind Turbines with Higher Energy Density Permanent Magnets,” *North American Power Symposium (NAPS)*, 2014, pp. 1-6, Sept. 2014.

- **H. A. Khazdozian**, R. L. Hadimani, D. C. Jiles, “Increased Efficiency of a Permanent Magnet Synchronous Generator through Optimization of NdFeB Magnet Arrays,” *American Physical Society March Meeting 2014*, Denver, CO, Mar. 2014.

Abstract Submitted
for the MAR16 Meeting of
The American Physical Society

Alternatives to Rare Earth Permanent Magnets for Energy Harvesting Applications[1] HELENA KHAZDOZIAN, RAVI HADIMANI, DAVID JILES, Department of Electrical and Computer Engineering, Iowa State University — Direct-drive permanent magnet generators (DDPMGs) offer increased reliability and efficiency over the more commonly used geared doubly-fed induction generator, yet are only employed in less than 1 percent of utility scale wind turbines in the U.S. One major barrier to increased deployment of DDPMGs in the U.S. wind industry is NdFeB permanent magnets (PMs), which contain critical rare earth elements Nd and Dy. To allow for the use of rare earth free PMs, the magnetic loading, defined as the average magnetic flux density over the rotor surface, must be maintained. Halbach cylinders are employed in 3.5kW Halbach PMGs (HPMGs) of varying slot-to-pole ratio to concentrate the magnetic flux output by a lower energy density PM over the rotor surface. We found that for high pole and slot number, the increase in magnetic loading is sufficient to allow for the use of strontium iron oxide hard ferrite PMs and achieved rated performance. Joule losses in the stator windings were found to increase for the hard ferrite PMs due to increased inductance in the stator windings. However, for scaling of the HPMG designs to 3MW, rated performance and high efficiency were achieved, demonstrating the potential for elimination for rare earth PMs in commercial scale wind turbines.

[1]This work was supported by the National Science Foundation under Grant No. 1069283 and a Barbara and James Palmer Endowment at Iowa State University

Helena Khazdozian
Department of Electrical and Computer Engineering, Iowa State University

Date submitted: 05 Nov 2015 Electronic form version 1.4

Abstract Submitted
for the MAR15 Meeting of
The American Physical Society

Size Reduction Techniques for Large Scale Permanent Magnet Generators in Wind Turbines[1] HELENA KHAZDOZIAN, RAVI HADIMANI, DAVID JILES, Department of Electrical and Computer Engineering, Iowa State University — Increased wind penetration is necessary to reduce U.S. dependence on fossil fuels, combat climate change and increase national energy security. The U.S Department of Energy has recommended large scale and offshore wind turbines to achieve 20% wind electricity generation by 2030. Currently, geared doubly-fed induction generators (DFIGs) are typically employed in the drivetrain for conversion of mechanical to electrical energy. Yet, gearboxes account for the greatest downtime of wind turbines, decreasing reliability and contributing to loss of profit. Direct drive permanent magnet generators (PMGs) offer a reliable alternative to DFIGs by eliminating the gearbox. However, PMGs scale up in size and weight much more rapidly than DFIGs as rated power is increased, presenting significant challenges for large scale wind turbine application. Thus, size reduction techniques are needed for viability of PMGs in large scale wind turbines. Two size reduction techniques are presented. It is demonstrated that 25% size reduction of a 10MW PMG is possible with a high remanence theoretical permanent magnet. Additionally, the use of a Halbach cylinder in an outer rotor PMG is investigated to focus magnetic flux over the rotor surface in order to increase torque.

[1]This work was supported by the National Science Foundation under Grant No. 1069283 and a Barbara and James Palmer Endowment at Iowa State University.

Helena Khazdozian
Department of Electrical and Computer Engineering, Iowa State University

Date submitted: 12 Nov 2014 Electronic form version 1.4

Abstract Submitted
for the MAR14 Meeting of
The American Physical Society

Increased Efficiency of a Permanent Magnet Synchronous Generator through Optimization of NdFeB Magnet Arrays[1] HELENA KHAZDOZIAN, RAVI HADIMANI, DAVID JILES, Department of Electrical and Computer Engineering, Iowa State University — The United States is currently dependent on fossil fuels for the majority of its energy needs, which has many negative consequences such as climate change. Wind turbines present a viable alternative, with the highest energy return on investment among even fossil fuel generation. Traditional commercial wind turbines use an induction generator for energy conversion. However, induction generators require a gearbox to increase the rotational speed of the drive shaft. These gearboxes increase the overall cost of the wind turbine and account for about 35 percent of reported wind turbine failures. Direct drive permanent magnet synchronous generators (PMSGs) offer an alternative to induction generators which eliminate the need for a gearbox. Yet, PMSGs can be more expensive than induction generators at large power output due to their size and weight. To increase the efficiency of PMSGs, the geometry and configuration of NdFeB permanent magnets were investigated using finite element techniques. The optimized design of the PMSG increases flux density and minimizes cogging torque with NdFeB permanent magnets of a reduced volume. These factors serve to increase the efficiency and reduce the overall cost of the PMSG.

[1]This work is supported by a National Science Foundation IGERT fellowship and the Barbara and James Palmer Endowment at the Department of Electrical and Computer Engineering of Iowa State University

Helena Khazdozian
Department of Electrical and Computer Engineering, Iowa State University

Date submitted: 15 Nov 2013 Electronic form version 1.4

APPENDIX C. WORKING PAPERS (UNDER REVIEW OR UNPUBLISHED)

- **H. A. Khazdozian**, R. L. Hadimani, D. C. Jiles, “Development of Rare Earth Free Permanent Magnet Generator using Halbach Cylinder Rotor Design,” *Renewable Energy*, under review.

- **H. A. Khazdozian**, R. L. Hadimani, D. C. Jiles, “Size Reduction of Permanent Magnet Generators using Magnetic Flux Focusing Techniques,” *Magnetics and Magnetic Materials 2016*, under review .

- **H.A. Khazdozian**, R. L. Hadimani, D. C Jiles, “Magnetic Flux Focusing for Rare Earth Free Permanent Magnet Generator Designs,” *2016 Magnetics Technology International*, working paper.

- **H. A. Khazdozian.** “Environmental, Social and Political Causes for Lack of U.S. Rare Earth Supply Policy,” *Renewable Energy*, working paper.

Development of Rare Earth Free Permanent Magnet Generator using Halbach Cylinder Rotor Design

Helena A. Khazdozian[1,2], Ravi L. Hadimani[3,2], and David C. Jiles[1,2]

[1]Wind Energy Science, Engineering and Policy, Iowa State University, Ames, IA, 50011, USA
[2]Department of Electrical and Computer Engineering, Iowa State University, Ames, IA, 50011, USA
[3]Department of Mechanical and Nuclear Engineering, Virginia Commonwealth University, Richmond, VA, 23284, USA
helenak@iastate.edu

Abstract

Direct-drive permanent magnet generators (DDPMGs) offer increased reliability and efficiency for wind turbine application over the more commonly used geared doubly-fed induction generators. However, deployment of DDPMGs is limited in the U.S. wind industry due to reliance on NdFeB permanent magnets, which contain critical rare earth elements Nd and Dy. To allow for the use of lower energy density, rare earth free permanent magnets, Halbach cylinders are employed as the rotor in a 3.5 kW PMG to concentrate magnetic flux over the rotor surface and increase magnetic loading. By varying the slot-to-pole ratio in Halbach PMGs (HPMGs), designs are developed which allow for the use of ceramic, or hard ferrite, strontium iron oxide permanent magnets. At the 3.5 kW scale, the ceramic HPMGs are able to achieve rated performance, though at reduced average efficiency of between 82 to 87%, due to the difference permanent magnet material properties. For scaling of the ceramic HPMGs to 3 MW, rated performance and high efficiency were achieved on average at rated speed, demonstrating the potential for a rare earth free PMG in commercial scale wind turbines.

Keywords: Halbach array, permanent magnet, permanent magnet generator, rare earth, wind energy

1. Introduction

The U.S. Department of Energy (DOE) has recommended the advancement of wind turbine drive train technology, including direct-drive permanent magnet generators (DDPMGs), to achieve the long-term goal of 35% wind electricity generation in the U.S. by 2050 [1-2]. Currently, the majority of wind turbines in the U.S. employ geared doubly-fed induction generators (DFIGs) for conversion of mechanical to electrical energy [1]. However, gearboxes account for the most downtime per failure in wind turbines, significantly increasing operation and maintenance costs [3]. By eliminating the gearbox, DDPMGs increase reliability and decrease operation and maintenance costs [4-5]. DDPMGs also have higher efficiency at both full and partial load than geared DFIGs [4-5]. Yet, as of September 2015 DDPMGs were only employed in less than 1% of utility scale (>100 kW) wind turbines in the U.S. wind industry [6].

NdFeB permanent magnets, used as the magnetic flux source in PMGs for wind turbines, contain rare earth elements Nd and Dy. Partial substitution of Dy for Nd in the NdFeB alloy is performed to increase anisotropy, which increases coercivity and temperature coefficient, allowing for high-temperature application without risk of demagnetization [7]. Nd and Dy are considered "critical materials" by the DOE due to their supply risk and importance to renewable energy

technologies [8]. This presents a major barrier to their increased deployment in the U.S. as an estimated 250 to 600 kg of permanent magnet material per MW is required [8, 9]. Elimination of rare earth NdFeB permanent magnets in DDPMGs is desirable to allow for their increased use in the U.S. wind industry.

1.1 Background

To generate rated power, DDPMGs must generate high torque at low speeds as described by equation (1).

$$P = T\omega \tag{1}$$

$$T = KBAV_r \tag{2}$$

where P is power, ω is rated speed, T is torque, K is the output coefficient, B is the magnetic loading, A is the electric loading and V_r is rotor diameter [10-11]. To generate high levels of torque at low speeds, large rotor volumes and high energy density NdFeB permanent magnets, which increase the magnetic loading B, are used. The magnetic loading B is defined as the average magnetic flux density over the rotor surface [10-11].

Permanent magnets have four figures of merit including the remanence B_r, coercivity H_c, energy product BH, and maximum working temperature T_w. The remanence B_r is the residual magnetic flux density remaining after an applied magnetic field is removed, the coercivity H_c is the magnetic field strength required to demagnetize the permanent magnet, the energy product BH is the energy density, and the maximum working temperature T_m is the maximum temperature the permanent magnet can operate at without becoming demagnetized. Rare earth permanent magnets such as NdFeB and SmCo have the highest energy product, or energy density, of all commercial permanent magnets (Table I). Rare earth free permanent magnets, such as hard ferrite (ceramic) permanent magnets require much more volume to produce the same magnetic flux. Thus, for the same volume, magnetic loading will be significantly reduced with the use of ceramic permanent magnets.

Table I. Typical properties of commercial permanent magnets [12].

	B_r (kG)	**H_c (kOe)**	**BH_{max} (MGOe)**	**T_m (°C)**
NdFeB	10.8 – 14.9	11.0 – 34.0	28 – 54	220
SmCo	8.7 – 11.6	8.2 – 10.9	18 – 31.5	350
Hard Ferrites	2.0 – 4.1	1.57 – 4.0	0.8 – 4.32	300
alnico	6.6 – 13.2	0.475 – 1.475	1.35 – 10.5	538

To maintain magnetic loading in a PMG when using lower energy density ceramic permanent magnets, the magnetic flux must be concentrated over the rotor surface. By concentrating magnetic flux over the rotor surface, the magnetic flux density can be increased without the need for a stronger permanent magnet or more permanent magnet volume. Halbach arrays can be used to concentrate magnetic flux [13-14]. A Halbach array is an arrangement of permanent magnets that causes magnetic flux to be concentrated to only one side of the magnet array (Fig. 1a). Halbach arrays can be arranged in a cylinder, or Halbach cylinder (HC), as shown in Fig. 1b to focus magnetic flux inside or outside of the cylinder. When used in machine application, HCs offer the benefit of elimination of the rotor back-iron and sinusoidal airgap flux density and back-EMF [15-16].

In part due to manufacturing costs, HCs have been limited in application. For a review of these applications, the reader is referred to reviews by Zhu and Howe [15-16]. The potential benefits of HCs in PMGs for wind turbines, especially elimination of rare earth permanent magnets, may make the trade-off for increased manufacturing costs worthwhile. Thus, we have investigated the use of HCs to accomplish this.

In this paper, we found PMG designs which increased magnetic loading, and consequently torque, by employing a HC as the rotor. Ceramic permanent magnets were substituted as the permanent magnet material in these designs and their performance was investigated at the 3.5 kW and 3 MW scale.

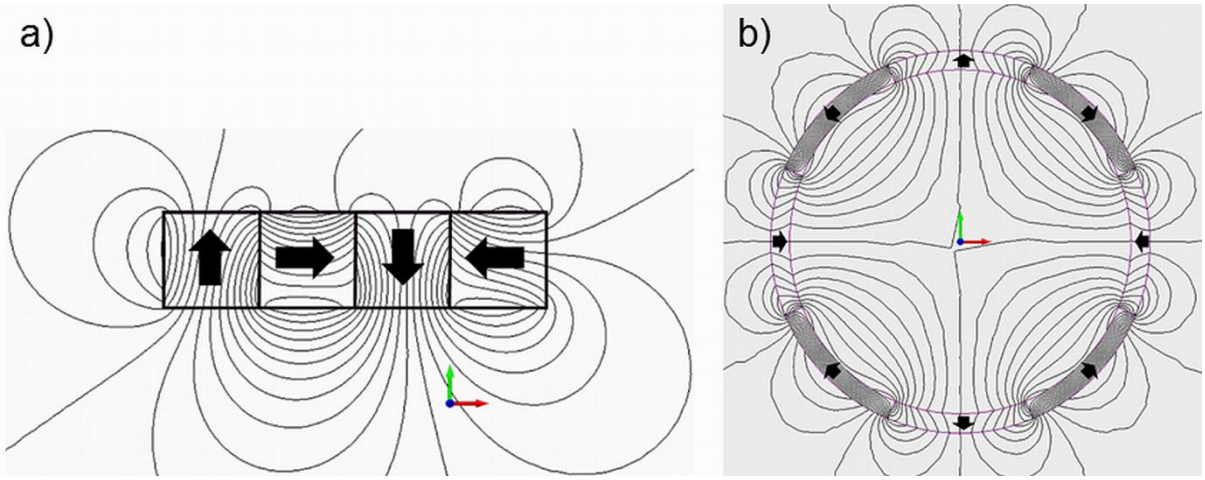

Fig. 1. Magnetic flux profile of a) 4 segment Halbach array and b) 8 segment Halbach cylinder. Arrows indicate magnetization direction.

2. Methodology

Halbach PMGs (HPMGs) with rated power of 3.5 kW were designed by employing a HC cylinder as the rotor, eliminating the rotor back-iron (Fig. 2). The number of magnetic poles (1 magnet segment per pole) was varied in allowed multiples of 4 (for a 24 slot machine), giving HPMGs with 4, 8, 16, 20, 28, 32 and 44 poles. The HCs used the magnetization scheme depicted in Fig. 1b (rotation of the magnetization by 90°) for all design variations. NdFeB 32/31 permanent magnets (see Table III for properties) were used initially to find designs which increased magnetic loading sufficiently for the use of ceramic permanent magnets by varying the slot-to-pole ratio for each design variation to optimize the efficiency of the magnetic flux path between the rotor and stator. Rotor volume, permanent magnet material volume, outer diameter, stack length, airgap length and machine ratings were kept constant (Table II) and were based on a design for a surface mounted PMG [17]. The dimensions of the inner stator were adjusted accordingly for each design to maximize efficiency

Finite element methods were used to calculate the torque, input and output power, airgap flux density, magnetic loading and cogging torque as a function of the rotor position, employing 2D steady-state, motion analysis in MotorSolve^{TM} by Infolytica Corporation. The advance angle was set to 180° to allow for simulation of generator operation at rated speed (333 rpm) and rated current (100 A). 24 sampling points per period for the best periodicity, 5 skew samples, and a harmonic amplitude threshold of $1x10^{-6}$ were used. Efficiency was calculated simply by taking the average

output power over the average input power. Finite element methods were also employed to determine the time-averaged hysteresis and eddy-current losses in each conducting component (stator windings and yoke) with 2D steady-state, motion analysis in MagNet by Infolytica Corporation™. Instantaneous windage losses were determined in MotorSolve™. Stray losses and thermal effects are ignored in these calculations.

For NdFeB HPMGs with rated power of 3.5kW that achieved more than twice the value of rated torque and power, ceramic 11 (C11), a strontium iron oxide grade permanent magnet, was substituted as the permanent magnet material in the HPMGs. No other design specifications were changed. C11 permanent magnets were selected as the rare earth free permanent magnet because it has one of the highest energy products among ceramic permanent magnets (Table III). C11 permanent magnets are fabricated from non-critical materials including strontium, carbonate and iron oxide [12].

Finally, the ceramic HPMGs which achieved rated torque and power were scaled to 3 MW to demonstrate a design which could be potentially adapted for commercial use. The performance was calculated utilizing the same finite element methods used for the 3.5 kW machines. The construction and assembly of the designs were not investigated to allow for an investigation of what is theoretically possible in terms of permanent magnetic material use.

Table II. 3.5 kW HPMG design specifications.

Rated Power (kW)	3.5
Rated Torque (Nm)	100
Rated Speed (rpm)	333
Outer Diameter (mm)	300
Stack Length (mm)	100
Airgap Length (mm)	1

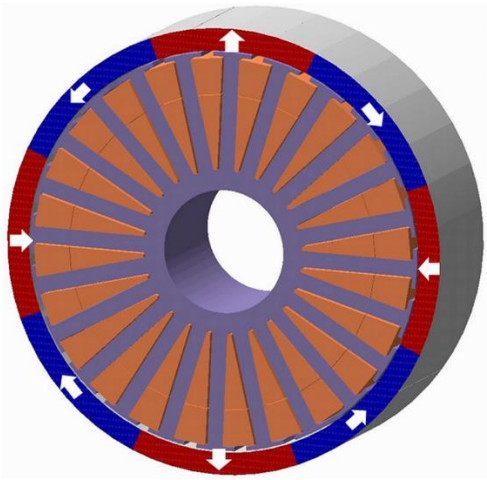

Fig. 2. Schematic of HPMG design (8 poles and 24 slots).

Table III. Permanent magnet properties.

	B_r (kG)	**H_c (kOe)**	**BH_{max} (MGOe)**
C11	4.3	3.94	4.1
NdFeB 32/31	11.7	11	32

3. Results & Discussion

3.1 Ceramic Halbach Permanent Magnet Generators: 3.5 kW

For the NdFeB HPMG design variations which achieved at least twice the value of rated torque (100 Nm) and power (3.5 kW) shown in Table IV, C11 permanent magnets were substituted as the permanent magnet material. Almost all the C11 HPMG designs achieved rated torque (100 Nm) on average at rated speed (Fig. 3a) with the exception of three designs (32 poles and 45 slots, 40 poles and 39 slots, and 44 poles and 39 slots). However, only 3 C11 HPMG designs achieved rated power (3.5 kW) on average at rated speed (Fig. 3b).

Table IV. 3.5 kW HPMGs with NdFeB 32/31 grade permanent magnets which achieved twice (or more) the value of rated torque and power.

# Poles	# Slots	Torque (Nm)	Input Power (kW)	Output Power (kW)	Efficiency (%)	Magnetic Loading (T)
32	45	229.91	8.03	7.38	92.00	0.791
32	48	244.78	8.55	7.94	92.87	0.792
40	39	248.77	8.68	8.13	93.67	0.833
40	42	262.63	9.17	8.55	93.22	0.845
40	45	273.83	9.56	8.85	92.61	0.795
40	48	283.58	9.90	9.10	91.91	0.805
44	39	254.17	8.87	8.30	93.55	0.836
44	42	273.00	9.53	8.89	93.32	0.841
44	45	286.93	10.02	9.30	92.87	0.839
44	48	299.14	10.44	9.64	92.28	0.840

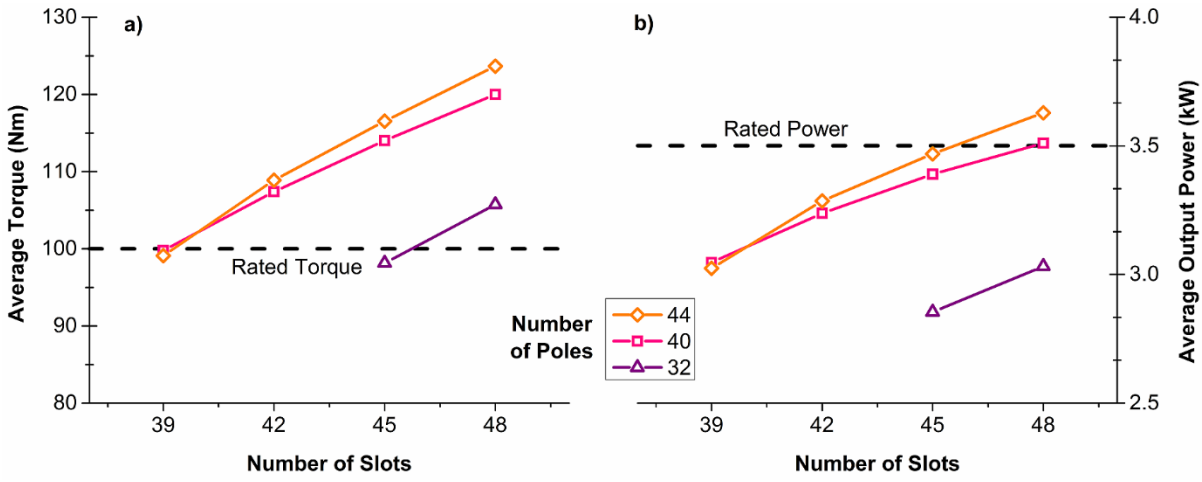

Fig. 3. Average torque (a) and output power (b) achieved in 3.5 kW HPMGs with C11 permanent magnets with varying pole and slot number.

In the C11 HPMGs, we observed that high pole and slot number contributed to the achievement of higher torque and power (Fig. 3), agreeing with previous results [18]. However, for constant pole number, the slot-to-pole ratio did not significantly affect the average magnetic flux density achieved over the rotor surface (Fig. 4a), with standard deviations of less than 1%. This is also consistent with previous results [18].

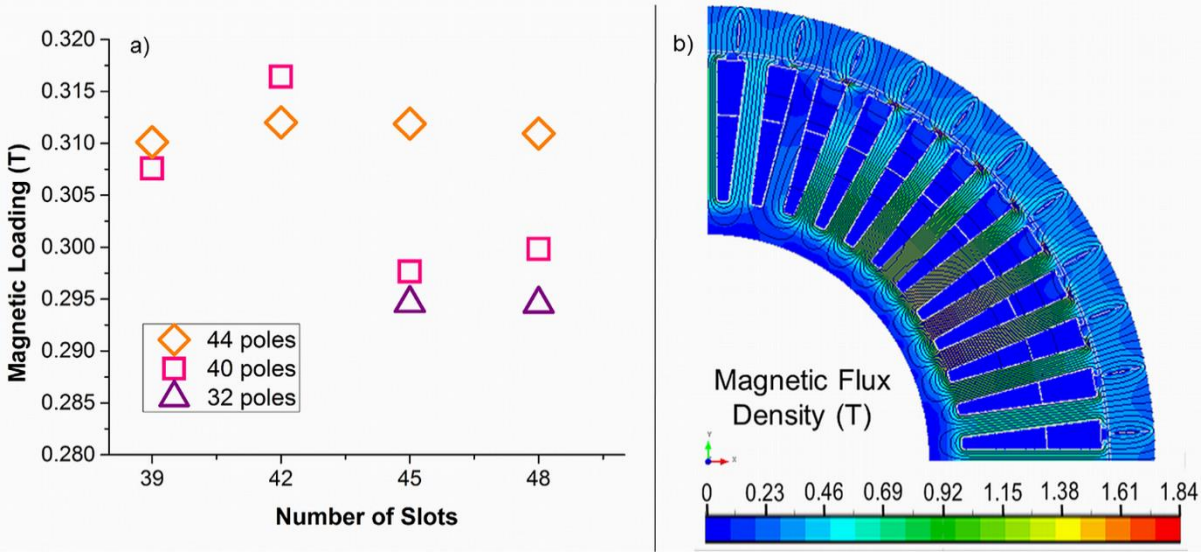

Fig. 4. Magnetic loading of 3.5 kW HPMGs with C11 permanent magnets and varying slot and pole number (a) and magnetic flux density distribution in a 3.5 kW HPMG with C11 permanent magnets and 44 poles and 48 slots (b).

3.1.1 Airgap Flux Density

A brief discussion of the airgap flux density calculated for the NdFeB HPMGs is merited to contextualize the airgap flux density of the C11 HPMGs. Significant variation in the airgap flux density can be seen for changing pole and slot number. For constant pole number, an increase in the number of slots resulted in more fringing present in the airgap flux density curve (Fig. 5). Slotting is known to cause this fringing effect [19], explaining the amplified fringing for higher slot number. For lower slot number, the airgap flux density resembles that of a Halbach cylinder with 2 magnet segments per pole, as expected [15-16]. However for higher slot number, the airgap flux density resembles that of a radially magnetized HC. Furthermore, for constant slot number, the fringing due to slotting was most prominent for low pole number than for high pole number in general (Fig. 6). The airgap flux density of the C11 HPMGs is consistent with this result (Fig. 7). From Fig. 8 it is apparent that for the C11 HPMGs, fringing was also more significant for higher slot number, though less amplified due to the high pole number.

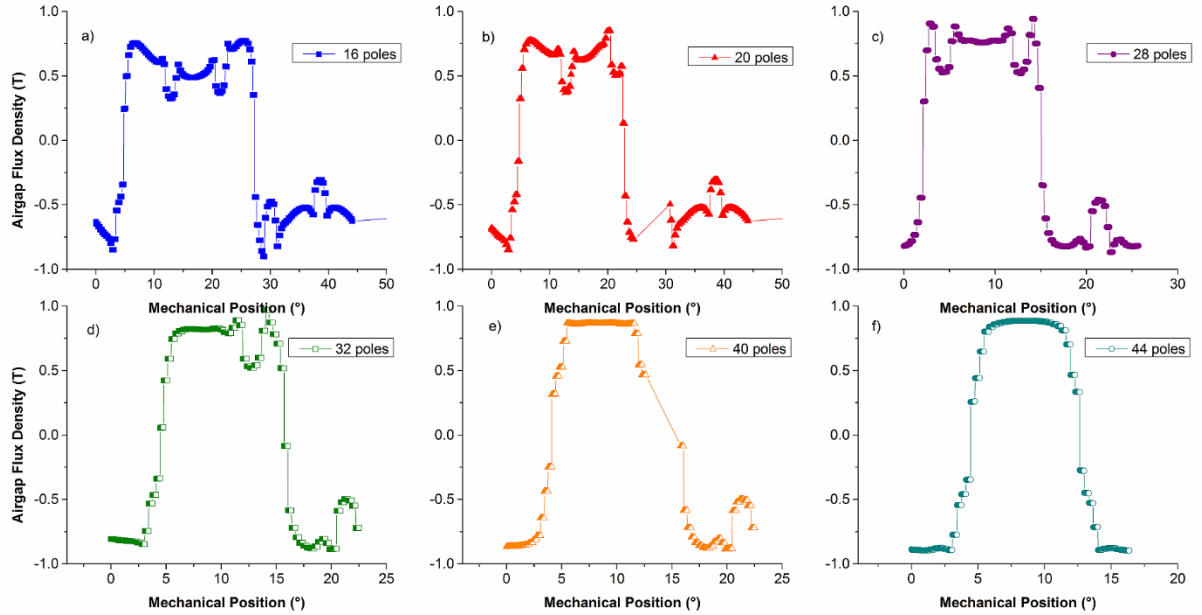

Fig. 5. Airgap flux density of NdFeB HPMGs, with a rated power of 3.5 kW, 42 slots and a) 16 poles, b) 20 poles, c) 28 poles, d) 32 poles, e) 40 poles, and f) 44 poles.

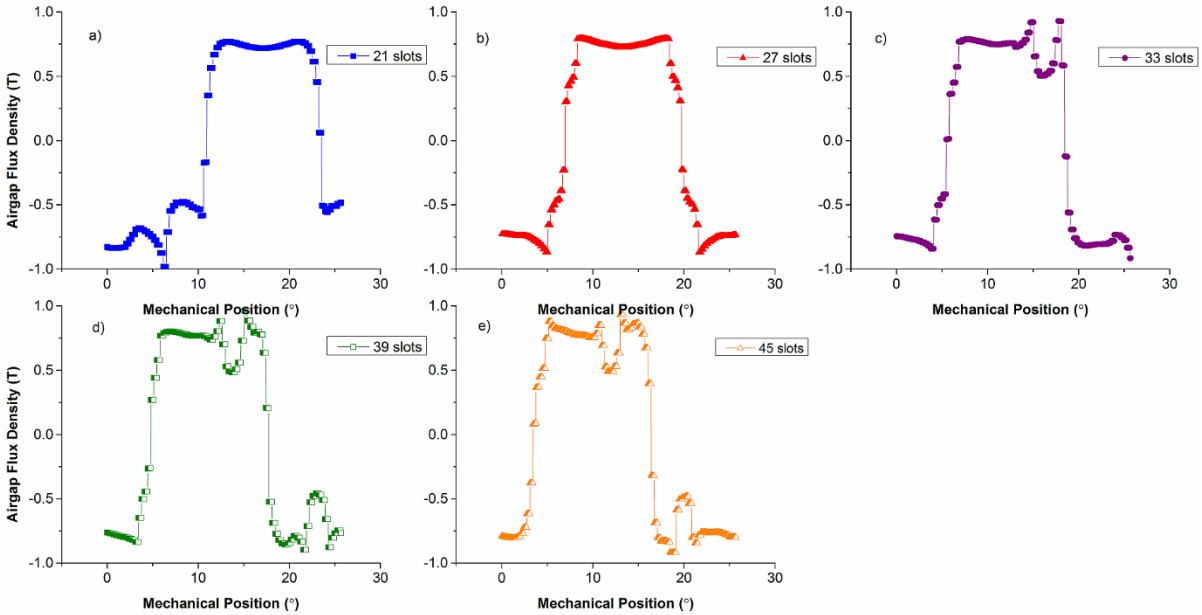

Fig. 6. Airgap flux density of NdFeB HPMGs, with a rated power of 3.5 kW, 28 poles and a) 21 slots, b) 27 slots, c) 33 slots, d) 39 slots, and e) 45 slots.

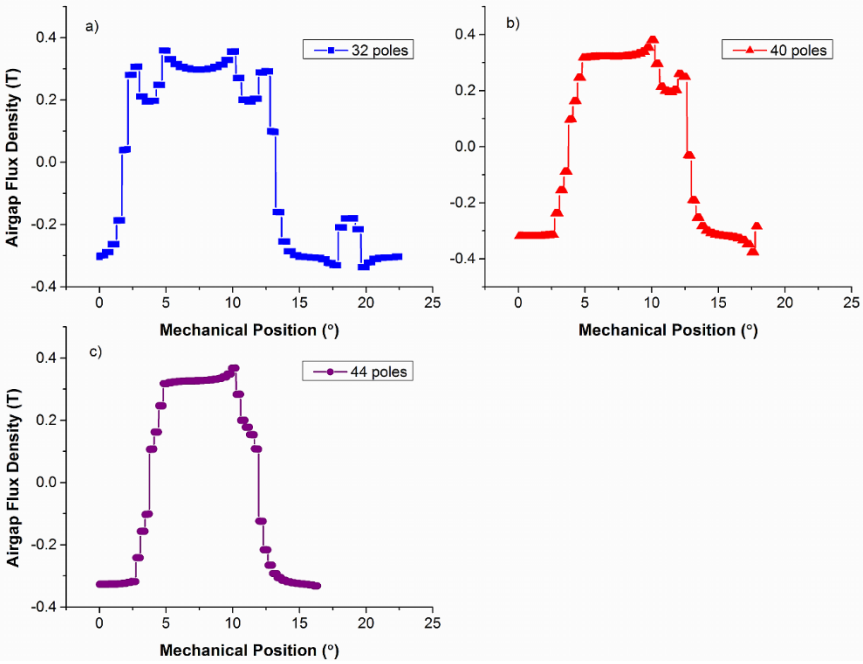

Fig. 7. Airgap flux density of C11 HPMGs, with a rated power of 3.5 kW, 48 slots and a) 32 poles, b) 40 poles, and c) 44 poles.

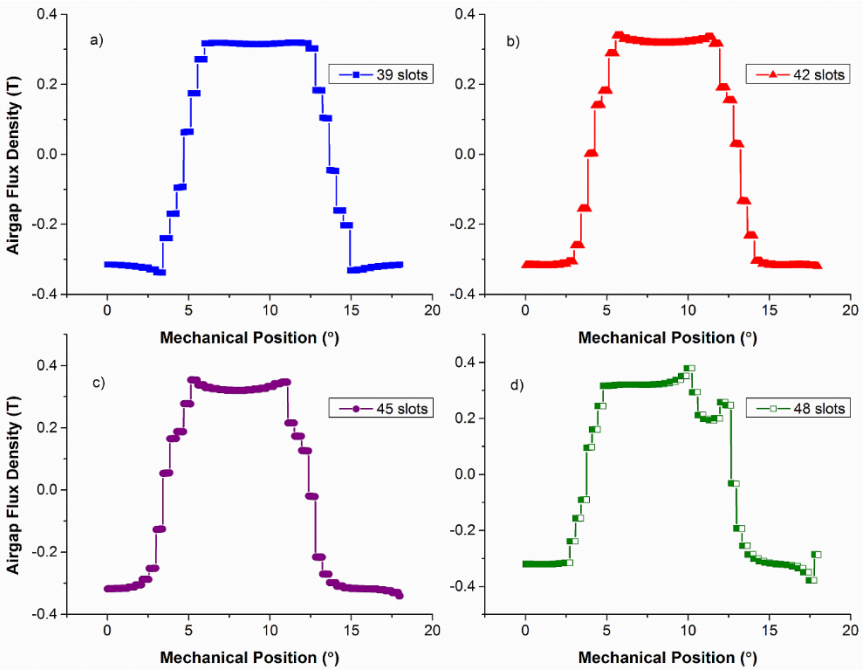

Fig. 8. Airgap flux density of C11 HPMGs, with a rated power of 3.5 kW, 40 poles and a) 39 slots, b) 42 slots, c) 45 slots, and d) 48 slots.

3.1.2 Cogging Torque

The cogging torque of the C11 HPMGs was found to be less than half a percent of rated torque with the exception of one machine (32 poles and 48 slots) as shown in Table V. The periodicity and shape of the cogging torque was a function of the generator design, specifically the slot-to-

pole ratio. However, the amplitude was directly related to the permanent magnet material. While the shape of the cogging torque was identical for the HPMGs regardless of permanent magnet material, the cogging torque of the NdFeB HPMGs was significantly higher than for the C11 HPMGs (Fig. 9). This is intuitive since the overall torque is reduced for the C11 HPMGs due to the reduction of energy product and consequently magnetic loading.

Table V. Cogging torque of 3.5 kW HPMGs with varying pole and slot number and permanent magnet material.

	Cogging Torque (Nm)	
Pole and slot configuration	**C11**	**NdFeB 32/31**
32 poles, 45 slots	0.0082	0.0651
32 poles, 48 slots	8.7857	77.1343
40 poles, 39 slots	0.0040	0.1980
40 poles, 42 slots	0.0240	0.1826
40 poles, 45 slots	0.0610	1.7432
40 poles, 48 slots	0.0294	4.8703
44 poles, 39 slots	0.0040	0.0416
44 poles, 42 slots	0.0240	0.2514
44 poles, 45 slots	0.0610	0.4478
44 poles, 48 slots	0.0294	0.4486

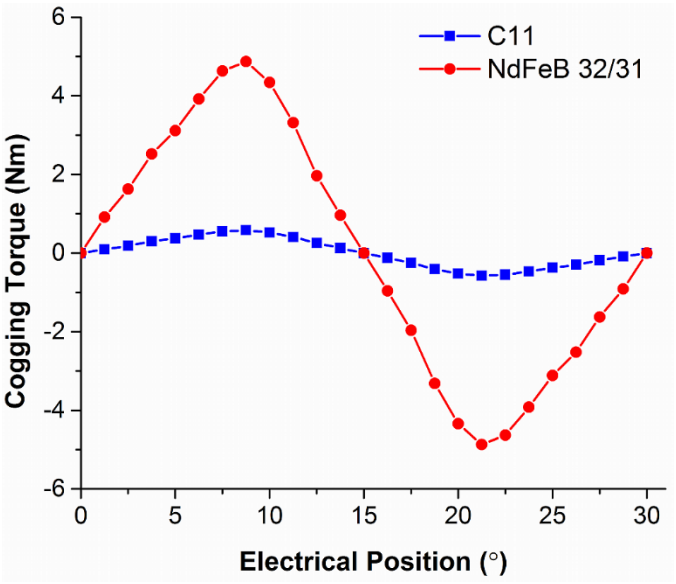

Fig. 9. Comparison of cogging torque for a 3.5 kW HPMGs with 40 poles and 38 slots.

3.1.3 Efficiency & Losses

We found that the average efficiency of the 3.5 kW HPMGs at rated speed (333 rpm) was reduced to between 82 and 87% with the use of C11 permanent magnets, compared to efficiencies between 91 and 94% for NdFeB permanent magnets (Table VI). The losses in the

HPMGs for each permanent magnet material were explored. Machine losses include Joule or copper losses W_{Cu}, iron losses W_{Fe}, friction and windage losses W_{mech}, and stray losses W_{stray}

$$W_T = W_{Cu} + W_{Fe} + W_{mech} + W_{stray} \quad (3)$$

$$W_{Cu} = mI_{ph}^2 R_{ph} \quad (4)$$

$$W_{Fe} = W_h + W_e \quad (5)$$

where W_T is the total loss, m is the number of phases (3), I_{ph} is the RMS phase current, R_{ph} is the phase resistance, W_h is the hysteresis loss and W_e is the eddy-current loss [20].

Table VI. Average efficiency of 3.5 kW HPMGs at rated speed with varying pole and slot number and permanent magnet material.

	Average Efficiency (%)	
Pole and slot configuration	**C11**	**NdFeB 32/31**
32 poles, 45 slots	83.31	92.00
32 poles, 48 slots	82.15	92.87
40 poles, 39 slots	87.49	93.67
40 poles, 42 slots	86.38	93.22
40 poles, 45 slots	85.16	92.61
40 poles, 48 slots	83.81	91.91
44 poles, 39 slots	87.43	93.55
44 poles, 42 slots	86.45	93.32
44 poles, 45 slots	85.27	92.87
44 poles, 48 slots	84.07	92.28

The total losses were determined for each design variation from the difference between the input and output power. The time-averaged ohmic, hysteresis and eddy-current losses were calculated as described in the methodology section. Copper losses are sometimes referred to as ohmic losses due to dependence on the resistance of the copper coils as shown in equation (4). Iron losses are composed of hysteresis and eddy-current losses as shown in the relationship in equation (5). Windage losses were calculated in MotorSolve and found to be on the order of 10^{-7} kW/mm^3 and thus were considered negligible. As described in the methodology section, friction and stray losses are ignored by the finite element calculations because no thermal analysis was performed and stray losses are generally negligible.

The percent of total losses due to iron losses decreased overall for the use of the C11 permanent magnets with a decrease in both hysteresis and eddy-current contributions (Fig. 10). This is explained by the dependence of hysteresis and eddy-current loss on the peak magnetic flux density, given by the relationships in equation (6) and (7) respectively. The peak magnetic flux density is higher for the use of NdFeB 32/31 permanent magnets because of higher energy product and remanence than C11 permanent magnets (Table III).

$$W_h = C_h B_{pk}^n \quad (6)$$

$$W_e = C_e B_{pk}^2 f^2 \quad (7)$$

where C_h is a coefficient of hysteresis, B_{pk}^n is the peak magnetic flux density, n is a material dependent non-constant exponent, varying between 1.6 to 2.2, C_e is a coefficient of eddy current, and f is frequency [20].

In terms of the percent of total losses, ohmic losses were increased slightly for the use of the C11 permanent magnets. However, it should be noted that the value of ohmic losses was equal for each HPMG design variation regardless of permanent magnet material due to the fact that the stator design was unchanged. Thus ohmic losses only accounted for a greater percentage of the total losses for the C11 HPMGs because the iron losses were reduced.

From Fig. 10, it is clear that the ohmic and iron losses do not account for 100% of the losses in the 3.5 kW HPMGs of either permanent magnet material. In permanent magnet machines, Joule losses will not be purely resistive. Self and mutual inductance in the coils will add a reactive component to the windings impedance, likely accounting for the remaining losses.

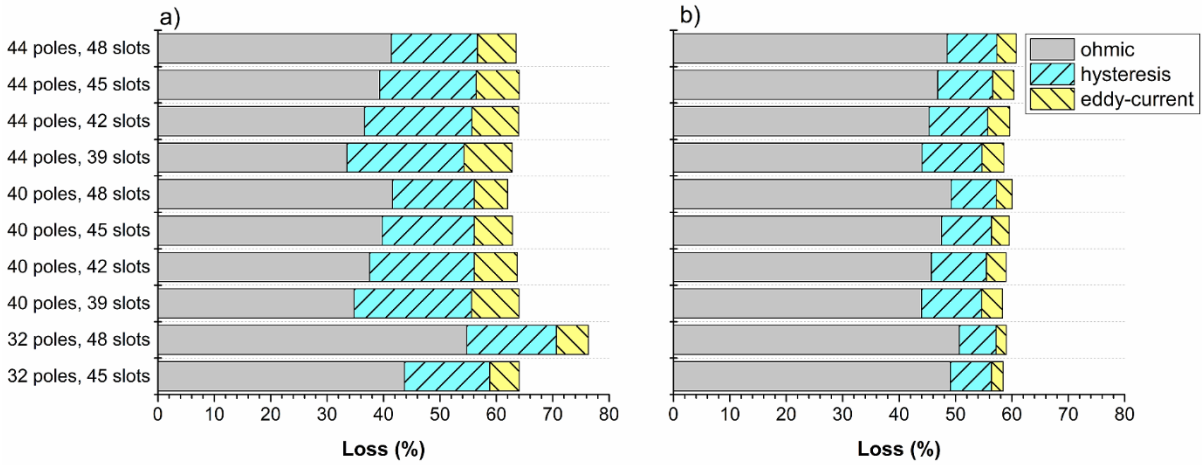

Fig. 10. Calculated losses in terms of percent of total loss for 3.5 kW HPMGs with a) NdFeB permanent magnets and b) C11 permanent magnets.

The only variable design factor in each 3.5 kW HPMG design was the permanent magnet material. Thus, the change in permanent magnet material properties must be responsible for the reduction in efficiency in the C11 HPMGs. To determine which property or properties were responsible for the reduction in efficiency, the energy product, remanence, coercivity and relative permeability of the NdFeB 32/31 permanent magnets were independently set to that of C11 and the torque, input and output power were calculated with finite element methods using the same methods described in the methodology section.

The reduced coercivity of the C11 permanent magnets was ultimately found to account for the decreased efficiency of the C11 3.5 kW HPMGs. The difference in coercivity of the C11 permanent magnets accounts for the higher relative permeability of the C11 permanent magnets with respect to the NdFeB 32/31 permanent magnets (Table III). To substantiate this, the coercivity of the NdFeB 32/31 permanent magnets was varied in a 3.5 kW HPMG with 44 poles and 48 slots, while *all* other parameters were left constant. From Fig. 11 below it is clear that there is a direct relationship between a decrease in coercivity of the permanent magnet and the efficiency, explaining the reduced efficiency of the C11 HPMGs. Thus, for the 3.5 kW HPMGs, the iron losses were reduced for the use of the C11 permanent magnets with lower energy product and remanence, and the reactive contribution to the copper losses was increased for the

use of C11 permanent magnets due to the reduced coercivity and consequently increased relatively permeability.

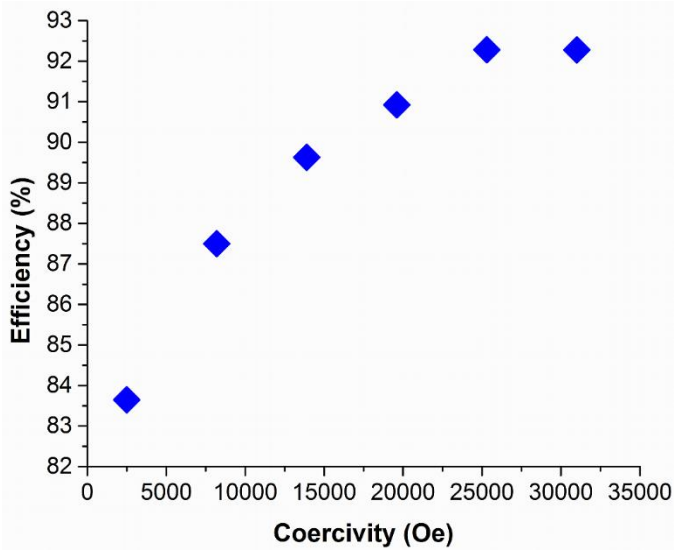

Fig. 11. Variation of efficiency with coercivity of NdFeB 32/31 permanent magnets in a 3.5 kW HPMG with 44 poles and 48 slots.

3.2 Ceramic Halbach Permanent Magnet Generators: 3 MW

The C11 HPMG designs which achieved rated torque (100 Nm) and power (3.5 kW) were scaled to 3 MW. For the 3 MW HPMGs with C11 permanent magnets, rated torque (85989.89 Nm) and power (3 MW) were achieved for all 3 designs (Fig. 12). 94% efficiency was achieved for all 3 HPMGs on average at rated speed. Larger machines tend to be more efficient than smaller ones, and it was found that ohmic losses were significantly reduced for the scaled 3 MW HPMG.

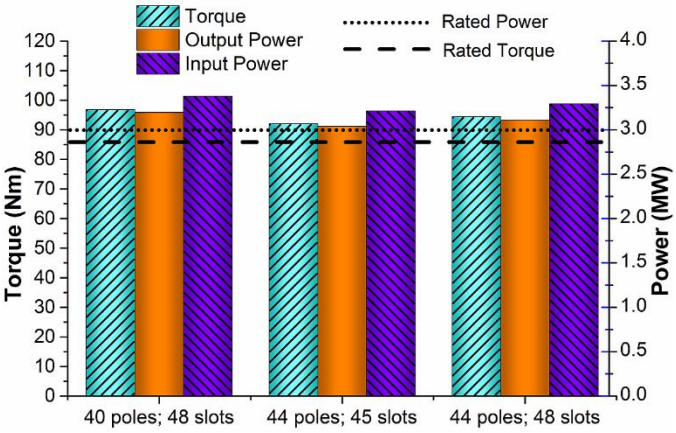

Fig. 12. Average torque and power achieved in 3 MW HPMGs with C11 permanent magnets and varying number of poles and slot.

When comparing the 3 MW HPMGs with C11 permanent magnets, we observed that higher pole number allowed for significant overall size reduction of the HPMG with the 44 pole machines being over 1 meter smaller in outer diameter than the 40 poles HPMG (3 meters vs. 4.1 meters) as shown in Table VII. The pole and slot number did not greatly affect the peak airgap flux density or airgap flux density distribution achieved (Fig. 13). Fringing due to slotting is

again more apparent for higher slot number and more prevalent for lower pole number in the 3 MW HPMGs (Fig. 14), which is consistent with the results for the 3.5 kW HPMGs. Finally, the cogging torque of the C11 3 MW HPMG with 40 poles and 48 slots was significant (Fig. 15a), but still less than 3% of the rated torque, while the cogging torque of the 44 pole, 3 MW HPMGs was less than 0.5% of rated torque. This gives some design flexibility when designing the 3 MW HPMG with the 44 pole, 45 slot machine being the best option in terms of cogging torque.

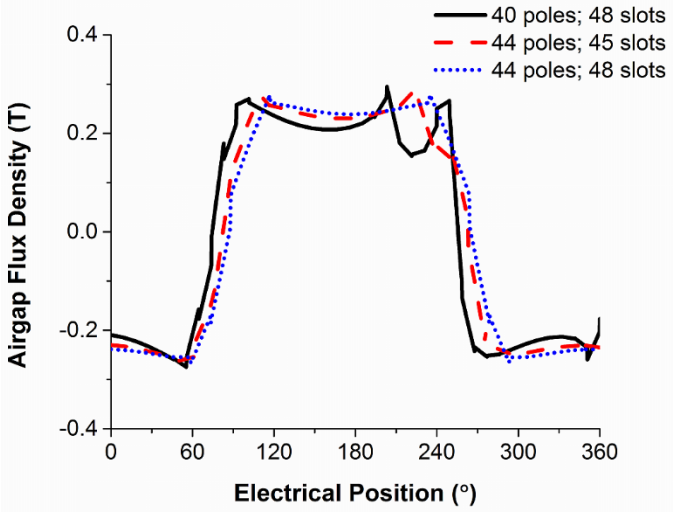

Fig. 13. Airgap flux density for 3 MW HPMGs with C11 permanent magnets and varying number of poles and slots.

Table VII. Dimensions of 3 MW HPMGs with C11 permanent magnets.

# Poles	40	44	44
# Slots	48	45	48
Outer Diameter (mm)	4100	3000	3000
Stack Length (mm)	1367	1000	1000

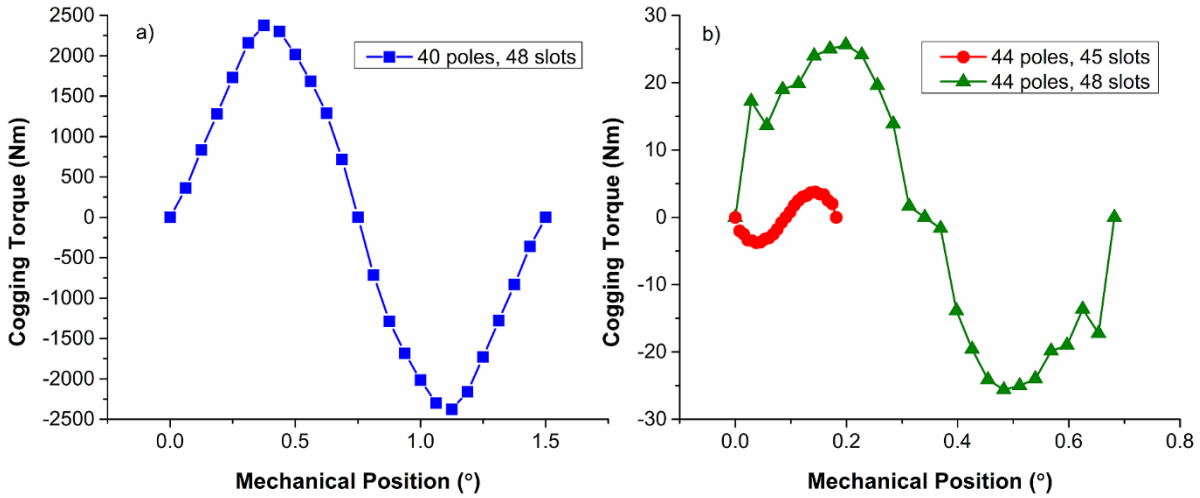

Fig. 14. Cogging torque of 3 MW HPMGs with C11 permanent and a) 40 poles and 48 slots and b) 44 poles and 45 or 48 slots.

4. Conclusions

We have demonstrated that by employing a Halbach cylinder (HC) as the rotor in 3.5 kW Halbach PMGs (HPMGs), sufficient magnetic flux is focused over the rotor surface to allow for the use of rare earth free, C11 strontium iron oxide permanent magnets. High pole and slot number are necessary for the use of ceramic permanent magnets. Rated torque and power was achieved for scaling of the C11 HPMGs to 3 MW on average at rated speed. High efficiency was achieved for the 3 MW HPMGs, demonstrating the potential for eliminating rare earth permanent magnets in commercial scale wind turbine generators. In future work, the use of HCs will be explored for PMGs rated at speeds in the range of direct-drive wind turbines.

Acknowledgement:

The work reported in this paper is funded under the U.S. National Science Foundation Grant No. 1069283 which supports the activities of the Integrative Graduate Education and Research Traineeship (IGERT) in Wind Energy Science, Engineering and Policy (WESEP) at Iowa State University as well as a Barbara and James Palmer Endowment at the Department of Electrical and Computer Engineering of Iowa State University.

The authors would also like to acknowledge Dr. Ayman El-Refaie of GE Global Research Center for useful discussions regarding this work.

References:

1. "Wind Vision: A New Era for Wind Power in the United States," U.S. Department of Energy, Oak Ridge, TN, Tech. Rep. DOE/GO-102015-4557, Apr. 2015.
2. "20% Wind Energy by 2030," U.S. Department of Energy, Oak Ridge, TN, Tech. Rep DOE/GO 102008-2567, July 2008.
3. S. S. Sheng. "Report on Wind Turbine Subsystem Reliability – A Survey of Various Databases," National Renewable Energy Laboratory, Golden, CO, Tech. Rep. NREL/PR-5000-59111, June 2013.
4. R. S. Semken, M. Polikarpova, P. Röyttä, J. Alexandrova, J. Pyrhönen, J. Nerg, A. Mikkola, J. Backman. "Direct-drive permanent magnet generators for high-power wind turbines: benefits and limiting factor," *IET Renewable Power Generation*, vol. 6, pp. 1-8, Jan. 2012. DOI: 10.1049/iet-rpg.2010.0191
5. H. Li, Z. Chen. "Overview of Different Wind Generator Systems and their Comparisons," *IET Renewable Power Generation*, vol. 2, pp. 123-128, June, 2008. DOI: 10.1049/iet-rpg:2007004
6. American Wind Energy Association, private communication, Sept. 2015.
7. K. H. J. Buschow. "Rare Earth Based Permanent Magnet Materials" in *Permanent Magnet Materials and Their Applications*. Ensfield, Trans Tech Publications Inc, 1998, ch. 3, sec. 3.1.3.1, pp. 27-31.
8. "Critical Materials Strategy," U.S. Department of Energy, Oak Ridge, TN, Tech. Rep. DOE/PI-0009, Dec. 2011.
9. S. Constantinides. "Rare Earth Materials Update," Presentation at the *Spring 2011 Management Conference*, submitted as part of Arnold Magnetics response to DOE Request for Information, 10 May 2011.
10. J. R. Hendershot, T. J. E. Miller. "Sizing & Computer-Aided Design," in *Design of Brushless Permanent-Magnet Motors*. Oxford, UK, Magna Physics Publishing and Clarendon Press, 1994, ch. 12, sec. 12.2, pp. 12-2 – 12-5.

11. J. R. Hendershot, T. J. E. Miller. "Basic Design Choices," in *Design of Brushless Permanent-Magnet Machines*. Venice, Motor Design Books LLC, 2010, ch. 3, sec. 3.3.1, pp. 87-91.
12. "Products," *Arnold Magnetic Technologies*, 2015. [Online]. Available: http://www.arnoldmagnetics.com/Products.aspx. [Accessed: 11-Aug-2015].
13. J. C. Mallinson. "One Sided Fluxes – A Magnetic Curiosity?" *IEEE Trans. Mag.*, vol. 9, no. 4, Dec. 1973. DOI: 10.1109/TMAG.1973.1067714
14. K. Halbach. "Design of Permanent Multipole Magnets with Oriented Rare Earth Cobalt Magnets," *Nucl. Instrum. Methods*, vol. 169, pp. 1-10, 1980. DOI: 10.1016/0029-554X(80)90094-4
15. Z Q. Zhu, D. Howe. "Halbach permanent magnet machines and applications: a review," *Electric Power Applications, IEE Proceedings*, vol. 148, no. 4, pp. 299-308, Jul. 2001. DOI: 10.1049/ip-epa:20010479
16. Z. Q. Zhu. "Recent Development of Halbach Permanent Magnet Machines and Applications," *Power Conversion Conference – Nagoya 2007. PCC '07*, pp. K-9 – K-16, Apr. 2007. DOI: 10.1109/PCCON.2007.372911
17. A. S. Abdel-Khalik, S. Ahmed, A. M. Massoud, A. A. Elserougi. "An improved performance direct-drive permanent magnet wind generator using a novel single-layer winding layout," *IEEE Trans. Magn*., vol. 49, pp. 5124-5134, Sept. 2013. DOI: 10.1109/TMAG.2013.2257823
18. H. A. Khazdozian, R. L. Hadimani, D. C. Jiles. "Size reduction of permanent magnet generators for wind turbines using halbach cylinders," *IEEE Magnetics Conference (INTERMAG)* 2015, pp. 1-1, 2015. DOI: 10.1109/INTMAG.2015.7156819.
19. Z. Q. Zhu, D. Howe, E. Bolte, B. Ackermann. "Instantaneous Magnetic Field Distribution in Brushless Permanent Magnet dc Motors, Part I: Open-Circuit Field," *IEEE Trans. Mag.*, vol. 29, no. 1, pp. 124-135, Jan. 1993. DOI: 10.1109/20.195558.
20. J. R. Hendershot, T. J. E. Miller. "Losses and Cooling," in *Design of Brushless Permanent-Magnet Machines*. Venice, Motor Design Books LLC, 2010, ch. 12, sec. 12.1-12.3, pp. 553-560.